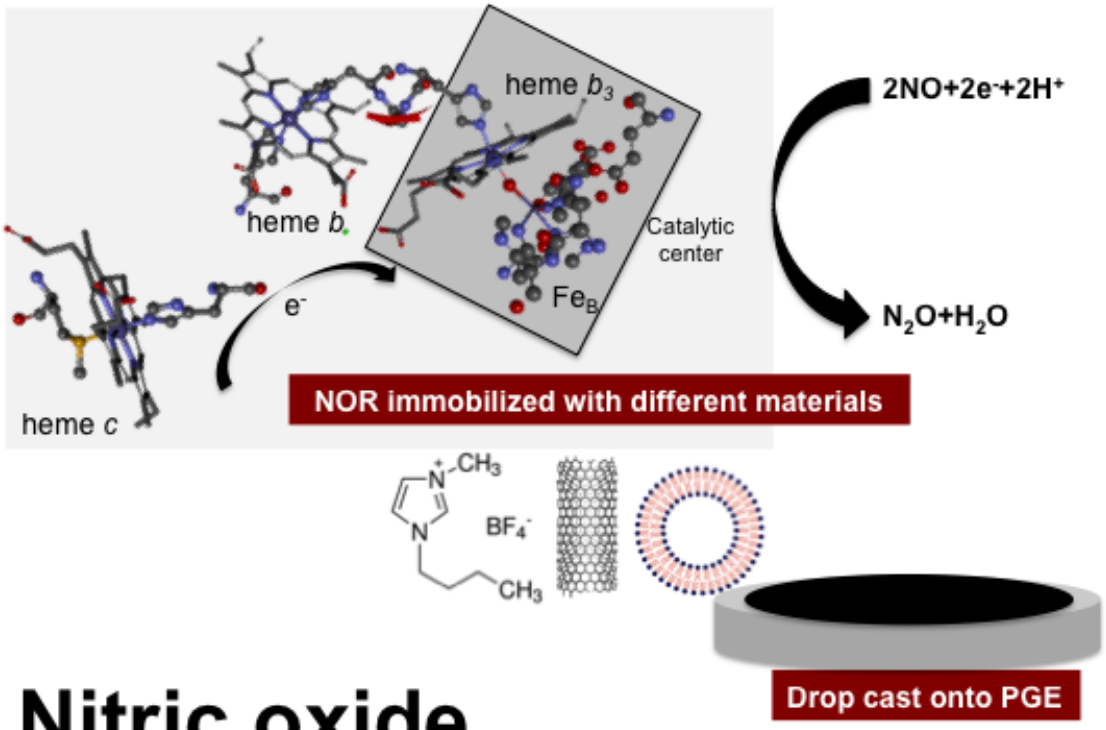

Nitric oxide detection using a Nitric Oxide Reductase-based Biosensor

Filipa Oliveira Gomes
Doutoramento em Química Sustentável
Departamento de Química e Bioquímica

Supervisor
Doctor Simone Barreira Morais
Professor Adjunto
REQUIMTE–LAQV, Instituto Superior de Engenharia, Instituto Politécnico do Porto

Co-supervisor
Doctor José João Galhardas de Moura
Professor Catedrático com Agregação
REQUIMTE-LAQV, Faculdade de Ciências e Tecnologia da Universidade Nova de Lisboa

2018

Nitric Oxide detection using a Nitric Oxide Reductase-based Biosensor

Filipa Oliveira Gomes

Supervisor

Doctor Simone Barreira Morais

Co-supervisor

Doctor José João Galhardas de Moura

A dissertation presented to the Faculty of Science from Porto University, Faculty of Science and Technology from Nova Lisboa University and Aveiro University for the degree of Doctor in Sustainable Chemistry

Porto

June 2018

The studies presented in this thesis were performed at the Environmental Chemistry and Health Group, member of the Associate Laboratory REQUIMTE-LAQV, at School of Engineering – Polytechnic of Porto (ISEP) in collaboration with REQUIMTE-LAQV at Faculty of Sciences and Technology, Nova University of Lisbon (FCT-UNL).

This work was supported by the PTDC/BBB-BQB/0129/2014 project (FCT/MCTES) and also by the Associate Laboratory Research Unit for Green Chemistry - Technologies and Processes Clean – LAQV, financed by national funds from FCT/MEC (UID/QUI/50006/2013) and co-financed by the ERDF under the PT2020 Partnership Agreement (POCI-01-0145-FEDER -007265). Funding through REQUIMTE project entitled “NOR-based biosensor for nitric oxide detection in biological and environmental samples” is also acknowledged. Filipa Gomes was supported by Fundação para a Ciência e a Tecnologia through the fellowship SFRH/BD/52502/2014.

ACKNOWLEDGMENTS

"There is no means of testing which decision is better, because there is no basis for comparison. We live everything as it comes, without warning, like an actor going on cold. And what can life be worth if the first rehearsal for life is life itself? That is why life is always like a sketch. No, "sketch" is not quite a word, because a sketch is an outline of something, the groundwork for a picture, whereas the sketch that is our life is a sketch for nothing, an outline with no picture."

Milan Kundera, The Unbearable Lightness of Being

This PhD dissertation consists in individual, colective and hard work during the last four years. As Milan Kundera says this was one of the rehearsal of my scientific life, the first one in this area (enzyme purification and bioelectrochemistry), without skecth…

…and feels so good not being prepared, living for the first time something...

However, during this four years, I had some difficulties and I receive all the support from special people.

Dedication

"In science, we must be interested in things, not in persons."

Marie Curie

Marie Curie was a huge phisical and chemistal scientist and received two nobels. She demonstrate that womans are strong human beings. However, I don't aggree with its citation. I think that in science we need to be interested in things but also in persons, because they help us to have some emocional support.

For this reason, I want to dedicate my dissertation to four special women in my life that deserve to be mentionated: to my grandmothers who unfortunately died in this professional course (Antónia da Silva and Lídia Antunes), to my mother (Irene Oliveira) and to my best friend (Diana Cruz).

I also had the privilege to count with the contribution of many people to whom I want to give a special thank.

I would like to thank to my supervisor, Doctor Simone Morais, for all the patience, scientific discussion and friendship. I think that Doctor Simone Morais is a polyvalent and serious researcher and I appreciate a lot her dynanism (that sometimes I can not keep up). The way she works is really to praise.

I also thank to my co-supervisor, Doctor José João Galhardas Moura for all the support namely in enzyme purification area (and other non-professional areas: art, cooking, photography, …) and guidance during the last four years.

A special thank to Doctor Luísa Maia for all the cooperation, dedication and teachings in the enzyme purification field at Faculty of Sciences and Technology, Nova University of Lisbon facilities. Thank you for your scientific and philosophical conversations and for your friendship.

I want to thank to Doctor Cristina Delerue-Matos, coordinator of Environmental Chemistry and Health Group - ISEP, for providing all the conditions needed in the development of this work.

I would also like to thank all colleagues from Faculty of Sciences and Technology, Nova University of Lisbon, particullarly to Cíntia Carreira, Cristina Cordas and Professor Isabel Moura and all colleagues from Environmental Chemistry and Health Group - ISEP, particularly to Idalina Bragança, Maria Freitas, Diana Rede, Paula Paíga, Luísa Correia de Sá e Fátima Barroso, for all the support, companionship and good moments since the beginning.

To my family, principaly to my mum and dad, my god mother, my brother (and its little family) and some cousins and aunts, a enormous thank you for all the encourage toughts and strengh to go ahead.

Thanks to Foundation for Science and Technology for granting a PhD scholarship (SFRH/BD/52502/2014), without which it would be impossible to carry out this work.

“God will never give you anything you can't handle, so don't stress.”

Kelly Clarkson

ABSTRACT

Nitric oxide (NO) is a key signaling molecule that plays an important role in humans. Although being essential, when produced in excess, may cause different pathologies. For this reason, new techniques for NO detection are required and, therefore, the topic has received increasing attention from the scientific community. Therefore, the main goal of this thesis was to develop novel third-generation enzymatic biosensors, taking advantage of the inherent specificity of *Marinobacter hydrocarbonoclasticus* nitric oxide reductase (NOR), which catalyzes the reduction of NO to nitrous oxide.

The **first stage** of this work consisted in NOR purification by ionic exchange chromatography, followed by chromatography in two hydroxyapatite columns using an optimized protocol. The NOR purity was assessed by its UltraViolet-Visible spectrum (with a $Absorbance_{410}/Absorbance_{280}$ ratio of 1.3) and by sodium dodecyl sulfate polyacrylamide gel electrophoresis (SDS-PAGE) with the observation of the two subunits of NOR: the α subunit (with the binuclear center responsible by the catalysis; SDS PAGE at 35-40 kDa) and the β subunit (responsible by the electron transfer; SDS PAGE at 17 kDa). Two batches of NOR were obtained with specific activities of 760 and 307 U/mg towards the reduction of NO.

The **second stage** of this work was to conduct direct electrochemical measurements of the immobilized NOR onto a pyrolytic graphite electrode (PGE), by cyclic and square-wave voltammetry under anaerobic conditions, and to evaluate the NO and dioxygen (O_2) bioelectrocatalysis (in independent and competitive studies). The greater NOR affinity for NO rather than for O_2 was corroborated.

The **subsequent steps** were related with the development and optimization, for the first time, of two novel NOR immobilization platforms and characterization of direct electrochemical behavior and electroanalytical performance towards NO reduction. The nanomaterials morphology and structure were characterized by scanning electron microscopy – energy dispersive X-ray spectroscopy, dynamic light scattering and attenuated total reflectance Fourier transform infrared spectroscopy. Cyclic and square-wave voltammetry, as well as electrochemical impedance spectroscopy, were used to characterize the interface properties of the modified electrodes surface during the different modifications steps. The first developed biosensor, composed by carboxylated multiwalled carbon nanotubes (MWCNTs), the selected ionic liquid (IL) 1-butyl-3-methylimidazolium tetrafluoroborate ($BMIMBF_4$) and NOR (PGE/[MWCNTs/$BMIMBF_4$/NOR]) showed high affinity for NO (Michaelis Menten

constant of 38.0 μmolL^{-1}) and acceptable electron transfer rate of 0.35 s^{-1}. The used nanocomposite for biosensor development demonstrated to be a favorable microenvironment for the immobilization of NOR due to excellent electric conductivity and large surface area of MWCNTs and biocompatibility and ionic conductivity of $BMIMBF_4$. Good electroanalytical characteristics were observed with a linear response to NO concentration between 0.23-4.76 μmolL^{-1} (detection limit of 0.07 μmolL^{-1}). The second biosensor, prepared with carboxylated SWCNTs, lipidic bilayer (DOPE:DOTAP:DSPE-PEG where 1,2-di-(9Z-octadecenoyl)-sn-glycero-3-phosphoethanolamine (DOPE), 1,2-di-(9Z-octadecenoyl)-3-trimethylammonium-propane (DOTAP) and 1,2-distearoyl-sn-glycero-3-phosphoethanolamine – polyethylene glycol (DSPE-PEG)) and NOR (PGE/[SWCNTs/(DOPA:DOTAP:DSPE-PEG)/NOR]) exhibited higher affinity for NO with a Michaelis Menten constant of 4.26 μmolL^{-1} and a wider linear range of 0.44 – 9.09 μmolL^{-1} (detection limit of 0.13 μmolL^{-1}) when compared to PGE/[MWCNTs/($BMIMBF_4$/NOR). The results obtained clearly show that NOR can be stabilized during at least during 1 month. Furthermore, PGE/[SWCNTs/(DOPA:DOTAP:DSPE-PEG)/NOR] biosensor revealed to provide the most suitable transducer surface due to the mimetic NOR environment achieved by the used lipidic bilayers.

The novel electrochemical third-generation biosensors based on NOR, constructed and optimized within this framework have the potential approach for *in vivo* NO biomonitoring.

Keywords: Third-generation biosensors; Direct electron transfer; Heme proteins; Porphyrins; Enzymatic biosensor; Nitric oxide reductase; Nitric oxide; Lipidic bilayer; Carbon nanotubes, Ionic liquid; Kinetic and electroanalytical parameters.

RESUMO

O óxido nítrico (NO) é uma molécula sinalizadora que desempenha um papel importante nos seres humanos. Embora o NO seja essencial, quando produzido em excesso, pode causar diferentes patologias. Por este motivo, o NO tem recebido especial atenção na comunidade científica sendo necessário o desenvolvimento de novas técnicas para a sua detecção. Assim, o objetivo principal desta tese foi desenvolver novos biossensores enzimáticos de terceira geração, tendo em conta a especificidade inerente à redutase do óxido nítrico (NOR) de *Marinobacter hydrocarbonoclasticus*, que catalisa a redução do NO a óxido nitroso.

A **primeira etapa** deste trabalho consistiu na purificação da NOR por cromatografia de troca iónica, seguida de cromatografia em duas colunas de hidroxiapatite utilizando um protocolo previamente otimizado. A pureza da NOR foi avaliada através do seu espectro Ultra Violeta-Visível (com uma relação $Absorvância_{410}/Absorvância_{280}$ de 1,3) e por eletroforese em gel de poliacrilamida com dodecil sulfato de sódio (SDS-PAGE) com a observação das duas subunidades da NOR: a subunidade α (centro binuclear responsável pela catálise; SDS PAGE a 35-40 kDa) e a subunidade β (responsável pela transferência electrónica; SDS PAGE a 17 kDa). Foram obtidos duas amostras de NOR com atividades específicas de 760 e 307 U/mg para a redução de NO.

A **segunda etapa** deste trabalho consistiu na realização de medições eletroquímicas diretas da NOR, imobilizada num elétrodo de grafite pirolítica (PGE), por voltametria cíclica e de onda quadrada sob condições anaeróbias, e avaliação da bioeletrocatálise do NO e do dioxigénio (O_2) (em estudos independentes e competitivos). A maior afinidade da NOR para o NO foi confirmada.

Os **passos seguintes** foram relacionados com o desenvolvimento e otimização, pela primeira vez, de duas novas plataformas de imobilização da NOR e com a caracterização do comportamento eletroquímico direto e do desempenho eletroanalítico em relação ao NO. A morfologia e a estrutura dos nanomateriais foram caracterizadas por microscopia eletrónica de varrimento - espectroscopia de raios X por dispersão de energia, dispersão de luz dinâmica e espectroscopia de infravermelho com transformada de Fourier. A voltametria cíclica e de onda quadrada, bem como a espectroscopia de impedância eletroquímica, foram utilizadas para caracterizar as propriedades de interface dos elétrodos modificados durante as diferentes etapas de modificação. O primeiro biossensor desenvolvido, composto por nanotubos de carbono de parede múltipla (MWCNTs) carboxilados, o liquido iónico selecionado – o tetrafluoroborato de 1-butil-3-metilimidazólio

($BMIMBF_4$) – e a NOR (PGE/[MWCNTs/$BMIMBF_4$/NOR]), demonstrou elevada afinidade para o NO (constante de Michaelis Menten de 38,0 $\mu molL^{-1}$) e uma velocidade de transferência electrónica aceitável de 0,35 s^{-1}. O nanocompósito utilizado para o desenvolvimento do biossensor demonstrou ser um microambiente favorável para a imobilização da NOR, devido à excelente condutividade elétrica e grande área superficial dos MWCNTs e à biocompatibilidade e condutividade iónica do $BMIMBF_4$. Foram também observadas boas características eletroanalíticas com uma resposta linear à concentração de NO entre 0,23-4,76 $\mu molL^{-1}$ (limite de deteção de 0,07 $\mu molL^{-1}$). O segundo biossensor, preparado com nanotubos de carbono de parede simples (SWCNTs) carboxilados, uma bicamada lipídica (DOPE: DOTAP: DSPE-PEG em que 1,2-di- (9Z-octadecenoil) -sn-glicero-3-fosfoetanolamina (DOPE), 1,2-di- 9Z-octadecenoil) -3-trimetilamonio-propano (DOTAP) e 1,2-distearoil-sn-glicero-3-fosfoetanolamina - polietilenoglicol (DSPE-PEG)) e NOR (PGE/[SWCNTs/(DOPA:DOTAP:DSPE-PEG)/NOR]), exibiu maior afinidade para o NO com uma constante de Michaelis Menten de 4.26 $\mu molL^{-1}$ e um maior intervalo linear de 0,44-9,09 $\mu molL^{-1}$ (limite de deteção de 0.13 $\mu molL^{-1}$) quando comparado com o biossensor PGE/[MWCNTs/($BMIMBF_4$/NOR)]. Os resultados obtidos mostram claramente que a NOR pode ser estabilizada durante pelo menos 1 mês. Além disso, o biossensor PGE/[SWCNTs/(DOPA:DOTAP:DSPE-PEG)/NOR] demonstrou apresentar o transdutor mais adequado devido ao ambiente mimético da NOR alcançado pelas bicamadas lipídicas usadas.

Os novos biossensores eletroquímicos de terceira geração baseados na NOR, construídos e otimizados no decorrer deste trabalho, têm como aplicação potencial a biomonitorização do NO *in vivo.*

Palavras-chave: Biossensores de terceira geração; Transferência eletrónica direta; Proteínas hémicas; Porfirinas; Biossensor enzimático; Redutase do óxido nítrico; Óxido nítrico; Bicamada lipídica; Nanotubos de carbono; Líquido iónico; Parâmetros cinéticos e eletroanalíticos.

PUBLICATIONS AND COMMUNICATIONS DEVELOPED UNDER THE PhD PROJECT

Publications of articles in journals of international circulation with scientific arbitration referenced in the Journal Citation Reports of ISI Web of Knowledge (***Orcid Id****: 0000-0002-9050-4557*)**:**

BOOK CHAPTER:

- F. Gomes, M. Freitas, H. Nouws, S. Morais, C. Delerue-Matos, Graphene as a Material for Bioelectrochemistry, Reference Module in Chemistry, Molecular Sciences and Chemical Engineering (2017). DOI: 10.1016/B978-0-12-409547-2.13519-X.

PAPERS IN SCIENTIFIC JOURNALS INCLUDED IN "SCIENTIFIC CITATION INDEX"

- F. Gomes, L.B. Maia, C. Cordas, C. Delerue-Matos, I. Moura, J.J.G. Moura, S. Morais, Nitric oxide detection using third-generation electrochemical biosensors based on heme proteins and porphyrins, Electroanalysis, *submitted*.
- F. Gomes, L.B. Maia, C. Delerue-Matos, I. Moura, J.J.G. Moura, S. Morais, Third-generation electrochemical biosensor based on nitric oxide reductase immobilized in a multiwalled carbon nanotubes/1-n-butyl-3-methylimidazolium tetrafluoroborate nanocomposite for nitric oxide detection, Sensors and Actuators B: Chemical, *submitted*.
- F. Gomes, L.B. Maia, C. Cordas, I. Moura, C. Delerue-Matos, J.J.G. Moura, S. Morais, Characterization of the direct Marinobacter hydrocarbonoclasticus nitric oxide reductase-catalysed nitric oxide and dioxygen reduction, Bioelectrochemistry, *in revision*.
- F. Gomes, L.B. Maia, J.A. Loureiro, M.C. Pereira, C. Delerue-Matos, I. Moura, J.J.G. Moura, S. Morais, Biosensor for direct bioelectrocatalysis detection of nitric oxide using nitric oxide reductase incorporated in carboxylated single-walled carbon nanotubes / lipidic bilayer nanocomposite, Sensors and Actuators B: Chemical, *submitted*.

ORAL COMMUNICATION IN INTERNATIONAL MEETING:

- F. Gomes, L.B. Maia, M.J. Ramalho, M.C. Pereira, I. Moura, C. Delerue-Matos, J.J.G. Moura, S. Morais, Nitric Oxide Reductase Based-Biosensor Modified with Liposomes and Gold Nanoparticles for Nitric Oxide Detection, 68th Annual Meeting of the International Society of Electrochemistry, 27 August-1 September 2017, Providence Rhode Island, USA.

POSTER COMMUNICATIONS IN INTERNATIONAL MEETINGS:

- F. Gomes, L.B. Maia, I. Moura, C. Delerue-Matos, J.J.G. Moura, S. Morais, Biosensor based on pyrolytic graphite electrode modified with Nitric Oxide Reductase-MWCNTs-$BMIMBF_4$ for nitric oxide determination, 13th European Biological Inorganic Chemistry Conference, 28 August-1 September 2016, Budapest, Hungary.
- F. Gomes, C. Cordas, L. Maia, I. Moura, C. Delerue-Matos, J. J. G. Moura, S. Morais, Nitric Oxide Reductase stabilization using carbon nanotubes, nanoPT2016, 16-19 February 2016, INL-Braga, Portugal.

POSTER COMMUNICATIONS IN NATIONAL MEETINGS:

- F. Gomes, L.B. Maia, I. Moura, C. Delerue-Matos, J.J.G. Moura, S. Morais, Nitric Oxide detection using a Nitric Oxide Reductase-based Biosensor: optimization of the immobilization strategy, 1st Scientific Meeting of the Doctoral Programme in Sustainable Chemistry, 26 September 2016, Universidade de Aveiro, Portugal.
- F. Gomes, C. Cordas, L.B. Maia, I. Moura, C. Delerue-Matos, J.J.G. Moura, S. Morais, Electrocatalytic behavior of Nitric Oxide Reductase toward NO and O_2, XX Meeting of the Portuguese Electrochemical Society, 21-23 October 2015, Braga, Portugal.

OTHER RELEVANT PARTICIPATIONS AND COURSES:

- Organizing Committee member (as student helper) at 68th Annual Meeting of the International Society of Electrochemistry. Providence Rhode Island, USA in 27 August to 1 September 2017.
- Organizing Committee member at the First Workshop on Electrochemistry Devices – (Bio) Sensors. Instituto Superior de Engenharia do Porto, Portugal in 13 and 14 October 2016.
- Curso de Especialização em Análise Quantitativa de Dados com SPSS, Laboratório de Engenharia Matemática – ISEP, Portugal in 20 February 2016 to 07 May 2016 (40h).
- Stripping electroanalytical techniques: SSCP and AGNES, given by Professor José Paulo Pinheiro from Laboratoire Interdisciplinaire des Environnements Continentaux – Université de Lorraine, Universidade do Minho in 19 and 20 October 2015 (14h).
- Protein electrophoresis, Universidade do Minho, Portugal in 2 and 3 July 2014 (16h).
- Short electrochemical impedance course, Universidade de Aveiro, Portugal in 29 June 2014 (8h).

TABLE OF CONTENTS

LIST OF FIGURES

CHAPTER 4 – Characterization of the direct *Marinobacter Hydrocarbonoclasticus* nitric oxide reductase-catalysed nitric oxide and dioxygen reduction

LIST OF TABLES

LIST OF ABBREVIATIONS

AuE	Gold electrode
AuNPs	Gold nanoparticles
AuPs	Gold particles
$BMIMBF_4$	1-n-butyl-3-methylimidazolium tetrafluoroborate
CAS	Catalase
CC	Cyanuric chloride
CEC	Cyanoethyl cellulose
CFM	Carbon fiber microelectrode
CHT-I e II	Ceramic Hydroxyapatite Type I and Type II
CPB	Cetylpyridinium bromide
CPE	Carbon paste electrode
CS	Chitosan
CTAB	Cetyl trimethylammonium bromide
CV	Cyclic voltammetry
Cys	Cysteamine
Cyt *c*	Cytochrome *c*
DDAB	Didodecyldimethylammonium bromide
DEAE Bio-gel	Diethylaminoethanol Bio-gel
DET	Direct electron transfer
DM	n-dodecyl-β-D-maltoside
DOAB	Dimethyldioctadecyl ammonium bromide
DOPE	2-di-(9Z-octadecenoyl)-sn-glycero-3-phosphoethanolamine
DOTAP	1,2-di-(9Z-octadecenoyl)-3-trimethylammonium-propane
DPV	Differential pulse voltammetry
DSPE-PEG	1,2-distearoyl-sn-glycero-3-phosphoethanolamine – polyethylene glycol
EDC/NHS	1-ethyl-3-(3-dimethylaminopropyl)carbodiimide/N-hydroxysuccinimide
EIS	Electrochemical impedance spectroscopy
Fe(4-TMPyP)	Iron(III) meso-tetrakis(N-methylpyridinium-4-yl)porphyrin
FTIR	Fourier-transform infrared spectroscopy
GCE	Glassy carbon electrode
GR	Graphene

Hb	Hemoglobin
HRP	Horseradish peroxidase
Mb	Myoglobin
MMT	Montmorillonite
MP	Microperoxidase
MSA	Methanesulfonic acid
MWCNTs	Multi walled carbon nanotubes
NO	Nitric oxide
NOR	Nitric oxide reductase
NYPA	Naphthalen-1-ylmethylphosphonic acid
PADDA	Poly(acrylamide-*co*-diallyldimethylammonium chloride
PAM	Polyacrylamide
PAN	Polyacrylonitrile
PC	Phosphatidylcholine
PE	2-phenylethanol
PEDGE	Poly(ethylene glycol diglycidylether)
PEI	Polyethyleneimine
PGE	Pyrolitic graphite electrode
PGMA	Poly(glycidyl methacrylate)
PIL	Polymerized ionic liquid
Pluoronic	Triblock copolymer poly(ethylene oxide)100-poly(propylene
films	oxide)65-poly(ethylene oxide)100
PME	Powder microelectrode
PNMP	Poly(N-(2-methacryloyloxyethyl) pyrrolidone)
PTFE	Polytetrafluoroehtylene
PTTCA	Poly-5,2':5",2''-terthiophene-3'- carboxylic acid
SCE	Saturated calomel electrode
SDS	Sodium dodecyl sulfate
SDS-PAGE	Sodium dodecyl sulfate polyacrylamide gel electrophoresis
SEM	Scanning electron microscopy
SOD	Superoxide dismutase
SWCNTs	Single walled carbon nanotubes
SWV	Square wave voltammetry
$TBABF_4$	Tetrabutylammonium tetrafluoroborate

LIST OF SYMBOLS

$-Z''$	Imaginary impedance
A	Geometric area of the working electrode
C	Concentration of the substrate
E	Peak potential
E_{cat}	Catalytic potential
$E^{o'}$	Formal potential
E_{pa}	Anodic peak potential
E_{pc}	Cathodic peak potential
F	Faraday constant
I_{max}	Maximum current measured under saturated substrate conditions
Ip	Peak current
I_{pa}	Anodic peak current
I_{pc}	Cathodic peak current
I_{ss}	Steady-state current after addition of the substrate
K_{app}	Apparent electron transfer rate constant
K_m	Michaelis Menten constant
k_s	Electron transfer constant
m	Parameter related to peak potential separation
n	Number of the electron transferred
Q	Charge involved in the reaction
R	Ideal gas constant
Rct	Charge transfer resistance
T	Temperature
v	Scan rate
Z'	Real impedance
ΔEp	Peak to peak separation
τ*	Surface concentration of the electroactive species

CHAPTER 1

PREFACE

1.1 Relevance and motivation

Bacterial nitric oxide reductase (NOR) is an integral membrane enzyme that catalyses the nitric oxide (NO) reduction to nitrous oxide (N_2O) in a two electron/proton reaction. Several types of NORs have been isolated from different bacteria organisms from the denitrification pathway [1-7]. The bacterial-denitrifying system (where NO_3^- is reduced to N_2) comprises four important reducing steps. Each step is mediated by different metalloenzymes, namely nitrate reductase ($NO_3^- \rightarrow NO_2^-$), nitrite reductase ($NO_2^- \rightarrow$ NO), NOR (NO $\rightarrow N_2O$) and nitrous oxide reductase ($N_2O \rightarrow N_2$) [8, 9]. In the step catalysed by NOR, a double N-N bond is formed in addition to the atom oxygen abstratction [9, 10]. *Marinobacter hydrocarbonoclasticus* NOR is purified as a cytochrome *bc* complex and is composed by two subunits (NorB and NorC) with three heme centers (heme *b*, heme *c* and heme b_3) and one non-heme Fe_B center [11–14]. Besides the NO reduction, NORs have also the ability to reduce O_2 to H_2O in a four electron/proton reaction [15–18].

Direct electron transfer of NOR was already performed (by cyclic voltammetry) by Cordas et al. [19] resulting in the determination of the redox potentials of the three heme and one non-heme centres of NOR. The binuclear center (composed by heme b_3 and non-heme Fe_B) demonstrated lower potential values [19]. The electrochemical behaviour of NOR in the presence of NO was also characterised by Cordas et al. [19] showing that the midpoint potential value of heme b_3 does not shift in the presence of NO. This was interpreted as indirect evidence that the catalytic mechanism should imply the two NO molecules binding to no-heme Fe_B center supporting the cis-Fe_B mechanism [19].

NO is a simple molecule that have important role in different physiological processes being a special type of transmitter in the nervous system, for example [20]. Additionally, in humans, NO regulate a wide range of vital functions namely vasodilation, platelet aggregation and gene expression [20]. Although, NO has also been implicated in different pathologies, such as chronic inflammation and infection conditions, septic shock syndrome, diabetes and Parkinson's and Alzheimer's diseases [21]. Briefly, in humans, NO is mainly generated by NO synthases that use arginine in a dioxygen and NADPH-dependent reaction to catalyse its formation [22]. In concert, under hypoxic conditions, several other proteins have been suggested to use nitrite to produce NO (e.g., hemoglobin and xanthine oxidase) [23].

Once formed, NO exerts its signalling function on the cellular target, mainly, by posttranslational modification of transition metal centres (mostly hemes and labile [4Fe-

4S] centres) and of cysteine residues and other thiols [24, 25]. Although of extreme importance, the *in vitro* characterization of those pathways, responsible for the NO formation and consumption, is not sufficient to fully understand the *in vivo* intra- and inter-cellular actions of NO.

The characteristics of NO make the *in vitro* and *in vivo* studies challenging tasks, namely its low concentration (10^{-9} - 10^{-7} molL^{-1}) and short half-life (typically within the seconds range), associated with the ability to freely permeate membranes [24, 25]. Consequently, there is a need to find efficient NO monitoring methodologies. For *in vitro*, and even *in vivo*, direct, sensitive, selective and real-time measurements, electrochemical biosensors are promising. There are some examples of heme proteins and porphyrins based-third generation biosensors to NO detection [27, 28], being hemoglobin and cytochrome *c* the most common choice [29, 30]; none was found based on NOR. Thus, taking advantage of the knowledge already gathered [17, 19, 31-32], novel approaches to build NO third-generation electrochemical biosensors based on NOR were explored. It is expected that the proposed biosensors based on the specific enzyme, NOR, that indeed possesses the higher affinity towards NO, may help to contribute to a better understanding of the cause-effect of NO and reactive nitrogen species at biological and physiological levels.

1.2 Objectives

The main goal of this work was to develop novel third-generation enzymatic biosensors for NO determination taking advantage of the inherent specificity of *Marinobacter hydrocarbonoclasticus* NOR.

In order to reach this goal, the specific objectives were:

- To purify and characterize NOR from *Marinobacter hydrocarbonoclasticus* bacterium based on previously developed protocols [6, 33];
- To immobilize *Marinobacter hydrocarbonoclasticus* NOR onto a pyrolitic graphite electrode by drop casting to study its direct electrochemical behaviour by square-wave voltammetry and to evaluate the competition under anaerobic environment between its two substrates (NO and O_2) acquiring information on the enzyme kinetics;
- To develop and optimize new distinctive platforms for NOR immobilization by testing different nanomaterials (combined or alone). The nanomaterials morphology and structure were characterized by scanning electron microscopy - energy-

dispersive X-ray spectroscopy, dynamic light scattering and attenuated total reflectance Fourier transform infrared spectroscopy. Cyclic and square-wave voltammetry, as well as electrochemical impedance spectroscopy were used to characterize the interface properties of the modified electrodes surface during the different modifications steps.

- To optimize the experimental parameters for NO bioelectrocatalytic reaction and evaluate the electroanalytical performance of the proposed NOR-based biosensors towards NO.

1.3 Thesis outline

This work is divided into seven chapters:

Chapter 1 (present chapter) is the preface of the thesis where the motivation and the objectives of the work, as well as the thesis outline are explained.

Chapter 2 provides the state of art concerning the NO importance and its detection using electrochemical third-generation biosensors–based on heme proteins and porphyrins. Chapters 3 reports the NOR purification from *Marinobacter hydrocarbonoclasticus*. Since this method was previously developed and optimized by the Moura and co-workers group [6, 33], only the more relevant results are presented.

Chapter 4 is dedicated to study the NOR direct electrochemical behaviour and its bioelectrocatalytic activity towards NO and O_2 in anaerobic environment.

Chapter 5 and 6 characterize the development of two novel biosensors constituted by multiwalled carbon nanotubes (MWCNTs), 1-n-butyl-3-methylimidazolium tetrafluoroborate ($BMIMBF_4$), and NOR (PGE/[MWCNTs/$BMIMBF_4$/NOR]; chapter 5), and carboxylated single-walled carbon nanotubes (SWCNTs), lipidic bilayer [1,2-di-(9Z-octadecenoyl)-sn-glycero-3-phosphoethanolamine (DOPE), 1,2-di-(9Z-octadecenoyl)-3-trimethylammonium-propane (DOTAP) and 1,2-distearoyl-sn-glycero-3-phosphoethanolamine – polyethylene glycol (DSPE-PEG)] and NOR (PGE/[SWCNTs/(DOPE:DOTAP:DSPE-PEG)/NOR]; chapter 6). The direct electron trasnfer behavior and electrocatalysis towards NO reduction of the optimized biosensors were investigated.

Finally, the concluding remarks and suggestions for future work are addressed in Chapter 7.

1.4 References

[1] J. Hoglen, T.C. Hollocher, Purification and some characteristics of nitric oxide reductase- containing vesicles from *Paracoccus denitrificans*, J. Biol. Chem., 264 (1989) 7556–7563.

[2] G.J. Carr, S.J. Ferguson, The nitric oxide reductase of *Paracoccus denitrificans*, J. Biochem., 269 (1990) 423–429.

[3] B. Heiss, K. Frunzke, W.G. Zumft, Formation of the N\N bond from nitric oxide by a membrane-bound cytochrome *bc* complex of nitrate-respiring (denitrifying) *Pseudomonas stutzeri*, J. Bacteriol., 171 (1989) 3288–3297.

[4] D.H. Kastrau, B. Heiss, P.M. Kroneck, W.G. Zumft, Nitric oxide reductase from *Pseudomonas stutzeri*, a novel cytochrome bc complex. Phospholipid requirement, electron paramagnetic resonance and redox properties, Eur. J. Biochem., 222 (1994) 293–303.

[5] H. Kumita, K. Matsuura, T. Hino, S. Takahashi, H. Hori, Y. Fukumori, I. Morishima, Y. Shiro, NO reduction by nitric-oxide reductase from denitrifying bacterium *Pseudomonas aeruginosa*: characterization of reaction intermediates that appear in the single turnover cycle, J. Biol. Chem., 279 (2004) 55247–55254.

[6] C.G. Timoteo, A.S. Pereira, C.E. Martins, S.G. Naik, A.G. Duarte, J.J. Moura, P. Tavares, B.H. Huynh, I. Moura, Low-spin heme b_3 in the catalytic center of nitric oxide reductase from *Pseudomonas nautica*, Biochemistry, 50 (2011) 4251–4262.

[7] M.C. Marquez, A. Ventosa, *Marinobacter hydrocarbonoclasticus* Gauthier, et al. 1992 and *Marinobacter aquaeolei* Nguyen et al. 1999 are heterotypic synonyms, Int. J. Syst. Evol. Microbiol., 55 (2005) 1349–1351.

[8] W.G. Zumft, Nitric oxide reductases of prokaryotes with emphasis on the respiratory, heme-copper oxidase type, J. Inorg. Biochem., 99 (2005) 194–215.

[9] P. Tavares, A.S. Pereira, J.J. Moura, I. Moura, Metalloenzymes of the denitrification pathway, J. Inorg. Biochem., 100 (2006) 2087–2100.

[10] N.J. Watmough, S.J. Field, R.J. Hughes, D.J. Richardson, The bacterial respiratory nitric oxide reductase, Biochem. Soc. Trans., 37 (2009) 392–399.

[11] P. Girsch, S. de Vries, Purification and initial kinetic and spectroscopic characterization of NO reductase from *Paracoccus denitrificans*, Biochim. Biophys. Acta, 1318 (1997) 202–216.

[12] J. Hendriks, A. Warne, U. Gohlke, T. Haltia, C. Ludovici, M. Lubben, M. Saraste, The active site of the bacterial nitric oxide reductase is a dinuclear iron center, Biochemistry, 37 (1998) 13102–13109.

[13] M.R. Cheesman, W.G. Zumft, A.J. Thomson, The MCD and EPR of the heme centers of nitric oxide reductase from *Pseudomonas stutzeri*: evidence that the enzyme is structurally related to the heme-copper oxidases, Biochemistry, 37 (1998) 3994–4000.
[14] Y. Shiro, Structure and function of bacterial nitric oxide reductases. Nitric oxide reductase, anaerobic enzymes, Biochim. Biophys. Acta, 1817 (2012) 1907–1913.
[15] N. Sakurai, T. Sakurai, Isolation and characterization of nitric oxide reductase from *Paracoccus halodenitrificans*, Biochemistry, 36 (1997) 13809–13815.
[16] U. Flock, N.J. Watmough, P. Adelroth, Electron/proton coupling in bacterial nitric oxide reductase during reduction of oxygen, Biochemistry, 44 (2005) 10711–10719.
[17] C.M. Cordas, A.S. Pereira, C.E. Martins, C.G. Timoteo, I. Moura, J.J. Moura, P. Tavares, Nitric oxide reductase: direct electrochemistry and electrocatalytic activity, Chembiochem, 7 (2006) 1878–1881.
[18] U. Flock, P. Lachmann, J. Reimann, N.J. Watmough, P. Adelroth, Exploring the terminal region of the proton pathway in the bacterial nitric oxide reductase, J. Inorg. Biochem., 103 (2009) 845–850.
[19] C.M. Cordas, A.G. Duarte, J.J.G. Moura, I. Moura, Electrochemical behaviour of bacterial nitric oxide reductase—Evidence of low redox potential non-heme Fe_B gives new perspectives on the catalytic mechanism, Biochim. Biophys. Acta, 1827 (2013) 233–238.
[20] S. Moncada, R.M. Palmer, E.A. Higgs, Nitric oxide: physiology, pathophysiology, and pharmacology, Pharmacol. Rev., 43 (1991) 109–142.
[21] J.P. Eiserich, R.P. Patel, V.B. O'Donnell, Pathophysiology of nitric oxide and related species: free radical reactions and modification of biomolecules, Mol. Aspects Med., 19 (1998) 221–357.
[22] D. J. Stuehr, Mammalian nitric oxide synthases, Biochim. Biophys. Acta, 1411 (1999) 217– 230.
[23] L.B. Maia, J.J.G. Moura, How Biology Handles Nitrite, Chemical Reviews, in press (available online), 2014, DOI 10.1021/cr400518y
[24] W.H. Koppenol, The basic chemistry of nitrogen monoxide and peroxynitrite, Free Radical Biol. Med., 25 (1998) 385–391.
[25] J.S. Beckman, W.H. Koppenol, Nitric oxide, superoxide, and peroxynitrite: the good, the bad, and ugly, Am. J. Physiol., 271 (1996) C1424–1437.
[26] X. Ye, S.S. Rubakhin, J.V. Sweedler, Detection of nitric oxide in single cells, Analyst, 133 (2008) 423–433.

[27] F. Bedioui, N. Villeneuve, Electrochemical Nitric Oxide Sensors for Biological Samples – Principle, Selected Examples and Applications, Electroanalysis, 15 (2003) 5–18.

[28] A.P. Gutierrez, S. Griveau, C. Richard, A. Pailleret, S.G. Granados, F. Bedioui, Hybrid materials from carbon nanotubes, nickel tetrasulfonated phthalocyanine and thin polymer layers for the selective electrochemical activation of nitric oxide in solution, Electroanalysis, 21 (2009) 2303–2310.

[29] S. Jia, J. Fei, J. Zhou, X. Chen, J. Meng, Direct electrochemistry of hemoglobin entrapped in cyanoethyl cellulose film and its electrocatalysis to nitric oxide, Biosens. Bioelectron., 24 (2009) 3049–3054.

[30] Z. Guo, J. Chen, H. Liu, C. Cha, Direct electrochemistry of hemoglobin and myoglobin at didodecyldimethylammonium bromide-modified powder microelectrode and application for electrochemical detection of nitric oxide, Anal. Chim. Acta, 607 (2008) 30–36.

[31] A.G. Duarte, C.M. Cordas, J.J.G. Moura, I. Moura, Steady-state kinetics with nitric oxide reductase (NOR): New considerations on substrate inhibition profile and catalytic mechanism, Biochim. Biophys. Acta, 1837 (2014) 375-384.

[32] S. Ramos, R.M. Almeida, C.M. Cordas, J.J.G. Moura, S.R. Pauleta, I. Moura, Insights into the recognition and electron transfer steps in nitric oxide reductase from *Marinobacter hydrocarbonoclasticus*, J Inorg Biochem., 177 (2017) 402-411.

[33] M. Prudêncio, A.S. Pereira, P. Tavares, S. Besson, I. Cabrito, K. Brown, et al., Purification, characterization, and preliminary crystallographic study of copper-containing nitrous oxide reductase from *Pseudomonas nautica* 617, Biochemistry, 39 (2000) 3899-3907.

CHAPTER 2

NITRIC OXIDE DETECTION USING ELECTROCHEMICAL THIRD-GENERATION BIOSENSORS–BASED ON HEME PROTEINS AND PORPHYRINS

Nitric oxide radical (NO) is a signalling molecule involved in diverse biological processes in virtually all forms of life, being also a key player in several prokaryotic "respiratory" pathways. The relevance of its biological roles led to the development of different analytical methodologies to assess the temporal and spatial fluxes of NO (formation and consumption) under the complex biological milieu. Third-generation electrochemical biosensors, or also known as unmediated biosensors, are promising tools for *in loco* and *in vivo* NO quantification and, over the past years, heme proteins (hemoglobin, myoglobin, cytochrome *c* and peroxidase) and porphyrins have been used in their design. Since there are some limitations with the biorecognition element directly adsorbed onto the electrode surface, nanomaterials (carbon nanotubes, gold nanoparticles, graphene, etc.) and polymers (cellulose, chitosan, nafion®, polyacrylamide, polyacrylonitrile, among others) have been explored to achieve high kinetics and better biosensor performance with improved stability and signal amplification. In this review, a broad overview of the field of electrochemical third-generation biosensors for NO electroanalysis is presented, discussing their main characteristics and aiming new outlooks and advances in this field.

2.1. Introduction

2.1.1. NO Biology

Nitric oxide radical (•NO, herein abbreviated as NO) is an ubiquitous molecule, involved in numerous biological processes in virtually all forms of life, from bacteria to humans. NO is known for long as key player of the biogeochemical cycle of nitrogen (Fig. 2.1), participating in different prokaryotic pathways crucial to the planet "recycling" of nitrogen and, consequently, to life on Earth [1]. In fact, NO may have been the first deep electron sink on Earth, before the emergence of dioxygen [2, 3]. Even today, the formation of the N-N bond, essential to ultimately produce dinitrogen and, thus, accomplish the complete biological "recycling" of nitrogen, is only possible with the oxidizing power of NO (as far as is known) [1].

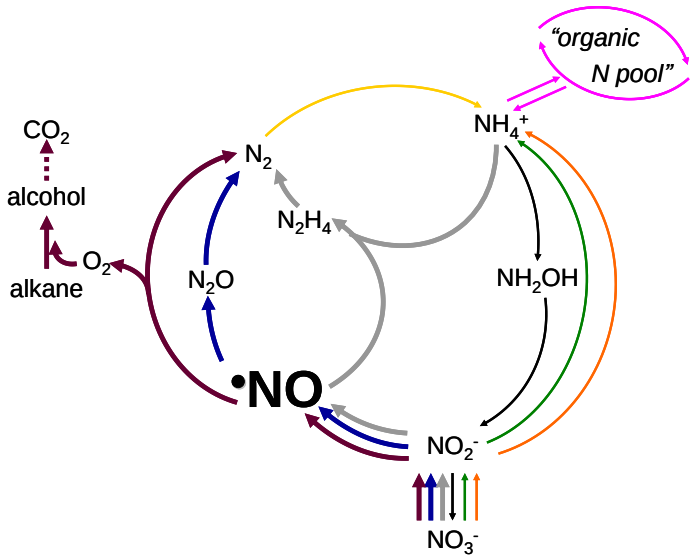

Fig. 2.1. Overview of the biochemical cycle of nitrogen. Denitrification, blue arrows; AnAmmOx, grey arrows; "denitrification/intra-aerobic methane oxidation", violet arrows; dinitrogen fixation, yellow arrow; assimilatory ammonification, orange arrows; "organic nitrogen pool", pink arrows; dissimilatory nitrate reduction to ammonium, green arrows; nitrification and ComAmmOx, black arrows. The pathways where NO participates are highlighted with thicker lines (denitrification, AnAmmOx and "denitrification/intra-aerobic methane oxidation"). Adapted from reference [1] with permission.

NO participates in two "classic" prokaryotic "respiratory" pathways, where nitrogen compounds are used as electron acceptors to derive energy: denitrification and anaerobic ammonium oxidation (AnAmmOx). In denitrification [4] (Fig. 2.1, blue arrows), nitrate is anaerobically reduced to dinitrogen, through four sequential reactions, catalysed by specific metalloenzymes. In this pathway, NO is formed from nitrite, in a reaction catalysed by nitrite reductases, and is converted into nitrous oxide by a nitric oxide reductase. In AnAmmOx [5] (Fig. 2.1, grey arrows), ammonium is anaerobically oxidised to dinitrogen in a two steps pathway, where ammonium is first oxidised by NO to yield hydrazine, in a reaction catalysed by the hydrazine synthase; the necessary NO is formed via nitrite reduction by nitrite reductases. In addition to these well-known "classic" pathways, several *new* processes are being identified, revealing the great biological versatility of NO [1]. Particularly interesting is the novel "denitrification/intra-aerobic methane oxidation" pathway that links the nitrogen and carbon cycles (Fig. 2.1, violet arrows) [6]. In this puzzling pathway, strictly anaerobic organisms use NO to produce their own (endogenous) dioxygen supply to oxidise methane and other alkanes, while simultaneously produce dinitrogen.

More recently, it became clear that NO is not just a "prokaryotic molecule" or an environmental issue (associated with the depletion of the ozone layer). In 1987, NO was identified as the elusive endothelium-derived relaxing factor that regulates blood vessel vasodilation in mammals cardiovascular system [7-10], a discovery that was latter (1998) distinguished with the Nobel Prize in Physiology or Medicine, awarded to Furchgott, Ignarro and Murad. Presently, it is clear that the signaling functions of NO are not restricted to mammals, but are ubiquitous in virtually all forms of life, from bacteria to humans.

In humans, NO controls a plethora of functions, not only the well-known vasodilation (through the activation of guanylate cyclase), but also neurotransmission, immune response, platelet aggregation, apoptosis and gene expression, and mediates a wide range of both anti-tumor and anti-microbial activities [11]. Consequently, NO is involved in several pathological conditions, either when it is not produced in sufficient concentrations, as is the case of hypertension [12, 13], impotence [14, 15], arteriosclerosis [16, 17] or susceptibility to infection [18, 19], or when it is produced in excess, as during chronic inflammation [20, 21], septic shock syndrome [22], diabetes [23], multiple sclerosis [24] or Parkinson’s and Alzheimer’s diseases [25]. In humans, three tissue-specific isoforms of NO synthases (NOS), neuronal, endothelial

and inducible NOS, catalyze the formation of NO from L-Arginine and dioxygen [26-28]. In addition, under hypoxic or anoxic conditions, when the dioxygen-dependent NOS activity is hampered, also nitrite is an important source of signalling NO [29-33]. The nitrite-dependent formation of NO is catalyzed by "non-dedicated" nitrite reductases, such as hemoglobin, myoglobin, xanthine oxidase and other metalloproteins present in the cells to carry out other functions.

This array of biological functions makes the metabolism of NO extremely important for the scientific community that pursuits *new* and *old* pathways of the nitrogen biogeochemical cycle, some of them linked with worrying environmental issues, as well as, *new* and *old* pathways of signaling NO and the associated physiological and pathological roles of NO. Yet, the advancement of our knowledge of the NO biology depends on methods capable of unequivocally identify it and precisely quantify it.

2.1.2. The challenges of detecting NO

Measuring NO under biological conditions is not an easy task. The NO fast diffusion ($k \approx 10^{10}$ - 10^{11} $mol^{-1}Ls^{-1}$) and high reactivity with dioxygen ($k \approx 10^{6}$ - 10^{7} $mol^{-1}Ls^{-1}$), superoxide anion ($k \approx 10^{9}$ - 10^{10} $mol^{-1}Ls^{-1}$) and other radicals, as well as, with metalloproteins (mostly hemes and labile [4Fe-4S] centres) cysteine residues and other thiols, determine that NO has a very short half-life (typically within the seconds range), which greatly hinders the precise and accurate NO quantification [11, 27, 34]. To further complicate the subject, the range of NO concentrations is very wide; for example, in humans, the NO physiological concentration can range from 10^{-10} to 10^{-7} $molL^{-1}$ and reach micromolar levels under pathological conditions and immune responses [11, 27, 34]. Moreover, the NO studies often require its detection in very complex systems, containing other potentially interfering species present in much higher concentrations than NO itself, such as nitrite, nitrate, dopamine or ascorbate. NO research has been increasing in the last years and this boost demands the development of analytical techniques capable of precisely and accurately quantify NO levels and rates of production. Moreover, several methodologies have been developed to measure NO: (i) indirect detection, quantifying cyclic guanosine monophosphate (cGMP), a biologically active second messenger [35, 36], or by the NO oxidation products, using fluorescent probes [37-42] or the Griess reaction [43-48]; (ii) direct detection, exploring different properties of NO, such as its radical nature, using electron paramagnetic resonance spectroscopy [41, 49-51], its reactivity towards some metalloproteins (*e.g.*, reaction with reduced hemoglobin and

methemoglobin formation) or its ability to react with ozone to produce light, using chemiluminescence detection [52-54]. While most of these approaches display high sensitivity and selectivity for NO, all present specific limitations, with one main issue being the spatial resolution *in vivo*, which cannot be obtained with a "bulk" method.

2.2. Electrochemical detection of NO

Electrochemistry has high potential to measure NO in biological fluids because it can detect NO in real time and *in situ* [55]. In addition, NO biosensors can be in the perfect size (small enough) to be used in many *in vivo* applications. According to the International Union of Pure and Applied Chemistry (IUPAC), sensors contain two basic functional units: a receptor and a transducer part. Sensors are normally designed to operate under well-defined conditions for specified analytes in specific samples [56]. Biosensors may be differentiated from sensors due to the biorecognition elements used in the receptor, which may be enzymes, antibodies, tissues, cells, organelles, membranes, among others [57, 58]. Depending on the type of signal transduced, the classification of biosensors can be electrochemical, optical, piezoelectric, thermal/calorimetric [59]. Electrochemical biosensors offer several advantages, such as excellent detection limits, high specificity, easy miniaturization, portability, and ability to be used in turbid biofluids and in extremely low analyte volumes [60, 61]. However, there may be some drawbacks to perform reliable electrochemical measurements in complex biological systems, such as lack of robustness, biofouling with surface electrode blockage, lack of stability, and/or deactivation of enzymatic activity [62, 63]. Still, the evolution of first- to third-generation electrochemical biosensors has helped to simplify and enhance the transduction pathway [64]. In third-generation biosensors, the electrons involved in the redox processes are transferred directly between the enzyme or redox protein and the electrode surface to generate the response signal; no redox mediators are used oppositely to the second-generation electrochemical biosensors [65]. Moreover, the use of third-generation biosensors can allow to understand the mechanisms regarding several electron transfer processes [66]. Electrochemical reduction may be employed for NO detection studies but it is often difficult due to interference from oxygen, whose happens faster than that of NO. As a result, the majority of electrochemical NO biosensors are based on the oxidation of NO to nitrite instead of NO reduction [67-69].

Biosensors of third-generation for NO detection were architected with hemoglobin (Hb), myoglobin (Mb) and cytochrome *c* (cyt *c*) proteins, peroxidase, as well as with porphyrins. This study is dedicated to review, discuss and compare the main characteristics of these biosensors, aiming new outlooks and advances in this field. The scientific literature available on NO reduction using electrochemical biosensors was reviewed from 1997 till 2017 and the following keywords were crossed in Thomson Reuters - Web of Science: direct electron transfer; third-generation biosensors; hemoglobin; myoglobin; cytochrome *c*; peroxidase; porphyrins; nitric oxide detection.

2.3. Direct electron transfer behavior of heme proteins and porphyrins in third-generation biosensors

The main advantages of these direct electron transfer (DET) systems are their simpler design and the potential to provide interference free detection [70]. However, one of the main problem in DET biosensors development may be the inaccessibility of the redox center of most redox enzymes and proteins, covered by several peptides, which may hamper the electron flow between the enzyme or protein and the electrode [71]. To promote DET, nanomaterials and polymers have been extensively used for electrode surface modification (table 2.1). Hb, Mb and cyt *c* proteins, peroxidase, and porphyrins have been all immobilized onto suitable physical transducers. The available immobilization techniques are adsorption on thin films (physical; electrostatic – layer-by-layer, electrochemical doping, pre-immobilization on ion-exchange beads; retention in a lipidic microenvironment), entrapment (electropolymerization; amphiphilic network; photopolimerization; sol-gel process; polysaccharide-based gel; carbon paste; clay-modified electrodes), cross-linking with natural or synthetic molecules (glutaraldehyde or carbodiimide), direct attachment by ionic or covalent bonding (activation of carboxylic or amino groups) and affinity (biotin-(strept)avidin; metal-ion chelator; lectin-carbohydrate) [72]. The selected strategy has a major impact on biosensor performance (sensitivity, reproducibility and response time) and stability. The biorecognition element structure and activity should remain unchanged after immobilization (to maximize sensitivity), and it should intimately and strongly link to the transducer surface (to maximize stability). In addition, the substrate diffusion should take place easily. The employed approaches for preparation of third-generation biosensors for NO detection (table

2.1) are mainly based on adsorption (physical [73, 74] and layer-by-layer [75-81]), entrapment [82-98] or covalent bonding [99-102]. Each method possesses its particular benefits and disadvantages. Adsorption have been mostly used due to its simplicity and because loss of activity is not significant [73-81]. However, leaching of the biocomponent has been reported as a problem due to the weak Van der Waal's forces and electrostatic or hydrophobic interactions established [103, 104]. Entrapment maintains the bioactivity and has been contributing to reduce heme proteins and porphyrins leakage [82-98], but diffusional limitations may happen while high bioelement concentrations are required for electropolymerization [82-98]. Regarding covalent attachment, its predominant advantages are the reached high stability (leaching of the bioelement is not significant) and the absence of mass transfer limitations although activity loss may be significant due to conformational changes of even denaturation of the enzyme or protein [72]. Also, toxic reagents (such as glutaraldehyde) have been commonly used for covalent coupling.

The choice of the working electrode is also crucial and several aspects, such as appropriate potential window, easy surface renewal, fast redox processes, reproducibility, easy miniaturization, low cost, the immobilized molecule and the substrate, should be considered. The privileged working electrodes have been glassy carbon (41%) (GCE) and graphite pyrolytic (PGE) (31%) electrodes, although gold electrodes (AuE) (9%), powder microelectrode (PME) [86], carbon paste electrodes (CPE) [74], SnO_2 and TiO_2 electrodes [73], platinum (Pt) microelectrode [100] and carbon fiber microelectrodes (CFM) [78, 101] have been also explored but in a much lesser extend (table 2.1).

Table 2.1. Immobilization and detection techniques, as well as kinetic parameters ($E^{0'}$ – formal potential; Γ^* –surface concentration of the electroactive species; k_s – electron transfer rate constant; K_m – Michaelis Menten constant) of heme proteins and porphyrins based third-generation biosensors for NO detection.

Biosensor	Immobilization	Detection technique	$E^{0'}$ heme-protein or porphyrin (V vs. SCE)	Γ^* (mol/cm^2)	k_s (s^{-1})	K_m ($\mu molL^{-1}$)	Ref.
		Hemoglobin (Hb)					
Hb-DNA/PGE	Hb mixed with DNA and then drop casted at electrode surface.	Cyclic voltammetry, Linear Sweep Voltammetry, Square Wave Voltammetry	-0.358	*n.r.*	*n.r.*	*n.r.*	[82, 83]
Hb-PC/PGE	Hb entrapped in a phosphatidylcholine film and drop casted at electrode surface.	Cyclic Voltammetry, Differential Pulse Voltammetry	-0.183	*n.r.*	*n.r.*	*n.r.*	[85]
Hb-AuPs-Cys/AuE	Modification of electrode surface with cysteamine; Immersion in colloidal gold solution; Immersion in Hb solution.	Cyclic Voltammetry, Differential Pulse Voltammetry, Amperometry	-0.051	*n.r.*	*n.r.*	190	[107]
Hb-PEI/PGE	Mixture of Hb with polyethyleneimine and then drop casted at electrode surface.	Cyclic Voltammetry	-0.205	*n.r.*	*n.r.*	*n.r.*	[92]
Hb-MMT-PVA/PGE	Mixture of Hb with montmorillonite and polyvinyl alcohol and then drop casted at electrode surface.	Cyclic Voltammetry	-0.358	*n.r.*	*n.r.*	*n.r.*	[95]
Hb-MMT/PGE	Mixture of Hb with montmorillonite and then drop casted at electrode surface.	Cyclic Voltammetry	-0.283	*n.r.*	*n.r.*	*n.r.*	[84]
Hb-DOAB/PGE	Mixture of Hb with dimethyldioctadecyl ammonium bromide and then drop casted at electrode surface.	Cyclic Voltammetry	-0.235	5.3×10^{-12}	0.10	*n.r.*	[93]
Hb-CPB-PAM/GCE	Modification of electrode surface with polyacrylamide; Mixture of Hb with cetylpyridinium bromide and then drop casted at modified electrode surface.	Cyclic Voltammetry	-0.216	*n.r.*	*n.r.*	*n.r.*	[87]

Table 2.1. Immobilization and detection techniques, as well as kinetic parameters ($E^{0'}$ – formal potential; τ^* –surface concentration of the electroactive species; k_s – electron transfer rate constant; K_m – Michaelis Menten constant) of heme proteins and porphyrins based third-generation biosensors for NO detection (continued).

Biosensor	Immobilization	Detection technique	$E^{0'}$ heme-protein or porphyrin (V vs. SCE)	τ^* (mol/cm^2)	k_s (s^{-1})	K_m ($\mu molL^{-1}$)	Ref.
Hb-PTFE/GCE	Mixture of Hb with polytetrafluoroethylene and then drop casted at electrode surface.	Cyclic Voltammetry	-0.281	3.45×10^{-11}	1.7	*n.r.*	[94]
Hb-C_{12}-C_3(OH)-C_{12}/GCE	Mixture of Hb with cationic gemini surfactant and then drop casted at electrode surface.	Cyclic Voltammetry, Amperometry	-0.320	1.36×10^{-10}	17.91	84.37	[97]
Hb-PNMP-*b*-PGMA/GCE	Mixture of Hb with poly [N-(2-methacryloyloxyethyl) pyrrolidone]-block- poly [glycidyl methacrylate] and then drop casted at electrode surface.	Cyclic Voltammetry, Differential Pulse Voltammetry	-0.409	2.51×10^{-11}	1.03±0.05	*n.r.*	[88]
Hb-CEC/GCE	Mixture of Hb with cyanoethyl cellulose and then drop casted at electrode surface.	Cyclic Voltammetry, Electrochemical Impedance Spectroscopy, Amperometry	-0.369	2.19×10^{-11}	1.10±0.05	75.39	[89]
Hb-Au/CPE	Mixture of graphite, gold colloid nanoparticles and paraffin to construct the carbon past electrode; Immersion in Hb solution.	Cyclic Voltammetry, Electrochemical Impedance Spectroscopy, Amperometry	-0.351	3.65×10^{-10}	3.72	105.8	[74]
Hb-CS-GR-CTAB/GCE	Mixture of hexadecyltrimethylammonium bromide with graphene and then drop casted at electrode surface; Mixture of Hb with chitosan and the drop casted at modified electrode surface.	Cyclic Voltammetry, Amperometry	-0.190	1.69×10^{-9}	60.3	0.315	[98]
Hb-AuNPs-GR-SDS/PGE	Mixture of gold nanoparticles with sodium dodecyl sulfate and graphene drop casted at electrode surface; Immersion in Hb solution.	Cyclic Voltammetry, Amperometry	-0.314	*n.r.*	48±5	*n.r.*	[81]
Hb-NYPA-MWCNTs-Nafion®/GCE	Mixture of Hb with phosphonate functionalized multi-walled carbon nanotubes and then drop casted at electrode surface.	Cyclic Voltammetry, Amperometry	-0.406	5.11×10^{-10}	12.69	*n.r.*	[91]

Table 2.1. Immobilization and detection techniques, as well as kinetic parameters ($E^{0'}$ – formal potential; τ^* –surface concentration of the electroactive species; k_s – electron transfer rate constant; K_m – Michaelis Menten constant) of heme proteins and porphyrins based third-generation biosensors for NO detection (continued).

Biosensor	Immobilization	Detection technique	$E^{0'}$ heme-protein or porphyrin (V vs. SCE)	τ^* (mol/cm^2)	k_s (s^{-1})	K_m ($\mu molL^{-1}$)	Ref.
Hb-AuNPs-Cellulose-PEGDGE/GCE	Mixture of Hb with gold nanoparticles (on a quaternized cellulose support) and poly(ethylene glycol diglycidyl ether) and then drop casted at electrode surface.	Cyclic Voltammetry, Electrochemical Impedance Spectroscopy, Chronoamperometry	-0.333	3.05×10^{-11}	0.92	2.6×10^{-3}	[90]
Hb-Pluronic film/PGE	Mixture of Hb with pluronic film and then drop casted at electrode surface.	Cyclic Voltammetry, Square Wave Voltammetry	-0.350	1.81×10^{-11}	36±6	*n.r.*	[96]
Hb-DDAB/PME	Mixture of Hb with acetylene black and didodecyldimethylammonium bromide.	Cyclic Voltammetry	-0.224	2.83×10^{-8}	*n.r.*	*n.r.*	[86]
Hb/SnO_2 or Hb/TiO_2	Drop cast of Hb at electrode surface.	Cyclic Voltammetry, Spetroelectrochemistry	-0.216	*n.r.*	1±0.03	*n.r.*	[73]
		Myoglobin (Mb)					
Mb-Pluronic film/PGE	Mixture of Mb with pluronic film and then drop casted at electrode surface.	Cyclic Voltammetry, Square Wave Voltammetry	-0.350	7.50×10^{-11}	69±6	*n.r.*	[96]
Mb-DDAB/PME	Mixture of Mb with acetylene black and didodecyldimethylammonium bromide.	Cyclic Voltammetry	-0.212	9.94×10^{-8}	*n.r.*	*n.r.*	[86]
Mb-MWCNTs/GCE	Drop cast of MWCNTs at electrode surface; Drop cast of Mb at modified electrode surface.	Cyclic Voltammetry, Amperometry	-0.128	$5.5\pm0.5\times10^{-11}$	*n.r.*	*n.r.*	[111]
		Cytochrome *c* (Cyt *c*)					
Cyt *c*/SnO_2 or Cyt *c*/TiO_2	Drop cast of cyt *c* at electrode surface.	Cyclic Voltammetry, Spetroelectrochemistry	0.050	*n.r.*	0.53±0.03	*n.r.*	[73]
Cyt *c*-4-Mercaptopyridine/AuE	Modification of electrode surface with 4-mercaptopyridine; Drop cast of cyt *c* at modified electrode surface.	Cyclic Voltammetry	-0.021	*n.r.*	*n.r.*	*n.r.*	[77]
Cyt *c*-MSA/AuE	Modification of electrode surface with mercaptosuccinic acid; Drop cast of cyt *c* at modified electrode surface	Cyclic Voltammetry, Amperometry	-0.088	*n.r.*	*n.r.*	*n.r.*	[79]

Table 2.1. Immobilization and detection techniques, as well as kinetic parameters ($E^{0'}$ – formal potential; τ^* –surface concentration of the electroactive species; k_s – electron transfer rate constant; K_m – Michaelis Menten constant) of heme proteins and porphyrins based third-generation biosensors for NO detection (continued).

Biosensor	Immobilization	Detection technique	E^* heme-protein or porphyrin (V vs. SCE)	τ^* (mol/cm^2)	k_s (s^{-1})	K_m ($\mu molL^{-1}$)	Ref.
Cyt *c*-DNA/GCE	Modification of electrode surface with DNA; Electrodeposition of cyt *c* at modified electrode surface.	Cyclic Voltammetry, Electrochemical Impedance Spectroscopy	0.089	2.46×10^{-8}	2.85±0.20	*n.r.*	[80]
Cyt *c*-PTTCA-Nafion®/Pt microelectrode	Eletropolymerization of PTTCA at electrode surface followed by EDC activation; Immersion in cyt *c* solution; Immersion in Nafion® solution.	Cyclic Voltammetry Chronoamperometry	0.244	2.51×10^{-10}	1.86	*n.r.*	[100]
Cyt *c*-SDS-PAM/GCE	Mixture of polyacrylamide and sodium dodecyl sulfate at electrode surface; Electrodeposition of cyt *c* at modified electrode surface.	Cyclic Voltammetry, Electrochemical Impedance Spectroscopy, Amperometry	0.068	$4.11\pm 0.02\times10^{-10}$	1.56	320	[76]
Cyt *c*- CC-PAN/GCE	Electropolymerization of poly(5-NH2-1-NAP) at electrode surface followed by immersion in an alcoholic solution of cyanuric chloride; Immersion in cyt *c* solution.	Cyclic Voltammetry	-0.226	*n.r.*	*n.r.*	*n.r.*	[102]
Cyt *c*-PIL-GR/PGE	Mixture of PIL and graphene at electrode surface; Immersion in cyt *c* solution.	Cyclic Voltammetry, Amperometry	-0.203	3.67×10^{-11}	2.93	25.6	[75]
		Peroxidase					
MP-CAS-SOD-MWCNTs-PTTCA-AuNPs/GCE	Mixture of gold nanoparticles, MWCNTs and PTTCA at electrode surface; Activation with EDC/NHS; Immersion on enzymatic solution.	Cyclic Voltammetry, Chronoamperometry	-0.300 (MP) -0.435 (CAS) -0.030 (SOD)	2.2×10^{-11} (MP)* 3.2×10^{-13} (CAS)* 2.3×10^{-12} (SOD)*	1.31 (MP) 1.27 (CAS) 0.48 (SOD)	*n.r.*	[99]

Table 2.1. Immobilization and detection techniques, as well as kinetic parameters ($E^{0'}$ – formal potential; τ^* –surface concentration of the electroactive species; k_s – electron transfer rate constant; K_m – Michaelis Menten constant) of heme proteins and porphyrins based third-generation biosensors for NO detection (continued).

Biosensor	Immobilization	Detection technique	$E^{0'}$ heme-protein or porphyrin (V vs. SCE)	τ^* (mol/cm^2)	k_s (s^{-1})	K_m ($\mu molL^{-1}$)	Ref.
		Porphyrin					
Hemin-MWCNTs-Chitosan/CFM	Electrodeposition of mixture of hemin, MWCNTs, chitosan and EDC/NHS.	Cyclic Voltammetry, Square Wave Voltammetry	-0.338	$1.7\pm0.9\times10^{-11}$	837±401	*n.r.*	[101]
Fe(4-TMPyP)-DNA-PADDA/PGE	Mixture of DNA and PADDA at electrode surface; Immersion in Fe(4-TMPyP) solution.	Cyclic Voltammetry Chronoamperometry	-0.130	*n.r.*	3.12	*n.r.*	[119, 120]
Metalloporphyrins (Mn and Co)-PP-$TBABF_4$/CFM	Electrodeposition of $TBABF_4$/metalloporphyrin solution.	Cyclic Voltammetry	-0.280	*n.r.*	*n.r.*	*n.r.*	[78]

n.r. – not reported.
* Obtained by quartz crystal microbalance analysis.

AuE, gold electrode; AuNPs, gold nanoparticles; AuPs, gold particles; CAS, catalase; CC, cyanuric chloride; CEC, cyanoethyl cellulose; CFM, carbon fiber microelectrode; CPB, cetylpyridinium bromide; CPE, carbon paste electrode; CS, chitosan; CTAB, cetyl trimethylammonium bromide; Cys, cysteamine; Cyt *c*, cytochrome *c*; DDAB, didodecyldimethylammonium bromide; DNA, deoxyribonucleic acid; DOAB, dimethyldioctadecyl ammonium bromide; EDC/NHS, 1-ethyl-3-(3-dimethylaminopropyl)carbodiimide/N-hydroxysuccinimide; Fe(4-TMPyP), Iron(III) meso-tetrakis(N-methylpyridinium-4-yl)porphyrin; GCE, glassy carbon electrode; GR, graphene; Hb, hemoglobin; Mb, myoglobin; MC, Methyl cellulose; MMT, montmorillonite; MP, microperoxidase; MSA, methanesulfonic acid; MWCNTs, multiwalled carbon nanotubes; NYPA, naphthalen-1-ylmethylphosphonic acid; PADDA, poly(acrylamide-*co*-diallyldimethylammonium chloride; PAM, polyacrylamide; PAN, polyacrylonitrile; PC, phosphatidylcholine; PEDGDE, poly(ethylene glycol diglycidylether); PEI, polyethyleneimine; PGE, pyrolitic graphite electrode; PIL, polymerized ionic liquid; Pluronic film, triblock copolymer poly(ethylene oxide)100-poly(propylene oxide)65-poly(ethylene oxide)100; PME, powder microelectrode; PNMP-*b*-PGMA, poly[N-(2-methacryloyloxyethyl) pyrrolidone]-block-poly[glycidyl methacrylate]; PP, protoporphyrin; PTFE, polytetrafluoroehtylene; PTTCA, poly-5,2':5",2"-terthiophene-3'- carboxylic acid; PVA, polyvinyl alcohol; SCE, saturated calomel electrode; SDS, sodium dodecyl sulfate; SOD, superoxide dismutase; $TBABF_4$, tetrabutylammonium tetrafluoroborate.

2.3.1. Hemoglobin

Hb is a hemic protein (containing four electroactive iron hemes – heme b groups) with a high molecular weight (64 500 g/mol) being a molecular vehicle of carbon dioxide and oxygen in red blood cells and also regulating the blood pH [105]. Hb is a molecule standard in bioelectrochemical studies due to its well-documented structure, known redox behavior in the vascular system of animals and because it is commercially available at moderated cost. Moreover, its heme *b* center catalyzes the NO reduction in biological systems. Therefore, there has been a huge interest to use Hb in NO biosensors development (around 59% of the total number of studies; table 2.1).

The working electrode material and the type of surface modification used in each biosensor contributed to changes in the Hb formal potential (Eº'- formal potential, attained as the midpoint of reduction and oxidation potentials). According to the table 2.1, a large Eº' window has been reported for modified GCE, ranging from -0.409 [88] and -0.190 [98] V *vs*. SCE. A pair of well-defined redox peaks at -0.384 V (anodic peak) and -0.434 V (cathodic peak), corresponding to the lowest reported Eº', were observed for a GCE modified by drop cast of a mixture of Hb with two polymers, the poly(o-nitro-benzyl-methacrylate-co-methyl-methacrylate-co-poly(ethylene-glycol)methacrylate) (PNMP) and the poly(glycidyl methacrylate) (PGMA) [88]. Based on the attained results, the direct electrochemistry of Hb when entrapped in the prepared polymeric matrix film was considered a quasi-reversible process with Hb exchanging electrons directly (electron transfer rate constant (k_s) = 1.03±0.05 s^{-1}) with the electrode. Authors concluded that the used of an amphiphilic linear block copolymer can form an ordered biomembrane-like film, which provided an environment similar to that of redox proteins in native systems [88]. A highly sensitive NO biosensor based on GCE modification with a Hb-chitosan (CS)-graphene (GR)-hexadecyltrimethylammonium bromide (CTAB) nanomatrix with the highest formal potential of -0.190 V vs. SCE was presented by Wen et al. [98]. CS, a natural biopolymer, showed good biocompatibility, nontoxicity, excellent film forming ability and high mechanical strength to immobilize proteins and also to act as dispersant for nanomaterials [98, 106]. The interesting inherent properties of the CTAB surfactant were used to obtain a good dispersion of GR without particles aggregation. The

composite film was deposited in a GCE and a combination of electrostatically and adsorptive interactions occurred, which improved the stability, selectivity and detectability making the developed approach suitable to use in amperometric devices. The reached very favorable electron transfer constant (k_s= 60.3 s^{-1}) was attributed to the fast electricity conduction and high effective surface area of GR offering electron-conducting tunnels that helped in electron transfer of the electroactive species [98]. In contrast to the considerable utilization of GCE, only one study reported the usage of Au electrodes due to their limited application for reduction processes detection [107]. Gu et al. [107] reported an Eº' of -0.051 V vs. SCE for an Au working electrode modified with gold particles (AuPs) and cysteamine (Cys) in a Hb-AuPs-Cys system. A pair of quasi-reversible redox peaks was also observed, with a significantly different cathodic (E_{pc}=-0.130 V vs. SCE) and anodic (E_{pa}=0.029 V vs. SCE) peak potentials due to the different transducer used, when compared with those reported for modified GCE [107]. In addition, for modified PGE, a similar Eº' range (-0.358 to -0.183 V vs. SCE) as the one indicated for modified GCE may be observed corroborating the analogous characteristics of these two types of electrodes. PME and CPE were used only in one study. Xu et al. [74] developed a novel biosensor based on Hb adsorbed on gold colloids modified carbon paste electrode (Hb/Au-CPE) with a Eº' of -0.224 V vs. SCE [74]. Guo et al. [86] reported -0.351 V vs. SCE for a modified PME (Hb/didodecyldimethylammonium bromide (DDAB)/PME i.e. a similar Eº' as some GCE and PGE based transducers [74, 82, 83, 89, 95, 96]. PME can be a promising electrode because it can contribute to decrease interferences from capacitive currents and uncompensated iR [108].

2.3.2. Myoglobin

Mb is a small water-soluble cytoplasmatic hemoprotein (consisting of a single polypeptide chain of 154 amino acids) with a similar structure of Hb, which has been also used in third-generation biosensors for NO analysis (table 2.1). Mb has an available sixth coordination position at the heme iron, which makes it attractive for the detection of small coordinating species such NO molecules [109]. However, its heme site is much more blocked when compared to other heme groups of other proteins, such as in cyt *c*, being the main disadvantage of this protein for electrochemical studies [110]. Thus, only three studies were found concerning the use of Mb for NO electroanalysis (table 2.1); comparison between Hb and Mb electrochemical behavior was made in two of the reported works [86, 96]. In the work

of [111], MWCNTs were used to enhance DET between Mb and the electrode conferring excellent electrical conductivity and chemical stability. The reported E°' was the highest, -0.128 V vs. SCE, while for the other reported transducers based on PGE [96] and PME [86], values ranged from -0.350 and -0.212 V vs. SCE, respectively. The formal potential and the structural conformation of Hb and Mb are similar and it was efficiently proved that both can be used for DET and for the design of NO biosensors.

2.3.3. Cytochrome *c*

Cyt *c* is a stable protein containing covalently bonded heme *c* groups with short-lived and transient response on a metal surface [80]. This protein plays an important role as electron transport in respiratory mitochondria chain, where cyt *c* reductase function as electron donos that delivers the electrons to cyt *c* oxidase – the electron acceptor. Cyt *c* shows peroxidase activity and can also catalyze several redox reactions such as hydroxylation and aromatic oxidation [112]. The E°' obtained in cyt *c*-based biosensors for NO detection were in the large range of -0.226 to 0.244 V vs. SCE. This huge window can be explained by microenvironment changes, namely due to the protein immobilization in different matrices and transducers. Cyt *c* works in several regions of the mitochondria and the cell, and changes in its environment may affect its redox characteristics. It is recognized that if a protein is not at the right potential in an electron transport chain, the consecutive steps may be disturbed affecting the whole process and promoting several reactions that could be undesirable [113]. Takahashi and de Torresi [102] reported the lowest value for the cyt *c* E°', -0.226 V vs. SCE, using GCE modified with poly(5-NH_2-1-NAP) (PAN) and cyt *c* covalently immobilized by cyanuric chloride (CC). The bridge component, CC, reacted with –OH groups of PAN and with the amino groups of the protein, attaching both by covalent bonds, revealing that the mechanism was not completely reversible and that the process at the surface electrode was not diffusional controlled, as expected for this type of immobilization system. The peak separation was larger than the value obtained from the theoretical electron transfer (Fe(III)/Fe(II) couple), probably because of the distance from heme of cyt *c* to the electrode surface [102]. On the other hand, a completely different E°' of 0.068 V vs. SCE was attained by Chen et al. [76] for the cyt *c* immobilized with polyacrylamide (PAM) and sodium dodecyl sulfate (SDS) forming a cyt *c*-SDS-PAM system used in the same working electrode (GCE). A quasi-reversible redox process was observed while no signals

were detected at the other electrodes without the immobilized protein. Also, the attained Nyquist plots and Randles circuit that fitted the impedance data showed that PAM, SDS and cyt *c* were efficiently deposited on the bare GCE surface forming different kinetic barriers (electron transfer resistance (Rct) of 240 Ω, 600 Ω and 1200 Ω for GCE, SDS/PAM/GCE and cyt *c*/SDS/PAM/GCE, respectively) [76]. So, the selected combination of polymer-surfactant, i.e. PAM-SDS, used as GCE surface modifiers allowed to form stable films with ordered multibilayer structure in aqueous solutions, indicating that DET between the cyt *c* heme protein and the SDS-PAM/GCE was improved [76]. The highest value of all previously reported E°', i.e. 0.244 V vs. SCE, was detected for Pt microelectrodes modified with two different polymers (poly(terthiophene-3-carboxylic acid) (PTTCA) and nafion®) [100]. The potential improvement was achieved by the use of microelectrodes due to the possibility to improve the signal-to-noise ratio and the ability to perform electrochemical measurements in highly resistive solutions. Less common working electrodes, namely AuE and SnO_2/TiO_2, were used to immobilized cyt *c* originating near zero E°' of -0.088 to -0.021 V [77, 79] and 0.050 V [73] vs. SCE, respectively.

2.3.4. Peroxidase

Peroxidase enzymes are redox glycoproteins presenting a Fe(III) protoporphyrin IX prosthetic group as the active site in enzyme catalyzed reactions [114]. Horseradish peroxidase (HRP) is the most studied of all peroxidase enzymes in amperometric biosensors using mostly mediators bound to the GCE surface to enhance the rate of electron transfer [106, 115]. Still, Abdelwahab et al. [99] tested another class of peroxidase enzymes, the microperoxidase (MP), in unmediated biosensors for NO detection and quantification. This simple and small enzyme was obtained by tryptic digestion of horse heart cyt *c* [99]. Abdelwahab et al. [99] tried to reduce the interferences of H_2O_2 and O_2^- during electroanalysis by co-immobilizing a multi-enzymes system with catalase (CAS) and superoxide dismutase (SOD), besides MP; -0.300 V vs. SCE was reported for E°' of MP. Authors used carbon nanomaterials (MWCNTs), gold nanoparticles (AuNPs) and poly-5,2':5'',2''-terthiophene-3'-carboxylic acid (PTTCA) forming a MWCNTs-PTTCA-AuNPs nanocomposite to modify the GCE surface to offer a huge surface area for immobilizing the selected enzymes (CAS, SOD and MP) through covalent bond formation [99].

2.3.5. Hemin and other porphyrins

Porphyrins are heterocyclic organic compounds that contain extensive π-system and form stable complexes with several metal ions [116]. Porphyrins can mimic the enzymatic or prosthetic centers and can also be used for NO detection and quantification. However, the electrocatalytic reduction of NO by adsorbed inorganic complexes such as porphyrins has been less considered than with heme proteins, but it is an interesting alternative approach considering the good affinity of NO to transition metals [117].

Hemin groups (a specific class of porphyrin) are known to adsorb rapidly on PGE surfaces forming an ordered structure. They are relatively inexpensive and have good stability in solution [118]. Other chemical groups, such as metalloporphyrins have been also tested in NO biosensors; formal potentials in the range of -0.338 [101] to -0.130 [119, 120] V vs. SCE have been reported. A cathodic and an anodic peak were attributed to the Fe(III)/Fe(II) couple of hemin at -0.370 ± 0.012 V and −0.305 ± 0.019 V vs. SCE, respectively, corresponding to the lowest E°' of −0.338 V vs. SCE at an hemin-MWCNTs-chitosan using carbon fiber microelectrodes (CFM) [101]. The iron(III) meso-tetrakis(N-methylpyridinium-4-yl)porphyrin (Fe(4-TMPyP) was used to prepare a novel Fe(4-TMPyP) (bio)sensor with Fe(4-TMPyP) co-immobilized with DNA and poly(acrylamide-co-diallyldimethylammonium chloride (PADDA), forming a DNA-bound-porphyrin complex more stable and biocompatible. The developed complex showed the highest transfer rate (k_s = 3.12 s^{-1}) and consequently the highest E°' of -0.130 V vs. SCE [119, 120]. The peak potentials of the Fe(III)/Fe(II) couple are in agreement with the other related studies (table 2.1) supporting the DET of porphyrins [78, 117].

2.4. Nitric oxide catalytic reduction on heme proteins and porphyrins based third-generation biosensors

The evaluation of the reported biosensors characteristics has been made using different electrochemical techniques. Cyclic voltammetry (CV), square wave voltammetry (SWV), differential pulse voltammetry (DPV), amperometry and electrochemical impedance spectroscopy (EIS) are the most usual methods for NO reduction studies (table 2.1).

2.4.1. Proposed mechanisms and catalytic potential of nitric oxide

The different catalytic potentials (E_{cat}) obtained for NO reduction are presented in table 2.2. A few works reported and discussed the possible mechanism of NO with heme-proteins, porphyrins and enzymes.

A NO E_{cat} between -0.880 V [97] and -0.580 V vs. SCE [85] was observed for Hb based-biosensors. Fan et al. [82] obtained a value of E_{cat} of -0.684 V vs. SCE for Hb-DNA/PGE and proposed as possible mechanism (Eq. (1) and (2)):

$$\text{Hb heme Fe(II)} + \text{NO} \rightarrow \text{Hb heme Fe (II)} - \text{NO} \qquad \text{Eq. (1)}$$

$$\text{Hb heme Fe(II)} - \text{NO} + \text{NO} + 2H^+ + 2e^- \rightarrow \text{Hb geme Fe (III)} + N_2O + H_2O \qquad \text{Eq. (2)}$$

Although He and Zhu [87] suggested the same mechanism, a different E_{cat} of -0.834 V vs. SCE was reported due to the different platform used for Hb immobilization (Hb-PAM-CPB/GCE). The use of water-absorbent polymers and surfactants such as PAM and cetylpyridinium bromide (CPB), respectively, could have contributed to the diminution of NO peak potential. It should be also mentioned that the lowest value of -0.880 V vs. SCE was also detected using a GCE modified with Hb entrapped in a cationic gemini surfactant film (Hb-C_{12}-C_3(OH)-C_{12}/GCE) [97]. The incorporation of MWCNTs in the immobilization strategy did not affect the NO mechanism but helped to increase the electron transfer rate and consequently the reported NO potential are more positive [91].

An analogous catalytic mechanism for NO reduction (Eq. (3) to Eq. (7)) was suggested for Mb entrapped in pluronic films [triblock copolymer poly(ethylene oxide)100-poly(propylene oxide)65-poly(ethylene oxide)100)] (E_{cat} of -0.800 V vs. SCE) [96]. Due to the interesting characteristics of pluronic films, such as the possibility to be used for controlled drug delivery, dispersion, and stabilization (among others), the selected polymers were used as a new type of materials that form films to immobilize successfully stabilize heme proteins at the PGE surface [96]. In the proposed mechanism, HNO_2 is firstly formed (Eq. (3)), being subsequently disproportionated to NO and NO_3^- (Eq. (4)). Then, the reaction showed in Eq. (5) was reported to occur at a formal potential of -0.350 V vs. SCE while -0.800 V vs. SCE was determined for the NO catalytic potential (Eq. (6)). In this reaction, $heme_{Fe(II)}$ from Mb is combined with NO, forming the ferrous nitrosyl intermediate complex of

$heme_{Fe(II)}$–NO. This complex is then reduced at the transducer surface (Eq. (7)) and releases $heme_{Fe(II)}$ again, forming a catalytic cycle. While the ultimate product of Eq. (7) is not yet clearly established, it is probably N_2O, as the literature suggested for other protein and enzymatic systems [96].

$$NO_2^- + H^+ \rightarrow HNO_2 \quad \text{Eq. (3)}$$

$$3HNO_2 \rightarrow 2NO + NO_3^- + H^+ + H_2O \quad \text{Eq. (4)}$$

$$heme_{Fe(III)} + H^+ + e^- \rightarrow heme_{Fe(II)} \quad \text{Eq. (5)}$$

$$heme_{Fe(II)} + NO \rightarrow heme_{Fe(II)} - NO \quad \text{Eq. (6)}$$

$$heme_{Fe(II)} - NO + H^+ + e^- \rightarrow heme_{Fe(II)} + product + H_2O \quad \text{Eq. (7)}$$

De Groot et al. [117] described a different mechanism for porphyrins, namely the hemin-NO reaction, which led to the formation of NH_2OH with an observed electrochemical followed by chemical reaction (EC) mechanism combined with proton transfer (Tafel slope of 62 mV/dec and pH dependence of -42 mV/pH). Some factors could have influenced these two different pathways including the mode of the electron transfer to the heme group, the residues surrounding the heme groups and the pH of the solution and more important the way in which a second NO bind to the active site [117]. In porphyrin based-biosensors, a E_{cat} from -0.776 to -0.566 V vs. SCE was reported for metalloporphyrins (Mn and Co)-PP-$TBABF_4$/CFM [78] and Fe(4-TMPyP)-DNA-PADDA/PGE [119, 120], respectively. Fe(4-TMPyP) influenced positively the electron transfer rate and the detected value was, in this way, more positive.

Cyt *c* based biosensors using modification with polymerized poly (1-vinyl-3-ethyl imidazolium)bromide (PIL)-GR, PTTCA-nafion®, DNA, SDS-PAM on PGE, Pt microelectrode or GCE showed similar E_{cat} values of -0.686, -0.656, -0.606, and -0.606 V vs. SCE for cyt *c*-PIL-GR/PGE [75], cyt *c*-PTTCA-nafion®/Pt microelectrode [100], cyt *c*-DNA/GCE [80] and cyt *c*-SDS-PAM/GCE [76], respectively, maybe due to the similar developed microenvironment. No NO potential was indicated for different working electrodes, such as AuE and SnO_2 or TiO_2 [73, 77, 79]. Still, a mechanism that consisted on NO binding on the ferrous derivative of Hb [Hb Fe(II) or deoxy Hb], forming a stable nitrosyl Hb species was proposed [73]. Deoxy Hb reacted with NO with a stoichiometry of one molecule of NO per heme (Hb Fe(II) + NO → Hb Fe(II) –

NO) as it was observed for Hb and Mb-based biosensors. The reaction requires anaerobic conditions because NO is quickly oxidized by O_2. Hb is normally in its oxidezed state (Hb Fe(III)), thus NO binding demands the previous reduction of Hb to Hb Fe(II) [73].

In biosensors constructed with microperoxidase (MP), a comparable NO reduction peak to those perceived using Hb, Mb, cyt *c* and porphyrin modified electrodes was observed at -0.706 V vs. SCE [99]. However, the mechanism of the reaction is not clear.

2.4.2. Kinetic parameters

Information on the kinetics of the reaction at the electrode surface is of great importance to understand the electron transfer processes and assess the success of protein or enzyme immobilization on the different surface electrodes. Therefore, the effect of scan rates on the redox peak currents has been examined in detail [73, 76, 93, 97, 121]; linear relationships have been reported suggesting that the involved reactions corresponded to surface-controlled processes.

Based on equation (8), it is possible to calculate the surface concentration of the electroactive species (***τ****) [60]:

$$Q=nFA\tau^* \qquad \text{Eq. (8)}$$

Where ***Q*** is the charge involved in the reaction; ***A*** is the geometric area of the working electrode; ***n*** is the number of the electron transferred; ***F*** is the Faraday constant. The majority of studies presented τ* of Hb, Mb, cyt *c*, peroxidase and porphyrins in the range of 10^{-10}-10^{-12} mol/cm^2 (table 2.1). However, there are some exceptions [80, 86]. The τ* values reported by Guo et al. [86] of 2.83×10^{-8} mol/cm^2 for Hb and 9.94×10^{-8} mol/cm^2 for Mb are much higher (100 – 10000) than those reached in the other studies possibly due to the large reported “real surface area/apparent electrode area” ratio of the DDAB–PME. Also, Liu et al. [80] reported the biggest value of surface concentration of 2.46×10^{-6} mol/cm^2 (10000 – 1000000 times higher when compared with most of the data; table 2.1) for cyt *c*-DNA/GCE biosensor that can possibly be explained by the formation of multilayers of cyt *c* together with DNA chain at the electrode surface. Despite these high results, the usual coverage of

electroactive species may still be considered low (10^{-10}-10^{-12} mol/cm^2), if very elevated sensitivity is desired, because all the active sites of the heme-proteins and porphyrins must be close to the electrode surface and with the proper orientation to promote an efficient electron transfer [122].

The $\mathbf{k_s}$, corresponding to the easiness that the electronic transfer occurs, was also reported for NO biosensors (table 2.1). This constant was estimated based on Laviron method according to the equation (9) if ΔE_p is greater than 200/n mV and equation (10) if the ΔE_p is lower than 200/n mV (where $\boldsymbol{\Delta E_p = E_{pa}-E_{pc}}$; $\boldsymbol{n}$ is the number of the electrons transferred; $\boldsymbol{\alpha}$ is the charge transfer coefficient; $\boldsymbol{R}$ is the ideal gas constant; $\boldsymbol{T}$ is temperature; $\boldsymbol{F}$ is Faraday constant; $\boldsymbol{v}$ is the scan rate and $\boldsymbol{m}$ is a parameter related to peak-to-peak separation) [123, 124].

$$\log k_s = \alpha\log(1-\alpha) + (1-\alpha)\log\alpha - \log(RT/nFv) - (1-\alpha)\alpha F\Delta E_p/(2.3RT) \quad \text{Eq. (9)}$$

$$k_s = mnFv/RT \quad \text{Eq. (10)}$$

The large k_s range for Hb protein was verified to be 0.10 [93] to 60.3 s^{-1} [98] (table 2.1). Wen at al. [98] obtained the highest value of the electron transfer rate of 60.3 s^{-1} in a Hb-CS-GR-CTAB/GCE biosensor. These authors described that the promotion of Hb electron transfer might be mainly due to the three-dimensional architecture of CTAB-GR film and the synergetic behavior of CS with GR. CS also helped to maintain the desirable conformation and activity of Hb preventing the protein leakage during the electrochemical assay [98].
The most common values reported for k_s for cyt *c* and MP are in the range of 0.530±0.03 [73] to 2.93 s^{-1} [75] and 1.31 s^{-1} [99], respectively (table 2.1), being overall in the same order of magnitude. The highest value of 837±40 s^{-1} was described for hemin-MWCNTs-CS-carbon fiber microelectrode corresponding to multilayers deposited at the microelectrode surface [101].

The Michaelis-Menten constant (K_m) is a measure of the affinity of the enzyme or protein for its substrate [125] and it can be determined by the Lineweaver–Burk equation (11) [123]:

$$1/I_{ss} = K_m/I_{max} \times 1/C + 1/I_{max} \quad \text{Eq. (11)}$$

Where $\boldsymbol{K_m}$ is the Michaelis-Menten constant; $\boldsymbol{I_{ss}}$ is the steady-state current after addition of the substrate; $\boldsymbol{C}$ is the concentration of the substrate; $\boldsymbol{I_{max}}$ is the maximum

current measured under saturated substrate conditions.

K_m was only reported for 25% of the studies (table 2.1). Gu et al. [107] obtained for Hb the highest K_m value of 190 $\mu molL^{-1}$ demonstrating that the system Hb-AuPs-Cys/AuE present the lowest affinity to NO substrate (table 2.1). On the other hand, the maximum affinity was assigned to Hb immobilized with gold nanoparticles (AuNPs), cellulose and poly(ethylene glycol diglycidylether) (PEDGE) forming the Hb-AuNPs-Cellulose-PEDGE/GCE biosensor (K_m of 0.0026 $\mu molL^{-1}$) [90], followed by Hb-CS-GR-CTAB/GCE (K_m of 0.315 $\mu molL^{-1}$) [98]. It is evident that the use of biopolymers, such as cellulose and chitosan, create adequate and compatible microenvironment benefiting the stabilization and the maintenance of the protein activity.

Greater K_m data were noted for cyt *c* based biosensors when compared to Hb but information needs to be analyzed with caution since only two studies proposed K_m values [75, 76]. The highest value of K_m of 320 $\mu molL^{-1}$ was achieved by a Cyt *c*-SDS-PAM/GCE biosensor [76], while Chen and Zhao [75] described a tenfold lower value of 25.6 $\mu molL^{-1}$ for Cyt *c*-PIL-GR/PGE, which can be explained by the use of a polymerized ionic liquid (PIL). PIL exhibit the properties of ionic liquids but also the merits of polymers contributing favorably for the immobilization of charged proteins. In addition, recent research studies with IL as alternative solvents for enzymatic catalysis exhibited higher enzymatic stability and activity, which make IL promising substitutes for organic solvents in biocatalysis at both laboratory and industrial scale [126]. No reported values of K_m were ascribed for Mb, enzymes and porphyrins used in NO third generation biosensors.

2.4.3. Electroanalytical performance

NO biosensing requires optimization of numerous parameters such as the linear range, limit of detection and quantification, sensitivity, selectivity, stability and response time (table 2.2). These analytical figures of merit are markedly influenced by the selected biorecognition element, the adopted immobilization strategy, and the applied detection technique. According to the real NO levels in biological systems, high accuracy and sensitivity coupled with low linear range and detection limit are desirable.

Sensitivity data were reported in most of the studies (table 2.2). The highest values were presented as being 6330, 1100 and 1068 $\mu A/mmolL^{-1}$ for Hb-PTFE [94], MP-

CAS-SOD-MWCNTs-PTTCA-AuNPs [99] and Mb-MWCNTs [111] modifications in GCE, respectively, while the lowest values were 0.031 and 1.7 ± 0.67 μA/mmolL^{-1} for Hb-C_{12}-C_3(OH)-C_{12}/GCE [97] and hemin-MWCNTs-CS/CFM [101], respectively. The utilization of nafion® and of some other polymers (PAM, PAN, PEDGDE, polyethyleneimine (PEI), among others) has shown to promote an increase in the biosensor resistance and consequently in sensitivity [91, 100], which can be counterbalanced by the use of highly conducting nanomaterials (AuNPs, MWCNTs and GR).

Table 2.2. Electroanalytical parameters of the reported NO biosensors (E_{cat} – catalytic potential).

Biosensor	Electrolyte	E_{cat} NO (V vs. SCE)	Sensitivity (μA/mmolL^{-1})	Linear range (μmolL^{-1})	Limit of detection (μmolL^{-1})	Cross-reactivity tests	Stability	Real Sample (μmolL^{-1})	Response time (sec.)	Ref.
Hemoglobin (Hb)										
Hb-DNA/PGE	0.1 molL^{-1} Na_2HPO_4-NaH_2PO_4 (pH=7) 0.1 molL^{-1} NaAc-HAc (pH=4)	-0.684	*n.r.*	*n.r.*	*n.r.*	Nitrite	*n.r.*	*n.r.*	*n.r.*	[82, 83]
Hb-PC/PGE	0.1 molL^{-1} citric acid (pH=2)	-0.580	*n.r.*	0.1-300	0.1	Nitrite, Ascorbate, Uric acid, Dopamine, Catechol, Cystine, Epinephrine	80% 2 months	*n.r.*	*n.r.*	[85]
Hb-AuPs-Cys/AuE	PBS (pH=7.2)	*n.r.*	610	0.012-5	4.0×10^{-3}	Arginine, Ascorbate, Nitrite, Uric acid, Cystine, Epinephrine	3 weeks	Raw blood (0.204±0.009)	3	[107]
Hb-PEI/PGE	0.1 molL^{-1} sodium acetate/acetic acid (pH=5.5)	-0.680	*n.r.*	0.1-8	40×10^{-3}	Ascorbate, Uric acid, Dopamine, Catechol, Cystine, Epinephrine	95% 1 month	*n.r.*	*n.r.*	[92]
Hb-MMT-PVA/PGE	Acetic buffer (pH=5.5)	-0.783	*n.r.*	1-250	0.5	Ascorbate, Uric acid, Dopamine, Catechol, Cystine, Epinephrine	90% 50 days	*n.r.*	*n.r.*	[95]
Hb-MMT/PGE	0.2 molL^{-1} NaAc-HAc (pH=5.5)	*n.r.*	*n.r.*	0.00004-5.0	20×10^{-6}	Dioxygen, Ascorbate, Dopamine, Uric acid, Nitrite, Epinephrine	80% 1 month	*n.r.*	*n.r.*	[84]

Table 2.2. Electroanalytical parameters of the reported NO biosensors (E_{cat} – catalytic potential) (continued).

Biosensor	Electrolyte	E_{cat} NO (V vs. SCE)	Sensitivity ($\mu A/mmolL^{-1}$)	Linear range ($\mu molL^{-1}$)	Limit of detection ($\mu molL^{-1}$)	Cross-reactivity tests	Stability	Real Sample ($\mu molL^{-1}$)	Response time (sec.)	Ref.
Hb-DOAB/PGE	0.1 $molL^{-1}$ HAc-NaAc (pH=5.0)	-0.850	*n.r.*	1-30	0.5	*n.r.*	*n.r.*	*n.r.*	*n.r.*	[93]
Hb-CPB-PAM/GCE	0.1 $molL^{-1}$ CH_3COOH–CH_3COONa (pH=4.22)	-0.834	*n.r.*	9.8-100	*n.r.*	*n.r.*	90% 7days	*n.r.*	*n.r.*	[87]
Hb-PTFE/GCE	0.1 $molL^{-1}$ PBS (pH=7.3)	-0.800	6330	1.8-14.4	*n.r.*	H_2O_2	*n.r.*	*n.r.*	*n.r.*	[94]
Hb-C_{12}-C_3(OH)-C_{12}/GCE	0.1 $molL^{-1}$ PBS (pH=7.4)	-0.880	49 0.031	0.225-18.0 18.0-164	2.0×10^{-4}	Dopamine, Ascorbic acid, Uric acid, Glucose, L-Arginine, Nitrite	92% 6 days	Rat liver (0.6 – 0.9)	*n.r.*	[97]
Hb-PNMP-b-PGMA/GCE	0.1 $molL^{-1}$ PBS (pH=7)	-0.760	323	0.45-10.0	0.32	*n.r.*	92% 10 days	*n.r.*	*n.r.*	[88]
Hb-CEC/GCE	0.1 $molL^{-1}$ PBS (pH=7)	-0.830	16/25	1.1-130	2.0×10^{-4}	Dopamine, Glucose, Nitrite, L-Arginine	88% 10 days	Rat liver (1.2 – 2.5)	<20	[89]
Hb-Au/CPE	0.1 $molL^{-1}$ PBS (pH=7)	-0.840	23/38	0.9-300	0.1	Uric acid, Glucose, Dopamine, Ascorbic acid, Nitrite, L-Arginine	94% 2 weeks	*n.r.*	*n.r.*	[74]
Hb-CS-GR-CTAB/GCE	0.1 $molL^{-1}$ PBS (pH=7)	-0.820	615	0.0225-2.64	6.75×10^{-3}	HPO_4^{2-}, K^+, NO_3^-, Ascorbic Acid, NO_2^-, H_2O_2	90% 4 weeks	Oilseed rape (*n.r.*)	5	[98]

Table 2.2. Electroanalytical parameters of the reported NO biosensors (E_{cat} – catalytic potential) (continued).

Biosensor	Electrolyte	E_{cat} NO (V vs. SCE)	Sensitivity ($\mu A/mmolL^{-1}$)	Linear range ($\mu molL^{-1}$)	Limit of detection ($\mu molL^{-1}$)	Cross-reactivity tests	Stability	Real Sample ($\mu molL^{-1}$)	Response time (sec.)	Ref.
Hb-AuNPs-GR-SDS/PGE	0.1 $molL^{-1}$ PBS (pH=7)	-0.776	*n.r.*	0.72-7.92	1.2×10^{-4}	*n.r.*	2 weeks	*n.r.*	<3	[81]
Hb-NYPA-MWCNTs-Nafion®/GCE	0.1 $molL^{-1}$ PBS (pH=7)	-0.780	*n.r.*	0.15-270	15×10^{-3}	H_2O_2	80% 1 month	*n.r.*	<3	[91]
Hb-AuNPs-Cellulose-PEGDGE/GCE	0.1 $molL^{-1}$ PBS 0.05 $molL^{-1}$ NaCl (pH=7)	-0.825	*n.r.*	0.9-160	12×10^{-3}	Ascorbic acid, Cysteine, L-Arginine, Nitrite, Dopamine, Glucose	93.3% 10 days	*n.r.*	*n.r.*	[90]
Hb-Pluronic film/PGE	0.05 $molL^{-1}$ citric acid, 0.05 $molL^{-1}$ potassium dihydrogen phosphates, or 0.05 $molL^{-1}$ boric acid.	-0.800	234 104	1-60	0.08	O_2, H_2O_2, Nitrite	1 month	*n.r.*	*n.r.*	[96]
Hb-DDAB/PME	0.1 $molL^{-1}$ PBS (pH=7)	-0.850	39.56 (cm^{-2})	1.90-28.08	<0.2	Ascorbic acid	1 month	*n.r.*	*n.r.*	[86]
Hb/SnO_2 or Hb/TiO_2	10 $mmolL^{-1}$ sodium phosphate (pH=7)	*n.r.*	*n.r.*	1-13	1	*n.r.*	2 weeks	*n.r.*	*n.r.*	[73]
Myoglobin (Mb)										
Mb-Pluronic film/PGE	0.05 $molL^{-1}$ citric acid, 0.05 $molL^{-1}$ potassium dihydrogen phosphates, or 0.05 $molL^{-1}$ boric acid.	-0.800	234 104	0.2-77	0.06	O_2, H_2O_2, Nitrite	1 month	*n.r.*	*n.r.*	[96]

Table 2.2. Electroanalytical parameters of the reported NO biosensors (E_{cat} – catalytic potential) (continued).

Biosensor	Electrolyte	E_{cat} NO (V vs. SCE)	Sensitivity ($\mu A/mmolL^{-1}$)	Linear range ($\mu molL^{-1}$)	Limit of detection ($\mu molL^{-1}$)	Cross-reactivity tests	Stability	Real Sample ($\mu molL^{-1}$)	Response time (sec.)	Ref.
Mb-DDAB/PME	0.1 $molL^{-1}$ PBS (pH=7)	-0.850	39.56 (cm^{-2})	1.90-28.08	<0.2	Ascorbic acid	1 month	*n.r.*	*n.r.*	[86]
Mb-MWCNTs/GCE	Phosphate buffer (pH=4.2)	-0.700	1068	0.2-40	8.0×10^{-4}	Nitrite, Ascorbate, L-cysteine, Oxygen, Dopamine	1 month	*n.r.*	*n.r.*	[111]
Cytochrome *c* (Cyt *c*)										
Cyt *c*/SnO_2 or Cyt *c*/TiO_2	10 $mmolL^{-1}$ sodium phosphate (pH=7)	*n.r.*	*n.r.*	1-13	1	*n.r.*	2 weeks	*n.r.*	*n.r.*	[73]
Cyt *c*-4-Mercaptopyridine/AuE	0.1 $molL^{-1}$ PBS (pH=7)	*n.r.*	*n.r.*	0.5-4.0	*n.r.*	*n.r.*	*n.r.*	*n.r.*	*n.r.*	[77]
Cyt *c*-MSA/AuE	5 $mmolL^{-1}$ Tris (pH=7.5)	*n.r.*	*n.r.*	100-600	*n.r.*	*n.r.*	*n.r.*	*n.r.*	*n.r.*	[79]
Cyt *c*-DNA/GCE	0.1 $molL^{-1}$ acetate buffer (pH=5)	-0.606	104	0.6-8	0.1	Ascorbic acid, Dopamine, K^+, Na^+, Ca^{2+}, Cu^{2+}, SO_4^{2-}, CO_3^{2-}, NO_3^{2-}, Cl^-	95% 1 week	*n.r.*	*n.r.*	[80]
Cyt *c*-PTTCA-Nafion®/Pt microelectrode	0.2 $molL^{-1}$ PBS (pH=7)	-0.656	117	2.4-55.0	13×10^{-3}	Superoxide, Oxygen, hydrogen peroxide	76% 2 months	Rat brain (1.13±0.03 and 2.13±0.05)**	<15	[100]
Cyt *c*-SDS-PAM/GCE	0.1 $molL^{-1}$ PBS (pH=7)	-0.606	140	0.8-95	0.1	Ascorbic Acid, Dopamine, K^+, Na^+, NH_4^+, Mg^{2+}, Al^{3+}, Ca^{2+}, Cu^{2+}, SO_4^{2-}, CO_3^{2-}, NO_3^{2-}, Cl^-	90% 2 weeks	*n.r.*	<2	[76]
Cyt *c*-CC-PAN/GCE	0.1 $molL^{-1}$ PBS (pH=7.4)	*n.r.*	*n.r.*	0-34	2.85	*n.r.*	*n.r.*	*n.r.*	*n.r.*	[102]

Table 2.2. Electroanalytical parameters of the reported NO biosensors (E_{cat} – catalytic potential) (continued).

Biosensor	Electrolyte	E_{cat} NO (V vs. SCE)	Sensitivity (μA/mmolL^{-1})	Linear range (μmolL^{-1})	Limit of detection (μmolL^{-1})	Cross-reactivity tests	Stability	Real Sample (μmolL^{-1})	Response time (sec.)	Ref.
Cyt c-PIL-GR/PGE	0.1 molL^{-1} PBS (pH=7)	-0.686	*n.r.*	1.05-13.7	0.7	Ascorbic acid, Uric acid, Dopamine, Catechol, Epinephrine	2 weeks	*n.r.*	*n.r.*	[75]
Peroxidase										
MP-CAS-SOD-MWCNTs-PTTCA-AuNPs/GCE	0.1 molL^{-1} PBS (pH=7)	-0.706	1100	1.0-40	4.3×10^{-3}	H_2O_2, $O_2^{\cdot-}$, Ascorbic acid, L-Arginine, Glucose	97% 1 month	Rat liver (3.82±0.83) AGS (3.91±0.27) HT-29cells (4.42±0.67)	*n.r.*	[99]
Porphyrin										
Hemin-MWCNTs-Chitosan/CFM	0.05 molL^{-1} PBS (pH=7.4)	-0.719	1.7±0.67	0.25-1.0	25×10^{-3}	Ascorbate, Dopamine, DOPAC, Nitrite, H_2O_2	*n.r.*	Rat brain (1)	10	[101]
Fe(4-TMPyP)-DNA-PADDA/PGE	0.05 molL^{-1} PBS (pH=7.4)	-0.566	49	0.1-90	30×10^{-3}	Nitrite, Ascorbate, Dopamine, Uric acid, Cysteine, Glucose	2 weeks	*n.r.*	1.5	[119, 120]
Metallo-porphyrins (Mn and Co)-PP-TBABF$_4$/CFM	0.1 molL^{-1} PBS (pH=7.4)	-0.776	*n.r.*	0.5-50	*n.r.*	*n.r.*	*n.r.*	*n.r.*	*n.r.*	[78]

n.r. – not reported

** Acute and repeated cocaine injections

AGS, gastric adenocarcinoma cells; AuE, gold electrode; AuNPs, gold nanoparticles; AuPs, gold particles; C_{12}-C_3(OH)-C12, cationic gemini surfactant film; CAS, catalase; CC, cyanuric chloride; CEC, cyanoethyl cellulose; CFM, carbon fiber microelectrode; CPB, cetylpyridinium bromide; CPE, carbon paste electrode; CS, chitosan; CTAB, cetyl trimethylammonium bromide; Cys, cysteamine; Cyt *c*, cytochrome *c*; DDAB, didodecyldimethylammonium bromide; DNA, deoxyribonucleic acid; DOAB, dimethyldioctadecyl ammonium bromide; DOPAC, 3,4–dihidroxifenilacético; Fe(4-TMPyP), Iron(III) meso-tetrakis(N-methylpyridinium-4-yl)porphyrin; GCE, glassy carbon electrode; GR, graphene; Hb, hemoglobin; HT-29, colon adenocarcinoma cells; Mb, myoglobin; MC, Methyl cellulose; MMT, montmorillonite; MP, microperoxidase; MSA, methanesulfonic acid; MWCNTs, multiwalled carbon nanotubes; NYPA, naphthalen-1-ylmethylphosphonic acid; PADDA, poly(acrylamide-*co*-diallyldimethylammonium chloride; PAM, polyacrylamide; PAN, polyacrylonitrile; PBS, phosphate buffer saline; PC, phosphatidylcholine; PEDGDE, poly(ethylene glycol diglycidylether); PEI, polyethyleneimine; PGE, pyrolitic graphite electrode; PIL, poliionic Liquid; Pluronic film, triblock copolymer poly(ethylene oxide)100-poly(propylene oxide)65-poly(ethylene oxide)100; PME, powder microelectrode; PNMP-*b*-PGMA, poly[N-(2-methacryloyloxyethyl) pyrrolidone]-block-poly[glycidyl methacrylate]; PP, protoporphyrin; PTFE, polytetrafluoroehtylene; PTTCA, poly-5,2':5",2"-terthiophene-3'- carboxylic acid; PVA, polyvinyl alcohol; SCE, saturated calomel electrode; SDS, sodium dodecyl sulfate; SOD, superoxide dismutase; TBABF$_4$, tetrabutylammonium tetrafluoroborate.

Linear ranges varying from 0.00004 – 5.0 $\mu molL^{-1}$ [84] to 0.1 – 300 $\mu molL^{-1}$ [85] were reported for Hb based-biosensors (table 2.2). The highest linear range [85] was obtained with Hb entrapped in a biological membrane component, phosphatidylcholine (PC), forming a Hb-PC/PGE biosensor. On the other hand, the use of montmorillonite (MMT) showed to help decreasing the NO linear range (0.00004 – 5.0 $\mu molL^{-1}$) and consequently its limit of detection (20×10^{-6} $\mu molL^{-1}$ for Hb-MMT/PGE) [84]. Moreover, other authors also described low linear ranges for Hb-based biosensors, namely 0.012 – 5 $\mu molL^{-1}$ for Hb-AuPs-Cys/AuE [107] and 0.0225 – 2.64 $\mu molL^{-1}$ for Hb-CS-GR-CTAB/GCE [98]. For a different protein, i.e. cyt *c*, the linear ranges varied from 0.5–4.0 $\mu molL^{-1}$ for cyt-*c*-4-mercaptopyridine/AuE [77] to 100 – 600 $\mu molL^{-1}$ for cyt *c*-MSA/AuE [79]. It is interesting to see that these two different linear ranges were obtained using different modification of the same bare electrode (AuE) indicating that the material of the bare electrode may not be the main influencing factor concerning NO catalysis. A similar linear range was presented for MP (with values of 1.0–40 $\mu molL^{-1}$ for MP-CAS-SOD-MWCNTs-PTTCA-AuNPs/GCE) [99]. For hemin biosensors, large linear ranges (0.1–90 $\mu molL^{-1}$ [119, 120]; 0.5–50 $\mu molL^{-1}$ [78]) were described with the exception for the hemin-MWCNTs-Chitosan/CFM biosensor (0.25–1.0 $\mu molL^{-1}$) [101] showing the advantages of the utilization of microelectrodes (in this case carbon fiber microelectrode) to reach low NO determination levels.

In terms of limits of detection (LOD), the achieved values were quite different ranging from 20×10^{-6} $\mu molL^{-1}$ to 2.85 $\mu molL^{-1}$ mainly due to the dissimilar reached sensitivity (table 2.2). Fan et al. [84] reached the lowest LOD (at the picomolar level) with a specific modification of Hb-MMT onto a PGE. It was demonstrated that this type of matrix provided an appropriate immobilization microenvironment, which significantly facilitated the electron communication between Hb and the PGE [84]. This biosensor exhibited also an acceptable stability retaining 80% of its initial response during one month. On the contrary, the largest LODs (1-2.85 $\mu molL^{-1}$) with no indication of the biosensor stability time [102] or only 2 weeks [73] were achieved with the cyt *c*-PAN-CC/GCE and cyt *c* or Hb/SnO_2 or cyt *c* or Hb/TiO_2 electrodes, but overall, the assessed LODs are in the order of 1×10^{-3} $\mu molL^{-1}$.

The biosensors cross-reactivity needs also to be carefully assessed. The most common tested compounds were nitrite, ascorbate, uric acid, cysteine, epinephrine, dopamine, ascorbic acid and glucose; overall they did not significantly interfere with NO detection. Furthermore, H_2O_2 and O_2 are two interfering species that can react with NO and form other electroactive species, therefore they were also tested in

about 27% of the studies. Gu et al. [107] suggested that H_2O_2 and O_2 interferences can be reduced by covering a nafion® film onto the modified electrode surface.

A few studies are described in the literature concerning the application of the previously referred biosensors to NO quantification in real samples, namely in oilseed rape (but no value of concentration was presented; [98]), raw blood [107], rat liver [89, 97, 99] and rat brain [100, 101]. According to the literature [89, 97], the NO levels in rat liver are in the range of 0.6–2.5 $\mu molL^{-1}$; still an higher concentration of 3.82 ± 0.83 $\mu molL^{-1}$ using microperoxidase as biological recognition element was reported by Abdelwahab et al. [99]. These last authors also analyzed the NO concentration in gastric adenocarcinoma (AGS) and colon adenocarcinoma (HT- 29) cells with high NO values of 3.91 ± 0.27 and 4.42 ± 0.67 $\mu molL^{-1}$, respectively [99]. Other successful applications were carried out at NO levels of 0.204±0.009 $\mu molL^{-1}$ in raw blood using the Hb-AuPs-Cys/AuE biosensor [107]. In rat brain, NO was also detected at levels varying from 1 $\mu molL^{-1}$ for hemin-MWCNTs-CS/CFM biosensor [101] to 1.13±0.03 $\mu molL^{-1}$ for cyt-*c*-PTTCA-nafion®/Pt microelectrode [100]. This last NO modified microelectrode, with cyt *c* immobilized onto a functionalized-conducting polymer (PTTCA) layer, was used, not only for acute, but also for repeated injections of abuse drug cocaine originating 2.13±0.05 $\mu molL^{-1}$ of NO concentration [100]. In all reported studies, the response time of NO biosensors was quite fast with a maximum reported of <20 seconds [89].

2.6. Final remarks and future perspectives

Third-generation biosensors show great potential for detection and quantification of NO in complex biological milieu, which is extremely important considering its key role in several physiological processes. They exhibit a plethora of advantages being the main ones, the simplicity (no redox mediator is used), sensitivity and selectivity (direct interaction between the redox protein or enzyme with its substrate), easy miniaturization and possibility of *in loco* measurements. Literature analysis revealed that hemoglobin is the most studied protein for NO detection and glassy carbon and pyrolytic graphite electrodes the most interesting working electrodes to perform biorecognition element immobilization. The use of carbon nanomaterials (carbon nanotubes and graphene) and gold nanoparticles promoted usually an increase in the effective surface area offering electron-conducting tunnels that enhanced the electron transfer rate of the redox protein and porphyrin with the electrode surface

and also yielding lower K_m values. The employment of polymers, in many reported works, provided a milieu similar to that of redox proteins and enzymes in native systems. Additionally, the combination of polymer-surfactant allowed forming stable films with ordered multibilayer structure increasing the direct electron transfer and stabilization of these biomolecules. Regardless of these great achievements, there are some limitations to solve. More fundamental research is clearly needed for full understanding the NO catalysis' mechanisms. Long-term stability, particularly in complex matrices and harsh conditions, and the need for lower detection limits are still major problems. Further advances in nanomaterials and proteins' immobilization strategies will allow to overcome these issues and to extend the *in vivo* applicability of these biosensors. In addition, special addition should be given to try to enlarge the scope of this type of biosensors. Only a limited number of biomolecules have been test to electrocatalyse NO via DET in biosensors. Nitric oxide reductase (NOR) enzyme, that can be isolated from different denitrifying organisms (*Pseudomonas aeruginosa, Marinobacter hydrocarbonoclasticus, Pseudonomas stutzeri* or *Paraccocus denitrificans*) and catalyzes the NO reduction to N_2O in a two electron/proton reaction [127] was not yet explored in the design of third-generation biosensors; it is a membrane enzyme with high potential for *in vivo* applications. Also, biotechnology, genetic and protein engineering may contribute with the development of new NO bioelectrocatalysts. Additionally, different biomolecules with DET capacity may be combined in order to obtain synergies and design novel biosensing platforms with enhanced kinetics and electroanalytical characteristics. It is predicted that third-generation biosensors for NO detection will have an increasingly important role in diagnostics of pathologic situations such as cancer, neurodegenerative diseases, amyotrophic lateral sclerosis, diabetes, among others.

2.7. References

[1] L.B. Maia, J.J.G. Moura, How biology handles nitrite, Chem Rev, 114 (2014) 5273-5357.

[2] B. Kartal, W.J. Maalcke, N.M. de Almeida, I. Cirpus, J. Gloerich, W. Geerts, et al.,Molecular mechanism of anaerobic ammonium oxidation, Nature, 479 (2011) 127-130.

[3] A.L. Ducluzeau, R. van Lis, S. Duval, B. Schoepp-Cothenet, M.J. Russell, W. Nitschke, Was nitric oxide the first deep electron sink?, Trends Biochem Sci, 34 (2009) 9-15.

[4] I. Moura, J.J. Moura, S.R. Pauleta, L.B. Maia, Metalloenzymes in denitrification: Applications and environmental impacts, Royal Society of Chemistry, 2016.

[5] M.S. Jetten, M. Strous, K.T. van de Pas-Schoonen, J. Schalk, U.G. van Dongen, A.A. van de Graaf, et al., The anaerobic oxidation of ammonium, FEMS Microbiol Rev., 22 (1998) 421-437.

[6] K.F. Ettwig, M.K. Butler, D. Le Paslier, E. Pelletier, S. Mangenot, M.M.M. Kuypers, et al., Nitrite-driven anaerobic methane oxidation by oxygenic bacteria, Nature, 464 (2010) 543-548.

[7] R.F. Furchgott, M.H. Carvalho, M.T. Khan, K. Matsunaga, Evidence for endothelium-dependent vasodilation of resistance vessels by acetylcholine, Blood vessels, 24 (1987) 145-149.

[8] L.J. Ignarro, G.M. Buga, K.S. Wood, R.E. Byrns, G. Chaudhuri, Endothelium-derived relaxing factor produced and released from artery and vein is nitric oxide, Proc Natl Acad Sci U S A, 84 (1987) 9265-9269.

[9] R.M. Palmer, A.G. Ferrige, S. Moncada, Nitric oxide release accounts for the biological activity of endothelium-derived relaxing factor, Nature, 327 (1987) 524-526.

[10] R.M. Rapoport, F. Murad, Agonist-induced endothelium-dependent relaxation in rat thoracic aorta may be mediated through cGMP, Circ Res, 52 (1983) 352-357.

[11] S. Moncada, R.M. Palmer, E.A. Higgs, Nitric oxide: physiology, pathophysiology, and pharmacology, Pharmacol. Rev, 43 (1991) 109-142.

[12] R.A. Johnson, R.H. Freeman, Sustained hypertension in the rat induced by chronic blockade of nitric oxide production, Am J Hypertens., 5 (1992) 919-922.

[13] V. Lahera, J. Salazar, M.G. Salom, J.C. Romero, Deficient production of nitric oxide induces volume-dependent hypertension, J Hypertens., 10 (1992) S179.

[14] G. Brock, L. Nunes, H. Padma-Nathan, S. Boyd, T.F. Lue, Nitric oxide synthase: a new diagnostic tool for neurogenic impotence, Urology, 42 (1993) 412-417.

[15] E. McGuffey, Can nitric oxide be used to treat impotence?, Am Pharm, (1993) 20.

[16] J. Koglin, T. Glysing-Jensen, J.S. Mudgett, M.E. Russell, Exacerbated transplant arteriosclerosis in inducible nitric oxide-deficient mice, Circulation, 97 (1998) 2059-2065.

[17] M. Weis, T.N. Kledal, K.Y. Lin, S.N. Panchal, S.Z. Gao, H.A. Valantine, et al., Cytomegalovirus infection impairs the nitric oxide synthase pathway: role of asymmetric dimethylarginine in transplant arteriosclerosis, Circulation, 109 (2004) 500-505.

[18] L. Fang, B.J. Nowicki, Y.L. Dong, C. Yallampalli, Localized increase in nitric oxide production and the expression of nitric oxide synthase isoforms in rat uterus with experimental intrauterine infection, Am J Obstet Gynecol, 181(1999) 601-609.

[19] N. Hopkins, Y. Gunning, D.F. O'Croinin, J.G. Laffey, P. McLoughlin, Anti-inflammatory effect of augmented nitric oxide production in chronic lung infection, J. Pathol, 209 (2006) 198-205.

[20] J.W. Choi, Nitric oxide production is increased in patients with rheumatoid arthritis but does not correlate with laboratory parameters of disease activity, Clin Chim Acta, 336 (2003) 83-87.

[21] J.J. Levine, M.J. Pettei, E. Valderrama, D.M. Gold, B.H. Kessler, H. Trachtman, Nitric oxide and inflammatory bowel disease: evidence for local intestinal production in children with active colonic disease, J Pediatr Gastroenterol Nutr, 26 (1998) 34-38.

[22] C. Martinez, Y. Juarranz, C. Abad, A. Arranz, B.G. Miguel, F. Rosignoli, et al., Analysis of the role of the PAC1 receptor in neutrophil recruitment, acute-phase response, and nitric oxide production in septic shock, J Leukoc Biol, 77 (2005) 729-738.

[23] G.M. Pieper, Review of alterations in endothelial nitric oxide production in diabetes: protective role of arginine on endothelial dysfunction, Hypertens., 31 (1998) 1047-1060.

[24] G.N. Andersen, K. Caidahl, E. Kazzam, A.S. Petersson, A. Waldenstrom, L. Mincheva-Nilsson, et al., Correlation between increased nitric oxide production and markers of endothelial activation in systemic sclerosis: findings with the soluble adhesion molecules E-selectin, intercellular adhesion molecule 1, and vascular cell adhesion molecule 1, Arthritis Rheum, 43 (2000) 1085-1093.

[25] E. Fabrega, F. Casafont, J. De La Pena, J. Berrazueta, G. De Las Heras, J. Amado, et al., Nitric oxide production in hepatic cell rejection of liver transplant patients, Transplantation proceedings, Elsevier, 1997, pp. 505-516.

[26] W.K. Alderton, C.E. Cooper, R.G. Knowles, Nitric oxide synthases: structure, function and inhibition, Biochem J, 357 (2001) 593-615.

[27] S. Pfeiffer, B. Mayer, B. Hemmens, Nitric oxide: Chemical puzzles posed by a biological messenger, Angew. Chem. Int. Ed., 38 (1999) 1714-1731.

[28] D.J. Stuehr, Mammalian nitric oxide synthases, Biochim. Biophys. Acta, 1411 (1999) 217-230.

[29] J.O. Lundberg, M.T. Gladwin, A. Ahluwalia, N. Benjamin, N.S. Bryan, A. Butler, et al., Nitrate and nitrite in biology, nutrition and therapeutics, Nat Chem Biol., 5 (2009) 865-869.

[30] J.O. Lundberg, E. Weitzberg, M.T. Gladwin, The nitrate-nitrite-nitric oxide pathway in physiology and therapeutics, Nat. Rev. Drug Discov, 7 (2008) 156-167.

[31] L.B. Maia, J.J. Moura, Nitrite reduction by xanthine oxidase family enzymes: a new class of nitrite reductases, J Biol Inorg Chem, 16 (2011) 443-460.

[32] L.B. Maia, J.J. Moura, Nitrite reduction by molybdoenzymes: a new class of nitric oxide-forming nitrite reductases, J Biol Inorg Chem, 20 (2015) 403-433.

[33] L.B. Maia, V. Pereira, L. Mira, J.J. Moura, Nitrite reductase activity of rat and human xanthine oxidase, xanthine dehydrogenase, and aldehyde oxidase: evaluation of their contribution to NO formation in vivo, Biochemistry, 54 (2015) 685-710.

[34] J.R. Lancaster, Jr., A tutorial on the diffusibility and reactivity of free nitric oxide, Nitric Oxide, 1 (1997) 18-30.

[35] M. Sato, N. Hida, Y. Umezawa, Imaging the nanomolar range of nitric oxide with an amplifier-coupled fluorescent indicator in living cells, Proc Natl Acad Sci USA, 102 (2005) 14515-14520.

[36] J.L. Wallace, R.C. Woodman, Detection of nitric oxide by bioassay, Methods, 7 (1995) 55-58.

[37] S. Hilderbrand, M. Lim, S. Lippard, In topics in fluorescence spectroscopy, Geddes, CD, Lakowicz, JR, Eds, Springer, 2005.

[38] H. Kojima, M. Hirotani, Y. Urano, K. Kikuchi, T. Higuchi, T. Nagano, Fluorescent indicators for nitric oxide based on rhodamine chromophore, Tetrahedron Lett., 41 (2000) 69-72.

[39] H. Kojima, N. Nakatsubo, K. Kikuchi, S. Kawahara, Y. Kirino, H. Nagoshi, et al., Detection and imaging of nitric oxide with novel fluorescent indicators: Diaminofluoresceins, Anal Chem, 70 (1998) 2446-2453.

[40] A.M. Miles, Y. Chen, M.W. Owens, M.B. Grisham, Fluorometric determination of nitric oxide, Methods, 7 (1995) 40-47.

[41] T. Nagano, T. Yoshimura, Bioimaging of nitric oxide, Chem Rev, 102 (2002) 1235-1270.

[42] E. Sasaki, H. Kojima, H. Nishimatsu, Y. Urano, K. Kikuchi, Y. Hirata, et al., Highly sensitive near-infrared fluorescent probes for nitric oxide and their application to isolated organs, J. Am. Chem. Soc., 127 (2005) 3684-3695.

[43] L.C. Green, D.A. Wagner, J. Glogowski, P.L. Skipper, J.S. Wishnok, S.R. Tannenbaum, Analysis of nitrate, nitrite, and [15N]nitrate in biological fluids, Anal Biochem., 126 (1982) 131-138.

[44] W.L. Daniel, M.S. Han, J.-S. Lee, C.A. Mirkin, Colorimetric nitrite and nitrate detection with gold nanoparticle probes and kinetic end points, J. Am. Chem. Soc., 131(2009) 6362-6363.

[45] D. Li, Y. Ma, H. Duan, W. Deng, D. Li, Griess reaction-based paper strip for colorimetric/fluorescent/SERS triple sensing of nitrite, Biosens Bioelectron, 99 (2018) 389-398.

[46] B.M. Jayawardane, S. Wei, I.D. McKelvie, S.D. Kolev, Microfluidic paper-based analytical device for the determination of nitrite and nitrate, Anal Chem, 86 (2014) 7274-7279.

[47] D.M. Zurcher, Y.J. Adhia, J.D. Romero, A.J. McNeil, Modifying a known gelator scaffold for nitrite detection, Chem Commun, 50 (2014) 7813-7816.

[48] N. Lopez-Ruiz, V.F. Curto, M.M. Erenas, F. Benito-Lopez, D. Diamond, A.J. Palma, et al., Smartphone-based simultaneous pH and nitrite colorimetric determination for paper microfluidic devices, Anal Chem, 86 (2014) 9554-9562.

[49] L.B. Maia, J.J. Moura, Detection of nitric oxide by electron paramagnetic resonance spectroscopy: Spin-trapping with iron-dithiocarbamates, Methods Mol Biol, 1424 (2016) 81-102.

[50] J. Vasquez-Vivar, P. Martasek, N. Hogg, H. Karoui, B.S. Masters, K.A. Pritchard, Jr., et al., Electron spin resonance spin-trapping detection of superoxide generated by neuronal nitric oxide synthase, Methods Enzymol., 301 (1999) 169-177.

[51] T. Yoshimura, H. Yokoyama, S. Fujii, F. Takayama, K. Oikawa, H. Kamada, In vivo EPR detection and imaging of endogenous nitric oxide in lipopolysaccharide-treated mice, Nat. Biotechnol., 14 (1996) 992-994.

[52] E.M. Hetrick, M.H. Schoenfisch, Analytical chemistry of nitric oxide, Annu Rev Anal Chem, 2 (2009) 409-433.

[53] J.L. Howland, Methods in nitric oxide research: Edited by M Feelisch and J S Stamler. pp 712. John Wiley and Sons, New York, 1996, ISBN 0-471-95524-8, Biochem Educ., 25 (1997) 184-195.

[54] A.M. Leone, V.W. Furst, N.A. Foxwell, S. Cellek, S. Moncada, Visualisation of nitric oxide generated by activated murine macrophages, Biochem. Biophys. Res. Commun, 221 (1996) 37-41.

[55] B.W. Allen, J. Liu, C.A. Piantadosi, Electrochemical detection of nitric oxide in biological fluids, Methods in enzymology, Academic Press, 2005, pp. 68-77.

[56] A. Hulanicki, S. Glab, F. Ingman, Chemical sensors: definitions and classification, Pure and Applied Chemistry, 1991, p. 1247.

[57] D.R. Thévenot, K. Toth, R.A. Durst, G.S. Wilson, Electrochemical biosensors:

recommended definitions and classification, International Union of Pure and Applied Chemistry: Physical Chemistry Division, Commission I.7 (Biophysical Chemistry); Analytical Chemistry Division, Commission V.5 (Electroanalytical Chemistry).1, Biosens Bioelectron, 16 (2001) 121-131.

[58] J. Castillo, S. Gáspár, S. Leth, M. Niculescu, A. Mortari, I. Bontidean, et al., Biosensors for life quality: Design, development and applications, Sens Actuators B Chem, 102(2004) 179-194.

[59] A. Koyun, E. Ahlatcioglu Özerol, Y. İpek, Biosensors and Their Principles, 2012.

[60] D. Grieshaber, R. MacKenzie, J. Vörös, E. Reimhult, Electrochemical biosensors - Sensor principles and architectures, Sensors, 8 (2008) 1400-1458.

[61] Jules L. Hammond, N. Formisano, P. Estrela, S. Carrara, J. Tkac, Electrochemical biosensors and nanobiosensors, Essays Biochem, 60 (2016) 69-80.

[62] D.W. Kimmel, G. LeBlanc, M.E. Meschievitz, D.E. Cliffel, Electrochemical sensors and biosensors, Anal Chem, 84 (2012) 685-707.

[63] B. Kowalewska, K. Jakubow, The impact of immobilization process on the electrochemical performance, bioactivity and conformation of glucose oxidase enzyme, Sens Actuators B Chem, 238 (2017) 852-861.

[64] N.J. Ronkainen, H.B. Halsall, W.R. Heineman, Electrochemical biosensors, Chem Soc Rev, 39 (2010) 1747-1763.

[65] W. Putzbach, N.J. Ronkainen, Immobilization techniques in the fabrication of nanomaterial-based electrochemical biosensors: A review, Sensors, 13 (2013) 4811-4840.

[66] P. Rafighi, M. Tavahodi, B. Haghighi, Fabrication of a third-generation glucose biosensor using graphene-polyethyleneimine-gold nanoparticles hybrid, Sens Actuators B Chem, 232 (2016) 454-461.

[67] C. Li, B. Guo, X.M. Guo, F. Wang, The electrochemical sensor based on electrochemical oxidation of nitrite on metalloporphyrin-graphene modified glassy carbon electrode, RSC Adv, 6 (2016) 90480-90488.

[68] Y.M. Liu, C. Punckt, M.A. Pope, A. Gelperin, I.A. Aksay, Electrochemical sensing of nitric oxide with functionalized graphene electrodes, ACS Appl Mater Interfaces., 5 (2013) 12624-12630.

[69] B.J. Privett, J.H. Shin, M.H. Schoenfisch, Tutorial review: Electrochemical nitric oxide sensors for physiological measurements, Chem Soc Rev, 39 (2010) 1925-1935.

[70] R.S. Freire, C.A. Pessoa, L.D. Mello, L.T. Kubota, Direct electron transfer: an approach for electrochemical biosensors with higher selectivity and sensitivity, J Braz Chem Soc, 14 (2003) 230-243.

[71] S.R. Chinnadayyala, A. Kakoti, M. Santhosh, P. Goswami, A novel amperometric alcohol biosensor developed in a 3rd generation bioelectrode platform using peroxidase coupled ferrocene activated alcohol oxidase as biorecognition system, Biosens Bioelectron, 55 (2014) 120-126.

[72] A. Sassolas, L.J. Blum, B.D. Leca-Bouvier, Immobilization strategies to develop enzymatic biosensors, Biotechnol Adv, 30 (2012) 489-511.

[73] E. Topoglidis, Y. Astuti, F. Duriaux, M. Grätzel, J.R. Durrant, Direct electrochemistry and nitric oxide interaction of heme proteins adsorbed on nanocrystalline tin oxide electrodes, Langmuir, 19 (2003) 6894-6900.

[74] Y. Xu, C. Hu, S. Hu, A reagentless nitric oxide biosensor based on the direct electrochemistry of hemoglobin adsorbed on the gold colloids modified carbon paste electrode, Sens Actuators B Chem, 148 (2010) 253-258.

[75] H. Chen, G. Zhao, Nanocomposite of polymerized ionic liquid and graphene used as modifier for direct electrochemistry of cytochrome *c* and nitric oxide biosensing, J Solid State Electrochem, 16 (2012) 3289-3297.

[76] X. Chen, H.-Y. Long, W.-L. Wu, Z.-S. Yang, Direct electrochemical behavior of cytochrome *c* on sodium dodecyl sulfate modified electrode and its application to nitric oxide biosensor, Thin Solid Films, 517 (2009) 2787-2791.

[77] T. Haruyama, S. Shiino, Y. Yanagida, E. Kobatake, M. Aizawa, Two types of electrochemical nitric oxide (NO) sensing systems with heat-denatured cyt *c* and radical scavenger PTIO, Biosens Bioelectron, 13 (1998) 763-769.

[78] C.Z. Li, S. Alwarappan, W. Zhang, N. Scafa, X. Zhang, Metallo protoporphyrin functionalized microelectrodes for electrocatalytic sensing of nitric oxide, Am J Med Sci, 1 (2009) 274-282.

[79] F. Lisdat, B. Ge, W. Stöcklein, F.W. Scheller, T. Meyer, Electrochemical behavior and nitric oxide interaction of immobilized cytochrome *c′* from *Rhodocyclus gelatinosus*, Electroanalysis, 12 (2000) 946-951.

[80] Y.-C. Liu, J. Zhao, W.-L. Wu, Z.-S. Yang, Direct electrochemical behavior of cytochrome *c* on DNA modified glassy carbon electrode and its application to nitric oxide biosensor, Electrochim Acta, 52 (2007) 4848-4852.

[81] M.Q. Xu, J.F. Wu, G.C. Zhao, Direct electrochemistry of hemoglobin at a graphene gold nanoparticle composite film for nitric oxide biosensing, Sensors, 13 (2013) 7492-7504.

[82] C. Fan, X. Chen, G. Li, J. Zhu, D. Zhu, H. Scheer, Direct electrochemical characterization of the interaction between haemoglobin and nitric oxide, Phys Chem Chem Phys, 2 (2000) 4409-4413.

[83] C. Fan, G. Li, J. Zhu, D. Zhu, A reagentless nitric oxide biosensor based on hemoglobin–DNA films, Anal Chim Acta, 423 (2000) 95-100.

[84] C. Fan, X. Liu, J. Pang, G. Li, H. Scheer, Highly sensitive voltammetric biosensor for nitric oxide based on its high affinity with hemoglobin, Anal Chim Acta, 523 (2004) 225-228.

[85] C. Fan, J. Pang, P. Shen, G. Li, D. Zhu, Nitric oxide biosensors based on Hb/phosphatidylcholine films, Anal Sci, 18 (2002) 129-132.

[86] Z. Guo, J. Chen, H. Liu, C. Cha, Direct electrochemistry of hemoglobin and myoglobin at didodecyldimethylammonium bromide-modified powder microelectrode and application for electrochemical detection of nitric oxide, Anal Chim Acta, 607 (2008) 30-36.

[87] X. He, L. Zhu, Direct electrochemistry of hemoglobin in cetylpyridinium bromide film: Redox thermodynamics and electrocatalysis to nitric oxide, Electrochem Commun, 8 (2006) 615-620.

[88] S. Jia, J. Fei, J. Deng, Y. Cai, J. Li, Direct electrochemistry and electrocatalysis of hemoglobin immobilized in an amphiphilic diblock copolymer film, Sens Actuators B Chem, 138 (2009) 244-250.

[89] S. Jia, J. Fei, J. Zhou, X. Chen, J. Meng, Direct electrochemistry of hemoglobin entrapped in cyanoethyl cellulose film and its electrocatalysis to nitric oxide, Biosens Bioelectron, 24 (2009) 3049-3054.

[90] F. Li, M. Nie, X. He, J. Fei, Y. Ding, B. Feng, Direct electrochemistry and electrocatalysis of hemoglobin on a glassy carbon electrode modified with poly(ethylene glycol diglycidyl ether) and gold nanoparticles on a quaternized cellulose support. A sensor for hydrogen peroxide and nitric oxide, Microchim Acta, 181 (2014) 1541-1549.

[91] P. Li, Y. Ding, Z. Lu, Y. Li, X. Zhu, Y. Zhou, et al., Direct electrochemistry of hemoglobin immobilized on the water-soluble phosphonate functionalized multi-walled carbon nanotubes and its application to nitric oxide biosensing, Talanta, 115 (2013) 228-234.

[92] X. Liu, L. Shang, J. Pang, G. Li, A reagentless nitric oxide biosensor based on haemoglobin/polyethyleneimine film, Biotechnol. Appl. Biochem, 38 (2003) 119-122.

[93] X. Liu, L. Shang, Z. Sun, G. Li, Direct electrochemistry of hemoglobin in dimethyldioctadecyl ammonium bromide film and its electrocatalysis to nitric oxide, J Biochem Biophys Methods, 62 (2005) 143-151.

[94] Q. Lu, S. Hu, Studies on direct electron transfer and biocatalytic properties of hemoglobin in polytetrafluoroethylene film, Chem. Phys. Lett., 424 (2006) 167-171.

[95] J. Pang, C. Fan, X. Liu, T. Chen, G. Li, A nitric oxide biosensor based on the multi-assembly of hemoglobin/montmorillonite/polyvinyl alcohol at a pyrolytic graphite electrode, Biosens Bioelectron, 19 (2003) 441-445.

[96] W. Shan, P. He, N. Hu, Electrocatalytic reduction of nitric oxide and other substrates on hydrogel triblock copolymer pluronic films containing hemoglobin or myoglobin based on protein direct electrochemistry, Electrochim Acta, 51 (2005) 432-440.

[97] F. Wang, X. Chen, Y. Xu, S. Hu, Z. Gao, Enhanced electron transfer for hemoglobin entrapped in a cationic gemini surfactant films on electrode and the fabrication of nitric oxide biosensor, Biosens Bioelectron, 23 (2007) 176-182.

[98] W. Wen, W. Chen, Q.-Q. Ren, X.-Y. Hu, H.-Y. Xiong, X.-H. Zhang, et al., A highly sensitive nitric oxide biosensor based on hemoglobin–chitosan/graphene–hexadecyltrimethylammonium bromide nanomatrix, Sens Actuators B Chem, 166-167 (2012) 444-450.

[99] A.A. Abdelwahab, W.C.A. Koh, H.-B. Noh, Y.-B. Shim, A selective nitric oxide nanocomposite biosensor based on direct electron transfer of microperoxidase: Removal of interferences by co-immobilized enzymes, Biosens Bioelectron, 26 (2010) 1080-1086.

[100] W.C.A. Koh, M.A. Rahman, E.S. Choe, D.K. Lee, Y.-B. Shim, A cytochrome *c* modified-conducting polymer microelectrode for monitoring in vivo changes in nitric oxide, Biosens Bioelectron, 23 (2008) 1374-1381.

[101] R.M. Santos, M.S. Rodrigues, J. Laranjinha, R.M. Barbosa, Biomimetic sensor based on hemin/carbon nanotubes/chitosan modified microelectrode for nitric oxide measurement in the brain, Biosens Bioelectron, 44 (2013) 152-159.

[102] S.H. Takahashi, S.I.C. de Torresi, Nitric oxide sensing by cytochrome *c* bonded to a conducting polymer modified glassy carbon electrode, Synth Met, 159 (2009) 2159-2161.

[103] J.G. Pacheco, M.F. Barroso, H.P.A. Nouws, S. Morais, C. Delerue-Matos, 21 - Biosensors A2 - Larroche, Christian, in: M.Á. Sanromán, G. Du, A. Pandey (Eds.), Current Developments in Biotechnology and Bioengineering, Elsevier, 2017, pp. 627-648.

[104] T. Jesionowski, J. Zdarta, B. Krajewska, Enzyme immobilization by adsorption: a review, Adsorption, 20 (2014) 801-821.

[105] C. Helms, D.B. Kim-Shapiro, Hemoglobin-mediated nitric oxide signaling, Free Radic Biol Med, 61 (2013) 464-472.

[106] A.R. Pereira, G.C. Sedenho, J.C.P. Souza, F.N. Crespilho, Advances in enzyme bioelectrochemistry, An Acad Bras Cienc., 90 (2018) 825-857.

[107] H.-Y. Gu, A.-M. Yu, S.-S. Yuan, H.-Y. Chen, Amperometric nitric oxide biosensor based on the immobilization of hemoglobin on a nanometer-sized gold colloid modified au electrode, Anal Lett, 35 (2002) 647-661.

[108] D. Pletcher, Studies of metal deposition and dissolution using microelectrodes, in: M.I. Montenegro, M.A. Queirós, J.L. Daschbach (Eds.), Microelectrodes: Theory and applications, Springer Netherlands, Dordrecht, 1991, pp. 463-475.

[109] G.A. Ordway, D.J. Garry, Myoglobin: an essential hemoprotein in striated muscle, J Exp Biol., 207 (2004) 3441-6.

[110] S. Kröning, F.W. Scheller, U. Wollenberger, F. Lisdat, Myoglobin-clay electrode for nitric oxide (NO) detection in solution, Electroanalysis, 16 (2004) 253-259.

[111] L. Zhang, G.-C. Zhao, X.-W. Wei, Z.-S. Yang, A nitric oxide biosensor based on myoglobin adsorbed on multi-walled carbon nanotubes, Electroanalysis, 17 (2005) 630-634.

[112] J. Wang, M. Li, Z. Shi, N. Li, Z. Gu, Direct electrochemistry of cytochrome *c* at a glassy carbon electrode modified with single-wall carbon nanotubes, Anal Chem, 74 (2002) 1993-1997.

[113] J. Petrović, R.A. Clark, H. Yue, D.H. Waldeck, E.F. Bowden, Impact of surface immobilization and solution ionic strength on the formal potential of immobilized cytochrome *c*, Langmuir, 21 (2005) 6308-6316.

[114] H.B. Dunford, T. Araiso, D. Job, J. Ricard, R. Rutter, L.P. Hager, et al., Peroxidases, in: H.B. Dunford, D. Dolphin, K.N. Raymond, L. Sieker (Eds.), The biological chemistry of iron: A look at the metabolism of iron and its subsequent uses in living organisms proceedings of the NATO advanced study - Institute held at Edmonton, Alberta, Canada, August 13 – September 4, 1981, Springer Netherlands, Dordrecht, 1982, pp. 337-55.

[115] E. Casero, M. Darder, F. Pariente, E. Lorenzo, Peroxidase enzyme electrodes as nitric oxide biosensors, Anal Chim Acta, 403 (2000) 1-9.

[116] J.H. Zagal, F. Bedioui, J.-P. Dodelet, N4-macrocyclic metal complexes: Springer Science & Business Media, 2007.

[117] M.T. de Groot, M. Merkx, A.H. Wonders, M.T.M. Koper, Electrochemical reduction of NO by hemin adsorbed at pyrolitic graphite, J Am Chem Soc, 127 (2005) 7579-7586.

[118] N.J. Tao, G. Cardenas, F. Cunha, Z. Shi, *In situ* STM and AFM study of protoporphyrin and iron(III) and zinc(II) protoporphyrins adsorbed on graphite in aqueous solutions, Langmuir, 11 (1995) 4445-4448.

[119] J. Lei, H. Ju, O. Ikeda, Supramolecular assembly of porphyrin bound DNA and its catalytic behavior for nitric oxide reduction, Electrochim Acta, 49 (2004) 2453-2460.

[120] J. Lei, H. Ju, O. Ikeda, A novel supramolecular assembly film of porphyrin bound DNA: Characterization and catalytic behaviors towards nitric oxide, Sensors, 5 (2005) 171-184.

[121] Y.-M. Li, H.-H. Liu, D.-W. Pang, Direct electrochemistry and catalysis of heme-proteins entrapped in methyl cellulose films, J Electroanal Chem, 574 (2004) 23-31.

[122] J. Yu, J. Ma, F. Zhao, B. Zeng, Direct electron-transfer and electrochemical catalysis of hemoglobin immobilized on mesoporous Al_2O_3, Electrochim Acta, 53 (2007) 1995-2001.

[123] E. Laviron, Adsorption, autoinhibition and autocatalysis in polarography and in linear potential sweep voltammetry, J Electroanal Chem Interfacial Electrochem, 52 (1974) 355-393.

[124] J.F. Rusling, B. Wang, S.-e. Yun, Electrochemistry of redox enzymes, Bioelectrochemistry, John Wiley & Sons, Ltd, 2008, pp. 39-85.

[125] R. Roskoski, Michaelis-Menten kinetics, The comprehensive pharmacology reference, Elsevier, New York, 2007, pp. 1-10.

[126] A.P. Tavares, O. Rodriguez, E.A. Macedo, Ionic liquids as alternative co-solvents for laccase: study of enzyme activity and stability, Biotechnol. Bioeng, 101 (2008) 201-207.

[127] P. Tavares, A.S. Pereira, J.J.G. Moura, I. Moura, Metalloenzymes of the denitrification pathway, J Inorg Biochem, 100 (2006) 2087-2100.

CHAPTER 3

NITRIC OXIDE REDUCTASE FROM *MARINOBACTER HYDROCARBONOCLASTICUS*

Protein purification is essential to understand its structure, function and interactions. It is also crucial to use the protein in the development of electrochemical biosensors, as is the case of the present thesis. The purification of the protein of interest from crude extract is usually achieved exploiting the differences in protein size, surface charge or binding affinity to specific ligands (such as substrates, inhibitors, activators). Herein, the nitric oxide reductase (NOR) enzyme was purified from *Marinobacter hydrocarbonoclasticus* bacterium membranes by ionic exchange chromatography in a DEAE-Biogel A column, followed by chromatography in two hydroxyapatite columns. The NOR purity was assessed by its UV-visible spectrum and by sodium dodecyl sulfate polyacrylamide gel electrophoresis (SDS-PAGE), as well as by the specific activity towards the reduction of nitric oxide radical (•NO) to nitrous oxide.

3.1. Introduction

Denitrification is an anaerobic "respiration" process, part of the nitrogen biogeochemical cycle, where nitrate is converted into dinitrogen through four reducing steps (1), catalysed by different metalloenzymes, namely nitrate reductase, that catalyses the reduction of nitrate to nitrite, nitrite reductase, that catalyses the subsequent reduction of nitrite to NO, NOR, responsible for the reduction of NO to nitrous oxide -the subject of this Thesis- and nitrous oxide reductase, that catalyses the final reduction of nitrous oxide to dinitrogen [1-4]. As such, denitrification is one of the major biological processes that returns the fixed nitrogen (in the form of nitrate) to the atmosphere (dinitrogen) [5, 6]. Additionally, this anaerobic process is an important source of NO, that causes ozone destruction, and of nitrous oxide (N_2O), an important greenhouse-effect gas that also consumes stratospheric ozone [7].

$$NO_3^- \rightarrow NO_2^- \rightarrow {}^{\bullet}NO \rightarrow N_2O \rightarrow N_2 \qquad (1)$$

3.1.1. Families and structural organization

NORs are integral membrane proteins that catalyze the two-electron reduction of NO to N_2O (2) [8].

$$2\,{}^{\bullet}NO + 2\,e^- + 2\,H^+ \longrightarrow N_2O + H_2O \qquad (2)$$

The bacterial NOR enzymes can be organized into three classes, namely, the cytochrome *c*-dependent NOR (cNOR), the quinol-dependent NOR (qNOR) and the copper-dependent NOR (Cu_ANOR) (Fig. 3.1) [9].

The cNOR (Fig. 3.1), found only in denitrifying bacteria -as is the case of the enzyme used in this Thesis, the NOR from *Marinobacter hydrocarbonoclasticus*- contains two subunits, denominated NorB and NorC (Fig 3.2). The NorC subunit (17 kDa), anchored in the membrane and facing the periplasm, harbors a *c*-type heme, bis-coordinated by a histidine and methionine residues. This subunit is involved in the electron transfer from the physiological electron donors ("soluble" proteins such as cytochrome *c* or pseudoazurin) to the active site. NorB, the larger (56 kDa), membrane subunit, is the catalytic subunit. It comprises three metal centers: (i) one *b*-type heme, bis-coordinated by two histidine residues, (ii) one *b*-type heme, pentacoordinated by a histidine residue, named b_3, (iii) and one non-heme iron,

named Fe_B, that is coordinated by three histidine residues. The pentacoordinated heme (heme b_3) and the non-heme iron (Fe_B) constitute the catalytic binuclear center, where the two iron atoms, in the absence of substrate, are connected by μ-oxo bridge (Fig. 3.2).

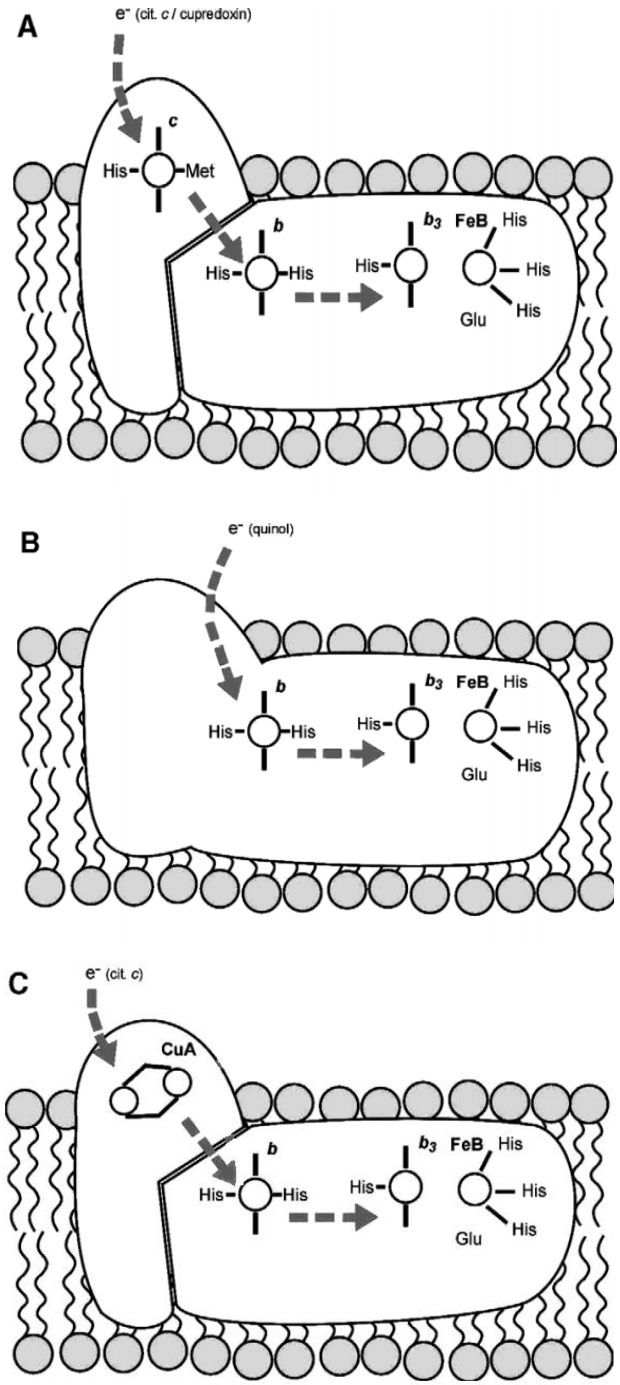

Fig. 3.1. Schematic representation of the three bacterial NOR classes: (A) *c*NOR; (B) qNOR; and (C) Cu_ANOR. Gray, broken, arrows represent the proposed electron transfer pathway from a periplasmic electron donor to the active site (adapted from Tavares et al. [4]).

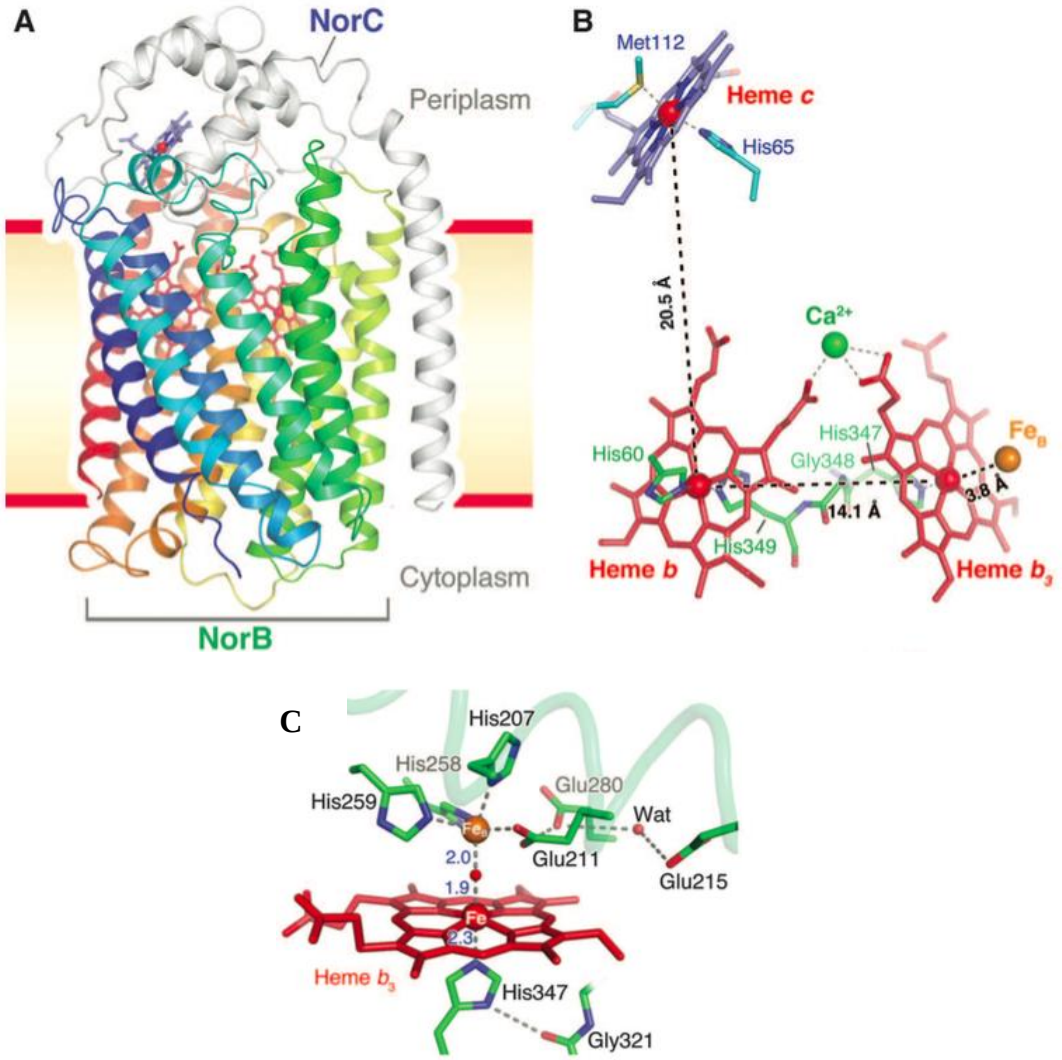

Fig. 3.2. Three-dimensional structure view of cNOR. (A) The NorC and NorB subunits are shown as ribbons in grey and other various colors, respectively. (B) Arrangement of the redox-active centers in the same orientation as in (A). Heme *c* is shown as blue sticks, and hemes *b* and b_3 are shown as red sticks and the Fe ions of these three centers are represented as red spheres. Fe_B and calcium ions are represented as orange and green spheres, respectively. The distances between redox centers are also indicated. (C) Structure of the binuclear center of cNOR. Non-heme iron (Fe_B) is coordinated by Glu211, His207, His258, and His259 that are conserved in cNOR. Amino acid residue numbering from *Pseudomonas aeruginosa* NOR. The structures shown are based on the PDB file 3O0R (adapted from Hino et al. [10]).

The qNOR (Fig. 3.1), on the contrary, is a monomeric enzyme that lacks the heme *c* and accepts electrons from the quinol pool. Nevertheless, the qNOR shares a high degree of similitude with cNOR: (i) the main body of qNOR is homologous to NorB and the qNOR active site also houses the binuclear center comprising one heme *b* and one non-heme Fe_B; (ii) the first transmembrane α-helix and the adjacent hydrophilic region of qNOR have a marked sequence similarity to NorC; (iii) and qNOR also harbors a transmembrane α-helix homologous to the region that connects NorC and NorB.

The Cu_ANOR (Fig. 3.1), which so far has only been found in bacilli, has the distinctive feature of harboring a binuclear copper center. In this dimeric enzyme, the smaller subunit contains two copper atoms (Cu_A) that are involved in electron transfer from the physiological electron donor (cytochrome *c*; it was recently described that quinol do not supported the NO reduction reaction). The larger subunit is the catalytic subunit and it harbors the three metal centers characteristic of qNOR and cNOR (two hemes *b* and one non-heme iron).

3.1.2. Reaction mechanism

The reaction mechanism of NO reduction by NOR is still under discussion. All proposed mechanisms suggest the biding of two NO molecules (2) in the heme b_3 and Fe_B binuclear center, after the reduction of the enzyme and dissociation of the bridging μ-oxo ligand in the form of a water molecule [9, 11]. It is the coordination of the NO molecules in the active site and the structure of the catalytic intermediate that raises the debate, as three different mechanisms were proposed.

In one of the mechanisms, named "*trans* mechanism" (Fig. 3.3), each iron atom of the binuclear active site (b_3 and Fe_B) binds one NO molecule, to form an iron-nitrosyl dimer intermediate. Subsequently, the close proximity of the two NO nitrogen atoms promotes the N-N bond formation, through an electrophilic attack or a radical coupling process, leading to the formation of a bound O-N-N-O intermediate. Finally, the O-N bond is cleaved and the N_2O is released.

In the other two mechanistic proposals, both NO molecules bind to the heme b_3 iron or to the non-heme Fe_B iron - the "*cis*-heme b_3 mechanism" and the "*cis*-Fe_B mechanism", respectively. In the "*cis*-heme b_3 mechanism" (Fig. 3.3), the first NO molecule binds to heme b_3 to form a $\{FeNO\}^7$ complex, which is then electrophilically attacked by the second NO molecule. There is little experimental evidence to support

this mechanism, although it is supported by theoretical calculations. In fact, the formation of the stable {FeNO}^{7}, one complex considered a catalytic "dead end", is one of the main criticisms raised against the "*cis*-heme b_3 mechanism". Moreover, a spectroscopic study suggested that ferrous heme b_3 is hexa-coordinated, what could result in a low affinity towards NO, and, thus, promote the formation of a ferrous-dinitrosyl complex at Fe_B.

In the "*cis*-Fe_B mechanism" (Fig. 3.3), as recently suggested by Duarte *et al*. [12], the first NO molecule binds to ferrous Fe_B. Subsequently, the second NO molecule binds to Fe_B or directly attacks the NO ligand of Fe_B, yielding an Fe_B-hyponitrite intermediate. In this mechanism, the role of the heme b_3, that remains hexa-coordinated, possibly with hydroxide ligand, could be to stabilize the Fe_B-hyponitrite intermediate and/or assist the cleavage of the N-O bond, to ultimately form N_2O and a water molecule.

Certainly, the debate about the mechanism of NO reduction by NOR will continue until new data concerning the structural and spectroscopic characterization of the reaction intermediate(s) is obtain.

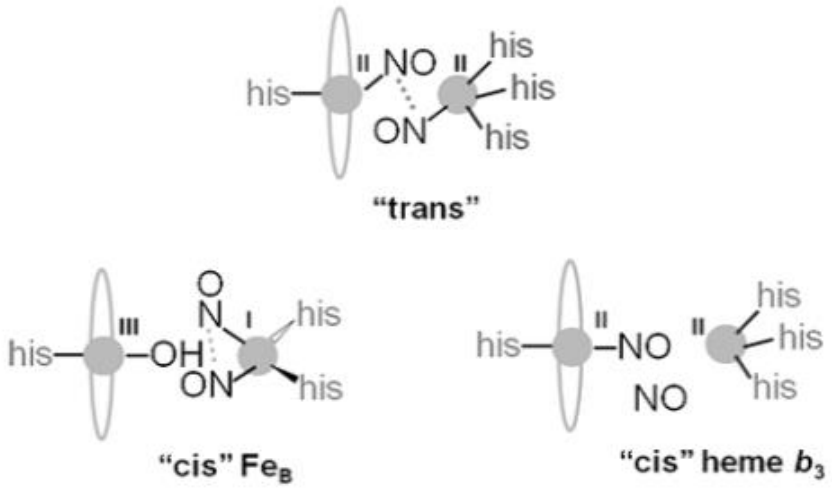

Fig. 3.3. Three possible modes of accommodating two molecules of NO at the active site/dinuclear center of NOR: trans, cis Fe_B and cis heme b_3. For simplicity, the ligands to Fe_B are shown as three histidine residues (corresponding to the homology models), except in the case of the cis-Fe_B model, which would require the co-ordination sphere to change (adapted from Watmough et al. [13]).

3.2. Purification of nitric oxide reductase from *Marinobacter hydrocarbonoclasticus*

3.2.1. Introduction

The purification of membrane proteins is more challenging than of "soluble" proteins, because the cellular membrane is essential for the stability of the enzyme (besides being also key to retard the proteolitic degradation). For this reason, the extraction of NOR from *Marinobacter hydrocarbonoclasticus (M. hydrocarbonoclasticus)* membranes is a delicate process [14]. So, in order to obtain a fruitful NOR purification is necessary to use an ideal non-ionic detergent that could play the stabilization role of the biological membrane. The choice of the ideal detergent may be an essential factor in the success achieved, since many detergents irreversibly inactivate the enzymes [15]. To enhance the *M. hydrocarbonoclasticus* NOR stability, n-dodecyl-*β*-D-maltoside (DM) and 2-phenylethanol (PE) were used during the all purification procedures, as previously described [12]. The NOR purification from the *M. hydrocarbonoclasticus* membranes was achieved using three different chromatographic processes: an anionic exchange in a DEAE-Biogel column and an adsorption in a CHT-type I and CHT-type II columns (pre-packed ceramic hydroxyapatite columns).

3.2.2. Materials and methods

a) Reagents

All the reagents were of the highest quality available (PA or superior) and were used as supplied.

b) Cell growth and membrane fraction preparation

The *M. hydrocarbonoclasticus* was isolated from a petroleum refinery outlet chronically polluted by hydrocarbons, in the Mediterranean Sea. This Gram negative, rod-shaped bacterium grows under NaCl concentrations between 0.08 and 3.5 $molL^{-1}$ and can use various hydrocarbons as the sole source of carbon and energy [16].

The *M. hydrocarbonoclasticus* cells (Institute Pasteur Collection, reference *Pseudomonas nautica* no. 617/1.85) were grown at the "Unité de Fermentation" (CNRS, Marselha), in a 300 L reactor, in artificial seawater, under denitrifying conditions in the presence of 10 $mmolL^{-1}$ nitrate (details can be found in Appendix A). The cells were collected by centrifugation, at the end of the stationary phase (the cellular growth resulted in approximately 1 g wet weight of cells per L of medium). The cells were suspended in 100 $mmolL^{-1}$ Tris-HCl pH 7.0, in a ratio of 1:2 (cells:buffer), and disrupted in a French Press at 9000 psi. The cellular extract was centrifuged (8000x*g* for 20 min), to eliminate the cellular debris, and ultracentrifuged (125000x*g* for 60 min), to separate the membrane fraction.

The membrane fraction was "washed" with 50 $mmolL^{-1}$ Tris-HCl, pH 8.0, collected by centrifugation (180000×*g* for 90 min), and homogenized in 50 $mmolL^{-1}$ Tris-HCl, pH 8.0, with 100 $mmolL^{-1}$ KCl, to a final concentration of 10 mg/mL of total protein. Subsequently, the membranes were sonicated in 500 mL portions, in an ice bath, with a 200 watts sonicator, at 24 kHz ultrasonic frequency, equipped with a S7 tip (7mm diameter). The sonicator amplitude was set to 60% and the pulse to 0.5 seconds. The sonication period was 10 minutes and this procedure was repeated twice. Afterwards the membrane fraction was centrifuged at 180000×*g*, for 90 minutes. The insoluble fraction containing the membranes was homogenized in 50 $mmolL^{-1}$ Tris-HCl pH 8.0, diluted to 10 mg/mL of total protein, and centrifuged, to "wash" to membranes and remove the KCl.

This membrane fraction was stored at -70ºC until it was used in the NOR purification.

c) Nitric oxide reductase purification from the membrane fraction

The NOR purification was performed as previously described [17] and all steps were carried out at 4ºC.The membrane fraction, prepared as described above, was diluted (if necessary) to a final protein concentration of 10 mg/mL, in 50 $mmolL^{-1}$ Tris-HCl, pH 8.0, and incubated with 0.8% DM and 0.02% PE, under steering, for 30 minutes. The solubilized membranes were collected by centrifugation (180000×*g*, for 90 min).

The membrane extract was first subjected to an anionic exchange chromatography in a DEAE Bio-gel column (Bio-Rad; Ø=50, h=25 cm), equilibrated with 50 $mmolL^{-1}$ Tris-HCl pH 8.0, with 0.02 % (w/v) DM, 0.01% (v/v) PE. After "washing" the column, the NOR was eluted using a linear NaCl gradient of 0-500 $mmolL^{-1}$, in the same buffer (in 3 column volumes). The fractions displaying NOR activity were pooled and concentrated using an ultrafiltration concentrator, with a 5 kDa cut-off membrane.

The sample ionic strength was, subsequently, lowered to 50 $mmolL^{-1}$ Tris-HCl pH 8.0, 0.02 % (w/v) DM, 0.01 % (v/v) PE, using the same device.

The next step in the NOR purification procedure was a chromatography in a CHT type II pre-packed column ("ceramic hydroxyapatite"; Bio-Rad), equilibrated with 50 $mmolL^{-1}$ Tris-HCl pH 8.0, 0.02 % (w/v) DM, 0.01 % (v/v) PE. NOR was eluted using a linear gradient with the equilibrating buffer against 1.5 $molL^{-1}$ potassium phosphates pH 7.0, also with 0.02% DM, 0.01% PE. The fractions exhibiting higher NOR activity were collected and concentrated using an ultrafiltration concentrator, with a 5 kDa cut-off membrane. The sample ionic strength was, subsequently, adjusted to 100 $mmolL^{-1}$ potassium phosphates pH 7.0, 0.02% (w/v) DM, 0.01% (v/v) PE, using the same device.

The third chromatographic step was carried out in a CHT type I pre-packed column (Bio-Rad; 20 mL), equilibrated with 100 $mmolL^{-1}$ potassium phosphates pH 7.0, 0.02% (w/v) DM, 0.01% (v/v) PE. A linear phosphate gradient of 0.1-1.5 $molL^{-1}$, in the same buffer, was applied to elute the NOR enzyme. The NOR fractions were pooled, concentrated and equilibrated in 100 $mmolL^{-1}$ potassium phosphates pH 7.0, 0.02% (w/v) DM, 0.01% (v/v) PE, as described above.

Throughout the purification procedure, the presence of NOR activity and the NOR purity were accessed measuring the NO reductase activity (as described below) and evaluating the UV-visible absorption spectra and the electrophoretic pattern in tricine, sodium dodecyl sulfate polyacrylamide gel electrophoresis (SDS-PAGE; performed as described in Appendix B). The protein concentration was determined by the Lowry method, using bovine serum albumin as a standard [44] (as described in Appendix C).

d) Nitric oxide reductase activity assay

The NOR activity was evaluated measuring the NO consumption (reduction) with a specific NO electrode (ISO-NO MarkII, with a 2 mm sensor, World Precision Instruments), as previously described [18]. Data were acquired "digitally" using the DataTrax™ software (World Precision Instruments) and a Quad 16/EFA-400 interface was used to connect the ISO-NO Mark II electrode with the computer.

The NO electrode calibration was performed as described by the manufacturer, using an acidic KI solution and a standard nitrite solution, according to the stoichiometric chemical reduction of nitrite to NO (3).

$$2\ KNO_2 + 2\ KI + 2\ H_2SO_4 \longrightarrow 2\ ^{\bullet}NO + I_2 + 2\ H_2O + 2\ K_2SO_4 \qquad (3)$$

The NOR activity assays were performed in an anaerobic chamber (1 mL) and the anaerobic conditions were maintained by a constant positive argon flux. The composition of the reaction mixture is described in Table 3.1 (the anaerobic solutions were added to the reaction chamber using gastight syringes). In all assays, a protein concentration of 6mg/mL was used and the reaction was started by the addiction of the enzyme sample. One unit of enzymatic activity corresponds to 1μmol of NO consumed/min.

Table 3.1. Reaction mixture used in the NOR activity assays.

Solution	**Concentration in stock solution**	**Amount added (μL)**	**Concentration at the assay**
Phosphate buffer, pH 6.0	20 $mmolL^{-1}$	850	≈17 $mmolL^{-1}$
DM	10 % (p/v)	2	0.02 % (p/v)
Cytochrome *c*	2 $mmolL^{-1}$	10	20 $\mu molL^{-1}$
Phenazine methosulfate	5 $mmolL^{-1}$	20	100 $\mu molL^{-1}$
Sodium ascorbate	500 $mmolL^{-1}$	20	10 $mmolL^{-1}$
NO stock solution	100 $\mu molL^{-1}$	[30-90]	[3-9] $\mu molL^{-1}$

The 100 $\mu molL^{-1}$ NO solution was prepared by bubbling a 5% NO / 95% He gas mixture (Air Liquid, Portugal) into a 5 $molL^{-1}$ KOH solution (aiming to hydrolyse any gaseous contaminants present in the gas mixture), subsequently in acidified water (pH 3) and, ultimately, in water (Fig. 3.4). The NO solution was prepared immediately before being used.

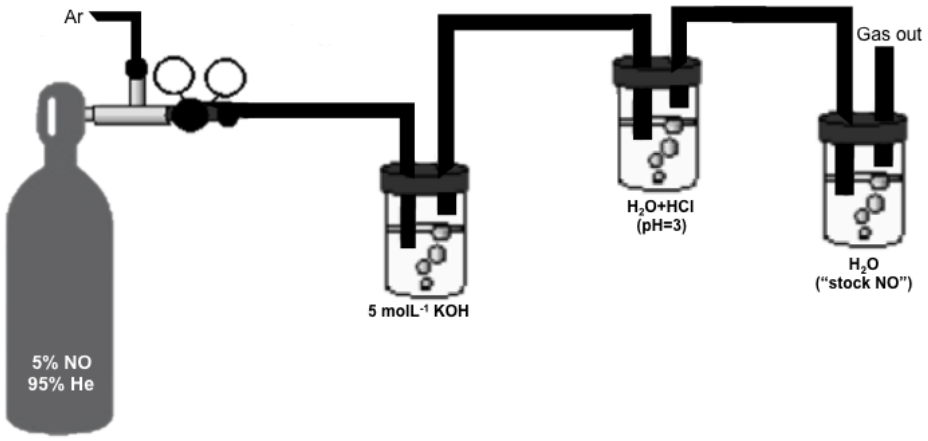

Fig. 3.4. Setup to prepare the NO solution.

3.2.3. Results and discussion

The NOR was purified from a previously prepared membrane fraction of *M. hydrocarbonoclasticus*, using three chromatographic steps, as previously described [18]. The first chromatographic process, an anionic exchange chromatography performed in a column with a large volume of DEAE Bio-gel, operated under gravity (without using a pressure pump), aimed to do a first, "coarse cleaning" of the membrane fraction. As expected from previous purifications processes [18], NOR was eluted during the gradient stage of the chromatography, at around 290 and 350 mmolL^{-1} NaCl. The next two purification steps were carried out in hydroxyapatite-based columns (CHT type II and I; Fig. 3.5) and resulted in a global purification of 3.24 times, with a recovery of 5.31% (Table 3.2). Although the global purification was not high (3.24x), the purification procedure resulted in a NOR sample with a significantly higher specific activity (760 U/mg) than that previously described in our Laboratory (162 U/mg, reported as 2700μM/s/mg by Duarte et al. [19]).

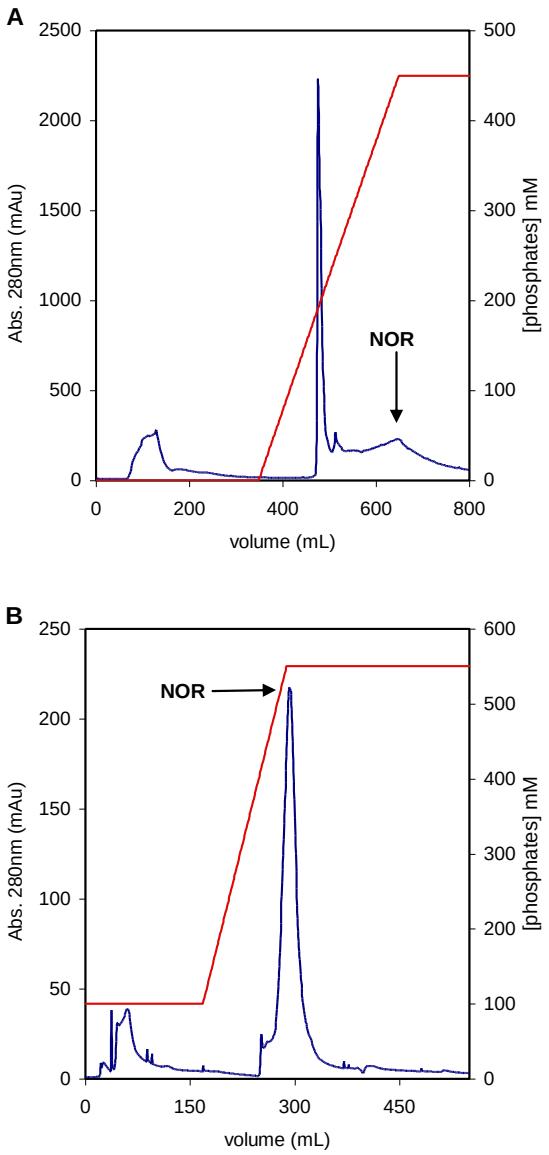

Fig. 3.5. Chromatograms of the separation of the NOR samples in CHT Type II (panel A) and CHT Type I (panel B) columns. The blue lines represent the absorbance at 280 nm (expressed in mAu, that correspond to absorbance values x10^3) and the red lines indicate the potassium phosphates gradient. The peaks containing NOR activity are indicated by the black arrows. Details of the chromatographic procedures can be found in section 3.2.2.-c).

Table 3.2. Table summarizing the NOR purification from *M. hydrocarbonoclasticus* membrane fraction.

Purification step	**Total protein (mg)**	**Total activity (kU)**	**Specific activity (U/mg)**	**Yield (%)**	**Purification fold (x)**
DEAE-Biogel	428	100	234	100	1.00
CHT Type II	61.5	30.1	489	30.0	2.09
CHT Type I	7.00	5.32	760	5.31	3.24

Nonetheless, in spite of its high specific activity, the purified NOR sample still exhibited the presence of some contaminants, as can be appreciated by the SDS-PAGE pattern present in Fig. 3.6, where, besides the two bands corresponding to the two NOR subunits, other bands can be observed. However, due to the low yield of the global process (5%; Table 3.2), no further purification of the sample was attempted.

Regarding the electrophoretic mobility of the two NOR subunits in the SDS-PAGE (Fig. 3.6), it must be noted that the NorB, due to its high hydrophobicity, presents a higher mobility, corresponding to a molecular mass between 35 and 40 kDa. This phenomenon is common to other cNOR [20, 21]. (The molecular mass values of the two NOR subunits, NorC (17 kDa) and NorB (56 kDa), were calculated according to the primary sequence.)

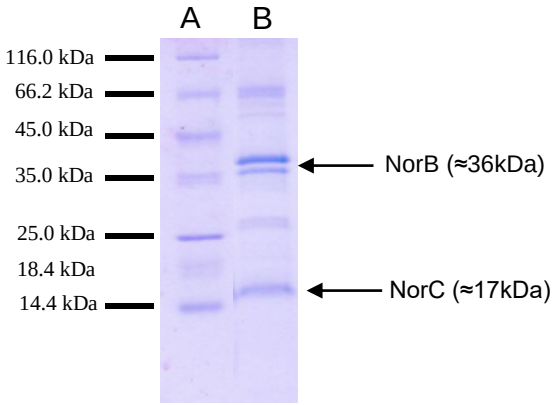

Fig. 3.6. Electrophoretogram of the separation under denaturating conditions (SDS-PAGE) of the purified NOR sample. Lane A - molecular mass markers (whose masses are indicated). Lane B - purified NOR fraction (where the bands corresponding to the two subunits of NOR are indicated). Details of the electrophoretic procedure can be found in Appendix B.

The UV-visible absorption spectrum of the purified NOR sample was also used as a measure of its purity. The as-isolated NOR spectrum (Fig. 3.7) is typical of heme-containing proteins and very similar to those of other highly purified cNORs [18]. It shows a peak around 270-280 nm, characteristic of all proteins, a heme Soret band at 411 nm, and a broad band centred around 550 nm, with two small shoulders at 528 and 558 nm. The observation of the two small absorbance shoulders indicates the presence of a small amount of reduced low-spin heme in the as-isolated form of the enzyme, what is in agreement with Mössbauer data [18]. The absorbance ratio

between the Soret band and the protein band (Abs_{411}/Abs_{280}) can be interpreted as a purity parameter (in an analogous way to the specific activity, that is defined as the ratio between the activity and the total protein). This ratio was determined to be 1.3 for the as-isolated purified NOR, a value identical to the ones determined for other highly purified NOR samples [18]. This excellent Abs_{411}/Abs_{280} value, together with the high specific activity attained, supported our decision to not further purify the NOR sample (because of the low yield obtained in the three purification steps performed (Table 3.2), the amount of NOR to be further purified was very low to compensate for the risk of ending the purification without sufficient sample to carry out the electrochemical studies).

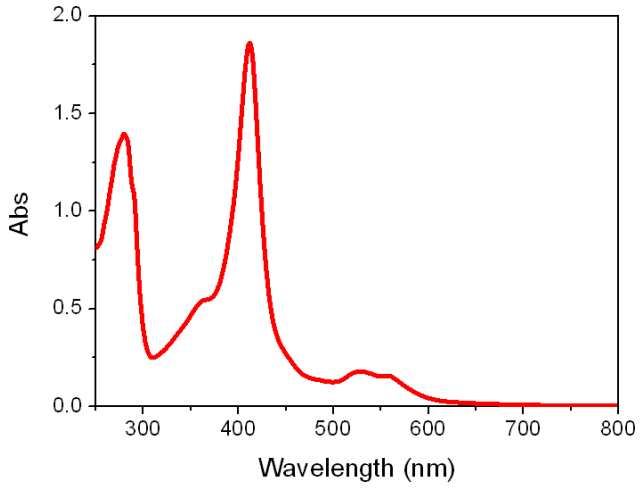

Fig. 3.7. The UV-visible absorption spectrum of the as-isolated purified NOR sample. The spectrum was acquired in 100mmolL^{-1} potassium phosphates pH 7.0, 0.02% (w/v) n-dodecyl-β-D-maltoside, 0.01% (v/v) 2-phenylethanol.

3.3. References

[1] L.I. Hochstein, G.A. Tomlinson, The enzymes associated with denitrification, Annu Rev Microbiol., 42 (1988) 231-261.

[2] I. Moura, J.J. Moura, S.R. Pauleta, L.B. Maia, Metalloenzymes in denitrification: Applications and environmental impacts, Royal Society of Chemistry, 2016.

[3] I. Moura, J.J.G. Moura, Structural aspects of denitrifying enzymes, Curr Opin Chem Biol., 5 (2001) 168-175.

[4] P. Tavares, A.S. Pereira, J.J. Moura, I. Moura, Metalloenzymes of the denitrification pathway, J Inorg Biochem, 100 (2006) 2087-2100.

[5] D.A. Martens, Denitrification A2 - Hillel, Daniel, Encyclopedia of soils in the environment, Elsevier, Oxford, 2005, pp. 378-82.

[6] P. Ambus, S. Zechmeister-Boltenstern, Chapter 22 - Denitrification and N-cycling in torest ecosystems A2 - Bothe, Hermann, in: S.J. Ferguson, W.E. Newton (Eds.), Biology of the Nitrogen Cycle, Elsevier, Amsterdam, 2007, pp. 343-58.

[7] R.W. Ye, B.A. Averill, J.M. Tiedje, Denitrification: production and consumption of nitric oxide, Appl Environ Microbiol, 60 (1994) 1053-1058.

[8] J.H.M. Hendriks, A. Jasaitis, M. Saraste, M.I. Verkhovsky, Proton and electron pathways in the bacterial nitric oxide reductase, Biochemistry, 41 (2002) 2331-2340.

[9] Y. Shiro, Structure and function of bacterial nitric oxide reductases: Nitric oxide reductase, anaerobic enzymes, Biochim. Biophys. Acta., 1817 (2012) 1907-1913.

[10] T. Hino, Y. Matsumoto, S. Nagano, H. Sugimoto, Y. Fukumori, T. Murata, et al., Structural basis of biological N_2O generation by bacterial nitric oxide reductase, Science, 330 (2010) 1666-1670.

[11] T. Hino, S. Nagano, H. Sugimoto, T. Tosha, Y. Shiro, Molecular structure and function of bacterial nitric oxide reductase, Biochim. Biophys. Acta., 1817 (2012) 680-687.

[12] A.G. Duarte, C.M. Cordas, J.J.G. Moura, I. Moura, Steady-state kinetics with nitric oxide reductase (NOR): New considerations on substrate inhibition profile and catalytic mechanism, Biochim. Biophys. Acta., 1837 (2014) 375-384.

[13] N.J. Watmough, S.J. Field, R.J. Hughes, D.J. Richardson, The bacterial respiratory nitric oxide reductase, Biochem Soc Trans., 37 (2009) 392-399.

[14] K. Ohlendieck, Extraction of membrane proteins, in: S. Doonan (Ed.) Protein purification protocols, Humana Press, Totowa, NJ, 1996, pp. 293-304.

[15] A. Anandan, A. Vrielink, Detergents in membrane protein purification and crystallisation, Adv. Exp. Med. Biol., 922 (2016) 13-28.

[16] M.J. Gauthier, B. Lafay, R. Christen, L. Fernandez, M. Acquaviva, P. Bonin, et al., *Marinobacter hydrocarbonoclasticus* gen. nov., sp. nov., a New, Extremely Halotolerant, Hydrocarbon-Degrading Marine Bacterium, International journal of systematic and evolutionary microbiology, 42 (1992) 568-576.

[17] M. Prudencio, A.S. Pereira, P. Tavares, S. Besson, I. Cabrito, K. Brown, et al., Purification, characterization, and preliminary crystallographic study of copper-containing nitrous oxide reductase from *Pseudomonas nautica* 617, Biochemistry, 39 (2000) 3899-3907.

[18] C.G. Timóteo, A.S. Pereira, C.E. Martins, S.G. Naik, A.G. Duarte, J.J.G. Moura, et al., Low-spin heme b_3 in the catalytic center of nitric oxide reductase from *Pseudomonas nautica*, Biochemistry, 50 (2011) 4251-4262.

[19] A.J.G. Duarte, Characterization of nitric oxide reductase (NOR) from *Pseudomonas nautica*, a study on biologic nitric oxide reduction, Universidade Nova de Lisboa (Portugal), 2011.

[20] P. Girsch, S. de Vries, Purification and initial kinetic and spectroscopic characterization of NO reductase from *Paracoccus denitrificans*, iochim. Biophys. Acta., 1318 (1997) 202-216.

[21] U.K. Laemmli, Cleavage of structural proteins during the assembly of the head of bacteriophage T4, Nature, 227 (1970) 680-685.

CHAPTER 4

CHARACTERIZATION OF THE DIRECT *MARINOBACTER HYDROCARBONOCLASTICUS* NITRIC OXIDE REDUCTASE-CATALYSED NITRIC OXIDE AND DIOXYGEN REDUCTION

Understanding the direct electron transfer processes between redox proteins and electrode surface is fundamental to understand the proteins mechanistic properties and for development of novel biosensors. In this study, nitric oxide reductase (NOR) extracted from *Marinobacter hydrocarbonoclasticus* bacteria was adsorbed onto a pyrolytic graphite electrode (PGE) to develop an unmediated enzymatic biosensor (PGE/NOR)) for characterization of NOR direct electrochemical behaviour and NOR bioelectrocatalytic activity towards NO and O_2. Square-wave voltammetry showed the reduction potential of all the four NOR redox centers: 0.095±0.002, -0.108±0.008, -0.328±0.001 and -0.635±0.004 V vs. SCE for heme *c*, heme *b*, heme b_3 and non-heme Fe_B, respectively. The determined sensitivity ($-4.00\times10^{-8}\pm1.84\times10^{-9}$ A/µmolL^{-1} and $-2.71\times10^{-8}\pm1.44\times10^{-9}$ A/µmolL^{-1} for NO and O_2, respectively), limit of detection (0.5 µmolL^{-1} for NO and 1.0 µmolL^{-1} for O_2) and the Michaelis Menten constant (2.1 and 7.0 µmolL^{-1} for NO and O_2, respectively) corroborated the higher affinity of NOR for its natural substrate (NO). No significant interference on sensitivity towards NO was perceived in the presence of O_2, while the O_2 reduction was markedly and negatively impacted (3.6 times lower sensitivity) by the presence of NO. These results clearly demonstrate the high potential of NOR for the design of innovative NO biosensors.

4.1. Introduction

Biological denitrification is an anaerobic pathway used by different bacteria to generate energy [1]. In denitrification, the reduction of nitrate to dinitrogen gas is accomplished by four different types of metalloenzymes (nitrate reductase, nitrite reductase, nitric oxide reductase (NOR) and nitrous oxide reductase) in four simple steps (nitrate → nitrite → nitric oxide → nitrous oxide → dinitrogen gas) [1]. In the third step, two nitric oxide radicals are conjugated to form nitrous oxide ($^{\bullet}NO$, herein abbreviated NO) and water in a two electron/proton reaction ($2NO + 2e^- + 2H^+ \rightarrow N_2O + H_2O$ (eq. 1)) with the involvement of NOR. NO is a signaling molecule involved in important biological processes in humans including neurotransmission, vasodilation, platelet aggregation, gene expression and apoptosis [2]. NO has also been implicated in a wide range of pathological processes, such as chronic infections and inflammations, diabetes, and neurological diseases (Parkinson and Alzheimer) [3]. Concerning NOR, three classes (*c*NOR, Cu_ANOR and *q*NOR) exist, which are composed by different electron transfer centers and subunits [4]. *c*NOR, the first class, is a membrane enzyme with two different subunits, a NorB (the catalytic center) and a NorC (responsible for electron transfer) [5, 6]. *c*NOR can be extracted from *Paracoccus denitrificans* [7-9], *Pseudomonas nautica* (also designated as *Marinobacter hydrocarbonoclasticus*) [5, 10, 11], *Pseudomonas aeruginosa* [12, 13] and *Halomonas halodenitrificans* [14].

Several methods have been applied to study the NO reduction by different NORs (table 4.1), which included density functional theory calculations (DFT) [7, 12, 15], fluorescence [16], Raman [17, 18] and UV/Vis spectroscopy [19, 20]. More recently, electrochemical methods, mainly cyclic voltammetry [5, 10, 11] and spectroelectrochemistry [8] have been also explored due to their inherent advantages, namely inexpensive instrumentation, possibility of miniaturization, requirement of low volumes, high sensitivity and low limits of detection (LOD) [21-24].

Table 4.1. NOR classes and representative organism for NO or O_2 detection.

NOR class	Representative organism	Substrate	Method	Electron donor	Purpose/application	Ref.
qNOR	*Geobacillus stearothermophilus*	O_2	Flow-flash technique	Ascorbate/PMS	Proton transfer pathway	[25]
qNOR	*Geobacillus stearothermophilus*	NO	Clark-type electrode equipped with an ISO-NO mark II system (WPI) Raman spectroscopy	Ascorbate/PMS	pH dependence of NO reduction	[18]
Liposomes reconstituted Cu_ANOR	*Bacillus azotoformans*	NO	Fluorescence	PESH	Cu_ANor can exploit NO reduction for increased cellular ATP production compared to organisms using cNor.	[16]
Liposomes reconstituted cNOR	*Paracoccus denitrificans expressed in Escherichia coli*	NO O_2	Optical flow-flash measurements	Not used	Proton transfer mechanism studies	[26]
cNOR	*Paracoccus denitrificans*	NO	DFT (B3LYP)	Not used	Mechanistic studies (Energy profile)	[7]
cNOR	*Paracoccus denitrificans*	CO NO	Ultrafast transient absorption spectroscopy	Not used	Ligand transfer pathways Time of the interaction of substrate with NOR	[9]
cNOR	*Paracoccus denitrificans*	CO	Spectroelectrochemistry	Not used	Effect of pH and CO exposure on cNOR reduction potentials	[8]
cNOR	*Paracoccus denitrificans*	NO	Raman spectroscopy and DFT	Not used	Bimetallic-bridging hyponitrite species in the reduction of NO	[17]
cNOR	*Paracoccus denitrificans*	O_2	DFT (B3LYP)	Cytochrome c	Mechanistic studies (Energy profile)	[15]
cNOR	*Pseudomonas nautica*	NO O_2	Electrochemistry (CV)	Not used	Protein redox centers pH dependence Catalytic mechanism	[10]
cNOR	*Pseudomonas nautica*	NO O_2	Electrochemistry (CV)	Cytochromes c_4, c_{549}, c_{551} and c_{552}	Mechanistic studies	[5]
sNorC	*Pseudomonas nautica*	NO	Molecular docking Electrochemistry −168 ± 15 for sNorC and +201 ± 34 mV for C_{552}	Not used	Increase of electron transfer when sNorC and cytochrome C_{552} are together.	[27]

Table 4.1. NOR classes and representative organism for NO or O_2 detection (continued).

NOR class	Representative organism	Substrate	Method	Electron donor	Purpose/application	Ref.
cNOR	*Halomonas halodenitrificans*	NO	Absorption, MCD and X-band ESR spectroscopy	Not used L-ascorbate as reducing agent	What happened to BNC when pH is <6	[14]
cNOR aa_3 (CcO)	*Pseudomonas aeruginosa* *Rhodobacter sphaeroides*	NO O_2	DFT (B3LYP)	Not used	Mechanistic studies (Energy profile)	[12]
cNOR	*Pseudomonas aeruginosa*	NO O_2 NO_2^- NO_3^-	ISO-NOP sensor in a bioreactor Nitrate/Nitrite Colorimetric Assay Kit which is based in a Griess assay	Not used	Pseudomonas aeruginosa use NorCB to prevent metabolic cycling of NO. Measurements in mutant cultures devoid of Fhp or NorCB (NO reductase) activity.	[13]
P450nor	*Cylindrocarpon tonkinense* and *Fusarium oxysporum*	NO	Flash-photolysis and Stopped-flow rapid scan Optical absorption	NADH or NADPH	NO reduction reaction for three Nor's from two denitrifying fungi	[28]
P450nor	*Fusarium oxysporum*	NO	Semiempirical method SAM1	Not used	NO reduction in synzyme (i.e. a heme site, a hydrogen-network-network, and an NADH binding site)	[29]
P450nor	*Fusarium oxysporum*	NO	Hartree–Fock and DFT calculations	NADH	The role of NADH as electron agent reducer	[30]
P450nor	*Fusarium oxysporum*	NO	UV/Vis spectroscopy	Not used	Mechanistic studies/Protecting the fungus from NO inhibition of mitochondria especially when O_2 becomes limiting	[20]
P450nor	*Fusarium oxysporum*	NO	DFT studies Monte Carlo multiple minimum algorithm	NADH as cofactor	Interaction between NOR, NO and NADH	[31]
P450nor	*Recombinant Anor from Escherichia coli*	NO	Spectroelectrochemistry	Not used	Quantify NOR activity from a P450-type NOR	[32]
NOR1	*Histoplasma capsulatum* (404 amino acid fragment of Nor1p was expressed in *Escherichia coli* and purified to homogeneity)	NO	UV/Vis Spectroscopy	NADH as the direct reductant	Detoxifying NO during infection/Persistent infection	[19]
Anor GDH Enzymes co-immobilized in epoxide- and carboxyl-functionalized microspheres	*NOR from Aspergillus oryzae – recombinant Anor from Escherichia coli and GDH isozyme from Bacillus megaterium*	NO	4-amino-5-methylamino- 2', 7 - difluorescein (DAF-FM) method and proliferation assay for cell viability	Not used	Quantitative reduction of NO in cell culture U937 cells Slow-releasing NO donor, SNAP	[33]

Table 4.1. NOR classes and representative organism for NO or O_2 detection (continued).

NOR class	Representative organism	Substrate	Method	Electron donor	Purpose/application	Ref.
Reduced heme/non-heme diiron(II) complex NOR model	*Not used*	NO O_2	UV/Vis, NMR, infrared and resonance Raman spectroscopy	Not used	NOR chemistry, and suggestions for the mechanism(s) of the observed reactions and product NO_x formation	[34]
$[(^5L)Fe^{II}...Fe^{II}-Cl]^+$						
Fe, FeFe or FeCu-PhOH catalyst models	*Not used*	O_2	Electrochemistry (CV, LSV in IDA AuE) and Raman spectroscopy	Not used	Generation of PROS Mechanistic studies	[35]
Cytochrome P450 55B1	*Chlamydomonas reinhardtii* *Expressed in Escherichia coli*	NO	Fluorescence	Not used	NO release from the rat liver homogenate stimulated by l-arginine was determined by the fluorescence NO biosensor.	[36]
Hexaheme cytochrome c NOR	*Desulfovibrio desulfuricans, Wolinella succinogenes and Escherichia coli*	NO	Mass spectrometry	Dithionite Ascorbate+PMS	N_2O production	[37]
nor_S-6H	*Ralstonia eutropha*	NO	EPR Optical absorption	NADH NADH+2-methyl-1,4-naphthoquinone NADH+tetramethyl-1,4-benzoquinone NADH+2,3-dimethoxy-5-methyl-1,4-benzoquinone NADH+cytochrome c (horse heart) TMPD+ascorbate PMS+ascorbate	NO reduction	[38]

BNC, binuclear center; CV, cyclic voltammetry; DFT, density functional theory calculations; EPR, electron paramagnetic resonance; FNOR, flavodiiron nitric oxide reductase; LSV, linear sweep voltammetry; MCD, magnetic circular dichroism; NADH, reduced nicotinamide adenine dinucleotide; NO, nitric oxide; NOR, nitric oxide reductase; PESH, reduced phenazine ethosulfate; PMS, phenazine methasulfate; PROS, partially reduced oxygen species.

Electrochemical biosensors, in particular third-generation biosensors (based on direct electron transfer (DET), i.e. in the absence of mediators, [39-43]) are the next promising step to detect NO in *in vivo* studies.

Recent works have permitted to obtain crucial information on NOR catalysis behaviour towards NO, however, some questions still remain unanswered due to controversial opinions [5, 10] One of those questions rely on the competition between the two most important substrates of this enzyme, NO and O_2. Therefore, in this study, NOR purified from *Marinobacter hydrocarbonoclasticus* was adsorbed onto a pyrolytic graphite electrode (PGE) to produce an unmediated enzymatic biosensor (PGE/NOR) for characterization of NOR direct electrochemical behaviour and NOR bioelectrocatalytic activity, as well as its electroanalytical features towards NO and O_2.

4.2. Materials and methods

4.2.1. Reagents

n-dodecyl-*β*-D-maltoside (DM), di-potassium hydrogen phosphate (K_2HPO_4, >99%) and sulfuric acid (H_2SO_4, 96%) were purchased from Panreac (Spain), 2-phenylethanol (PE, ≥ 99.0%) from Sigma-Aldrich (Germany) and ethanol (>96%) from Carlo Erba (Italy). Potassium hydroxide (KOH, 87.50%) and potassium dihydrogen phosphate (KH_2PO_4, 99.50%) were bought from Pronolab (Mexico) and Merck (USA), respectively. NO and O_2 with the desired concentrations were prepared by dilution from buffer stock solutions. NO solutions of different concentrations were prepared by dilution from a buffer stock solution of 100 $\mu molL^{-1}$ prepared by bubbling a 5% NO/95% He gas mixture (Air Liquid, Portugal) into phosphate buffer 100 $mmolL^{-1}$ pH 6.0. For the O_2 effect study, the O_2 concentration was varied by adding different volumes of air-equilibrated water (assumed as being 245 $\mu molL^{-1}$ at 25°C) to the anaerobic reaction mixture. All solutions and stock were prepared immediately before being used. Ultrapure water obtained from a Millipore water purification system (18 MΩ, Milli-Q; Millipore, Molsheim, France) was used in all experiments.

4.2.2. NOR purification and characterization

NOR is not commercially available and it was purified from membrane extracts of *Marinobacter hydrocarbonoclasticus* grown anaerobically as described by Prudêncio

et al. [44]. The enzyme purity was estimated by its UV-visible spectrum (Abs_{410}/Abs_{280} ratio of 1.3; UV 1800-Shimadzu, Germany) [45] and electrophoresis assays under denaturation conditions (tricine SDS-PAGE) (Bio-Rad, Mini-PROTEAN® Tetra Handcast Systems, Portugal) based on the protocol of Laemmli [46]. Two bands corresponding to NOR subunits (NorC (17 kDa) and NorB (35-40 kDa)) were obtained and are in agreement with those presented by Girsch and de Vries [47]. Moreover, the specific activity of the purified NOR of 760 U/mg was determined by amperometry with an ISO-NO sensor (2 mm, World Precision Instruments, Inc., UK: one unit corresponds to 1 µmol of NO/min) as described previously by Timóteo et al. [45].

4.2.3. Biosensor preparation

PGE was sequentially hand polished with 5.0, 1.0 and 0.3 µm alumina (Gravimeta Lda, Portugal), briefly sonicated with ethanol and finally rinsed with ultrapure water. Surface activation was performed by cyclic voltammetry (CV) in 0.5 M H_2SO_4 at 100 mVs^{-1} in the range of 0 to 1.6 V *vs*. saturated calomel electrode (SCE). NOR (7 µL of 14 mg/mL – 760 U/mg) was then immobilized on the PGE surface (0.4 cm diameter) using the solvent casting technique and dried using ultra-pure argon [48]. All the assays were conducted inside an anaerobic chamber (MBraun UniLab, Germany), at room temperature, where O_2 concentration was set to 0.1 ppm.

4.2.4. Electrochemical measurements

The PGE/NOR was set as the working electrode, and a platinum wire and SCE were the secondary and reference electrodes, respectively. The three-electrode system was connected to an µAUTOLAB potentiostat controlled by GPES 4.9.7 software (Eco Chimie). The redox behaviour of NOR was evaluated by CV at different scan rates (from 0.10 to 2.0 Vs^{-1}) in a potential range of 0.4 to -0.9 V with a previous deoxygenation of the buffer solution (100 $mmolL^{-1}$ potassium phosphate buffer, 0.02% (v/v) DM and 0.01% PE at pH 6.0) using ultra-pure argon gas during 20 minutes. For the O_2 effect study, the O_2 concentration was varied by adding different volumes of air-equilibrated water (assumed as being 245 $\mu molL^{-1}$ at 25°C) to the anaerobic reaction mixture. Bioelectrocatalytic studies of NO and O_2 reduction were performed by CV at 5 mVs^{-1} and by square wave voltammetry (SWV) at 8 Hz, step

potential of 6 mV and amplitude of 20 mV in the same, as previously described, potential range.

4.3. Results and discussion

4.3.1. Characterization of the nitric oxide reductase-based biosensor

The characterization of the DET of the purified NOR was firstly performed by CV at 0.50 Vs^{-1} in buffer solution (100 $mmolL^{-1}$ potassium phosphate, 0.02% DM and 0.01% PE) at pH 6.0 under anaerobic conditions (Fig. 4.1-(A)). The pH of 6.0 was chosen based on the previous data reported by Duarte et al. [5] and Garny et al. [49] since, at this value, maximum enzyme catalytic activity was attained due to the protonation of the residues surrounding the catalytic centre. A cathodic (at 0.28 V) and an anodic (at 0.26 V) peak were detected with a formal potential ($E^{0'}$) of -0.27 ± 0.01 V at 0.50 Vs^{-1} corresponding to the low spin heme b_3 of the NOR bi-nuclear catalytic center, which is related to the reduction/oxidation of heme–(Fe(III)/Fe(II)) groups in accordance with Cordas et al. [10]. The observed cathodic (I_{pc}) and anodic (I_{pa}) peak current ratio (I_{pa}/I_{pc}) ≈ 1 and the linear regressions of the I_{pc} and I_{pa} *versus* the tested scan rates (v; 0.10 to 2.0 Vs^{-1})) (Fig. 4.1-(B)); $I_{pc}(A) = - 2.56\times10^{-6} \pm 4.70\times10^{-8}$ v (Vs^{-1}) $- 1.32\times10^{-7} \pm 3.68\times10^{-8}$; r^2=0.997; n=10 and $I_{pa}(A) = 2.60\times10^{-6} \pm 4.90\times10^{-8}$v ($Vs^{-1}$) + $7.17\times10^{-8} \pm 3.83\times10^{-8}$; r^2=0.997; n=10) indicated that this is a surface electron-transfer process with no diffusion control [50]. The peak to peak separation (ΔEp) was ≈ 0 mV for the highest scan rates (0.35 to 2.00 Vs^{-1}), which is in agreement with the theoretical value for ideal surfaces, but ΔEp ≈ 30 mV for the lowest scan rates (0.1 to 0.23 Vs^{-1}). This profile could be influenced by the amino acids around the heme b_3, the protonation states of ligands to the heme iron or the protonation of the water molecule coordinated to the iron center [51]. SWV assays allowed to observe the other three peaks of heme NOR centers in addition to the redox signal of the previously described heme b_3-center (Fig. 4.1-(C)), due to the SWV higher sensitivity when compared with CV. The NOR reduction potential was determined for heme *c*, heme *b*, heme b_3 and non-heme Fe_B as being 0.095±0.002, -0.108±0.008, -0.328±0.001 and -0.635±0.004 V, respectively (Fig. 4.1-(C)) (at 50 Hz, step potential of 5 mV and amplitude of 20 mV). These results are in agreement with those previously reported for formal potentials of NOR by Cordas et al. [10] except for heme *c* with a value of 0.059 V with non-significant deviations for the others three centers. Moreover, dependence between the peak current and the scan rate was perceived for all three redox centers that were not detected by CV (heme *c:* I_p (A) = -

$9.83\times10^{-7} \pm 1.62\times10^{-7}$ v (Vs^{-1}) – $2.75\times10^{-8} \pm 3.64\times10^{-8}$; r^2=0.995; n=6; heme *b*: I_p (A) = - $1.04\times10^{-6} \pm 6.28\times10^{-8}$ v (Vs^{-1}) + $4.09\times10^{-8} \pm 2.33\times10^{-8}$; r^2=0.99; n=7; non-heme Fe_B: I_p (A) = - $2.05\times10^{-6} \pm 1.67\times10^{-7}$ v (Vs^{-1}) – $2.75\times10^{-7} \pm 4.66\times10^{-8}$; r^2=0.994; n=7) (Fig. 4.1-(D)).

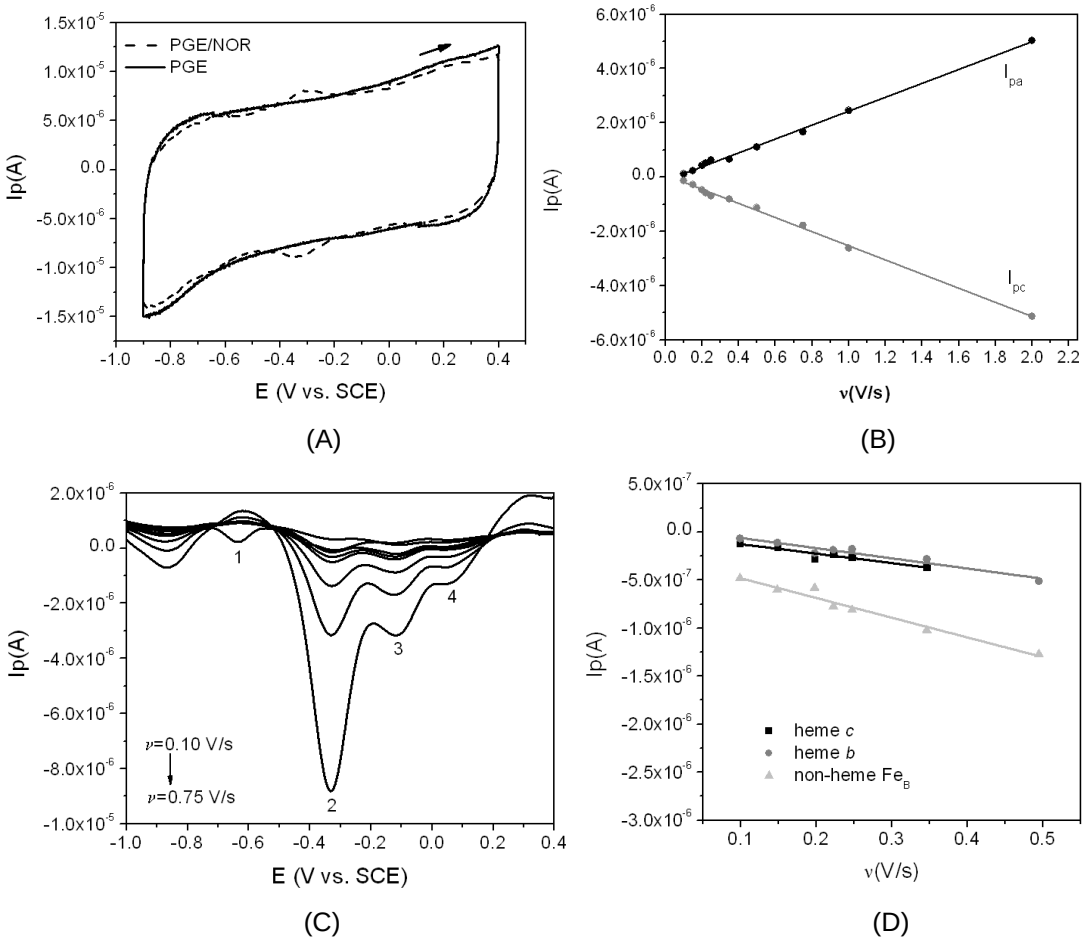

Fig. 4.1. (A) Representative cyclic voltammograms of the electrochemical behavior of PGE and PGE/NOR in buffer solution at 0.50 Vs^{-1}. (B) Influence of the scan rate (0.10, 0.15, 0.20, 0.22, 0.25, 0.35, 0.50, 0.75, 1.0 and 2.0 Vs^{-1}) on the oxidation and reduction peak current of the principal heme center of NOR (heme b_3). (C) Square-wave voltamograms of PGE/NOR biosensor at different frequencies (20, 30, 40, 45, 50, 70, 100 and 150 Hz) (step potential of 5 mV and amplitude of 20 mV) showing the non-heme Fe_B (1), heme b_3 (2), heme *b* (3) and heme *c* (4) peak centers. (D) Influence of the scan rate (0.10, 0.15, 0.20, 0.22, 0.25, 0.35 and 0.50 Vs^{-1}) on the reduction peak current of non-heme Fe_B, heme *b* and heme *c* peak centers. Experimental conditions: Assays were performed under anaerobic conditions in 100 $mmolL^{-1}$ potassium phosphate pH 6.0, 0.02% n-dodecyl-*β*-D-maltoside and 0.01% 2-phenylethanol.

The surface concentration of the electroactive species, rate constant and Michaelis Menten constant were also determined using the obtained electrochemical data. The surface concentration of the electroactive species (**τ***, molcm^{-2}) was estimated based on equation 2 [52]:

$$Q=nFA\tau^* \qquad \text{(Eq. 2)}$$

where **Q** (A.s) is the charge involved in the reaction, **A** (cm^2) is the geometric area of the working electrode, **n** is the number of the electron transferred, **F** (sA.mol^{-1}) is the Faraday constant, as being 1.2×10^{-11} molcm^{-2}, corresponds to a multilayer coating. By applying the Laviron model [53], a value of the rate constant, k_s, for the redox reaction of the catalytic heme b_3 centre was assessed as 0.60 s^{-1}, demonstrating the high electron transfer between NOR and the electrode surface.

4.3.2. Nitric oxide bioelectrocatalysis

In this work, the NO bioelectrocatalysis by the PGE/NOR was followed by SWV and CV (Fig. 4.2). Heme proteins-modified electrodes using haemoglobin, myoglobin, cytochrome *c*, among others, have been applied for the detection of NO [54-56]. NOR, a specific bacterial heme protein, bioelectrocatalyses directly the NO to N_2O reduction (-0.71 ± 0.01 V; Fig. 4.2-(A)) with the release of water according to the reaction $2NO+2e^-+2H^+\rightarrow N_2O+H_2O$ (eq. 3) [7], thus avoiding the necessity of using electroactive mediators. The irreversible behavior of NO reduction at the developed biosensor may be observed in Fig. 4.2-(B); the respective insets exhibit the attained calibration curve data (square wave voltammograms and corresponding mean regression equation) when the PGE/NOR was exposed to different concentration of dissolved NO (0.50 to 6.98 µmolL^{-1}): I_p (A) = $-4.00\times10^{-8} \pm 1.84\times10^{-9}$ [NO] (µmolL^{-1}) - $1.36\times10^{-7} \pm 6.78\times10^{-9}$; r^2=0.99; n=6; (Fig. 4.2-(B)). These results were used to determine the detection (LOD; 3× the standard deviation of the y-intercept (Sy)/slope) and quantification (LOQ; 10×Sy-intercept/slope) limits [57], as being 0.5 and 1.7 µmolL^{-1}, respectively. The apparent Michaelis Menten constant ($\boldsymbol{K_m}$, µmolL^{-1}) was also estimated according to the Lineweaver/Burk equation (eq. 4).

$$1/I_{ss}=K_m/I_{max}\times1/C+1/I_{max} \qquad \text{(Eq. 4)}$$

where $\mathbf{I_{ss}}$ (A) is the steady-state current after addition of the substrate; **C** ($\mu molL^{-1}$) is the concentration of the substrate; $\mathbf{I_{max}}$ (A) is the maximum current measured under saturated substrate conditions [58]. The attained K_m value, 2.1 $\mu molL^{-1}$, is similar than 2.2 $\mu molL^{-1}$, which was reported by Duarte et al. [5] proving the great affinity of this purified NOR for the NO substrate. This behaviour may be due to the efficient orientated immobilization of the catalytic center of NOR and its availability for NO reduction [5].

NOR was shown to be a divergent member of the superfamily of O_2-reducing heme-copper oxidases [59]. This enzyme was also reported to be catalytically active towards O_2 reduction trough the following reaction: $O_2+4H^++4e^-\rightarrow 2H_2O$ (eq. 5) [15]. Therefore, the influence of O_2 (at 5.98 $\mu molL^{-1}$) on the NO reduction was similarly characterized. No significant interference on sensitivity towards NO was perceived since the following data were achieved: I_p (A) = $-3.76\times10^{-8} \pm 1.95\times10^{-9}$ [NO] ($\mu molL^{-1}$) – $9.87\times10^{-8} \pm 7.19\times10^{-9}$; r^2=0.99; n=6) (Fig. 4.2-(C)); the ratio between regression equation slopes (in the absence and presence of O_2) was 1.06. Therefore, the attained biosensor sensitivity seems adequate to determine the NO release in biological systems or in environmental studies under anaerobic or aerobic conditions.

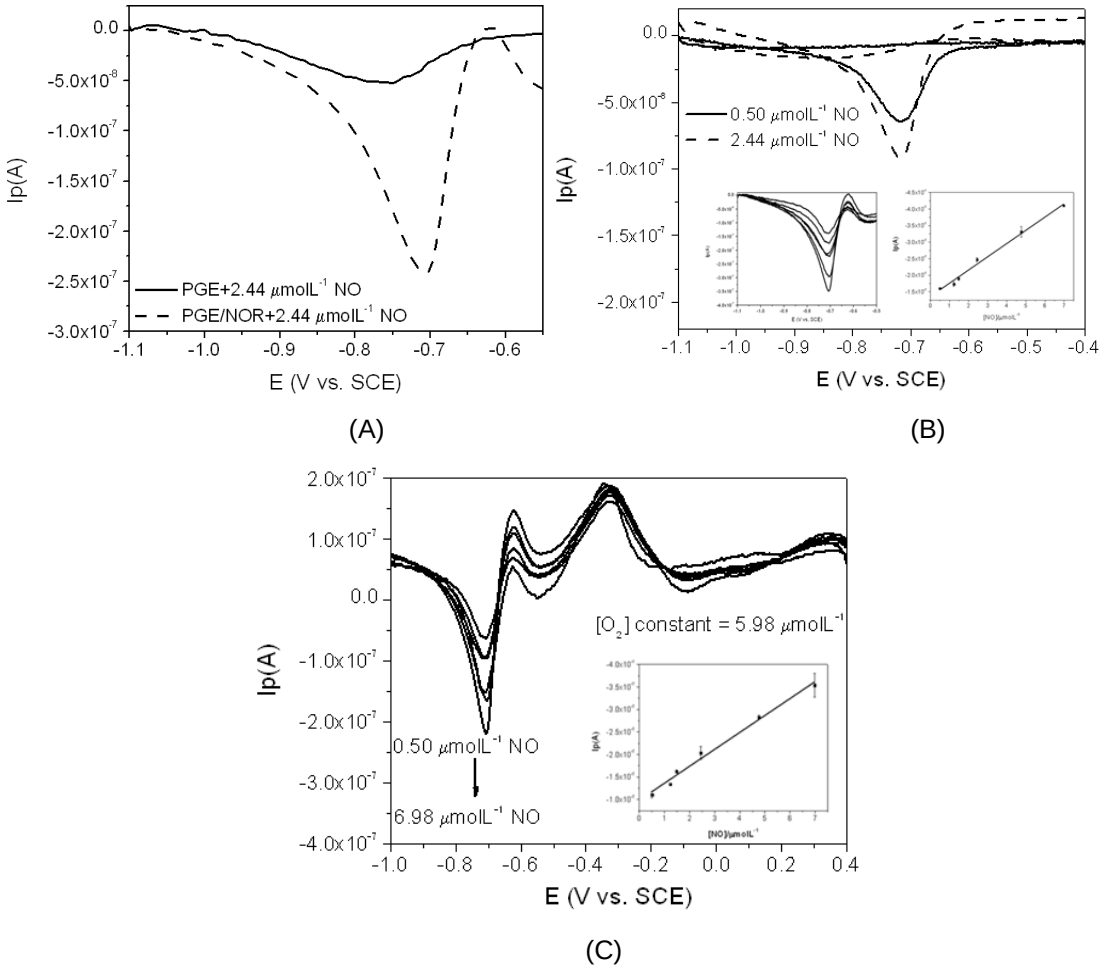

Fig. 4.2. (A) Comparative square-wave voltammograms of the PGE and PGE/NOR exposed to 2.44 μmolL^{-1} NO. (B) Cyclic voltammograms of PGE/NOR biosensor exposed to two different NO concentrations (0.50 and 2.44 μmolL^{-1}); Inset: Square-wave voltamograms of NOR – catalysed NO reduction at 0.50, 1.23, 1.48, 2.44, 4.76, 6.98 μmolL^{-1} and the respective peak current vs NO concentration curve. (C) Square-wave voltamograms of NOR – catalysed NO reduction at the same concentrations as indicated in (B) but in the presence of 5.98 μmolL^{-1} of O_2; Inset: Respective peak current vs NO concentration curve. Experimental conditions: Assays were performed under anaerobic conditions in 100 mmolL^{-1} potassium phosphate pH 6.0, 0.02% n-dodecyl-*β*-D-maltoside and 0.01% 2-phenylethanol at 5 mVs^{-1} for CV and at frequency of 8 Hz, step potential of 6 mV and amplitude of 20 mV for SWV.

4.3.3. Dioxygen bioelectrocatalysis

Using the same approach as the one applied for NO, the O_2 bioelectrocatalysis by NOR was studied by CV and SWV in the absence (Fig. 4.3-(A)-(B)) and in the presence (Fig. 4.3-(C)) of NO. The efficient O_2 bioelectrocatalysis by NOR promoted the appearance of an irreversible reduction peak at -0.25 ± 0.02 V (Fig. 4.3-(A)-(B)), which increased linearly with the O_2 concentration from 1.22 to 11.67 $\mu molL^{-1}$. When NO was introduced at the 2.44 $\mu molL^{-1}$ level, a significant negative impact on the biosensor sensitivity towards O_2 was perceived with a value about 3.6 times lower (I_p (A)=-7.57×10^{-9} ± 2.71×10^{-10} [O_2] ($\mu molL^{-1}$) - 8.06×10^{-10} ± 1.09×10^{-9}; r^2=0.994; n=6) than the reached in the absence of NO (I_p (A)=-2.71×10^{-8} ± 1.44×10^{-9} [O_2] ($\mu molL^{-1}$) - 3.93×10^{-8} ± 9.89×10^{-9}; r^2=0.99; n=6). On the other hand, the peak current of NO did not suffered any marked effect due to the augmentation of the O_2 concentration in the electrolyte, being stable at 1.89 ×10^{-7} ± 9.00 ×10^{-9} A (RSD = 4.8% at 2.44 $\mu molL^{-1}$; n=6) (Fig. 4.3-(C)). As expected, the determined LOD (1.0 $\mu molL^{-1}$) and LOQ (3.2 $\mu molL^{-1}$) values for O_2 electroanalysis were considerably higher than those reached for NO detection. Also, the greater Michaelis Menten constant value (7.0 $\mu molL^{-1}$), when compared to the K_m obtained for the bioelectrocatalysis of NO (2.1 $\mu molL^{-1}$), reinforced the higher affinity of NOR to NO and the preference of this enzyme for its natural substrate.

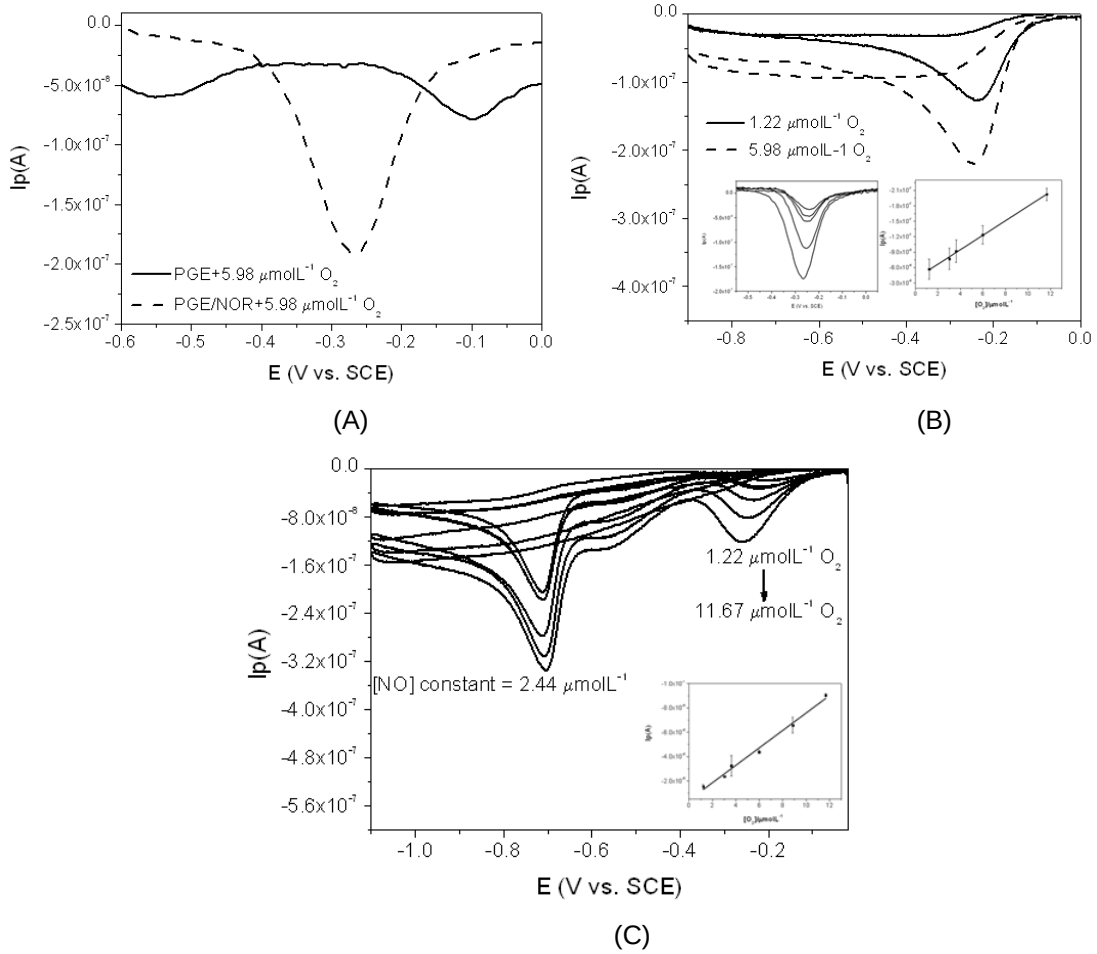

Fig. 4.3. (A) Comparative square-wave voltammograms of the PGE and PGE/NOR exposed to 5.98 µmolL^{-1} O_2. (B) Cyclic voltammograms of PGE/NOR biosensor exposed to two different O_2 concentrations (1.22 and 5.98 µmolL^{-1}); Inset: Square-wave voltamograms of NOR – catalysed O_2 reduction at 1.22, 3.02, 3.62, 5.98, 11.67 µmolL^{-1} and the respective peak current vs O_2 concentration curve. (C) Cyclic voltamograms of NOR – catalysed O_2 reduction at the same concentrations as indicated in (B) but in the presence of 2.44 µmolL^{-1} of NO; Inset: Respective peak current vs O_2 concentration curve. Experimental conditions: Assays were performed under anaerobic conditions in 100 mmolL^{-1} potassium phosphate pH 6.0, 0.02% n-dodecyl-β-D-maltoside and 0.01% 2-phenylethanol at 5 mVs^{-1} for CV and at frequency of 8 Hz, step potential of 6 mV and amplitude of 20 mV for SWV.

4.4. Conclusions

A third generation biosensor composed by PGE/NOR was used to characterize the NOR electrochemical behaviour. Considering that NOR is catalytically active towards NO and O_2 reduction, the bioelectrocatalysis of these two substrates, under anaerobic conditions, was studied when both existed separately and when the two substrates were in competitive environment. NOR demonstrated to have affinity for both substrates but exhibited a lower Michaelis Menten constant (2.1 for NO *vs.* 7.0 $\mu molL^{-1}$ for O_2) for its natural substrate (NO). The attained high sensitivity for NO suggests the potential applicability of this NOR-based biosensor to real biological samples in aerobic conditions and demonstrate the possibility of using NOR in the design of unmediated nitric oxide biosensors. Still, further studies are needed to characterize other possible interfering substrates existing in real matrices. Moreover, future research is being undertaken to enhance the NOR electron transfer rate and lifetime at the PGE.

4.5. References

[1] P. Tavares, A.S. Pereira, J.J.G. Moura, I. Moura, Metalloenzymes of the denitrification pathway, J Inorg Biochem., 100 (2006) 2087-2100.

[2] S. Moncada, R.M. Palmer, E.A. Higgs, Nitric oxide: physiology, pathophysiology, and pharmacology, Pharmacol. Rev, 43 (1991) 109-142.

[3] F.X. Guix, I. Uribesalgo, M. Coma, F.J. Muñoz, The physiology and pathophysiology of nitric oxide in the brain, Prog Neurobiol., 76 (2005) 126-152.

[4] W.G. Zumft, Nitric oxide reductases of prokaryotes with emphasis on the respiratory, heme-copper oxidase type, J Inorg Biochem., 99 (2005) 194-215.

[5] A.G. Duarte, C.M. Cordas, J.J.G. Moura, I. Moura, Steady-state kinetics with nitric oxide reductase (NOR): New considerations on substrate inhibition profile and catalytic mechanism, Biochim. Biophys. Acta., 1837 (2014) 375-384.

[6] Faye H. Thorndycroft, G. Butland, David J. Richardson, Nicholas J. Watmough, A new assay for nitric oxide reductase reveals two conserved glutamate residues form the entrance to a proton-conducting channel in the bacterial enzyme, Biochem J, 401 (2007) 111-119.

[7] L.M. Blomberg, M.R.A. Blomberg, P.E.M. Siegbahn, Reduction of nitric oxide in bacterial nitric oxide reductase—a theoretical model study, Biochim. Biophys. Acta., 1757 (2006) 240-252.

[8] S.J. Field, M.D. Roldan, S.J. Marritt, J.N. Butt, D.J. Richardson, N.J. Watmough, Electron transfer to the active site of the bacterial nitric oxide reductase is controlled by ligand binding to heme b_3, Biochim. Biophys. Acta., 1807 (2011) 451-457.

[9] S.M. Kapetanaki, S.J. Field, R.J. Hughes, N.J. Watmough, U. Liebl, M.H. Vos, Ultrafast ligand binding dynamics in the active site of native bacterial nitric oxide reductase, Biochim. Biophys. Acta., 1777 (2008) 919-924.

[10] C.M. Cordas, A.G. Duarte, J.J.G. Moura, I. Moura, Electrochemical behaviour of bacterial nitric oxide reductase—Evidence of low redox potential non-heme Fe_B gives new perspectives on the catalytic mechanism, Biochim. Biophys. Acta., 1827 (2013) 233-238.

[11] C.M. Cordas, A.S. Pereira, C.E. Martins, C.G. Timóteo, I. Moura, J.J.G. Moura, et al., Nitric oxide reductase: Direct electrochemistry and electrocatalytic activity, ChemBioChem, 7 (2006) 1878-1881.

[12] M.R. Blomberg, P.E. Siegbahn, Why is the reduction of NO in cytochrome *c* dependent nitric oxide reductase (cNOR) not electrogenic?, Biochim. Biophys. Acta., 1827 (2013) 826-833.

[13] J.L. Robinson, J.M. Jaslove, A.M. Murawski, C.H. Fazen, M.P. Brynildsen, An integrated network analysis reveals that nitric oxide reductase prevents metabolic cycling of nitric oxide by *Pseudomonas aeruginosa*, Metab Eng, 41 (2017) 67-81.

[14] T. Sakurai, S. Nakashima, K. Kataoka, D. Seo, N. Sakurai, Diverse NO reduction by *Halomonas halodenitrificans* nitric oxide reductase, Biochem. Biophys. Res. Commun, 333 (2005) 483-7.

[15] M.R.A. Blomberg, P. Adelroth, The mechanism for oxygen reduction in cytochrome *c* dependent nitric oxide reductase (cNOR) as obtained from a combination of theoretical and experimental results, Biochim. Biophys. Acta., 1858 (2017) 884-894.

[16] S. Al-Attar, S. de Vries, An electrogenic nitric oxide reductase, FEBS Lett, 589 (2015) 2050-2057.

[17] V. Daskalakis, T. Ohta, T. Kitagawa, C. Varotsis, Structure and properties of the catalytic site of nitric oxide reductase at ambient temperature, Biochim. Biophys. Acta., 1847 (2015) 1240-1244.

[18] E. Terasaka, N. Okada, N. Sato, Y. Sako, Y. Shiro, T. Tosha, Characterization of quinol-dependent nitric oxide reductase from *Geobacillus stearothermophilus*: enzymatic activity and active site structure, Biochim. Biophys. Acta., 1837 (2014) 1019-1026.

[19] L.Y. Chao, J. Rine, M.A. Marletta, Spectroscopic and kinetic studies of Nor1, a cytochrome P450 nitric oxide reductase from the fungal pathogen histoplasma capsulatum, Arch Biochem Biophys, 480 (2008) 132-137.

[20] A. Daiber, H. Shoun, V. Ullrich, Nitric oxide reductase (P450nor) from *Fusarium oxysporum*, J Inorg Biochem, 99 (2005) 185-193.

[21] F. Wu, P. Yu, L. Mao, Bioelectrochemistry for in vivo analysis: Interface engineering toward implantable electrochemical biosensors, Curr. Opin. Electrochem., 5 (2017) 152-157.

[22] T.M.B.F. Oliveira, M.F. Barroso, S. Morais, M. Araújo, C. Freire, P. de Lima-Neto, et al., Sensitive bi-enzymatic biosensor based on polyphenoloxidases–gold nanoparticles–chitosan hybrid film–graphene doped carbon paste electrode for carbamates detection, Bioelectrochemistry, 98 (2014) 20-9.

[23] T.M.B.F. Oliveira, M. Fátima Barroso, S. Morais, M. Araújo, C. Freire, P. de Lima-Neto, et al., Laccase–Prussian blue film–graphene doped carbon paste modified electrode for carbamate pesticides quantification, Biosens Bioelectron, 47 (2013) 292-299.

[24] F.W.P. Ribeiro, M.F. Barroso, S. Morais, S. Viswanathan, P. de Lima-Neto, A.N. Correia, et al., Simple laccase-based biosensor for formetanate hydrochloride quantification in fruits, Bioelectrochemistry, 95 (2014) 7-14.

[25] L. Salomonsson, J. Reimann, T. Tosha, N. Krause, N. Gonska, Y. Shiro, et al., Proton transfer in the quinol-dependent nitric oxide reductase from *Geobacillus stearothermophilus* during reduction of oxygen, Biochim. Biophys. Acta., 1817 (2012) 1914-1920.

[26] J. Reimann, U. Flock, H. Lepp, A. Honigmann, P. Adelroth, A pathway for protons in nitric oxide reductase from *Paracoccus denitrificans*, Biochim. Biophys. Acta., 1767 (2007) 362-373.

[27] S. Ramos, R.M. Almeida, C.M. Cordas, J.J.G. Moura, S.R. Pauleta, I. Moura, Insights into the recognition and electron transfer steps in nitric oxide reductase from *Marinobacter hydrocarbonoclasticus*, J Inorg Biochem., 177 (2017) 402-411.

[28] N. Toritsuka, H. Shoun, U.P. Singh, S.Y. Park, T. Iizuka, Y. Shiro, Functional and structural comparison of nitric oxide reductases from denitrifying fungi *Cylindrocarpon tonkinense* and *Fusarium oxysporum*, Biochim. Biophys. Acta., 1338 (1997) 93-99.

[29] K. Tsukamoto, S. Nakamura, K. Shimizu, SAM1 semiempirical calculations on the catalytic cycle of nitric oxide reductase from *Fusarium oxysporum*, J Mol Struc Theochem, 624 (2003) 309-322.

[30] K. Tsukamoto, T. Watanabe, U. Nagashima, Y. Akiyama, Hartree–Fock and density functional theory calculations for the reaction mechanism of nitric oxide reductase cytochrome P450nor from *Fusarium oxysporum*, J Mol Struc Theochem, 732 (2005) 87-98.

[31] D.K. Menyhárd, G.M. Keserű, Binding mode analysis of the NADH cofactor in nitric oxide reductase: A theoretical study, J Mol Graph Model, 25 (2006) 363-372.

[32] S. Garny, J. Verschoor, N. Gardiner, J. Jordaan, Spectrophotometric activity microassay for pure and recombinant cytochrome P450-type nitric oxide reductase, Anal Biochem, 447 (2014) 23-29.

[33] S. Garny, N. Beeton-Kempen, I. Gerber, J. Verschoor, J. Jordaan, The co-immobilization of P450-type nitric oxide reductase and glucose dehydrogenase for the continuous reduction of nitric oxide via cofactor recycling, Enzyme Microb Technol, 85 (2016) 71-81.

[34] T.D. Ju, A.S. Woods, R.J. Cotter, P. Moënne-Loccoz, K.D. Karlin, Dioxygen and nitric oxide reactivity of a reduced heme/non-heme diiron(II) complex $[(5L)Fe^{II}\cdot\cdot Fe^{II}Cl]^{+}$ using a tethered tetraarylporphyrin for the development of an active site reactivity model for bacterial nitric oxide reductase, Inorg Chim Acta, 297 (2000) 362-372.

[35] J.P. Collman, A. Dey, Y. Yang, S. Ghosh, R.A. Decreau, O_2 reduction by a functional heme/nonheme bis-iron NOR model complex, Proc Natl Acad Sci U S A, 106 (2009) 10528-10533.

[36] Y. Li, Q. Liu, X. Liang, Q. Xiao, Y. Fang, Y. Wu, A new fluorescence biosensor for nitric oxide detection based on cytochrome P450 55B1, Sens Actuators B Chem, 230 (2016) 405-410.

[37] C. Costa, A. Macedo, I. Moura, J.J. Moura, J. Le Gall, Y. Berlier, et al., Regulation of the hexaheme nitrite/nitric oxide reductase of *Desulfovibrio desulfuricans*, *Wolinella succinogenes* and *Escherichia coli*. A mass spectrometric study, FEBS Lett, 276 (1990) 67-70.

[38] R. Cramm, A. Pohlmann, B. Friedrich, Purification and characterization of the single-component nitric oxide reductase from *Ralstonia eutropha* H16, FEBS Lett, 460(1999) 6-10.

[39] Y. Wu, S. Hu, Biosensors based on direct electron transfer in redox proteins, Microchim Acta, 159 (2007) 1-17.

[40] W. Zhang, G. Li, Third-generation biosensors based on the direct electron transfer of proteins, Anal Sci, 20 (2004) 603-609.

[41] X. Wu, F. Zhao, J.R. Varcoe, A.E. Thumser, C. Avignone-Rossa, R.C.T. Slade, Direct electron transfer of glucose oxidase immobilized in an ionic liquid reconstituted cellulose–carbon nanotube matrix, Bioelectrochemistry, 77 (2009) 64-68.

[42] T. Kuwahara, T. Asano, M. Kondo, M. Shimomura, Bioelectrocatalytic O_2 reduction with a laccase-bearing poly(3-methylthiophene) film based on direct electron transfer from the polymer to laccase, Bioelectrochemistry, 91 (2013) 28-31.

[43] D. Nie, Y. Liang, T. Zhou, X. Li, G. Shi, L. Jin, Electrochemistry and electrocatalytic of hemoglobin immobilized on FDU-15-Pt mesoporous materials, Bioelectrochemistry, 79 (2010) 248-253.

[44] M. Prudencio, A.S. Pereira, P. Tavares, S. Besson, I. Cabrito, K. Brown, et al., Purification, characterization, and preliminary crystallographic study of copper-containing nitrous oxide reductase from *Pseudomonas nautica* 617, Biochemistry, 39 (2000) 3899-3907.

[45] C.G. Timóteo, A.S. Pereira, C.E. Martins, S.G. Naik, A.G. Duarte, J.J.G. Moura, et al., Low-spin heme b_3 in the catalytic center of nitric oxide reductase from *Pseudomonas nautica*, Biochemistry, 50 (2011) 4251-4262.

[46] U.K. Laemmli, Cleavage of structural proteins during the assembly of the head of bacteriophage T4, Nature, 227 (1970) 680-685.

[47] P. Girsch, S. de Vries, Purification and initial kinetic and spectroscopic characterization of NO reductase from *Paracoccus denitrificans*, Biochim. Biophys. Acta, 1318(1997) 202-16.

[48] U. Siemann, Solvent cast technology – a versatile tool for thin film production, Scattering Methods and the Properties of Polymer Materials, Springer Berlin Heidelberg, Berlin, Heidelberg, 2005, pp. 1-14.

[49] S. Garny, N. Beeton-Kempen, I. Gerber, J. Verschoor, J. Jordaan, The co-immobilization of P450-type nitric oxide reductase and glucose dehydrogenase for the continuous reduction of nitric oxide via cofactor recycling, Enzyme Microb Technol, 85 (2016) 71-81.

[50] J.E. Frew, H.A. Hill, Direct and indirect electron transfer between electrodes and redox proteins, Eur J Biochem, 172 (1988) 261-269.

[51] F. Li, M. Nie, X. He, J. Fei, Y. Ding, B. Feng, Direct electrochemistry and electrocatalysis of hemoglobin on a glassy carbon electrode modified with poly(ethylene glycol diglycidyl ether) and gold nanoparticles on a quaternized cellulose support. A sensor for hydrogen peroxide and nitric oxide, Microchim Acta, 181 (2014) 1541-1549.

[52] D. Grieshaber, R. MacKenzie, J. Vörös, E. Reimhult, Electrochemical biosensors - sensor principles and architectures, Sensors, 8 (2008) 1400.

[53] E. Laviron, General expression of the linear potential sweep voltammogram in the case of diffusionless electrochemical systems, J Electroanal Chem Interfacial Electrochem, 101 (1979) 19-28.

[54] H. Chen, G. Zhao, Nanocomposite of polymerized ionic liquid and graphene used as modifier for direct electrochemistry of cytochrome *c* and nitric oxide biosensing, J Solid State Electrochem, 16 (2012) 3289-3297.

[55] C. Fan, J. Pang, P. Shen, G. Li, D. Zhu, Nitric oxide biosensors based on Hb/phosphatidylcholine films, Anal Sci, 18 (2002) 129-132.

[56] L. Zhang, G.-C. Zhao, X.-W. Wei, Z.-S. Yang, A nitric oxide biosensor based on myoglobin adsorbed on multi-walled carbon nanotubes, Electroanalysis, 17 (2005) 630-634.

[57] J. Mocak, A. Bond, S. Mitchell, G. Scollary, A statistical overview of standard (IUPAC and ACS) and new procedures for determining the limits of detection and quantification: application to voltammetric and stripping techniques (technical report), Pure Appl. Chem., 69 (1997) 297-328.

[58] E. Laviron, Adsorption, autoinhibition and autocatalysis in polarography and in linear potential sweep voltammetry, J Electroanal Chem Interfacial Electrochem, 52 (1974) 355-393.

[59] J.A. Sigman, H.K. Kim, X. Zhao, J.R. Carey, Y. Lu, The role of copper and protons in heme-copper oxidases: kinetic study of an engineered heme-copper center in myoglobin, Proc Natl Acad Sci U S A, 100 (2003) 3629-3634.

CHAPTER 5

THIRD-GENERATION ELECTROCHEMICAL BIOSENSOR BASED ON NITRIC OXIDE REDUCTASE IMMOBILIZED IN A MULTIWALLED CARBON NANOTUBES/1-N-BUTYL-3-METHYLIMIDAZOLIUM TETRAFLUOROBORATE NANOCOMPOSITE FOR NITRIC OXIDE DETECTION

Nitric oxide (NO) has a crucial role in signaling and cellular physiology in humans. Herein, a novel third-generation biosensor based on the *Marinobacter hydrocarbonoclasticus* metalloenzyme (nitric oxide reductase (NOR)), responsible for the NO reduction in the denitrifying processes, was developed through the direct adsorption of a new nanocomposite (multiwalled carbon nanotubes (MWCNTs)/1-n-butyl-3-methylimidazolium tetrafluoroborate ($BMIMBF_4$)/NOR) onto a pyrolytic graphite electrode (PGE) surface. The NOR direct electron transfer behavior (formal potential of -0.255±0.003 V *vs.* Ag/AgCl) and electrocatalysis towards NO reduction (−0.68±0.03 V *vs*. Ag/AgCl) of the PGE/[MWCNTs/$BMIMBF_4$/NOR] biosensor were investigated in phosphate buffer at pH 6.0. Large enzyme loading (2.04×10^{-10} mol/cm^2), acceptable electron transfer rate between NOR and the PGE surface (k_s= 0.35 s^{-1}), and high affinity for NO (K_m=2.17 μmolL^{-1}) were observed with this biosensor composition. A linear response to NO concentration (0.23-4.76 μmolL^{-1}) was perceived with high sensitivity (0.429 μA/μmolL^{-1}), a detection limit of 0.07 μmolL^{-1}, appropriate repeatability (9.1% relative standard deviations (RSD)), reproducibility (6.0-11% RSD) and 80-102% recoveries. The biosensor was stable during 1 month retaining 79-116% of its initial response. These data confirmed that NOR incorporated in the MWCNTs/$BMIMBF_4$ nanocomposite can efficiently maintain its bioactivity paving a new and effective way for NO biosensing.

5.1. Introduction

Nitric oxide radical (•NO, herein abbreviated as NO), produced in humans from *L*-arginine by the action of NO synthases, is one of three fundamental gasotransmitters (together with hydrogen sulfide and carbon monoxide) [1, 2]. NO sensing is needed in a variety of applications, including medical and pharmaceutical industry [3], asthma monitoring [4], human breath [5], rat kidney monitoring [6], among others. Excessive amounts of NO can damage cells and cause many pathological conditions including neurodegenerative diseases, endothelial dysfunction and cancer [7]. Therefore, the development of efficient, fast and selective methods capable of NO detection in the cellular milieu has been in the last years a hot research topic [8].

In bacteria, NO is an intermediate in denitrification, a "respiratory" pathway, where nitrate is reduced to dinitrogen [9]. In this pathway, NO is reduced into nitrous oxide (N_2O), in a reaction catalyzed by the specific nitric oxide reductase (NOR) enzyme [10, 11]. The specificity and efficiency of this enzyme towards NO make them a very interesting target to develop a new biosensor for the NO detection. Until now, NOR has not been used in electrochemical biosensors but, concerning its electrochemical characteristics reported by few authors, its application in third-generation biosensors development could be considered [12-15]. Third generation biosensors are based on the direct electron transfer (DET) of proteins, where the absence of mediator is the main advantage providing high selectivity [16]. Because they operate in a closer potential window to the redox potential of the protein, these biosensors are less prone to interfering reactions [16]. However, the stabilization of the enzyme within the biosensor can be a major problem [17, 18]. Multiwalled carbon nanotubes (MWCNTs) have been widely used as solid platforms to immobilize enzymes in electrochemical biosensors due to their unique physical and chemical properties, namely easy functionalization, high electric conductivity and large surface area, enhancing the electrocatalysis [19-22]. Additionally, room temperature ionic liquids (ILs) may act as electrolytes and solvents in biosensor design [23] being good dispersants for MWCTNs [24]. ILs are a broad class of salts that are liquid below 100 °C [25] and have been recognized as green solvents (as alternative to volatile organic solvents) due to their negligible vapor pressure, good thermal stability and biocompatibility [26]. These sustainable characteristics offer benefits, namely simplicity of containment, recovery and recycling facility [27]. In electrochemistry, ILs also exhibit a wide potential window and appropriate intrinsic conductivity and

viscosity [23, 28]. Recently, they have been successfully explored in the preparation of IL-carbon nanomaterial hybrids since synergistic effects have been noticed, offering unique advantages for electrodeposition, electrosynthesis and electrocatalysis [29]. Furthermore, these composite materials can also be used as immobilization matrix to entrap proteins and enzymes [29, 30].

$BMIMBF_4$ is composed by a small anion tetrafluoroborate and a large organic cation 1-n-butyl-3-methylimidazolium. The high potential applicability of this IL for electrochemical biosensors development can be assessed by the reported studies regarding enzymatic and heme-protein third generation biosensors (Table 5.1 and 5.2). The main applied enzymes (presented by decreasing order of number of studies) were glucose oxidase, horseradish peroxidase, but others, such as choline oxidase, laccase, catalase, superoxide dismutase and chloroperoxidase have been also tested but in a more limited way; the involved substrates were methomyl, superoxide anion, glucose, cholesterol, choline, trichloroacetic acid and hydrogen peroxide (Table 5.1). Furthermore, and because NOR is a hemic enzyme, the heme-protein biosensors that have been described using $BMIMBF_4$ were also reviewed (Table 5.2). Hemoglobin, myoglobin and cytochrome *c* were exploited for H_2O_2, trichloroacetic acid and nitrite biosensing [31-33]. As far as we know, $BMIMBF_4$ or NOR enzyme were not yet explored for the development of biosensors for NO.

Thus, the main aim of this study was to develop a novel third-generation enzymatic biosensor for NO determination taking advantage of the inherent features of *Marinobacter hydrocarbonoclasticus* NOR, MWCNTs and $BMIMBF_4$. With this goal in mind, the selected metalloenzyme (which is not commercially available) was purified, characterized, and subsequently incorporated in an optimized MWCNTs/$BMIMBF_4$ nanocomposite, which was used to modify a pyrolytic graphite electrode (PGE). The DET behavior and electrocatalysis towards NO reduction of the PGE/[MWCNTs/$BMIMBF_4$/NOR] biosensor were investigated. The optimized approach provided high biosensor sensitivity and stability.

Table 5.1. Review of the reported enzymatic biosensors using $BMIMBF_4$.

Transducer	Enzyme	Immobilization	Detection technique	Analyte	Substrate/detected species	Linear range ($\mu mol L^{-1}$)	Limit of detection ($\mu mol L^{-1}$)	Γ^* (mol/cm^2)	k_s (s^{-1})	K_m ($\mu mol L^{-1}$)	Ref.
Carbon ionic liquid electrode	Laccase	Platinum nanoparticles dispersed in $BMIMBF_4$ and mixed with montmorillonite; Enzyme solution drop cast on modified electrode.	Square Wave and Cyclic voltammetry	Pesticide	Methomyl	0.98–9.0	0.235	n.r.	n.r.	n.r.	[34]
Glassy carbon electrode	Catalase	Drop cast of amino functionalized multiwalled carbon nanotubes dispersed in dimethylformamide; Immersion of modified electrode on $BMIMBF_4$; Immersion of modified electrode on enzyme solution.	Cyclic voltammetry and amperometry	H_2O_2	H_2O_2	0.0086–0.14	0.0037	2.88×10^{-10}	2.23	0.118	[35]
Glassy carbon electrode	Superoxide dismutase	Mixture of $HAuCl_4$, $BMIMBF_4$ and chitosan solution; Electrode incubated in this mixture; Enzyme solution drop casted on modified electrode.	Cyclic voltammetry	O_2^-	O_2^-	0.0056–2.7	0.0017	4.55×10^{-10}	4.7	n.r.	[36]
Glassy carbon electrode	Chloroperoxidase	Nafion–ethanol solution was cast onto the electrode surface; Drop cast of $BMIMBF_4$–ethanol onto the modified electrode; Mixture of enzymie and konjac glucomannan onto the modified electrode.	Cyclic voltammetry	H_2O_2	H_2O_2	0–100	n.r.	n.r.	0.7–3.5	n.r.	[37]
Glassy carbon electrode	Cholesterol oxidase	Amino functionalize multiwalled carbon nanotubes dispersed in dimethylformamide drop casted on surface electrode; Modified electrode incubated on $BMIMBF_4$ solution; Modified electrode incubated on enzyme solution.	Cyclic voltammetry Amperometry	Cholesterol	Cholesterol	0.026–3.4	0.012	n.r.	3.11	1.4	[38]

Table 5.1. Review of the reported enzymatic biosensors using $BMIMBF_4$ (continued).

Transducer	Enzyme	Immobilization	Detection technique	Analyte	Substrate/ detected species	Linear range ($\mu mol L^{-1}$)	Limit of detection ($\mu mol L^{-1}$)	Γ^* (mol/cm^2)	k_s (s^{-1})	K_m ($\mu mol L^{-1}$)	Ref.
Glassy carbon electrode	Choline oxidase	Drop cast of amino functionalized multiwalled carbon nanotubes dispersed in dimethylformamide; Immersion of modified electrode on $BMIMBF_4$; Immersion of modified electrode on enzyme solution.	Cyclic voltammetry and amperometry	Choline	Choline	6.9–67	2.7	n.r.	2.74	320	[39]
Glassy carbon electrode	Choline oxidase	Drop cast of amino functionalized multiwalled carbon nanotubes dispersed in dimethylformamide; Immersion of modified electrode on $BMIMBF_4$; Immersion of modified electrode on enzyme solution.	Cyclic voltammetry and amperometry	Choline	Choline	8–700	4.40	5.83×10^{-10}	1.91	n.r.	[40]
Glassy carbon electrode	Choline oxidase	Carboxylated carbon nanotubes (single walled or multi walled) dispersed in dimethylformamide onto the electrode surface; Immersion on $BMIMBF_4$ solution; Immersion on enzyme solution.	Cyclic voltammetry and amperometry	Choline	Choline	10–700 10–800	10 100	9.07×10^{-9} 1.38×10^{-8}	0.78 2.47	790 1070	[41]
Gold electrode	Glucose oxidase	Electrodeposition of gold nanoparticles; Mixture of p-benzoquinone, chitosan, glucose oxidase and $BMIMBF_4$ for electrodeposition.	Amperometry	Glucose	H_2O_2	3.0–9000	1.5	n.r.	n.r.	7800	[42]
Platinum electrode	Glucose oxidase	Deposition of Prussian blue at electrode surface; The modified platinum electrode was immersed on enzyme and $BMIMBF_4$ in chitosan solution.	Cyclic voltammetry and Chronoampero metry	Glucose	Glucose	10 to 4200	5	n.r.	n.r.	6600	[43]
Glassy carbon electrode	Glucose oxidase	Copper hexacyanoferrate/polypyrrole modified electrode; Glutaraldehyde-enzyme-$BMIMBF_4$.	Chronoampero metry	Glucose	Glucose	100–800	14–190	n.r.	n.r.	390	[44]
Glassy carbon electrode	Glucose oxidase	Mixture of Polyhydroxy-C60 with enzyme solution drop casted on surface electrode; $BMIMBF_4$ on modified electrode.	Cyclic voltammetry	Glucose	Glucose	20–2000	1	5.33×10^{-10}	n.r.	1450	[45]

Table 5.1. Review of the reported enzymatic biosensors using $BMIMBF_4$ (continued).

Transducer	Enzyme	Immobilization	Detection technique	Analyte	Substrate/ detected species	Linear range ($\mu molL^{-1}$)	Limit of detection ($\mu molL^{-1}$)	Γ^* (mol/cm^2)	k_s (s^{-1})	K_m ($\mu molL^{-1}$)	Ref.
Carbon paste electrode	Glucose oxidase	Mixture of Ppy–Co_3O_4 with $BMIMBF_4$ drop casted onto electrode; Drop cast of enzyme onto the modified electrode.	Cyclic voltammetry and amperometry	H_2O_2	H_2O_2	2.0–910	0.71	1.59×10^{-9}	1.67	530	[46]
Glassy carbon electrode	Glucose oxidase	Mixture of multiwalled carbon nanotubes dispersed in $BMIMBF_4$, hyaluronic acid and enzyme solution casted onto electrode surface.	Cyclic voltammetry	Glucose	Glucose	100–2000	30	8.5×10^{-9}	0.51	9800	[47]
Gold electrode	Glucose oxidase	Three-dimensional ordered macroporous gold film at electrode surface; Mixture of $BMIMBF_4$, dimethylformamide and enzyme solution drop casted onto the modified electrode.	Cyclic voltammetry	Glucose	Glucose	0.010–0.125	0.0033	4.18×10^{-12}	1.95	18	[48]
Glassy carbon electrode	Glucose oxidase	Preparation of gold nanoparticles with $BMIMBF_4$, $HAuCl_4$, $NaBH_4$ and chitosan (red solution); Mixture of multiwalled carbon nanotubes with the previous mixture drop casted onto surface electrode; Drop cast of enzyme solution onto the modified electrode.	Cyclic voltammetry	Glucose	Glucose	10–100	n.r.	7.26×10^{-10}	9.36	13.7	[49]
Glassy carbon electrode	Horseradish peroxidase	Enzyme deposited at electrode surface; Nafion or agarose on enzyme/electrode modification; Immersed in $BMIMBF_4$.	Cyclic voltammetry	H_2O_2	H_2O_2	< 6000	n.r.	n.r.	0.55	n.r.	[50]
Glassy carbon electrode	Horseradish peroxidase	Mixture of titanate nanotubes coated with Au nanoparticles with enzyme solution and $BMIMBF_4$; Drop casted on surface electrode; Nafion at surface modified electrode.	Cyclic voltammetry and Chronoamperometry	H_2O_2	H_2O_2	15–750	2.2	n.r.	n.r.	n.r.	[51]

Table 5.1. Review of the reported enzymatic biosensors using $BMIMBF_4$ (continued).

Transducer	Enzyme	Immobilization	Detection technique	Analyte	Substrate/ detected species	Linear range ($\mu molL^{-1}$)	Limit of detection ($\mu molL^{-1}$)	Γ^* (mol/cm^2)	k_s (s^{-1})	K_m ($\mu molL^{-1}$)	Ref.
Carbon fiber ultramicroel ectrode	Horseradish peroxidase	Singlewalled carbon nanotubes dispersed on hexadecyltrimethyl ammonium bromide; Drop cast of the previous carbon dispersion; Drop cast of enzyme solution with $BMIMBF_4$ on modified electrode.	Cyclic voltammetry and amperometry	H_2O_2	H_2O_2	> 10.2	0.13	n.r.	n.r.	15.4	[52]
Glassy carbon electrode	Horseradish peroxidase	Mixture of β-ciclodextrin, $BMIMBF_4$ and enzyme solution drop casted onto the electrode surface.	Cyclic voltammetry and amperometry	H_2O_2	H_2O_2	4.0–84	2.65	3.80×10^{-11}	n.r.	68.6	[53]
Carbon ionic liquid electrode	Horseradish peroxidase	Carbon paste was prepared using $EMIMEtOSO_3$ ionic liquid; Mixture of CdS nanorods, $BMIMBF_4$, hyaluronic acid and enzyme solution drop casted onto the electrode surface.	Cyclic voltammetry	Trichloroac etic acid	Trichloroac etic acid	1600–18000	530	1.74×10^{-9}	0.655	345	[54]
Glassy carbon electrode	Horseradish peroxidase	Mixture of microbial exocellular polysaccharide-gellan gum, $BMIMBF_4$ and enzyme solution drop casted onto the electrode surface.	Cyclic voltammetry	H_2O_2	H_2O_2	0.05–0.5	0.02	4.5×10^{-9}	15.8	0.67	[55]
Glassy carbon electrode	Horseradish peroxidase	Mixture of chitosan, $BMIMBF_4$ and enzyme solution drop casted onto the electrode surface.	Cyclic voltammetry	H_2O_2	H_2O_2	0.75–135	0.25	1.03×10^{-10}	n.r.	n.r.	[56]
Glassy carbon electrode	Horseradish peroxidase	$BMIMBF_4$ mixed with sol gel tetraethyl orthosilicate; Enzyme solution was added to the previous mixture drop casted onto the electrode surface.	Cyclic voltammetry and amperometry	H_2O_2	H_2O_2	10–260	1.1	n.r.	n.r.	2000	[57]

n.r. – not reported

Table 5.2. Review of the reported heme-based biosensors $BMIMBF_4$.

Transducer	Heme protein	Immobilization	Detection technique	Analyte	Substrate/ detected species	Linear range ($\mu molL^{-1}$)	Limit of detection ($\mu molL^{-1}$)	Γ^* (mol/cm^2)	k_s (s^{-1})	K_m ($\mu molL^{-1}$)	Ref.
Gold electrode	Cytochrome *c*	11-mercaptoun-decanoic acid and 6-mercapto-1-hexanol to modify the gold electrode; Mixture of poly(diallyldimethylammonium chloride), graphene oxide, gold nanoparticles and $BMIMBF_4$ and drop casted on the electrode surface; Mixture of Nafion and protein solution was drop casted on the modified electrode.	Cyclic voltammetry and amperometry	H_2O_2	H_2O_2	10–4450	2.5	4.9×10^{-11}	3.14	1680	[33]
Glassy carbon electrode	Cytochrome *c*	Multi-walled carbon nanotubes dispersed with dimethylformamide and casted on electrode surface; $BMIMBF_4$ at modified electrode; Gold nanoparticles at modified electrode; Protein solution drop casted on the modified electrode.	Cyclic voltammetry and amperometry	H_2O_2	H_2O_2	50–1150	3.0	n.r.	3.89	n.r.	[58]
Carbon ionic liquid electrode	Cytochrome *c*	Mixture of [5,10,15,20- (4-carboxyphenyl)porphyrin]Co(III) and $BMIMBF_4$; Protein casted on surface electrode; $BMIMBF_4$ casted on modified electrode.	Cyclic voltammetry and amperometry	Nitrite	Nitrite	3.5–2800	1.1	2.69×10^{-10}	4.76	280	[59]
Carbon ionic liquid electrode	Myoglobin	Drop casted of protein solution onto the electrode surface; Mixture of LaF_3 doped CeO_2 with $BMIMBF_4$ and drop casted on the modified surface.	Cyclic voltammetry and amperometry	Nitrite	Nitrite	5–4650	2	2.07×10^{-9}	1.01	2190	[60]
Carbon ionic liquid electrod	Myoglobin	Magnetic ferroferric oxide carbon aerogel mixed with $BMIMBF_4$; Protein casted on surface electrode.	Cyclic voltammetry and amperometry	H_2O_2	H_2O_2	10–1450	3.2	4.10×10^{-10}	1.30	880	[61]

Table 5.2. Review of the reported heme-based biosensors $BMIMBF_4$ (continued).

Transducer	Heme protein	Immobilization	Detection technique	Analyte	Substrate/ detected species	Linear range ($\mu molL^{-1}$)	Limit of detection ($\mu molL^{-1}$)	Γ^* (mol/cm^2)	k_s (s^{-1})	K_m ($\mu molL^{-1}$)	Ref.
Carbon ionic liquid electrode	Myoglobin	Mixture of $BMIMBF_4$, paraffin and graphite powder; Adsorption of mixture of $BMIMBF_4$, graphene, protein and Co_3O_4 nanoflower; Incubation of modified electrode on chitosan solution.	Cyclic voltammetry	Trichloroacetic acid	Trichloroacetic acid	1000–20000	180	6.81×10^{-9}	0.675	980	[31]
Carbon ionic liquid electrode	Myoglobin	$BMIMBF_4$ used to prepare the carbon paste electrode; Carbon coated Fe_2O_3 nanospindles at electrode surface; Protein solution drop casted on electrode surface; $EMIMEtOSO_3$ at modified electrode.	Cyclic voltammetry	Trichloroacetic acid	Trichloroacetic acid	1000–20000	333	2.24×10^{-9}	0.610	1390	[62]
Carbon ionic liquid electrode	Myoglobin	Mixture of dsDNA and $BMIMBF_4$ and drop casted on electrode surface; Protein solution at modified electrode; Dextran at modified electrode.	Cyclic voltammetry	Trichloroacetic acid H_2O_2	Trichloroacetic acid H_2O_2	200–32000 0.1–280	72	2.93×10^{-9}	0.84 n.r.	4800 280	[63]
Glassy carbon electrode	Myoglobin	Mixture of cellulose diacetate, $BMIMBF_4$ and protein solution and drop casted on electrode surface.	Amperometry	H_2O_2	H_2O_2	5.0–100	2.0	n.r.	n.r.	175.8	[64]
Glassy carbon electrode	Myoglobin	Mixture of silica-coated gold nanorods with protein solution and $BMIMBF_4$ with tetraethoxysilane and drop casted onto the electrode surface.	Cyclic voltammetry and amperometry	H_2O_2	H_2O_2	0.2–180	0.12	7.65×10^{-9}	4.7	420	[65]
Glassy carbon electrode	Myoglobin	Mixture of montemorillonite-$BMIMBF_4$ clay with protein solution and drop casted on electrode surface.	Amperometry	H_2O_2	H_2O_2	3.90–2590	0.733	4.90×10^{-11}	3.58	17.6	[66]

Table 5.2. Review of the reported heme-based biosensors $BMIMBF_4$ (continued).

Transducer	Heme protein	Immobilization	Detection technique	Analyte	Substrate/ detected species	Linear range ($\mu molL^{-1}$)	Limit of detection ($\mu molL^{-1}$)	Γ^* (mol/cm^2)	k_s (s^{-1})	K_m ($\mu molL^{-1}$)	Ref.
Carbon ionic liquid electrode	Hemoglobin	Mixture of $BMIMBF_4$, paraffin and graphite powder; Adsorption of mixture of $BMIMBF_4$, graphene, protein and SnO_2 nanosheet; Incubation of modified electrode on nafion solution.	Cyclic voltammetry	Trichloroacetic acid	Trichloroacetic acid	2000–11000	615	6.77×10^{-9}	0.973	17870	[67]
Carbon ionic liquid electrode	Hemoglobin	Mixture of SnS_2 nanoflowers, $BMIMBF_4$ and protein solution and drop casted onto the electrode surface; Nafion drop casted onto the modified electrode.	Cyclic voltammetry	Trichloroacetic acid	Trichloroacetic acid	800–21000	270	3.28×10^{-9}	0.725	14700	[68]
Carbon ionic liquid electrode	Hemoglobin	Mixture of $BMIMBF_4$, paraffin and graphite powder; Protein solution drop casted on electrode surface; Urchinlike MnO_2 nanoparticles mixed with chitosan and deposited on the modified electrode.	Cyclic voltammetry	Trichloroacetic acid	Trichloroacetic acid	15–16000	167	8.52×10^{-9}	0.406	1227	[69]
Carbon ionic liquid electrode	Hemoglobin	Mixture of gellan gum, $BMIMBF_4$ and protein solution and drop casted on electrode surface.	Cyclic voltammetry and amperometry	Trichloroacetic acid H_2O_2	Trichloroacetic acid H_2O_2	20–9100 4.6–782.6	6.8 1.5	3.93×10^{-9}	2.0	4300 130	[70]
Carbon ionic liquid electrode	Hemoglobin	Mixture of carbon aerogel-$HAuCl_4$ with $BMIMBF_4$ and drop casted on electrode surface; Drop casted of protein solution on modified electrode.	Cyclic voltammetry and amperometry	H_2O_2 Nitrite	H_2O_2 Nitrite	5–950 5–1320	2.0 H_2O_2 1.3 Nitrite	3.11×10^{-9}	1.32	450 260	[71]

Table 5.2. Review of the reported heme-based biosensors $BMIMBF_4$ (continued).

Transducer	Heme protein	Immobilization	Detection technique	Analyte	Substrate/ detected species	Linear range ($\mu molL^{-1}$)	Limit of detection ($\mu molL^{-1}$)	Γ^* (mol/cm^2)	k_s (s^{-1})	K_m ($\mu molL^{-1}$)	Ref.
Glassy carbon electrode	Hemoglobin	ZrO_2 nanotubes dispersed on chitosan solution and mixed with $BMIMBF_4$ and protein solution; Mixture was casted on electrode surface.	Cyclic voltammetry	Nitrite	Nitrite	0.5–500	0.2	n.r.	n.r.	n.r.	[32]
Glassy carbon electrode	Hemoglobin	Carbon-coated nickel magnetic nanoparticle–chitosan–dimethylformamide composite films; Protein with $BMIMBF_4$ on modified electrode.	Cyclic voltammetry and amperometry	H_2O_2	H_2O_2	2–210	0.6	16.1×10^{-11}	30.07	310	[72]
Glassy carbon electrode	Hemoglobin	Carboxylic acid functionalized multi walled carbon nanotubes were dispersed in $BMIMBF_4$; Drop casted of protein solution on modified electrode.	Cyclic voltammetry and amperometry	H_2O_2	H_2O_2	10–300 34–310	2.60 3.02	2.72– 3.65×10^{-10}	0.63– 0.70	40–61	[73]
Glassy carbon electrode	Hemoglobin	Mixture of protein solution with gold nanoparticles, poly(3,4-ethylenedioxythiophene) nanowhiskers and $BMIMBF_4$ and drop casted on electrode surface.	Cyclic voltammetry and amperometry	H_2O_2	H_2O_2	1–1100	0.6	2.89×10^{-11}	n.r.	38	[74]
Glassy carbon electrode	Hemoglobin	Mixture of protein, $BMIMBF_4$ and carrageenan and drop casted on surface electrode.	Cyclic voltammetry	H_2O_2	H_2O_2	5.0–150	0.212	5.77×10^{-10}	2.02	20	[75]

Table 5.2. Review of the reported heme-based biosensors $BMIMBF_4$ (continued).

Transducer	Heme protein	Immobilization	Detection technique	Analyte	Substrate/ detected species	Linear range ($\mu molL^{-1}$)	Limit of detection ($\mu molL^{-1}$)	Γ^* (mol/cm^2)	k_s (s^{-1})	K_m ($\mu molL^{-1}$)	Ref.
Glassy carbon electrode	Hemoglobin	Halloysite nanotubes dispersed in chitosan solution and drop casted on surface electrode; Protein solution was drop casted on modified electrode; $BMIMBF_4$ was drop casted on modified electrode.	Cyclic voltammetry	H_2O_2	H_2O_2	7.5–97.5	2.4	6.50×10^{-10}	1.51	369	[76]
Glassy carbon electrode	Hemoglobin	Mixture of multi walled carbon nanotubes, $BMIMBF_4$, nafion and protein solution and drop casted onto the electrode surface.	Cyclic voltammetry	H_2O_2	H_2O_2	2.0–2500	0.8	n.r.	3.35	340	[77]
Glassy carbon electrode	Hemoglobin	Mixture of hyaluronic acid, $BMIMBF_4$ and protein solution and drop casted on electrode surface.	Cyclic voltammetry	H_2O_2	H_2O_2	4.0–100.0	1.8	8.20×10^{-11}	1.49	86.9	[78]
Glassy carbon electrode	Hemoglobin	Mixture of chitosan, $BMIMBF_4$ and protein solution and drop casted onto the electrode surface.	Cyclic voltammetry and amperometry	HCH	HCH	0.2–1.0	0.06	9.30×10^{-11}	0.5525	1.634	[79]
Glassy carbon electrode	Hemoglobin	Mixture of graphene, chitosan, $BMIMBF_4$ and protein solution and drop casted on electrode surface.	Amperometry	Nitromethane	Nitromethane	0.002–0.230	0.0006	7.70×10^{-10}	57.3	0.16	[80]

Table 5.2. Review of the reported heme-based biosensors $BMIMBF_4$ (continued).

Transducer	Heme protein	Immobilization	Detection technique	Analyte	Substrate/ detected species	Linear range ($\mu molL^{-1}$)	Limit of detection ($\mu molL^{-1}$)	Γ^* (mol/cm^2)	k_s (s^{-1})	K_m ($\mu molL^{-1}$)	Ref.
Glassy carbon electrode	Hemoglobin Myoglobin Cytochrome *c*	Mixture of dimethylformamide–chitosan organo/hydrogel films with $BMIMBF_4$ and protein solution and drop casted on electrode surface.	Cyclic voltammetry	H_2O_2	H_2O_2	23.6–1340 83.4–497 92.9–1470	7.1 2.5 2.8	6.49×10^{-11} 7.61×10^{-11} 3.13×10^{-11}	29.08 25.43 27.54	850 600 590	[82]
Glassy carbon electrode	Hemoglobin Myoglobin	Mixture of agarose hydrogel, $BMIMBF_4$ and protein solution and drop casted on electrode surface.	Cyclic voltammetry	H_2O_2	H_2O_2	26.56–912.80 1.28–708.49	n.r.	2.30×10^{-11} 2.18×10^{-11}	36.1 29.1	755 593	[83]
Indium oxide glass electrode	Hemoglobin	Poly(diallyldimethylammonium chloride) at electrode surface; Negatively charged DNA at modified electrode; $BMIMBF_4$ at modified electrode; Protein solution drop casted at modified electrode.	Cyclic voltammetry and amperometry	H_2O_2	H_2O_2	1.0–380	0.1	1.39×10^{-11}	0.91	690	[84]

HCH, 3,4'-bis-(4-hydro-3-xycoumarin)-2,5-hexanediol
n.r. – not reported

5.2. Materials and methods

5.2.1. Reagents

MWCNTs-COOH (thin, extent of labeling: >8% carboxylic acid functionalized, avg. diam. × L 9.5 nm × 1.5 μm), $BMIMBF_4$ (≥97.0%), 2-phenylethanol (PE; ≥ 99.0%), potassium hexa-cyanoferrate (II) trihydrate ($C_6FeK_4N_6.3H_2O$; ≥ 99%), N,N-dimethylformamide (DMF; 99%), potassium hexa-cyanoferrate (III) ($C_6FeK_3N_6$; ≥ 99%) were purchased from Sigma-Aldrich (Steinhein, Germany). Ethanol (EtOH; 99.5%), sulfuric acid (H_2SO_4; 96%) and n-dodecyl-β-D-maltoside (DM) were obtained from Panreac (Barcelona, Spain). Potassium dihydrogen phosphate (KH_2PO_4, p.a.) and di-potassium hydrogen phosphate (K_2HPO_4, p.a.) were used to prepare phosphate buffer (100 $mmolL^{-1}$, pH 6.0); they were bought from Riedel-de-Haën (Germany) as well as potassium hydroxide (p.a.). NO solutions of different concentrations were prepared by dilution from a buffer stock solution of 100 $\mu molL^{-1}$, prepared by bubbling a 5% NO/95% He gas mixture (Air Liquid, Portugal) into buffer 100 $mmolL^{-1}$ phosphate buffer pH 6.0. All solutions and stock were prepared immediately before being used. Ultrapure water obtained from a Millipore water purification system (18 MΩ, Milli-Q, Millipore, Molsheim, France) was used in all assays.

5.2.2. NOR purification and characterization

NOR was purified from membrane extracts of *Marinobacter hydrocarbonoclasticus* grown anaerobically as described by Prudêncio *et al.* [85]; the NOR preparation used in these studies was evaluated by sodium dodecyl sulfate polyacrylamide gel electrophoresis (SDS-PAGE) (Bio-Rad, Mini-PROTEAN® Tetra Handcast Systems, Portugal) based on the protocol of Laemmli [86] and UV–visible spectrum (UV 1800-Shimadzu, 250-800 nm, Germany). An ISO-NO Mark II amperometric sensor (2 mm, World Precision Instruments, Inc., UK: one unit corresponds to 1 μmol of NO/min) was used to achieve the specific activity of 760 U/mg (14 mg/mL) (determined as described previously by Timóteo *et al.* [87].

5.2.3. Biosensor fabrication

Preparation of the modified electrode included the pretreatment of a pyrolytic graphite electrode (PGE; A=7.07 mm^2; ALS Co., Ltd; Tokyo, Japan) and subsequent immobilization of the prepared nanocomposite on it. The PGE was successively polished with alumina powder (1.0 and 0.3 μm, Gravimeta Lda, Portugal), ultrasonicated with ethanol and washed with ultra-pure water for 10 min. PGE surface activation was performed by cyclic voltammetry (CV) in H_2SO_4 0.5 $molL^{-1}$ at 100 mV/s in the range of 0 V to 1.6 V *vs*. Ag/AgCl/Cl^- sat. For the preparation of MWCNTs/$BMIMBF_4$/NOR nanocomposite, the optimum amount of 6 μL of 1.0 mg/mL MWCNTs (dispersed in DMF) was mixed with 4 μL of $BMIMBF_4$ and 4 μL of NOR (760 U/mg; 14 mg/mL). The as prepared nanocomposite was immobilized on the PGE surface by the solvent casting technique and the solvent was evaporated with a very gentle nitrogen flow.

5.2.4. Electrochemical measurements

A three-electrode cell consisting in the modified PGE (PGE/MWCNTs; PGE/[MWCNTs/$BMIMBF_4$], PGE/[MWCNTs/$BMIMBF_4$/NOR] or PGE/NOR) as the working electrode, and a platinum wire and silver/silver chloride saturated with KCl 3 $molL^{-1}$ as the secondary and reference electrodes, respectively. Electrochemical experiments were performed with an Autolab PGSTAT 204 potentiostat-galvanostat controlled by GPES 4.9.7 and Nova 1.10 software (Metrohm Autolab). The assays were conducted in one conventional compartment cell using as electrolyte 100 $mmolL^{-1}$ of phosphate buffer with 0.02% DM and 0.01% PE at pH 6.0 for NOR redox behavior and NO bioelectrocatalysis or the same buffer with 5.0 $mmolL^{-1}$ $[Fe(CN)_6]^{3-/4-}$ for characterization of the biosensor construction. The redox behavior of NOR was evaluated by CV applying a step potential of 3 mV and a potential range of 0.4 to -1.0 V, with a previous deoxygenation of the electrolyte using nitrogen gas during 20 minutes. NO bioelectrocatalysis was performed in the same potential window using square wave voltammetry (SWV) at a frequency of 10 Hz, amplitude of 20 mV and step potential of 3 mV. Electrochemical impedance spectroscopy (EIS) assays were performed in the buffer solution with 5.0 $mmolL^{-1}$ $[Fe(CN)_6]^{3-/4-}$ (pH 6.0) applying a frequency range from 10^{-1} to 10^5 Hz with an amplitude perturbation of 5 mV and 0.2 V as conditioning potential.

5.2.5. Morphological characterization

The morphological biosensor characterization was realized by a High resolution Environmental Scanning Electron Microscope with X-Ray Microanalysis and Electron Backscattered Diffraction analysis: Quanta 400 FEG ESEM / EDAX Genesis X4M (Schottky).

5.2.6. Statistical analysis

Statistical analysis was performed using SPSS software (IBM SPSS Statistics 20). The non-parametric Wilcoxon Mann-Whitney U-test was used due to non-normal distribution of the data. Statistical significance was defined at $p \leq 0.05$.

5.3. Results and discussion

5.3.1. Biosensor construction

a) Electrochemical characterization

CV and EIS were used to characterize the impact of each modification on the electrochemical behavior and interface properties of the biosensor and thus to optimize its construction. Assays were performed with 5.0 $mmolL^{-1}$ $[Fe(CN)_6]^{3-/4-}$ as redox probe in phosphate buffer (pH 6.0).

Firstly, the optimum MWCNTs:$BMIMBF_4$ ratio in the nanocomposite was established by testing six different proportions (0:10, 2:8, 4:6, 6:4, 8:2 and 10:0 (v/v)) and maintaining constant the total drop cast volume (10 μL) (Fig. 5.1-(A)). Synergetic effects were attained since higher sensitivity was reached when both composite constituents were present, when compared with the electrode modification with only one of the individual component (MWCNTs or $BMIMBF_4$) ((Fig. 5.1-(A)-(B)). The decrease of the MWCNTs volume from 10 till 6 μL and simultaneous increase of $BMIMBF_4$ in the nanocomposite from 0 till 4 μL originated the best significant ($p < 0.05$) enhancement of the signal (72.5% higher current for PGE/[MWCNTs/$BMIMBF_4$] than PGE) ((Fig. 5.1-(B)), thus the 6:4 (v/v) MWCNTs:$BMIMBF_4$ ratio was considered the optimum one. Moreover, it can be observed that MWCNTs contributed more

significantly than $BMIMBF_4$ to the marked positive impact on the PGE current intensity and on the process reversibility. These data are in accordance with the MWCNTs properties, i.e. high electric conductivity, electrocatalytic activity and electroactive surface area [22, 88]. $BMIMBF_4$ has high viscosity (99.9 cP at 20 °C [89]; which may increase the resistance), but may support charge transport by behaving as a fortifying source of ion carriers (conductivity of 0.35 S/m at 25 °C [89]) [90]. This electrochemical behavior is in agreement with those observed by Zhang et al. [91] and Shangguan et al. [47].

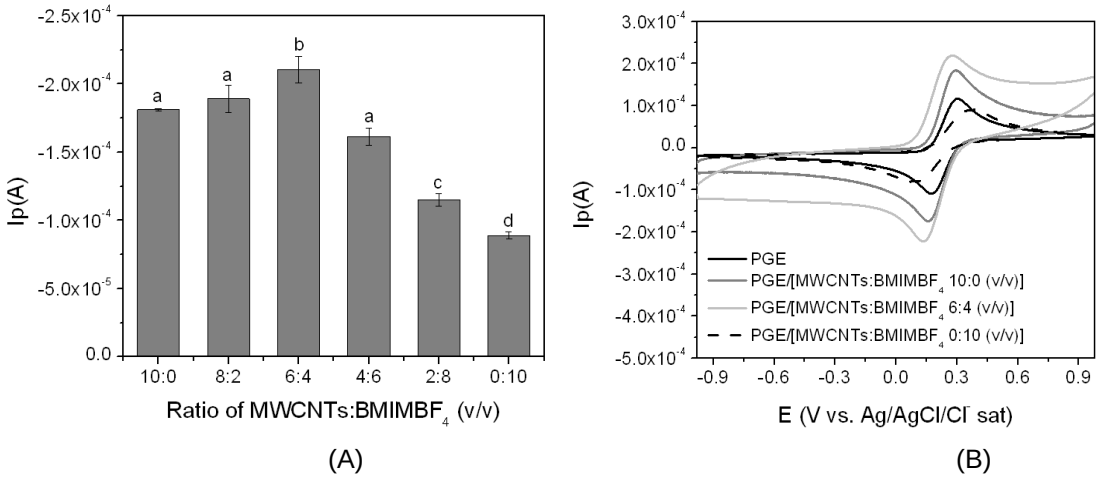

Fig. 5.1. Optimization of the MWCNTs:$BMIMB_4$ ratio: (A) Effect of the MWCNTs:$BMIMB_4$ ratio (10:0, 8:2, 6:4, 4:6, 2:8 and 0:10, v/v) on the peak current of the modified pyrolytic graphite electrode (PGE). Different letters indicate that the given medians are significantly different (Wilcoxon Mann-Whitney U-test at $p < 0.05$). (B) Cyclic voltammograms of the bare and modified PGE with the MWCNTs:$BMIMB_4$ ratio (v/v) of 10:0 (PGE/MWCNTs), 6:4 (PGE/[MWCNTs/$BMIMBF_4$]) and 0:10 (v/v) (PGE/$BMIMBF_4$). Experimental conditions: 5.0 $mmolL^{-1}$ $[Fe(CN)_6]^{3-/4-}$ in phosphate buffer (pH 6.0) at 100 mV/s.

Fig. 5.2 displays the representative cyclic voltammograms (Fig. 5.2 – (A)) and the impedance spectra represented as Nyquist plots (Fig. 5.2 – (B)) of the PGE, PGE/NOR, PGE/[MWCNTs/$BMIMBF_4$] and PGE/[MWCNTs/$BMIMBF_4$/NOR].

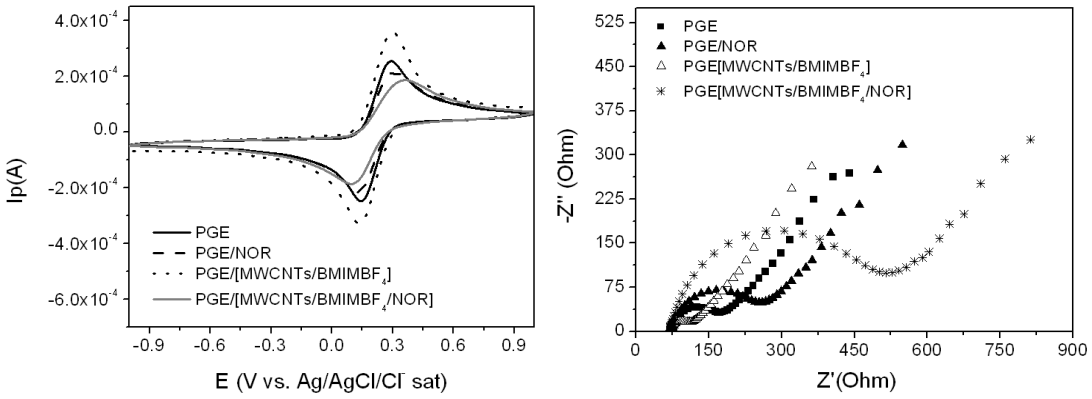

Fig. 5.2. Effect of enzyme immobilization on (A) cyclic voltammetric behavior and (B) Nyquist plots of the PGE and PGE/[MWCNTs/BMIMBF$_4$] in 5.0 mmolL^{-1} $[Fe(CN)_6]^{3-/4-}$ in phosphate buffer (pH 6.0). Cyclic voltammetry parameters: scan rate of 100 mV/s and step potential of 3 mV. Electrochemical impedance spectroscopy conditions: frequency range from 10^{-1} to 10^5 Hz with an amplitude perturbation of 5 mV and 0.2 V as conditioning potential.

The impedance spectra were fitted to the Randles equivalent electric circuit with a constant phase element with charge transfer resistance indicated by the diameter of the semicircle [92], while the linear part locating at lower frequency gave information on the diffusion process [47]. The observed changes in the cyclic voltammograms (Fig. 5.2 – (A)), caused by enzyme incorporation, are in agreement with those exhibited by the EIS profiles (Fig. 5.2 – (B)) of the different modified electrodes suggesting the successful immobilization of MWCNTs/BMIMBF$_4$/NOR or simply NOR at the PGE surface. The charge transfer resistance (Rct) increased from 81.7 to 147 Ω after NOR adsorption onto the PGE surface, while a tenfold increment was noticed between the Rct values of PGE/[MWCNTs/BMIMBF$_4$] (33.8 Ω) and PGE/[MWCNTs/BMIMBF$_4$/NOR] (360 Ω). In agreement with previous studies, the inclusion of the enzyme on the proposed nanocomposite promoted a significant increase of the semi-circle in the impedimetric plots [93]. A similar Rct of 300 Ω was reported by Karimi et al. [38] for another biosensor based on cholesterol oxidase incorporated in NH$_2$-MWCNTs/BMIMBF$_4$ nanocomposite and adsorbed onto a glassy carbon electrode [38]. NOR at pH 6.0 is positively charged [94] and hence can bind to BMIMBF$_4$ and the MWCNTs through ionic interactions. Additionally, BMIMBF$_4$ may interact with the carbon nanotubes by π-π, π–cationic and/or hydrophobic–hydrophobic interactions [35, 95]. For that reason, the selected IL combined with the

MWCNTs had an essential role in NOR entrapment.

b) Morphological characterization

Since the electrochemical responses are also dependent of the surface morphology, SEM characterization of each modified electrode (PGE/MWCNTs, PGE/[MWCNTs/$BMIMBF_4$] and PGE/[MWCNTs/$BMIMBF_4$/NOR]) was performed to complement the electrochemical data. Representative SEM images spectra are exhibited in Fig. 5.3. Fig. 5.3 –(A) shows the typical morphology of well-dispersed functionalized MWCNTs onto the electrode surface, which displays a spaghetti-like porous reticular structure with MWCNTs entangled in one another [35]. After mixing $BMIMBF_4$ with MWCNTs (Fig. 5.3 –(B)), the pores of the MWCNTs network were fully eliminated and filled with the viscous IL increasing the uniformity and smoothness of the film, being in accordance with previous studies [35]. This layer (MWCNTs/$BMIMBF_4$), as it can be noticed in Fig. 5.3 –(C), provided an adequate microenvironment for NOR entrapment by combining the solvation ability (and high ionic conductivity) of the selected IL with the high tensile strength (and electric conductivity) of MWCNTs [35, 38, 47].

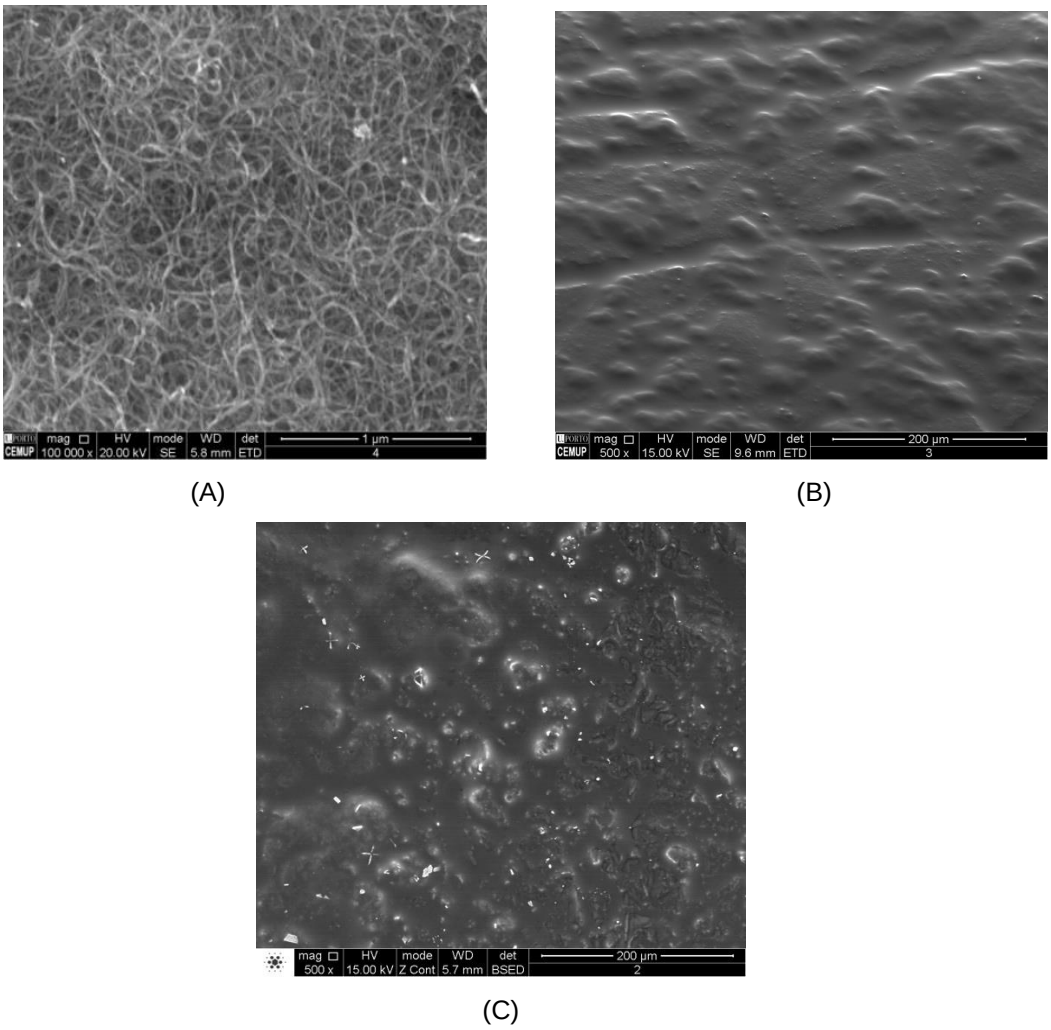

Fig. 5.3. Scanning electron microscopy images of (A) PGE/MWCNTs, (B) PGE/[MWCNTs/$BMIMBF_4$] and (C) PGE/[MWCNTs/$BMIMBF_4$/NOR].

5.3.2. Direct electron transfer behavior of NOR on the PGE/[MWCNTs/$BMIMBF_4$/NOR] biosensor

The DET behavior of NOR on the proposed biosensor immersed in 100 $mmolL^{-1}$ phosphate buffer, 0.02 %DM and 0.01% PE at pH 6.0 is presented in Fig. 5.4. Since enzymatic activity is markedly influenced by the pH, all assays were executed at the optimum pH for NOR, i.e. 6.0 [14]. The electrochemical response of NOR corresponded to a pair of well-defined cathodic and anodic peaks (Fig. 5.4 at -0.261 ± 0.003 and -0.249 ± 0.002 V (formal potential of -0.255 ± 0.003 V), respectively, at scan rate of 0.25 V/s, which is ascribed to the heme b_3 center in the bi-nuclear site of NOR [14]. Good linearity was obtained between the peak current and the scan rate (0.150 – 0.750 V/s) for both anodic and cathodic signals (Fig. 5.4) (I_{pa} (A)=1.44×10^{-5} ±

6.14×10^{-7}v (V/s) - 1.73×10^{-6} ± 2.58×10^{-7}; r^2=0.991; n=6 and I_{pc} (A)=-1.82×10^{-5} ± 4.53×10^{-7}v (V/s)+1.92×10^{-6} ± 1.90×10^{-7}; r^2=0.997; n=6) indicative of a characteristic surface-controlled electrochemical process as anticipated for immobilized structures [96]. Moreover, the formal potential was not dependent of the scan rate pointing to a facile charge transfer kinetic in the tested range of scan rates (150 to 750 mV/s) [35].

The NOR surface coverage (**τ***, mol/cm^2) of the biosensor was estimated based on equation (1):

$$Q=nFA\tau^* \qquad \text{(Eq. 1)}$$

where **Q** (A.s) is the charge involved in the reaction, **A** (cm^2) is the geometric area of the working electrode, **n** is the number of the electron transferred, and **F** (s.A/mol) is the Faraday constant [97]. The obtained τ* value (2.04×10^{-10} mol/cm^2) indicated a high quantity of adsorbed NOR due to the large specific surface area of the nanocomposite-modified PGE. This is the first time that NOR was used to prepare a biosensor, but some previous catalytic studies, with NOR directly adsorbed onto the PGE, reported a one order of magnitude lower value of surface coverage (1.52×10^{-11} - 2.37×10^{-11} mol/cm^2) [12-14] evidencing the advantages of the proposed immobilization approach. Moreover, the previously reported τ* for enzymatic and heme-based-biosensors that included $BMIMBF_4$ ranged from 4.18×10^{-12} to 9.07×10^{-9} mol/cm^2 and 1.39×10^{-11} to 6.81×10^{-8} mol/cm^2, respectively (Table 5.1 and 5.2). Both lowest values of surface coverage were obtained for biosensors that did not include nanomaterials in their construction [48, 84]. On the other hand, the higher loadings were reported when enzyme immobilization involved carbon nanomaterials [31, 41]. Recently, Kang et al. [31] reported very high τ* (6.81×10^{-8} to mol/cm^2) for a carbon ionic liquid electrode modified with a biocomposite composed by myoglobin, $BMIMBF_4$, graphene and cobalt oxide nanoflower, possibly due to the porous and three-dimensional structure of the nanoflowers combined with the use of other nanomaterials. Comparable values as the one reached in this study were reported for biosensors based on catalase [35], horseradish peroxidase [56] and hemoglobin [73] developed for hydrogen peroxide detection.

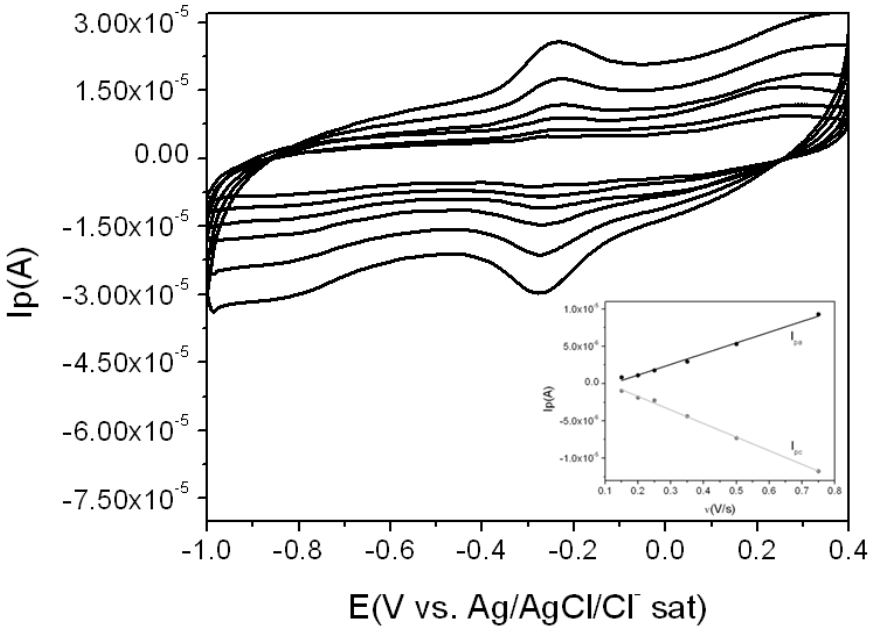

Fig. 5.4. Cyclic voltammograms of direct electrochemical behavior of NOR on PGE/[MWCNTs/$BMIMBF_4$/NOR] biosensor in 100 $mmolL^{-1}$ of phosphate buffer with 0.02% n-dodecyl-β-D-maltoside and 0.01% 2-phenylethanol (pH 6.0) at several scan rates (150, 200, 250, 350, 500 and 750 mV/s). Inset: Anodic (I_{pa}) and cathodic (I_{pc}) peak current *vs* the scan rate.

According to Laviron theory [98], and since the potential separation of the peaks was less than 200 mV, the electron transfer rate constant (**k_s**, s^{-1}) was calculated using equation (2):

$$k_s = mnFv/RT \qquad \text{(Eq. 2)}$$

where **m** is the parameter related to peak potential separation (V), **n** the number of electrons involved in the reaction, **v** is the scan rate (V/s) and all other symbols have their usual meanings. A k_s value of 0.35 s^{-1} was obtained being in the same range as those described for some enzymatic biosensors (0.51 s^{-1} for glucose oxidase [47]; 0.55 [50] and 0.655 s^{-1} [54] for horseradish peroxidase; 0.7 s^{-1} for chloroperoxidase [37]; and 0.78 s^{-1} for choline oxidase based-biosensor [41]) and heme-based biosensors (0.406 s^{-1} [69], 0.5525 s^{-1} [79], 0.63-0.70 s^{-1} [73] and 0.725 s^{-1} [68] for hemoglobin based-biosensors; 0.610 s^{-1} [62], 0.675 s^{-1} [31] for myoglobin based devices) with $BMIMBF_4$ (Table 5.1 and 5.2). This information demonstrated that the

electron transfer between NOR and the modified electrode is efficiently facilitated by the developed nanocomposite.

5.3.3. Nitric oxide reduction on the PGE/[MWCNTs/BMIMBF$_4$/NOR] biosensor

To investigate the electrocatalytic activity of NOR towards NO reduction, SWV voltammograms (at the optimal conditions of 10 Hz frequency, 20 mV amplitude and 3 mV step potential) were executed in 100 mmolL^{-1} phosphate buffer, 0.02 %DM and 0.01% PE (pH 6.0). The obtained results are illustrated in Fig. 5.5. NOR entrapped on MWCNTs/BMIMBF$_4$ acts as an effective catalyst towards reduction of NO, with an irreversible peak at − 0.68 ± 0.03 V (Fig. 5.5). Moreover, the biosensor response to 0.50 – 6.98 µmolL^{-1} of NO was evaluated. Linearity with low dispersion of data (I_{pc} (A)=-4.29×10^{-7} ± 2.48×10^{-8} [NO] (µmolL^{-1})-1.24×10^{-7} ± 6.84×10^{-8}; n=6) and appropriate correlation coefficient (0.991) was perceived till 4.76 µmolL^{-1}, which was followed by saturation of the signal tending to a plateau after 5.88 µmolL^{-1} (characteristic of enzymatic kinetics of second order [99]) (Fig. 5.5). The limit of detection (LOD) and limit of quantification (LOQ) were assessed as being 0.07 and 0.23 µmolL^{-1}, respectively, based on 3*Sy-intercept/slope (for LOD) and 10*Sy-intercept/slope (for LOQ), where Sy-intercept is the standard deviation of the y-intercept [100]. Satisfactory sensitivity of 0.429 µA/µmolL^{-1} was also established. These data compare favorably with those described by Xu et al. [101] for hemoglobin and myoglobin-based biosensors using HIMIMPF$_6$ and didodecyldimethylammonium bromide (linear ranges from 1.8–21.6 and 1.8–23 µmolL^{-1} with no reported LOD and LOQ) and by Zhang et al. [91] for a basal plane graphite electrode modified by successive layers of nafion/ethanol, EMIMBF$_4$/ethanol and myoglobin (linearity between 0.7–7.0 µmolL^{-1} and a LOD of 0.2 µmolL^{-1}). Only these two studies were found concerning NO biosensors that include an IL and heme-proteins in their construction.

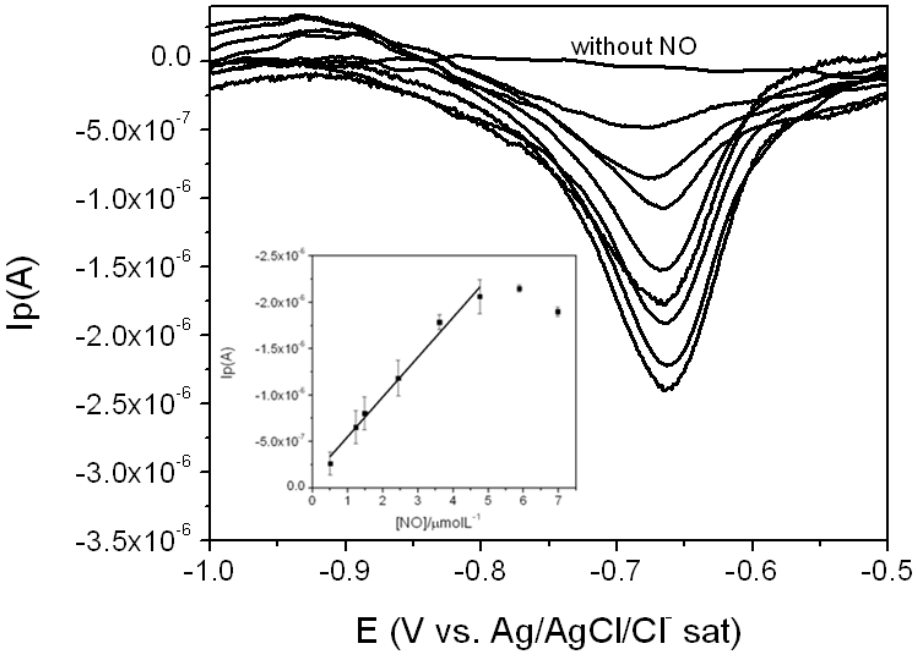

Fig. 5.5. Square wave voltammograms obtained with PGE/[MWCNTs/$BMIMBF_4$/NOR] biosensor in the absence of NO and in the presence of standard NO concentrations of 0.50, 1.23, 1.48, 2.44, 3.61 and 4.76 $\mu molL^{-1}$ in 100 $mmolL^{-1}$ of phosphate buffer with 0.02% n-dodecyl-β-D-maltoside and 0.01% 2-phenylethanol (pH 6.0). Inset: Peak current vs NO concentration and respective linearity zone. Experimental conditions: frequency of 10 Hz, amplitude of 20 mV and step potential of 3 mV.

The affinity of a substrate for the enzymatic centre can be assessed by the Michaelis Menten constant (K_m, $molL^{-1}$), which decreases as the enzyme affinity increases [99]. Biochemically, it indicates a higher probability of formation of the NOR-NO intermediate, which originates an increased NO concentration to be electrochemically reduced. K_m ($\mu molL^{-1}$) was estimated by the Lineweaver–Burk equation (3):

$$1/I_{ss}=K_m/I_{max}\times 1/[NO]+1/I_{max} \qquad \text{(Eq. 3)}$$

where $\mathbf{I_{ss}}$ (A) is the steady-state current after addition of the substrate; **[NO]** ($molL^{-1}$) is the concentration of the substrate and $\mathbf{I_{max}}$ (A) is the maximum current measured [98]. The value obtained for the PGE/[MWCNTs/$BMIMBF_4$/NOR] biosensor of 2.17 $\mu molL^{-1}$ indicated high bioactivity performance, which could be ascribed to the ionic microenvironment generated by the prepared MWCNTs/$BMIMBF_4$ nanocomposite, allowing NOR to retain its native structure and high affinity towards its natural

substrate, and at the same time promoting efficient NOR–substrate interaction. To the best of our knowledge, no Michaelis Menten constant was yet established for NO biosensors that include the selected IL ($BMIMBF_4$) or other IL [91, 101]. In general, the achieved K_m is significantly lower than those reported for heme-based (0.16 – 17870 $\mu molL^{-1}$) and enzymatic (0.118 – 9800 $\mu molL^{-1}$) biosensors using $BMIMBF_4$ (Table 5.1 and 5.2) with some exceptions [35, 38, 48, 49, 52, 55, 66, 75, 79, 80]. The best reported affinity was reached for laccase immobilized in a $BMIMBF_4/NH_2$-MWCNTs nanocomposite (K_m of 0.118 $\mu molL^{-1}$) tested for hydrogen peroxide quantification [35]; for heme-protein biosensors 0.16 $\mu molL^{-1}$ was attained for hemoglobin incorporated in a chitosan/graphene/$BMIMBF_4$ matrix proposed for nitromethane biosensing [80].

The repeatability and reproducibility of the PGE/[MWCNTs/$BMIMBF_4$/NOR] biosensor were examined by the relative standard deviation (RSD) of several experiments. The reduction current of 2.44 $\mu molL^{-1}$ NO was measured during six independent assays and a RSD of 9.1% was displayed showing that the proposed approach had high repeatability. Concerning reproducibility, it was tested with eight biosensors, independently prepared under equivalent experimental circumstances, and the RSD varied from 6.0% (at 4.76 $\mu molL^{-1}$) to 11% (at 0.50 $\mu molL^{-1}$), indicating good reproducibility. Recovery values ranged from 80 – 102% for concentrations in the 0.50 – 4.76 $\mu molL^{-1}$ range. In addition, the long-term stability and electroanalytical performance of the developed biosensor was intermittently (once or twice per week) characterized during one month. The results showed that the developed biosensor was active and retained 79 – 116% of its initial response during all the tested period. These data confirmed that NOR incorporated in the MWCNTs/$BMIMBF_4$ nanocomposite can efficiently maintain its bioactivity for a significant period of time.

5.4. Conclusions

The importance of NO in signaling and cellular physiology in humans has been increasingly recognized in biomedical sciences over the last decade, what has led to an exponential growth in the development of new methods and tools. In this work, a MWCNTs/$BMIMBF_4$ nanocomposite was successfully developed to entrap NOR, for the first time, and prepare a novel third-generation enzymatic biosensor for NO detection. The excellent electric conductivity, together with the large surface area of

MWCNTs, combined with the suitable biocompatibility, viscosity and ionic conductivity of the selected IL provided a suitable microenvironment for the immobilization of NOR and for preservation of its activity. Synergetic effects were perceived between MWCNTs and $BMIMBF_4$, which facilitated the direct electron transfer between NOR and the transducer (k_s of 0.35 s^{-1}) and the unmediated NOR-NO interaction. Therefore, these results suggest that this novel PGE/[MWCNTs/$BMIMBF_4$/NOR] biosensor can be a simple, sensitive and excellent strategy for bioelectrochemical NO biomonitoring applications.

5.5. References

[1] N. Kumar, V. Bhalla, M. Kumar, Recent developments of fluorescent probes for the detection of gasotransmitters (NO, CO and H_2S), Coord. Chem. Rev., 257 (2013) 2335-2347.

[2] X. Zhou, S. Lee, Z. Xu, J. Yoon, Recent progress on the development of chemosensors for gases, Chem Rev, 115 (2015) 7944-8000.

[3] C.W. Chang, G. Maduraiveeran, J.C. Xu, G.W. Hunter, P.K. Dutta, Design, fabrication, and testing of MEMS-based miniaturized potentiometric nitric oxide sensors, Sens Actuators B Chem, 204 (2014) 183-189.

[4] H.K. Gatty, S. Leijonmarck, M. Antelius, G. Stemme, N. Roxhed, An amperometric nitric oxide sensor with fast response and ppb-level concentration detection relevant to asthma monitoring, Sens Actuators B Chem, 209 (2015) 639-644.

[5] C. Sun, G. Maduraiveeran, P. Dutta, Nitric oxide sensors using combination of p- and n-type semiconducting oxides and its application for detecting NO in human breath, Sens Actuators B Chem, 186 (2013) 117-125.

[6] Y. Peng, Y. Ji, D. Zheng, S. Hu, In situ monitoring of nitric oxide release from rat kidney at poly(eosin-b)-ionic liquid composite-based electrochemical sensors, Sens Actuators B Chem, 137 (2009) 656-661.

[7] V. Calabrese, C. Mancuso, M. Calvani, E. Rizzarelli, D.A. Butterfield, A.M. Stella, Nitric oxide in the central nervous system: neuroprotection versus neurotoxicity, Nat Rev Neurosci., 8 (2007) 766-775.

[8] D. O'Hare, Biosensors and sensor systems, Body Sensor Networks, Springer, 2014, pp. 55-115.

[9] J.A. Cole, Chapter 2 Nitric oxide production, damage and management during anaerobic nitrate reduction to ammonia, Metalloenzymes in denitrification:

Applications and environmental impacts, The Royal Society of Chemistry, 2017, pp. 11-38.

[10] Y. Shiro, Structure and function of bacterial nitric oxide reductases: Nitric oxide reductase, anaerobic enzymes, Biochim. Biophys. Acta., 1817 (2012) 1907-1913.

[11] Nicholas J. Watmough, Sarah J. Field, Ross J.L. Hughes, David J. Richardson, The bacterial respiratory nitric oxide reductase, Biochem Soc Trans., 37 (2009) 392-399.

[12] C.M. Cordas, A.G. Duarte, J.J.G. Moura, I. Moura, Electrochemical behaviour of bacterial nitric oxide reductase—Evidence of low redox potential non-heme Fe_B gives new perspectives on the catalytic mechanism, Biochim. Biophys. Acta., 1827 (2013) 233-238.

[13] C.M. Cordas, A.S. Pereira, C.E. Martins, C.G. Timoteo, I. Moura, J.J. Moura, et al., Nitric oxide reductase: direct electrochemistry and electrocatalytic activity, Chembiochem, 7 (2006) 1878-1881.

[14] A.G. Duarte, C.M. Cordas, J.J.G. Moura, I. Moura, Steady-state kinetics with nitric oxide reductase (NOR): New considerations on substrate inhibition profile and catalytic mechanism, Biochim. Biophys. Acta., 1837 (2014) 375-384.

[15] S. Ramos, R.M. Almeida, C.M. Cordas, J.J.G. Moura, S.R. Pauleta, I. Moura, Insights into the recognition and electron transfer steps in nitric oxide reductase from *Marinobacter hydrocarbonoclasticus*, J Inorg Biochem, 177 (2017) 402-411.

[16] W. Zhang, G. Li, Third-generation biosensors based on the direct electron transfer of proteins, Anal Sci, 20 (2004) 603-609.

[17] J.M. Guisan, Immobilization of enzymes and cells, Springer, 2006.

[18] N. Rueda, J.C.S. dos Santos, C. Ortiz, R. Torres, O. Barbosa, R.C. Rodrigues, et al., Chemical modification in the design of immobilized enzyme biocatalysts: Drawbacks and opportunities, Chem Rec, 16 (2016) 1436-1455.

[19] X. Che, R. Yuan, Y. Chai, J. Li, Z. Song, W. Li, et al., A glucose biosensor based on chitosan-Prussian blue-multiwall carbon nanotubes-hollow PtCo nanochains formed by one-step electrodeposition, Colloids Surf B Biointerfaces, 84 (2011) 454-461.

[20] G. Fu, Z. Dai, Efficient immobilization of glucose oxidase by in situ photo-cross-linking for glucose biosensing, Talanta, 97 (2012) 438-444.

[21] F.W.P. Ribeiro, M.F. Barroso, S. Morais, S. Viswanathan, P. de Lima-Neto, A.N. Correia, et al., Simple laccase-based biosensor for formetanate hydrochloride quantification in fruits, Bioelectrochemistry, 95 (2014) 7-14.

[22] T.M. Oliveira, M. Fatima Barroso, S. Morais, P. de Lima-Neto, A.N. Correia, M.B. Oliveira, et al., Biosensor based on multi-walled carbon nanotubes paste electrode modified with laccase for pirimicarb pesticide quantification, Talanta, 106 (2013) 137-143.

[23] M. Galiński, A. Lewandowski, I. Stępniak, Ionic liquids as electrolytes, Electrochim Acta, 51 (2006) 5567-5580.

[24] N. Hameed, J.S. Church, N.V. Salim, T.L. Hanley, A. Amini, B.L. Fox, Dispersing single-walled carbon nanotubes in ionic liquids: a quantitative analysis, RSC Adv, 3 (2013) 20034-20039.

[25] I. Krossing, J.M. Slattery, C. Daguenet, P.J. Dyson, A. Oleinikova, H. Weingärtner, Why are ionic liquids liquid? A simple explanation based on lattice and solvation energies, J. Am. Chem. Soc., 128 (2006) 13427-13434.

[26] P. Sun, D.W. Armstrong, Ionic liquids in analytical chemistry, Anal Chim Acta, 661 (2010) 1-16.

[27] S. Mallakpour, M. Dinari, Ionic liquids as green solvents: Progress and prospects, in: A. Mohammad, D. Inamuddin (Eds.), Green Solvents II: Properties and Applications of Ionic Liquids, Springer Netherlands, Dordrecht, 2012, pp. 1-32.

[28] R. Toniolo, R. Bortolomeazzi, R. Svigelj, N. Dossi, I.G. Casella, C. Bragato, et al., Use of an electrochemical room temperature ionic liquid-based microprobe for measurements in gaseous atmospheres, Sens Actuators B Chem, 240 (2017) 239-247.

[29] M.J.A. Shiddiky, A.A.J. Torriero, Application of ionic liquids in electrochemical sensing systems, Biosens Bioelectron, 26 (2011) 1775-1787.

[30] F. Xiao, C. Ruan, L. Liu, R. Yan, F. Zhao, B. Zeng, Single-walled carbon nanotube-ionic liquid paste electrode for the sensitive voltammetric determination of folic acid, Sens Actuators B Chem, 134 (2008) 895-901.

[31] S. Kang, W. Zhao, X. Li, Z. Wen, X. Niu, B. He, et al., Electrochemical behaviors of myoglobin on ionic liquid-graphene-cobalt oxide nanoflower composite modified electrode and its electrocatalytic activity, Int J Electrochem Sci, 12 (2017) 2184-2193.

[32] Y. Ma, G. Zhan, M. Ma, X. Wang, C. Li, Direct electron transfer of hemoglobin in a biocompatible electrochemical system based on zirconium dioxide nanotubes and ionic liquid, Bioelectrochemistry, 84 (2012) 6-10.

[33] Y. Song, H. Liu, L. Wan, Y. Wang, H. Hou, L. Wang, Direct electrochemistry of cytochrome *c* based on poly (diallyldimethylammonium chloride)- graphene

nanosheets/gold nanoparticles hybrid nanocomposites and its biosensing, Electroanalysis, 25 (2013) 1400-1409.

[34] E. Zapp, D. Brondani, I.C. Vieira, C.W. Scheeren, J. Dupont, A.M.J. Barbosa, et al., Biomonitoring of methomyl pesticide by laccase inhibition on sensor containing platinum nanoparticles in ionic liquid phase supported in montmorillonite, Sens Actuators B Chem, 155 (2011) 331-339.

[35] P. Rahimi, H.-A. Rafiee-Pour, H. Ghourchian, P. Norouzi, M.R. Ganjali, Ionic-liquid/NH_2-MWCNTs as a highly sensitive nano-composite for catalase direct electrochemistry, Biosens Bioelectron, 25 (2010) 1301-1306.

[36] L. Wang, W. Wen, H. Xiong, X. Zhang, H. Gu, S. Wang, A novel amperometric biosensor for superoxide anion based on superoxide dismutase immobilized on gold nanoparticle-chitosan-ionic liquid biocomposite film, Anal Chim Acta, 758 (2013) 66-71.

[37] L. Yang, X.Q. Wu, R. Wang, Z.Q. Lu, W.J. Hou, H.X. Li, Ionic liquid modified GC electrode for the direct electrochemistry of chloroperoxidase, Chin Chem Lett, 19 (2008) 1483-1486.

[38] S. Karimi, H. Ghourchian, P. Rahimi, H.-A. Rafiee-Pour, A nanocomposite based biosensor for cholesterol determination, Anal Methods, 4 (2012) 3225-3231.

[39] S. Sajjadi, H. Ghourchian, H.-A. Rafiee-Pour, P. Rahimi, Accelerating the electron transfer of choline oxidase using ionic-liquid/NH_2-MWCNTs nano-composite, J. Iran. Chem. Soc., 9 (2012) 111-119.

[40] P. Rahimi, H. Ghourchian, S. Sajjadi, Effect of hydrophilicity of room temperature ionic liquids on the electrochemical and electrocatalytic behaviour of choline oxidase, Analyst, 137 (2012) 471-475.

[41] S. Sajjadi, H. Ghourchian, P. Rahimi, Different behaviors of single and multi wall carbon nanotubes for studying electrochemistry and electrocatalysis of choline oxidase, Electrochim Acta, 56 (2011) 9542-9548.

[42] X. Zeng, X. Li, L. Xing, X. Liu, S. Luo, W. Wei, et al., Electrodeposition of chitosan–ionic liquid–glucose oxidase biocomposite onto nano-gold electrode for amperometric glucose sensing, Biosens Bioelectron, 24 (2009) 2898-2903.

[43] Y. Zhang, Y. Liu, Z. Chu, L. Shi, W. Jin, Amperometric glucose biosensor based on direct assembly of Prussian blue film with ionic liquid-chitosan matrix assisted enzyme immobilization, Sens Actuators B Chem, 176 (2013) 978-984.

[44] K.S. Galhardo, R.M. Torresi, S.I.C. de Torresi, Improving the performance of a glucose biosensor using an ionic liquid for enzyme immobilization. On the chemical

interaction between the biomolecule, the ionic liquid and the cross-linking agent, Electrochim Acta, 73 (2012) 123-128.

[45] T. Yang, X.L. Yang, Y.S. Zhang, B. Xiao, J. Hong, Glucose biosensing using glassy carbon electrode modified with polyhydroxy-C60, glucose oxidase and ionic-liquid, Biomed Mat Eng, 24 (2014) 2197-2202.

[46] S. Dong, L. Peng, D. Liu, Q. Yang, T. Huang, Design synthesis of polypyrrole–Co_3O_4 hybrid material for the direct electrochemistry of hemoglobin and glucose oxidase, Bioelectrochemistry, 98 (2014) 87-93.

[47] X. Shangguan, J. Zheng, H. Zhang, H. Tang, Direct electrochemistry and electrocatalysis behaviors of glucose oxidase based on hyaluronic acid-carbon nanotubes-ionic liquid composite film, Chin. J. Chem., 28 (2010) 1890-1896.

[48] X. Chen, J. Xuan, L. Jiang, J. Zhu, Preparation of the glucose sensor based on three-dimensional ordered macroporous gold film and room temperature ionic liquid, Sci. China, Ser. B, 52 (2009) 1999.

[49] J. Li, F. Zhao, G. Wang, Z. Gui, F. Xiao, B. Zeng, Novel composite of multiwalled carbon nanotubes and gold nanoparticles stabilized by chitosan and hydrophilic ionic liquid for direct electron transfer of glucose oxidase, Electroanalysis, 21 (2009) 150-156.

[50] L. Lu, X. Huang, Y. Qu, Effect of the structure of imidazolium cations in $[BF_4]^-$-type ionic liquids on direct electrochemistry and electrocatalysis of horseradish peroxidase in Nafion films, Colloids Surf B Biointerfaces, 87 (2011) 61-66.

[51] X. Liu, H. Feng, J. Zhang, R. Zhao, X. Liu, D.K.Y. Wong, Hydrogen peroxide detection at a horseradish peroxidase biosensor with a Au nanoparticle–dotted titanate nanotube|hydrophobic ionic liquid scaffold, Biosens Bioelectron, 32 (2012) 188-194.

[52] Q.-Q. Ren, J. Wu, W.-C. Zhang, C. Wang, X. Qin, G.-C. Liu, et al., Real-time i*n vitro* detection of cellular H_2O_2 under camptothecin stress using horseradish peroxidase, ionic liquid, and carbon nanotube-modified carbon fiber ultramicroelectrode, Sens Actuators B Chem, 245 (2017) 615-621.

[53] A. Cao, H. Ai, Y. Ding, C. Dai, J. Fei, Biocompatible hybrid film of β-cyclodextrin and ionic liquids: A novel platform for electrochemical biosensing, Sens Actuators B Chem, 155 (2011) 632-638.

[54] Z. Zhu, X. Li, Y. Wang, Y. Zeng, W. Sun, X. Huang, Direct electrochemistry and electrocatalysis of horseradish peroxidase with hyaluronic acid-ionic liquid-cadmium sulfide nanorod composite material, Anal Chim Acta, 670 (2010) 51-56.

[55] X. Shangguan, J. Zheng, Q. Sheng, Direct electron transfer of horseradish peroxidase in gellan gum–hydrophilic ionic liquid gel film, Electroanalysis, 21 (2009) 1469-1474.

[56] X. Lu, Q. Zhang, L. Zhang, J. Li, Direct electron transfer of horseradish peroxidase and its biosensor based on chitosan and room temperature ionic liquid, Electrochem Commun, 8 (2006) 874-878.

[57] Y. Liu, L. Shi, M. Wang, Z. Li, H. Liu, J. Li, A novel room temperature ionic liquid sol-gel matrix for amperometric biosensor application, Green Chem, 7 (2005) 655-6558.

[58] C. Xiang, Y. Zou, L.-X. Sun, F. Xu, Direct electron transfer of cytochrome *c* and its biosensor based on gold nanoparticles/room temperature ionic liquid/carbon nanotubes composite film, Electrochem Commun, 10 (2008) 38-41.

[59] M. Tong, S. Dong, K. Wang, G. Suo, A porphyrin MOF and ionic liquid biocompatible matrix for the direct electrochemistry and electrocatalysis of cytochrome *c*, J. Electrochem. Soc, 164 (2017) B200-B204.

[60] S. Dong, N. Li, T. Huang, H. Tang, J. Zheng, Myoglobin immobilized on LaF_3 doped CeO_2 and ionic liquid composite film for nitrite biosensor, Sens Actuators B Chem, 173 (2012) 704-709.

[61] M. Li, S. Dong, N. Li, H. Tang, J. Zheng, Magnetic Fe_3O_4 carbon aerogel and ionic liquid composite films as an electrochemical interface for accelerated electrochemistry of glucose oxidase and myoglobin, RSC Adv, 5 (2015) 14704-14711.

[62] Y. Ke, Y. Zeng, X. Pu, X. Wu, L. Li, Z. Zhu, et al., Electrochemistry and electrocatalysis of myoglobin on carbon coated Fe_3O_4 nanospindle modified carbon ionic liquid electrode, RSC Adv, 2 (2012) 5676-5682.

[63] Z. Zhu, Z. Sun, Y. Wang, Y. Zeng, W. Sun, X. Huang, Application of ionic liquid–dsDNA biocomposite film for the direct electrochemistry of myglobin on carbon ionic liquid electrode, J. Electroanal. Chem., 650 (2010) 31-35.

[64] S.-Y. Dong, G.-Z. Gu, Z.-Q. Yu, Y.-Z. Zhou, H.-S. Tang, J.-B. Zheng, Hydrogen peroxide biosensor based on cellulose diacetate-ionic liquid film immobilizing myoglobin, Chin. J. Anal. Chem, 39 (2011) 1358-1362.

[65] W.-L. Zhu, Y. Zhou, J.-R. Zhang, Direct electrochemistry and electrocatalysis of myoglobin based on silica-coated gold nanorods/room temperature ionic liquid/silica sol–gel composite film, Talanta, 80 (2009) 224-230.

[66] Z. Dai, Y. Xiao, X. Yu, Z. Mai, X. Zhao, X. Zou, Direct electrochemistry of myoglobin based on ionic liquid–clay composite films, Biosens Bioelectron, 24 (2009) 1629-1634.

[67] L. Kong, Z. Du, Z. Xie, R. Chen, S. Jia, R. Dong, et al., Electrochemistry of hemoglobin-ionic liquid-graphene-SnO_2 nanosheet composite modified electrode and electrocatalysis, Int J Electrochem Sci, 12 (2017) 2297-2305.

[68] Y. Zeng, W. Li, H. Zhang, X. Wu, W. Sun, Z. Zhu, et al., Application of flower-like SnS_2 nanoparticles for direct electrochemistry of hemoglobin and its electrocatalysis, Anal Methods, 6 (2014) 404-409.

[69] Z. Zhu, L. Qu, Q. Niu, Y. Zeng, W. Sun, X. Huang, Urchinlike MnO_2 nanoparticles for the direct electrochemistry of hemoglobin with carbon ionic liquid electrode, Biosens Bioelectron, 26 (2011) 2119-2124.

[70] L.F. Qiao, J.B. Zheng, R.F. Gao, Q.L. Sheng, Direct electron transfer of hemoglobin in a hydrophilic ionic liquid/gellan gum composite film modified carbon ionic liquid electrode, J Chin Chem Soc., 57 (2010) 718-725.

[71] L. Peng, S. Dong, N. Li, G. Suo, T. Huang, Construction of a biocompatible system of hemoglobin based on AuNPs-carbon aerogel and ionic liquid for amperometric biosensor, Sens Actuators B Chem, 210 (2015) 418-424.

[72] T. Wang, L. Wang, J. Tu, H. Xiong, S. Wang, Direct electrochemistry and electrocatalysis of heme proteins immobilised in carbon-coated nickel magnetic nanoparticle–chitosan–dimethylformamide composite films in room-temperature ionic liquids, Bioelectrochemistry, 94 (2013) 94-99.

[73] A. Banaei, H. Ghourchian, P. Rahimi, A.A. Moosavi Movahedi, R. Amjadi, Different electrochemical behavior of adult and fetal hemoglobin at ionic liquid-carbon nanotube nanocomposite, J. Iran. Chem. Soc., 12 (2015) 687-694.

[74] Y. Chen, P. Gai, L. Jin, D. Zhu, D. Tian, E.S. Abdel-Halim, et al., Fabrication of PEDOT nanowhiskers for electrical connection of the hemoglobin active center for H_2O_2 electrochemical biosensing, J Mater Chem, 1 (2013) 3451-3457.

[75] C. Sheng, Y. Zhang, L. Wang, N. Jia, Immobilization and bioelectrochemistry of hemoglobin based on carrageenan and room temperature ionic liquid composite film, Chinese J Chem, 30 (2012) 1565-1570.

[76] Y. Zhang, H. Cao, W. Fei, D. Cui, N. Jia, Direct electrochemistry and electrocatalysis of hemoglobin immobilized into halloysite nanotubes/room temperature ionic liquid composite film, Sens Actuators B Chem, 162 (2012) 143-148.

[77] Y. Zhang, J. Zheng, Direct electrochemistry and electrocatalysis of hemoglobin based on nafion-room temperature ionic liquids-multiwalled carbon nanotubes composite film, Chinese J Chem, 29 (2011) 685-690.

[78] R. Gao, X. Shangguan, G. Qiao, J. Zheng, Direct electrochemistry of hemoglobin and its electrocatalysis based on hyaluronic acid and room temperature ionic liquid, Electroanalysis, 20 (2008) 2537-2542.

[79] S. Dong, Z. Li, Z. Yu, Y. Zhou, H. Tang, Direct electrochemistry of hemoglobin immobilized in chitosan-room temperature ionic liquid film and application in its interaction with 3,4'-bis-(4-hydro-3-xycoumarin)-2,5-hexanediol, Colloids Surf B Biointerfaces, 100 (2012) 133-7.

[80] L. Wang, X. Zhang, H. Xiong, S. Wang, A novel nitromethane biosensor based on biocompatible conductive redox graphene-chitosan/hemoglobin/graphene/room temperature ionic liquid matrix, Biosens Bioelectron, 26 (2010) 991-995.

[81] X. Lu, J. Hu, X. Yao, Z. Wang, J. Li, Composite system based on chitosan and room-temperature ionic liquid: direct electrochemistry and electrocatalysis of hemoglobin, Biomacromolecules, 7 (2006) 975-980.

[82] H.Y. Xiong, T. Chen, X.H. Zhang, S.F. Wang, Electrochemical property and analysis application of biosensors in miscible nonaqueous media—Room-temperature ionic liquid, Electrochem Commun, 9 (2007) 1648-1654.

[83] S.-F. Wang, T. Chen, Z.-L. Zhang, D.-W. Pang, K.-Y. Wong, Effects of hydrophilic room-temperature ionic liquid 1-butyl-3-methylimidazolium tetrafluoroborate on direct electrochemistry and bioelectrocatalysis of heme proteins entrapped in agarose hydrogel films, Electrochem Commun, 9 (2007) 1709-1714.

[84] R. Gao, J. Zheng, L. Qiao, Direct electrochemistry of hemoglobin in layer-by-layer films assembled with DNA and room temperature ionic liquid, Electroanalysis, 22 (2010) 1084-1089.

[85] M. Prudêncio, A.S. Pereira, P. Tavares, S. Besson, I. Cabrito, K. Brown, et al., Purification, characterization, and preliminary crystallographic study of copper-containing nitrous oxide reductase from *Pseudomonas nautica* 617, Biochemistry, 39 (2000) 3899-3907.

[86] U.K. Laemmli, Cleavage of structural proteins during the assembly of the head of bacteriophage T4, Nature, 227 (1970) 680-5.

[87] C.G. Timóteo, A.S. Pereira, C.E. Martins, S.G. Naik, A.G. Duarte, J.J.G. Moura, et al., Low-spin heme b_3 in the catalytic center of nitric oxide reductase from *Pseudomonas nautica*, Biochemistry, 50 (2011) 4251-4262.

[88] T.M. Oliveira, M. Fatima Barroso, S. Morais, M. Araujo, C. Freire, P. de Lima-Neto, et al., Laccase-Prussian blue film-graphene doped carbon paste modified electrode for carbamate pesticides quantification, Biosens Bioelectron, 47 (2013) 292-299.

[89] F. Faridbod, M.R. Ganjali, P. Norouzi, S. Riahi, H. Rashedi, Application of room temperature ionic liquids in electrochemical sensors and biosensors, Ionic liquids: applications and perspectives, InTech, 2011.

[90] W. Wei, H.-H. Jin, G.-C. Zhao, A reagentless nitrite biosensor based on direct electron transfer of hemoglobin on a room temperature ionic liquid/carbon nanotube-modified electrode, Microchim Acta, 164 (2009) 167-71.

[91] Q. Zhang, W. Wei, G.C. Zhao, Direct electrochemistry of myoglobin on a room temperature ionic liquid modified electrode and its application to nitric oxide biosensing, Electroanalysis, 20 (2008) 1002-1007.

[92] M.C. Rodriguez, A.-N. Kawde, J. Wang, Aptamer biosensor for label-free impedance spectroscopy detection of proteins based on recognition-induced switching of the surface charge, Chem Commun, (2005) 4267-4269.

[93] Y. Zheng, Z. Liu, Y. Jing, J. Li, H. Zhan, An acetylcholinesterase biosensor based on ionic liquid functionalized graphene–gelatin-modified electrode for sensitive detection of pesticides, Sens Actuators B Chem, 210 (2015) 389-397.

[94] J.E. Nielsen, J.A. McCammon, Calculating pKa values in enzyme active sites, Protein Sci, 12 (2003) 1894-1901.

[95] Q. Zhao, D. Zhan, H. Ma, M. Zhang, Y. Zhao, P. Jing, et al., Direct proteins electrochemistry based on ionic liquid mediated carbon nanotube modified glassy carbon electrode, Front Biosci. 10 (2005) 326-334.

[96] Y. Yin, Y. Lü, P. Wu, C. Cai, Direct Electrochemistry of redox proteins and enzymes promoted by carbon nanotubes, Sensors, 5 (2005) 220-234.

[97] D. Grieshaber, R. MacKenzie, J. Vörös, E. Reimhult, Electrochemical biosensors - Sensor principles and architectures, Sensors, 8 (2008) 1400-1458.

[98] E. Laviron, Adsorption, autoinhibition and autocatalysis in polarography and in linear potential sweep voltammetry, J Electroanal Chem Interfacial Electrochem, 52 (1974) 355-393.

[99] J. Berg, J. Tymoczko, L. Stryer, The Michaelis-Menten model accounts for the kinetic properties of many enzymes, Biochemistry, 5 (2002).

[100] A. Shrivastava, V. Gupta, Methods for the determination of limit of detection and limit of quantitation of the analytical methods, Chron. Young Sci., 2 (2011) 21-25.

[101] Y. Xu, C. Hu, S. Hu, Electrochemical behavior of biocatalytical composite based on heme-proteins, didodecyldimethylammonium bromide and room-temperature ionic liquid, Anal Chim Acta, 663 (2010) 19-26.

CHAPTER 6

BIOSENSOR FOR DIRECT BIOELECTROCATALYSIS DETECTION OF NITRIC OXIDE USING NITRIC OXIDE REDUCTASE INCORPORATED IN CARBOXYLATED SINGLE-WALLED CARBON NANOTUBES / LIPIDIC BILAYER NANOCOMPOSITE

An enzymatic biosensor for nitric oxide (NO) detection was prepared by deposition onto a pyrolytic graphite electrode (PGE) of a nanocomposite constituted by carboxylated single-walled carbon nanotubes (SWCNTs), lipidic bilayer [1,2-di-(9Z-octadecenoyl)-sn-glycero-3-phosphoethanolamine (DOPE), 1,2-di-(9Z-octadecenoyl)-3-trimethylammonium-propane (DOTAP) and 1,2-distearoyl-sn-glycero-3-phosphoethanolamine – polyethylene glycol (DSPE-PEG)] and nitric oxide reductase (NOR). NOR (307 U/mg) was purified from *Marinobacter hydrocarbonoclasticus*. NOR direct electron transfer behavior and NO bioelectrocatalysis were characterized by several electrochemical techniques; biosensor development was also followed by scanning electron microscopy and Fourier transform infrared spectroscopy. 4/2.5/4 (v/v/v) was the optimum ratio for the SWCNTs/(DOPE:DOTAP:DSPE-PEG)/NOR nanocomposite, which biomimicked the NOR environment improving its stability and the electron transfer (apparent rate constant of 1.96×10^{-4} $cm.s^{-1}$). The PGE/[SWCNTs/(DOPE:DOTAP:DSPE-PEG)/NOR] biosensor exhibited a low Michaelis-Menten constant (4.26 $\mu molL^{-1}$), wide linear range (0.44 – 9.09 $\mu molL^{-1}$), low detection limit (0.13 $\mu molL^{-1}$), high repeatability (4.1% RSD), reproducibility (7.0% RSD), and stability (*ca*. 5 weeks). Selectivity tests towards L-arginine, ascorbic acid, sodium nitrate, sodium nitrite and glucose showed that these physiologically relevant compounds did not significantly interfere in NO biosensing (91.0±9.3% to 98.4±5.3% recoveries). The proposed biosensor, by incorporating the benefits of biomimetic features of phospholipid bilayer with SWCNT´s inherent properties and NOR bioelectrocatalytic activity and selectivity, is a promising tool for NO detection.

6.1. Introduction

Nitric oxide reductase (NOR) is a key enzyme in the denitrification pathway, where nitrate is reduced to dinitrogen, through four sequential steps ($NO_3^- \rightarrow NO_2^- \rightarrow {}^{\bullet}NO \rightarrow N_2O \rightarrow N_2$), catalyzed by specific metalloenzymes. NOR catalyzes the reduction of nitric oxide radical (NO) to nitrous oxide (N_2O) in a two-electron/proton reaction [1]. This enzyme is a membrane-bound metalloprotein containing two subunits: the NorC subunit harbors one heme *c* and is responsible for the electron transfer from the physiological electron donor to the catalytic subunit; the NorB subunit, the catalytic subunit, is constituted by two hemes *b*, heme *b* and heme b_3, and one non-heme iron, Fe_B; heme b_3 and Fe_B are bridged by a μ-oxo/hydroxo group and, together, form the catalytic diiron center [2]. NOR can be isolated from different organisms, including denitrifying bacteria, such as *Paracoccus denitrificans*, *Pseudomonas stutzeri*, *Pseudomonas aeruginosa* or *Marinobacter hydrocarbonoclasticus* [2].

In the last decades, NO has been under a tremendous scrutiny due to the environmental importance of the denitrification pathway [3] and to the involvement of NO in a plethora of biological events in all forms of life (cell differentiation, regulation of blood flow, heart and neurodegenerative diseases, among many others) [4]. NO reacts promptly with several biological compounds, including O_2, heme proteins (e.g., hemoglobin), thiols (e.g., cysteine residues, glutathione), and other radicals (e.g., superoxide anion radical) and, as a consequence, has a short half-life, which has been reported to be in the range of 5–15 s [5]. Moreover, NO exists in a broad range of concentrations, from $pmolL^{-1}$ to $\mu molL^{-1}$. These NO features make its detection and quantification a challenging task. Therefore, appropriate analytical techniques to study NO should have a wide working range and rapid response times [6]. In this scenario, third-generation electrochemical biosensors are the approach of choice for direct, real-time, selective and sensitive measurements, for both *in vitro* and *in vivo* studies of NO metabolism and homeostasis [7]. Moreover, third-generation biosensors are a powerful tool to study catalytic mechanisms of redox enzymes [8].

Previously architected enzymatic biosensors for NO detection have been mainly based on peroxidases (horseradish peroxidase (HRP) and microperoxidase (MP)) [9, 10]. In this work, a new biosensor using the NOR from *Marinobacter hydrocarbonoclasticus* is described. This enzyme was the subject of a very limited number of studies [11-15], where it was directly immobilized onto a graphite

electrode, with the only goal of characterizing its electrochemical behavior and catalytic mechanism.

The major challenge to develop enzymatic biosensors is to succeed in the stabilization of the enzyme on the solid support. For this reason, carbon nanotubes (CNTs) are the most reported nanomaterials, because they keep high biological activity of the enzyme, decrease the redox potential of the reaction and increase the sensitivity, stability and lifetime of the biosensor [16]. Considering that NOR is a membrane-bound enzyme, a lipidic bilayer (liposomes composed by different phospholipids) is an interesting alternative for its immobilization, since it will allow to mimic the cellular NOR environment and keep enzyme conformation. Recently, lipidic structures were used in other systems to amplify the signal intensity, with clear benefits on the reached sensitivity and detection limits [17]. Anionic and zwitterionic phospholipids [1-hexadecanoyl-2-(9Z-octadecenoyl)-sn-glycero-3-phosphocholine (POPC); N-glutaryl-phosphatidylethanolamine (NGPE); 1,2-dihexadecanoyl-sn-glycero-3-phospho-(1'-rac-glycerol) (sodium salt) (DPPG); 1-hexadecanoyl-2-(9Z-octadecenoyl)-sn-glycero-3-phospho-(1'-rac-glycerol) (sodium salt) (POPG); 1,2-dimyristoyl-sn-glycero-3-phospho- (1-rac-glycerol) (DMPG); lyso-1-heptadecanoyl-sn-glycero-3-phosphocholine (LPC)] and Langmuir-Blodgett films composed by arachidic acid have been the most tested for the development of enzymatic biosensors (Table 6.1); the enzymes used on those studies were glucose oxidase (GOD), monoamine oxidase B (MAO-B), tyrosinase (Tyr), acetylcholinesterase (AChE), HRP and MP. Still, the number of studies is very limited [18-24]. Cationic and other zwitterionic phospholipids, such as 1,2-di-(9Z-octadecenoyl)-sn-glycero-3-phosphoethanolamine (DOPE), 1,2-di-(9Z-octadecenoyl)-3-trimethylammonium-propane (DOTAP) and 1,2-distearoyl-sn-glycero-3-phosphoethanolamine (DSPE) have not yet been tested for preservation, stabilization and immobilization of enzymes. Moreover, the insertion of hydrophilic polymers, such as polyethylene glycol (PEG), in the lipidic bilayer may help to avoid liposomes fusion, while promoting excellent biocompatibility, low immunogenicity and antigenicity for *in vivo* assays [25]. PEG is non-ionic, low fouling and possesses high solubility in both aqueous and has different molecular weights, influencing, in this way, the lipidic bilayer permeability [26]. Pegylated lipidic bilayer has been widely applied for drug delivery systems [25], but not yet applied in electrochemical enzymatic biosensors [27].

Therefore, in this study, and for the first time, carboxylated single-walled carbon nanotubes (SWCNTs) were combined with the lipidic bilayer DOPE:DOTAP:DSPE-PEG and NOR to modify a pyrolytic graphite electrode (PGE) in order to develop a novel and sensitive third-generation electrochemical biosensor for NO detection.

Table 6.1. Review of the reported enzymatic biosensors based on lipidic bilayer.

Transducer	Enzyme	Lipidic bilayer	Immobilization	Method	Analyte	Substrate /detected species	Linear range ($\mu molL^{-1}$)	Limit of detection ($\mu molL^{-1}$)	Ref.
Tin oxide doped with indium	Glucose Oxidase	POPC/NGPE/ cholesterol	Encapsulated enzyme PAH/MnO_x electrodeposited film Carboxylic groups of NGPE with EDC/NHS Incubation PAH/MnO_x with liposomal glucose oxidase	Amperometry	Glucose	H_2O_2	19600–107100	13000	[18]
Tin oxide doped with indium	Monoamine oxidase B	DPPG/POPG	Electrode surface modification with Prussian blue Immersion in a PEI solution alternated with enzyme solution (Layer-by-layer)	Amperometry	Dopamine	H_2O_2	1400–10000	860±16	[19]
Tin oxide doped with indium	Tyrosinase	LB films	Mixture of lutetium bisphthalocyanine and arachidic acid LB filmes were immersed in glutaraldehyde	Cyclic Voltammetry	Antioxidants	Caffeic acid	10–400	1.98	[20]
Glassy carbon electrode	Tyrosinase	LPC	Lipid film's hydration technique LPC: cholesterol: Tyr: pyranine Porin was added giving the TLB CS deposited on electrode surface Immersed on TLB	Cyclic Voltammetry	Phenolic compounds	Phenol	0.25×10^{-3}–25	0.091×10^{-3}	[21]
Glassy carbon electrode	Acetylcholin esterase	LPC	Lipid film's hydration technique LPC: Cholesterol: AChE: pyranine Porin was added giving the ALB CS deposited on electrode surface MWCNTs deposited on CS modified electrode (multiple layers) and immersed on ALB solution Process repeated 6 times	Cyclic Voltammetry	Organophosphate Pesticides	Acetylthiocholine chloride	0.25–1.75 2.00–10.00	0.68±0.076 µg/L	[22]
Glassy carbon electrode	Horseradish peroxidase	N,N'-bis(10-undecenyl)-2-methylimidazolium bromide	Ionic liquid modified lipid Potassium persulfate Thermal polymerization IL-polysomes/PVA cast on electrode Immersed on enzyme solution	Cyclic Voltammetry	H_2O_2	H_2O_2	10–2300	3.33	[23]
Glassy carbon electrode	Microperoxidase	DMPG	Graphene oxide was dispersed in DMPG L-ascorbic acid was mixed with the previous suspension.	Cyclic Voltammetry	H_2O_2	H_2O_2	2.0–450	0.72	[24]

AChE, acetylcholinesterase; ALB, AChE liposomes bioreactor; CS, chitosan ; DMPG, 1,2-dimyristoyl-sn-glycero-3-phospho- (1-rac-glycerol); DPPG, dipalmitoyl phosphatidyl glycerol; EDC/NHS, N-ethyl-N'-(3-(dimethylamino)propyl)carbodiimide/N-hydroxysuccinimide; LB, Langmuir-Blodgett; LPC, L- phosphocholine; MWCNTs, multi walled carbon nanotubes; NGPE, N-glutaryl-phosphatidylethanolamine; PAH, poly- (allylamine hydrochloride); PEI, polyethylene imine; POPC, 1-palmitoyl-2- oleoyl-sn-glycero-3-phosphocholine; POPG, palmitoyl phosphatidyl glicera; PVA, polyvinyl alcohol; TLB, lyr liposomes bioreactor.

6.2. Materials and methods

6.2.1. Reagents

SWCNTs-COOH, chloroform ($CHCl_3$, p.a.), N,N-dimethylformamide (DMF; 99%), HEPES buffer (10 $mmolL^{-1}$, pH 7.4), 2-phenylethanol (PE; ≥ 99.0%), potassium hexa-cyanoferrate (II) trihydrate ($C_6FeK_4N_6.3H_2O$; ≥ 99%), potassium hexa-cyanoferrate (III) ($C_6FeK_3N_6$; ≥ 99%) and L-Arginine (≥ 98%) were purchased from Sigma-Aldrich (Steinhein, Germany). Sulfuric acid (H_2SO_4; 96%), ethanol (EtOH; 99.5%) and n-dodecyl-β-D-maltoside (DM) were obtained from Panreac (Barcelona, Spain). DOTAP (chloride salt, 698.54 g mol^{-1}; >99%), DOPE (744.03 g mol^{-1}; > 99%) and DSPE-PEG (1,2-distearoyl-sn-glycero3-phosphoethanolamine-N-[amino(polyethylene glycol)-2000] (ammonium salt, 2790.49 g mol^{-1}; > 99%) were purchased from Avanti Polar Lipids (Alabama, USA). Di-potassium hydrogen phosphate (K_2HPO_4, p.a.) and potassium dihydrogen phosphate (KH_2PO_4, p.a.) were used to prepare phosphate buffer (100 $mmolL^{-1}$, pH 6.0); they were bought from Riedel-de-Haën (Germany) as well as potassium hydroxide (p.a.), ascorbic acid (p.a.) and sodium nitrate (p.a.). Sodium nitrite (p.a.) was acquired from M&B and D-glucose anhydrous (ACS) from Scharlau (Barcelona, Spain).

NO solutions of different concentrations were prepared by dilution from a buffer stock solution of 100 $\mu molL^{-1}$ [28] prepared by bubbling a 5% NO/95% He gas mixture (Air Liquid, Portugal) into phosphate buffer 100 $mmolL^{-1}$ pH 6.0. All solutions and stock were prepared immediately before being used.

Ultrapure water obtained from a Millipore water purification system (18 MΩ, Milli-Q, Millipore, Molsheim, France) was used in all experiments.

6.2.2. NOR purification

NOR is not commercially available and it was purified from membrane extracts of *Marinobacter hydrocarbonoclasticus* grown anaerobically as described by Prudêncio *et al.* [29]. NOR purity was assessed by its UV–visible spectrum (UV 1800-Shimadzu, 250-800 nm, Germany) and by sodium dodecyl sulfate polyacrylamide gel electrophoresis (SDS-PAGE) (Bio-Rad, Mini-PROTEAN® Tetra Handcast Systems, Portugal) based on the protocol of Laemmli [30]. The NOR preparation used in these studies had a specific activity of 307 U/mg, determined as described previously by

Timóteo et al. [31], using an ISO-NO Mark II amperometric sensor (2 mm, World Precision Instruments, Inc., UK: one unit corresponds to 1 μmol of NO/min).

6.2.3. Lipidic structures

Liposomes as lipidic bilayer were prepared by lipid film hydration method [32]. DOPE (zwitterionic phospholipids), DOTAP (cationic phospholipids) and DSPE-PEG (zwitterionic pegylated phospholipids) dispersed in chloroform were mixed at the volume ratio of 74.5:70:5.7. Then, the solvent was evaporated with nitrogen flow until getting a lipid film. The obtained dried film was dispersed in HEPES buffer and vortexed for 15 minutes in order to obtain multilamellar vesicles. The suspension was sonicated in an ultrasonic processor (Hielscher ultrasound technology UP400S; amplitude: 20%; cycle: 1; time: 1 minute; pulse on: 10 s; pulse off: 15 s) in order to obtain unilamellar vesicles with low and homogenous size. The hydrodynamic size average measurements were performed by dynamic light scattering (DLS) (Malvern Zetasizer NANO ZS instrument). The zeta-potential was also assessed with the same equipment by the laser Doppler velocimetry technique. The liposomes with a concentration of 10 $mmolL^{-1}$ exhibit a *D*-average of 228 ± 10 nm and a zeta potential of 29.7 ± 4 mV evaluated at a 1:15 dilution (liposomes: HEPES buffer, v/v). After deposition in the electrode, the liposomes were dehydrated, forming a lipidic bilayer.

6.2.4. Biosensor fabrication

Firstly, the PGE (A = 7.07 mm^2; ALS Co., Ltd; Tokyo, Japan) was successively treated by hand polished with 1.0 and 0.3 μm alumina (Gravimeta Lda, Portugal), briefly sonicated with EtOH and finally rinsed with ultrapure water. The surface activation was performed by cyclic voltammetry (CV) in H_2SO_4 0.5 $molL^{-1}$ at 100 mV/s in the range of 0 V to 1.6 V *vs*. Ag/AgCl/Cl^- sat.. SWCNTs were prepared in DMF with a final concentration of 1.0 mg/mL. 10.5 μL of the nanocomposite [SWCNTs/(DOPE:DOTAP:DSPE-PEG)/NOR], prepared by mixing 4 μL of SWCNTs suspension at 0.5 mg/mL (dilution of the SWCNTs stock suspension with phosphate buffer; 1:1, v/v) with 2.5 μL of (DOPE:DOTAP:DSPE-PEG) at 74.5:70:5.7 volume ratio and 4 μL of NOR at 307 U/mg, were immobilized on the PGE surface using the solvent casting technique and left overnight at 4ºC.

6.2.5. Electrochemical measurements

The modified PGE (PGE/SWCNTs; PGE/[SWCNTs/(DOPE:DOTAP:DSPE-PEG)] or PGE/[SWCNTs/(DOPE:DOTAP:DSPE-PEG)/NOR]) was set as the working electrode, and a platinum wire and silver/silver chloride saturated with KCl 3 $molL^{-1}$ were the secondary and reference electrodes, respectively. The three-electrode system was connected to an Autolab PGSTAT 204 potentiostat-galvanostat controlled by GPES 4.9.7 and Nova 1.10 software (Metrohm Autolab). The assays were conducted in one compartment cell using as electrolyte 100 $mmolL^{-1}$ of phosphate buffer with 0.02% DM and 0.01% PE at pH 6.0 for NOR redox behavior and NO bioelectrocatalysis or the same buffer with 2.5 $mmolL^{-1}$ $[Fe(CN)_6]^{3-/4-}$ for characterization of the biosensor construction. The redox behavior of NOR was evaluated by square-wave voltammetry (SWV) at the optimum parameters of 100 Hz, amplitude of 20 mV and step of 3 mV in a potential scale range of +0.4 to -1.0 V with a previous deoxygenation of the electrolyte using nitrogen gas during 20 minutes. NO bioelectrocatalysis was performed in the same potential window and using the same SWV conditions with the exception of the frequency that was 10 Hz. Electrochemical impedance spectroscopy (EIS) assays were performed in the buffer solution with 2.5 $mmolL^{-1}$ $[Fe(CN)_6]^{3-/4-}$ (pH 6.0) applying a frequency range from 10^{-1} to 10^{5} Hz with an amplitude perturbation of 5 mV and 0.2 V of conditioning potential.

6.2.6. Morphological and structural characterization

Scanning electron microscopy (SEM) with energy-dispersive X-ray spectroscopy (EDS) (High Resolution (Schottky) Environmental Scanning Electron Microscope with X-Ray Microanalysis and Electron Backscattered Diffraction analysis (Quanta 400 FEG ESEM / EDAX Genesis X4M)) and *Fourier* transform infrared spectroscopy with attenuated total reflectance (FTIR-ATR) (Nicolet 6700 FTIR spectrometer (Thermo Scientific) controlled by OMNIC software) were used to characterize the biosensor construction.

6.3. Results and discussion

6.3.1. Biosensor construction

a) Electrochemical characterization

SWV and EIS assays performed using $Fe(CN)_6^{3-/4-}$ as electroactive indicator in the supporting electrolyte (pH = 6.0) were used to characterize the different steps involved in the biosensor development. pH has a marked effect on NOR activity and it was maintained at the optimum value of 6.0 [13, 33] during all the experiments.

Fig. 6.1-(A) displays the square-wave voltammograms obtained with the PGE, PGE/SWCNTs, PGE/[SWCNTs/(DOPE:DOTAP:DSPE-PEG)] and PGE/[SWCNTs/(DOPE:DOTAP:DSPE-PEG)/NOR]. As expected, the characteristic reduction peak of the electroactive indicator was detected at around 0.14-0.20 V by all the (bare and modified) electrodes. However, significantly different current intensities were attained showing the impact of the performed modifications. Drop casting of 2 µL SWCNTs at 1 mg/mL onto the PGE surface promoted the biggest current increase (about 2.5 times). CNT-based biosensors generally have higher sensitivity and lower limit of detection due to the faster electron transfer kinetics, larger surface areas and electrocatalytic properties [7]. The amount of SWCNTs deposited on the surface of the PGE was optimized by testing three different volumes namely 1.0, 2.0, and 5.0 µL. An increase of the current peak almost proportional to the increase of SWCNTs quantity was observed between 1 and 2 µL. No significant current differences were observed between 2 and 5 µL and, due to the difficulty to have reproducible results with this last volume, the optimum result was considered to be 2.0 µL of 1.0 mg/mL SWCNTs or the equivalent amount (i.e. 4.0 µL of 0.5 mg/mL SWCNTs when SWCNTs were mixed with DOPE:DOTAP:DSPE-PEG and/or NOR) since it proved to be enough to cover the electrode surface while promoting a low standard deviation of the peak current.

The selected lipidic suspension (DOPE:DOTAP:DSPE-PEG; 74.5:70:5.7 volume ratio) was mixed with SWCNTs in order to mimic the environment of the enzyme and to increase its stability and lifetime [25]. The composition of the lipidic bilayer had high amount of DOPE phospholipids in order to simulate biological membranes. However, to increase its stability on the electrode surface, positive charged phospholipids (DOTAP) were included. In this way, the lipidic bilayer interacted

electrostatically with the negative charged (due to functionalization with carboxylic groups) SWCNTs. The influence of the concentration of lipidic bilayer on the PGE/[SWCNTs/(DOPE:DOTAP:DSPE-PEG)] signal was evaluated by comparison with the current intensity reached with PGE/SWCNTs. 2.5 μL of five different concentrations of the lipidic bilayer mixture (1:5000, 1:500, 1:250, 1:25 and 1:15 liposomes:HEPES buffer ratio; v/v) were tested and results are presented in Fig. 6.2. The ratios of 1:5000, 1:500 and 1:250 (with not detectable, 6.0 and 13.9% peak reduction, respectively) did not promote a significant impact on the peak current of the PGE/[SWCNTs/(DOPE:DOTAP:DSPE-PEG)] suggesting insufficient amount of lipidic bilayer; the successful incorporation of phospholipids in a biosensor platform is expected to promote the diminution of the current peak caused by the negative effect on electron transfer reaction [34]. When the ratio was increased to 1:25 and 1:15 (v/v), the peak current markedly decreased (21.9 – 34.1%) showing that the lipidic bilayer significantly interacted with the SWCNTs. These results can be due to the presence of higher amount of lipidic bilayer and by the electrostatic interactions between the positive charges of the lipidic bilayer (zeta potential of 29.7 mV) and the negative charges of the carboxilated groups of the SWCNTs. As the lipidic bilayer was highly diluted (1:250 to 1:5000, v/v), the zeta potential decreased and became less positive hampering the interactions. Therefore, the 1:15 (v/v) (DOPE:DOTAP:DSPE-PEG):HEPES buffer ratio was considered the optimum concentration to prepare the nanocomposite. These results are not comparable with literature data since no similar study was found regarding enzymatic biosensors development. The integration of NOR in the prepared nanocomposite [SWCNTs/(DOPE:DOTAP:DSPE-PEG)/NOR] (4/2.5/4, v/v/v)), used to modify the PGE, produced a significant deviation of the electroactive indicator peak potential (0.137 ± 0.009 V instead of the initial potential of 0.200 ± 0.009 V) and a significant decrease of the current (23 times lower when compared with the PGE/[SWCNTs/(DOPE:DOTAP:DSPE-PEG)] and 29 times lower with PGE/SWCNTs). This behavior suggested successful entrapment of NOR. No significant differences were detected when 7 μL were tested instead of 4 μL of NOR.

EIS assays (Fig. 6.1-(B)-(C)) were also performed to supplement SWV data. In this technique, the changes of charge transfer resistance or also called polarization resistance (Rct) are observed, and the resistance of the electrolyte (Rs), Warburg impedance (W) and capacitance of the system (Cp) are maintained constant. Therefore, EIS measurements were employed to characterize the electron transfer

efficiency of the proposed biosensor using a circuit of Rs(Cp[RctW]) (Fig. 6.1-(C)), where polarization is due to a combination of kinetic and diffusion models [35].

Significant differences between the attained Rct of the PGE, PGE/SWCNTs, PGE/[SWCNTs/(DOPE:DOTAP:DSPE-PEG)] and PGE/[SWCNTs/(DOPE:DOTAP:DSPE-PEG)/NOR] can be observed (Fig. 6.1-(B)). The redox process at PGE displayed low resistance with a value of 653 Ω. When the SWCNTs were casted on the PGE surface, no semicircle was observed indicating that the interfacial electron transfer was improved due to the inherent SWCNTs properties. With the incorporation of the lipid bilayer, and subsequently NOR, the Rct considerably increased reaching 7.70 kΩ, which explain the decreased peak currents noticed in SWV. Therefore, these results further reinforce that the immobilization of NOR in the prepared nanocomposite was effectively accomplished. Moreover, the time for stabilization of the PGE/[SWCNTs/(DOPE:DOTAP:DSPE-PEG)/NOR] signal, using five freshly prepared biosensors, was assessed during ten consecutive days. From day zero to day one, a 35% current augmentation was perceived while no further meaningful changes were noted during the tested period ($-2.49 \times 10^{-6} \pm 3.71 \times 10^{-7}$ A (day 0); $-3.37\times 10^{-6} \pm 3.32 \times 10^{-7}$ A (day 1) to $-3.57\times 10^{-6} \pm 3.59 \times 10^{-7}$ A (day 10); n=5). One day appeared enough to have NOR in the perfect rearrangement/conformation in the proposed biosensor. Compared to the free forms, immobilizing enzymes in nano- or bio-materials, including lipidic bilayer, can confer longer stability, improvement in selectivity and activity, and easier manipulation [36, 37]. This time span was chosen as the operational stabilization time before the electroanalytical application of the proposed biosensor.

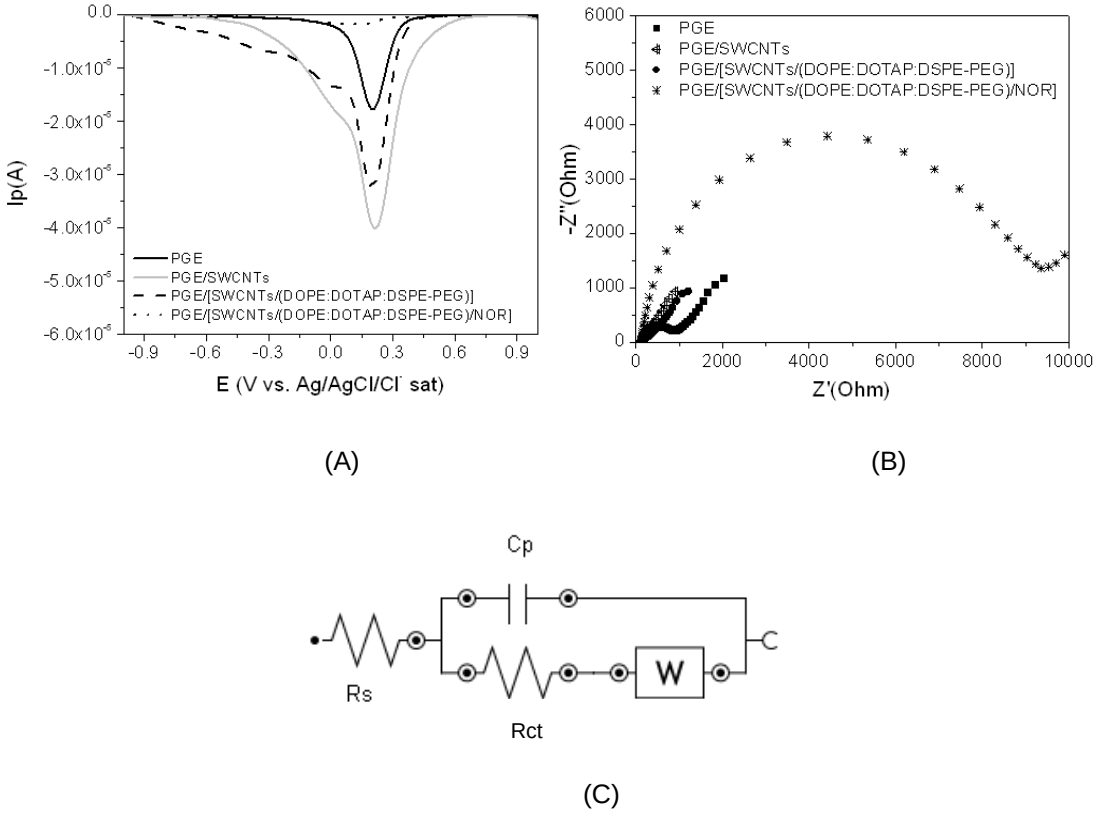

Fig. 6.1. (A) Square-wave voltammograms and (B) Nyquist plots of the different stages of the PGE biosensor development obtained in 2.5 mmolL^{-1} $[Fe(CN)_6]^{3-/4-}$ and 100 mmolL^{-1} of phosphate buffer with 0.02% n-dodecyl-β-D-maltoside and 0.01% 2-phenylethanol (pH 6.0). Square-wave voltammetry parameters: frequency of 50 Hz, amplitude of 50 mV and step potential of 2 mV; electrochemical impedance spectroscopy conditions: frequency range from 10^{-1} to 10^{5} Hz with an amplitude perturbation of 5 mV and 0.2 V of conditioning potential. (C) Equivalent electrical circuit composed by the resistance of the solution (Rs/Ω), the Warburg impedance (W/Ω), the double-layer capacitance (Cp/F), and the electron transfer resistance (Rct/Ω).

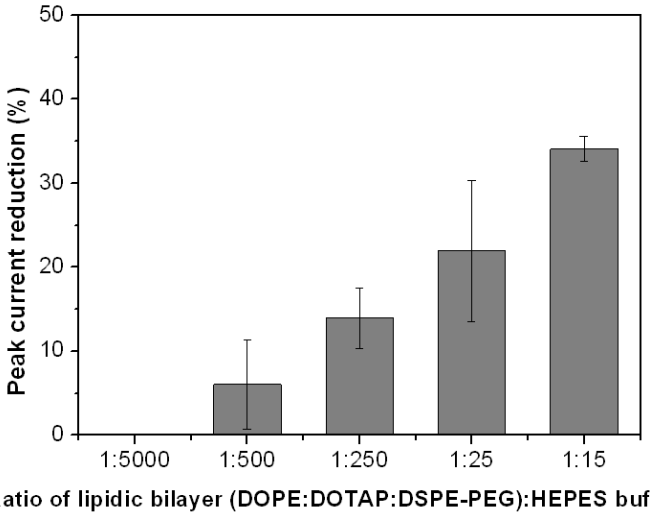

Fig. 6.2. Peak current reduction (%) of the PGE/[SWCNTs/(DOPE:DOTAP:DSPE-PEG)] (when compared with PGE/SWCNTs) *versus* ratio of lipidic bilayer (DOPE:DOTAP:DSPE-PEG; 74.5:70:5.7 (v/v/v)):HEPES buffer (v/v). Experimental square-wave voltammetry conditions: frequency of 50 Hz, amplitude of 50 mV and step potential of 2 mV, 2.5 $mmolL^{-1}$ $[Fe(CN)_6]^{3-/4-}$ in 100 $mmolL^{-1}$ of phosphate buffer with 0.02% n-dodecyl-β-D-maltoside and 0.01% 2-phenylethanol (pH 6.0).

b) Morphological and structural characterization

Fig. 6.3 illustrates the surface morphology of the biosensor at the different stages of construction. The PGE/SWCNTs surface shows a common morphology [38] with carbon nanotube filaments well-distributed and forming an homogeneous film without damage (Fig. 6.3-(A)). When the lipidic bilayer was mixed with the SWCNTs (Fig. 6.3-(B)), some prominences, protuberances and shadows were perceived originating a consistent film structure, which may still be considered homogeneous. It has been proposed that, after the SWCNTs incorporation in lipids or other amphiphilic surfactants, the tubes could be adsorbed by the surfactants in a randomly distributed form or either created the core of cylindrical micelles [39]. The introduction of NOR in the nanocomposite resulted in a completely different surface morphology (Fig. 6.3-(C)) (when compared to the PGE/[SWCNTs/(DOPE:DOTAP:DSPE-PEG)]; Fig. 6.3-(B)), i.e. significantly less flat, more irregular, with a film similar to a gel demonstrating the well distribution of NOR in the prepared nanocomposite.

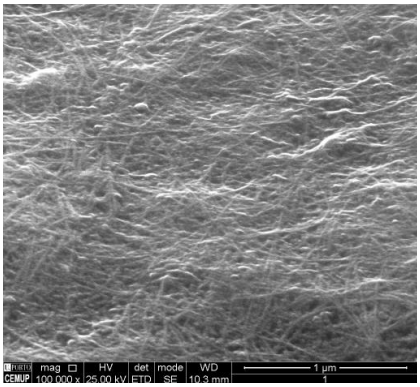

(A)

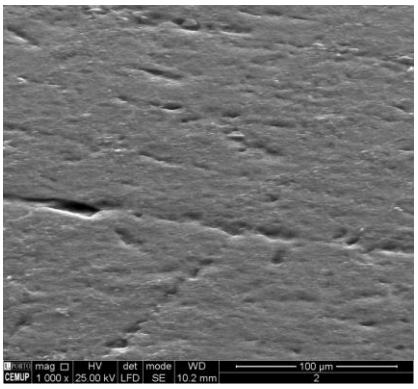

(B)-1

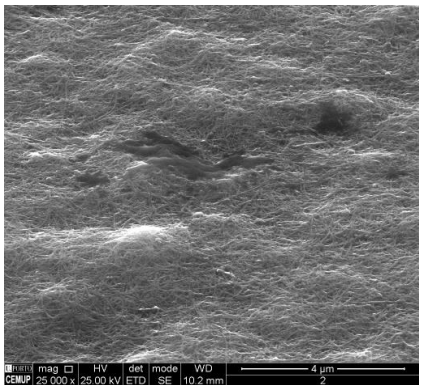

(B)-2

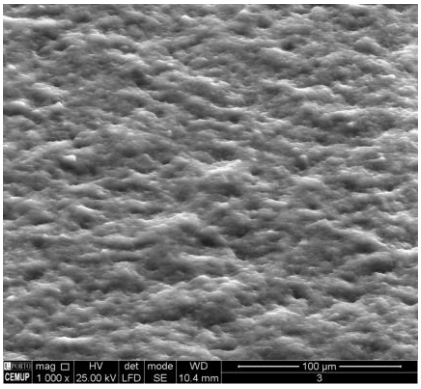

(C)-1

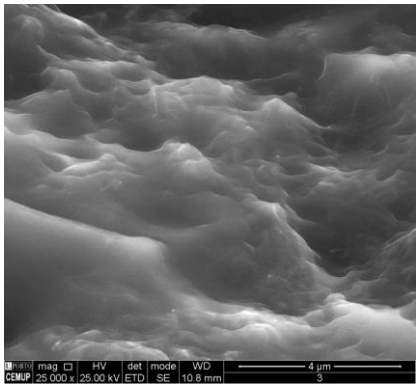

(C)-2

Fig. 6.3. Scanning electron microscopy images of (A) PGE/SWCNTs, (B) PGE/[SWCNTs/(DOPE:DOTAP:DSPE-PEG) and (C PGE/[SWCNTs(DOPE:DOTAP:DSPE-PEG)/NOR].

Regarding the results of FTIR spectroscopy (Fig. 6.4), the spectrum of NOR displayed the presence of two principal bands, one at 1643 cm^{-1} (C=C, C=N, C=O) and the other between 2848 – 3700 cm^{-1} (N-H or O-H). The strongest SWCNTs band appeared at *ca.* 1650 cm^{-1} and can be attributed to COOH stretching confirming

carbon nanotubes functionalization with carboxylic groups; other bands with wavenumber of 1064, 1103, 1253, 1388, 1436, 1498, and 3023 – 3646 cm^1 are common with those of the solvent used to prepared the SWCNTs suspension (DMF). The spectra of [SWCNTs/(DOPE:DOTAP:DSPE-PEG)] and [SWCNTs/(DOPE:DOTAP:DSPE-PEG)/NOR] were similar with the one of SWCNTs, being the main difference related with the reduction of the observed transmittance values of COOH band (70, 59 and 33 a.u. for SWCNTs, SWCNTs/(DOPE:DOTAP:DSPE-PEG) and SWCNTs/(DOPE:DOTAP:DSPE-PEG)/NOR, respectively). Clearly, the stability of the film and consequent enhanced performance of the proposed biosensor resulted from the hydrogen-bond interactions among the carboxylic acid groups of SWCNTs, the protonated imine nitrogen atom of the lipidic bilayer and the amine group of the NOR enzyme.

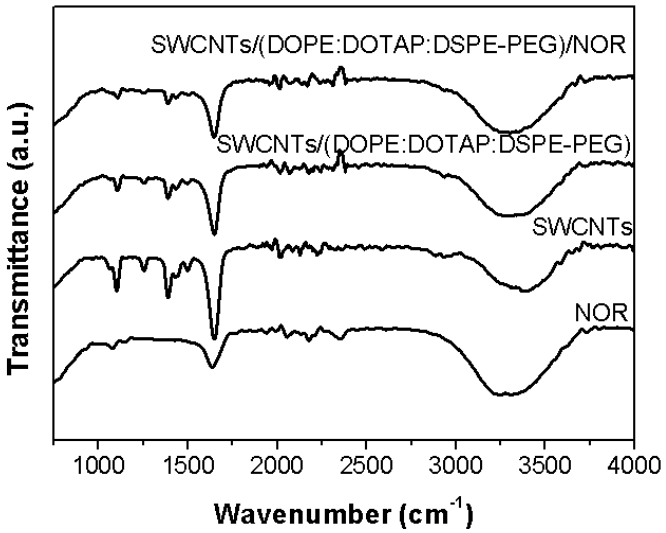

Fig. 6.4. Fourier transform infrared spectroscopy spectra of NOR enzyme and of the different stages of the biosensor development.

6.3.2. Direct electron transfer behavior of nitric oxide reductase

Comparative square-wave voltammograms of the direct electrochemical response of NOR on PGE and on the proposed biosensor in buffer (at pH 6.0) are exhibited in Fig. 6.5. To attain the best electroanalytical signal, the parameters of SWV were optimized. Briefly, the frequency was ranged from 10 to 285 Hz, the amplitude from 5 to 50 mV and the step from 1 to 4 mV. A frequency of 100 Hz, a pulse amplitude of 20 mV and a step potential of 3 mV were selected as the most adequate for

subsequent NOR direct electron transfer (DET) characterization considering peak baseline, definition and current. The high sensitivity of SWV allowed to perceive two centers of the enzyme at -0.406 ± 0.002 V for heme b_3 (peak 1) and at -0.272 ± 0.004 V for heme *b* (peak 2) on PGE/NOR (Fig. 6.5).

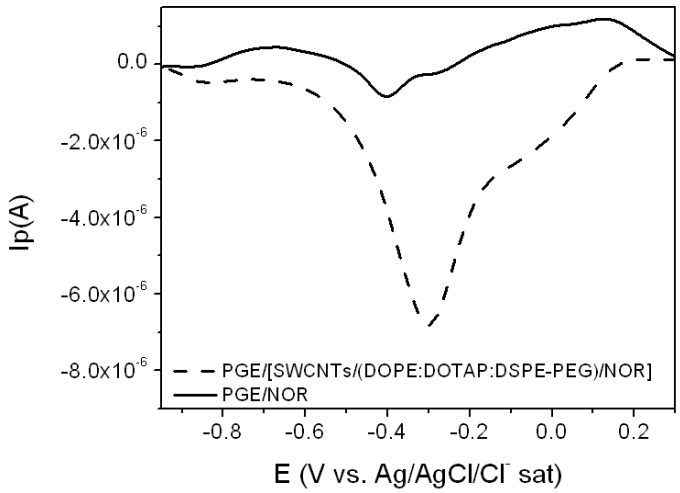

Fig. 6.5. Comparative square wave voltammograms of direct electrochemical behavior of NOR on PGE and PGE/[SWCNTs/(DOPE:DOTAP:DSPE-PEG)/NOR]. Peaks 1 and 2 correspond to heme b_3 and heme *b* centers, respectively. Experimental conditions: frequency of 100 Hz, amplitude of 20 mV and step potential of 3 mV in 100 mmolL^{-1} of phosphate buffer with 0.02% n-dodecyl-β-D-maltoside and 0.01% 2-phenylethanol (pH 6.0).

The other NOR centers (heme *c* and non-heme Fe_B at *ca.* 0.05 V and -0.58 V, respectively) can only be detected in anaerobic conditions. These results are in agreement with those previously reported by Cordas et al. [11] with non-significant deviations in heme potentials. Regarding DET of NOR on PGE/[SWCNTs/(DOPE:DOTAP:DSPE-PEG)/NOR], only the peak corresponding to the low spin heme b_3 bi-nuclear catalytic center was distinctly observed at a lesser negative potential, -0.308 ± 0.003 V. Moreover, an enhanced sensitivity was noticed with the reduction current of heme–(Fe(III)/Fe(II) eight times higher on the developed biosensor than on PGE/NOR. This favorable behavior is directly linked with the adopted immobilization strategy and with the fast electron-transfer rates between heme *c*/heme *b*, and heme *b*/heme b_3 in the bi-nuclear site [13]. Using different square-wave frequencies (10 to 285 Hz; n=8), the surface concentration of the electroactive species (τ^*, mol/cm^2) was estimated for PGE/[SWCNTs/(DOPE:DOTAP:DSPE-PEG)/NOR] biosensor using the Faradic

equation [40] considering the geometric area of the electrode since the real area of the modified electrode cannot be determined due to unidentified diffusion coefficient. The attained value was 1.10×10^{-10} mol/cm^2 for the constructed biosensor, which is about 7 times higher than the one reported by Cordas et al. [12] for PGE/NOR (1.52×10^{-11} mol/cm^2), as a consequence of the large specific surface area of SWCNTs and DOPE:DOTAP:DSPE-PEG that permitted the existence of additional active sites of NOR. Furthermore, the determined surface coverage is comparable with others from previous reported biosensors, namely those based on DET of hemoglobin adsorbed on the gold colloids modified carbon paste electrode or captured in a cationic gemini surfactant film [41].

The influence of surface PGE modification in kinetics performance was also evaluated using the apparent electron transfer rate constant (K_{app}, cm.s^{-1}) estimated by equation 1 [42]:

$$K_{app}=RT(n^2F^2AR_{ct}C)^{-1} \qquad \text{(Eq. 1)}$$

where **R** is the ideal gas constant (J mol^{-1} K^{-1}), **T** is the temperature (K), **n** is the number of electrons involved in reaction (n = 1), **F** is the Faraday constant (C mol^{-1}), **A** is the electrode area (cm^2), $\mathbf{R_{ct}}$ is the charge transfer resistance (Ω) and C is the concentration of the redox species (mol/cm^3). A value of 1.96×10^{-4} cm.s^{-1} was reached for the PGE/[SWCNTs/(DOPE:DOTAP:DSPE-PEG)/NOR] biosensor, which unequivocally demonstrates its fast electron transfer process, being comparable with values reported for other enzymatic biosensors [43].

6.3.3. Direct bioelectrocatalytic analysis of nitric oxide

Since NO is reduced by the selected bacterial NOR enzyme with the formation of nitrous oxide and water (equation 2), the response of the proposed biosensor to NO was studied (Fig. 6.6). The reduction potential of NO was evidenced at -0.69 ± 0.02 V, which is near to the reported values for other heme-protein (hemoglobin and myoglobin) sensors [44, 45]. The optimum SWV parameters for NO bioelectrocatalysis were determined as being 10 Hz, 20 mV and 3 mV for the frequency, pulse amplitude and the staircase step, respectively.

$2NO+2e^-+2H^+ \longrightarrow N_2O+H_2O$ (Eq. 2)

The majority of studies reported in the literature regarding the interaction of NO with different types of NOR are theoretical studies [46-48]; only a few works are based on electrochemical techniques [11-15]. Several possible mechanisms for the bioelectrocatalytic NO reduction by NOR have been described based on experimental and computational data, namely the trans-mechanism, the cis-Fe_B and the cis-heme b_3 mechanism [49]. However, due to the very limited information regarding this enzyme, the real mechanism is not yet established and is a still a matter of debate [11, 13, 48].

The apparent Michaelis-Menten constant (K_m; $\mu molL^{-1}$), that reveals the biological activity including the kinetic constants of immobilized enzymes, was determined using the Lineweaver–Burk equation (eq. 3) [50]:

$1/I_{ss}=K_m/I_{max}\times 1/[NO]+1/I_{max}$ (Eq. 3)

where $\boldsymbol{I_{ss}}$ (A) is the steady-state current after addition of the substrate*;* **[NO]** *(*$molL^{-1}$) is the concentration of the substrate and $\boldsymbol{I_{max}}$ (A) is the maximum current measured [50]. The estimated K_m was 4.26 $\mu molL^{-1}$ suggesting that the bioactivity of the immobilized enzyme was well preserved on the prepared biosensor. Also, this result evidenced the high affinity of NOR to NO, which compares favourably with most of the published apparent Michaelis-Menten constants for NO biosensors [51, 52], with the exception of data from Wen et al. [53] and Li et al. [54].

Fig. 6.6 displays the biosensor response to different standard NO concentrations under the optimized conditions (the blank is also included). The attained calibration curve (I (A) = $-7.70\times10^{-7} \pm 4.65\times10^{-8}$ log[NO; $\mu molL^{-1}$] + $1.80\times10^{-7} \pm 3.37\times10^{-8}$, n=6) presented good sensitivity (0.77 $\mu A/log\mu molL^{-1}$), satisfactory linear range (0.44 to 9.09 $\mu molL^{-1}$ NO), data with low standard deviation (0.4 to 9.5%) and acceptable quadratic correlation coefficient (r^2=0.986). Values of 0.13 $\mu molL^{-1}$ for limit of detection (LOD) and 0.44 $\mu molL^{-1}$ for limit of quantification (LOQ) were estimated based on 3*Sy-intercept/slope and 10*Sy-intercept/slope, respectively, where Sy-intercept is the standard deviation of the y-intercept [55].

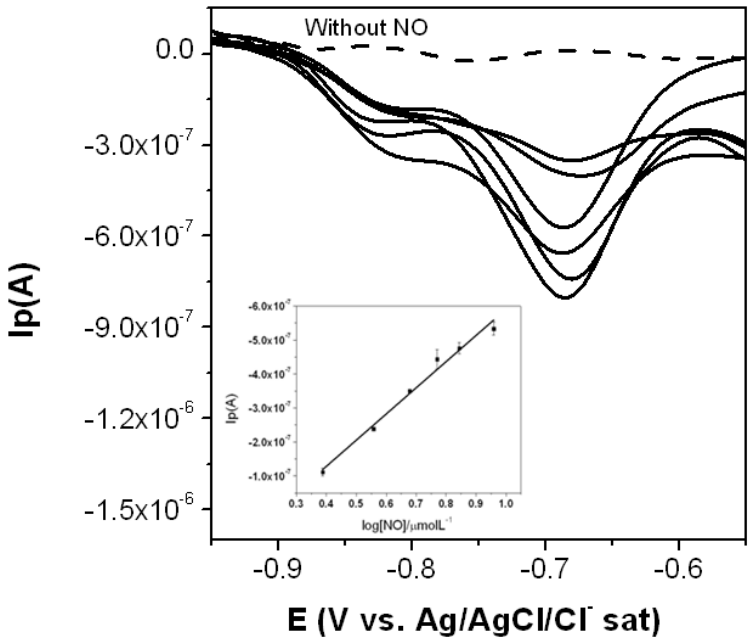

Fig. 6.6. Square wave voltammograms obtained with PGE/[SWCNTs/(DOPE:DOTAP:DSPE-PEG)/NOR] in the absence of NO and in the presence of standard NO concentrations of 2.44, 3.61, 4.76, 5.88, 6.98 and 9.09 $\mu molL^{-1}$. Inset: Respective calibration curve. Experimental conditions: frequency of 10 Hz, amplitude of 20 mV and step potential of 3 mV in 100 $mmolL^{-1}$ of phosphate buffer with 0.02% n-dodecyl-β-D-maltoside and 0.01% 2-phenylethanol (pH 6.0).

The main figures of merit compares favourably with those previously published for hemoglobin- [52, 56] and cyt *c*- based sensors [51, 57]. The proposed PGE/[SWCNTs/(DOPE:DOTAP:DSPE-PEG)/NOR] biosensor may be applicable to screen NO levels released from biological systems. Previous *in vivo* studies have been reporting NO concentrations in the order of 1 to 3 $\mu molL^{-1}$ in rat liver and brain [58-60].

The intra-day repeatability and the reproducibility of the device were estimated by carrying out five analyses in the same day and by independently preparing and testing five biosensors, respectively. The values of relative standard deviation ranged from 4.1 to 7.0% for the NO concentration level of 4.76 $\mu molL^{-1}$. In addition, the long-term stability and the continuous activity of the built biosensor were examined during five weeks. The results showed that it retained approximately 97% of the initial

response after one week and 83.5% after five weeks, confirming that the selected NOR immobilization approach allows to maintain the bioelectrocatalytic activity for a long period of time.

The selectivity of the PGE/[SWCNTs/(DOPE:DOTAP:DSPE-PEG)/NOR] was also evaluated at a concentration of 4.76 $\mu molL^{-1}$ NO by testing the presence of compounds that potentially co-exist with NO (or are promoters of NO production) in biological systems. L-arginine (L-Arg), ascorbic acid (AA), sodium nitrate (NO_3^-), sodium nitrite (NO_2^-) and glucose (Glu) are the most common species that may cause interference during the electrochemical detection of NO [54] and, thus, their individual effect on the NO peak current was tested at 200 $\mu molL^{-1}$ for L-Arg, NO_3^- and NO_2^-, 20 $\mu molL^{-1}$ for AA and 800 $\mu molL^{-1}$ for Glu. The biosensor demonstrated excellent performance with recovery values of 98.4 ± 5.3 %, 97.3 ± 2.3 %, 91.0 ± 9.3 %, 91.4 ± 3.0 % and 98.4 ± 8.9 % for L-Arg, AA, NO_3^-, NO_2^- and Glu, respectively.

6. 4. Conclusions

For the first time, a biosensor based on NOR was developed. A biomimetic nanocomposite prepared with carboxylated SWCNTs, lipidic bilayer (DOPE:DOTAP:DSPE-PEG) and NOR was optimized and used to modify a PGE to construct a new third generation enzymatic biosensor. Regarding DET of NOR, the peak corresponding to the heme b_3 bi-nuclear catalytic center displayed enhanced current and was detected at a lesser negative potential when compared to the PGE/NOR. The proposed PGE/[SWCNTs/(DOPE:DOTAP:DSPE-PEG)/NOR] exhibited excellent structural stability and selectivity, combined with good bioelectrocatalytic activity and sensitivity towards NO detection. Thus, it has the potential to constitute an interesting approach for monitoring the spatial and temporal profiles of NO formation and consumption in real biological systems.

6.5. References

[1] P. Tavares, A.S. Pereira, J.J.G. Moura, I. Moura, Metalloenzymes of the denitrification pathway, J. Inorg. Biochem, 100 (2006) 2087-2100.

[2] J. Hendriks, A. Oubrie, J. Castresana, A. Urbani, S. Gemeinhardt, M. Saraste, Nitric oxide reductases in bacteria, Biochim. Biophys. Acta, 1459 (2000) 266-273.

[3] D.E. Canfield, A.N. Glazer, P.G. Falkowski, The evolution and future of earth's nitrogen cycle, Science, 330 (2010) 192-196.

[4] V. Calabrese, C. Cornelius, E. Rizzarelli, J.B. Owen, A.T. Dinkova-Kostova, D.A. Butterfield, Nitric oxide in cell survival: a janus molecule, Antioxid Redox Signal, 11 (2009) 2717-2139.

[5] K.C. Wood, R.A. Alvarez, A.C. Straub, Chapter 18 - Diffusional control of nitric oxide in the vessel wall A2 - Ignarro, Louis J, in: B.A. Freeman (Ed.) Nitric Oxide (Third Edition), Academic Press, 2017, pp. 237-46.

[6] F. Schreiber, P. Wunderlin, K.M. Udert, G.F. Wells, Nitric oxide and nitrous oxide turnover in natural and engineered microbial communities: biological pathways, chemical reactions, and novel technologies, Front Microbiol, 3 (2012) 1-24.

[7] H. Qi, C. Zhang, X. Li, Amperometric third-generation hydrogen peroxide biosensor incorporating multiwall carbon nanotubes and hemoglobin, Sens Actuators B Chem, 114 (2006) 364-370.

[8] M. Baghayeri, H. Veisi, M. Ghanei-Motlagh, Amperometric glucose biosensor based on immobilization of glucose oxidase on a magnetic glassy carbon electrode modified with a novel magnetic nanocomposite, Sens Actuators B Chem, 249 (2017) 321-330.

[9] A.A. Abdelwahab, W.C.A. Koh, H.-B. Noh, Y.-B. Shim, A selective nitric oxide nanocomposite biosensor based on direct electron transfer of microperoxidase: Removal of interferences by co-immobilized enzymes, Biosens. Bioelectron, 26 (2010) 1080-1086.

[10] E. Casero, M. Darder, F. Pariente, E. Lorenzo, Peroxidase enzyme electrodes as nitric oxide biosensors, Anal. Chim. Acta, 403 (2000) 1-9.

[11] C.M. Cordas, A.G. Duarte, J.J.G. Moura, I. Moura, Electrochemical behaviour of bacterial nitric oxide reductase—Evidence of low redox potential non-heme Fe_B gives new perspectives on the catalytic mechanism, Biochim. Biophys. Acta, 1827 (2013) 233-238.

[12] C.M. Cordas, A.S. Pereira, C.E. Martins, C.G. Timóteo, I. Moura, J.J.G. Moura, P. Tavares, Nitric oxide reductase: Direct electrochemistry and electrocatalytic activity, ChemBioChem, 7 (2006) 1878-1881.

[13] A.G. Duarte, C.M. Cordas, J.J.G. Moura, I. Moura, Steady-state kinetics with nitric oxide reductase (NOR): New considerations on substrate inhibition profile and catalytic mechanism, Biochim. Biophys. Acta, 1837 (2014) 375-384.

[14] S.J. Field, M.D. Roldan, S.J. Marritt, J.N. Butt, D.J. Richardson, N.J. Watmough, Electron transfer to the active site of the bacterial nitric oxide reductase is controlled by ligand binding to heme b_3, Biochim. Biophys. Acta, 1807 (2011) 451-457.

[15] S. Ramos, R.M. Almeida, C.M. Cordas, J.J.G. Moura, S.R. Pauleta, I. Moura, Insights into the recognition and electron transfer steps in nitric oxide reductase from *Marinobacter hydrocarbonoclasticus*, J. Inorg. Biochem, 177 (2017) 402-411.

[16] N. Yang, X. Chen, T. Ren, P. Zhang, D. Yang, Carbon nanotube based biosensors, Sens Actuators B Chem, 207 (2015) 690-715.

[17] T. Mahmoudi-Badiki, E. Alipour, H. Hamishehkar, S.M. Golabi, Dopamine-loaded liposome and its application in electrochemical DNA biosensor, J. Biomater. Appl, 31 (2016) 273-282.

[18] C. Apetrei, P. Alessio, C.J.L. Constantino, J.A. de Saja, M.L. Rodriguez-Mendez, F.J. Pavinatto, E.G.R. Fernandes, V. Zucolotto, O.N.Jr. Oliveira, Biomimetic biosensor based on lipidic layers containing tyrosinase and lutetium bisphthalocyanine for the detection of antioxidants, Biosens. Bioelectron, 26 (2011) 2513-2519.

[19] H. Guan, X. Liu, W. Wang, Encapsulation of tyrosinase within liposome bioreactors for developing an amperometric phenolic compounds biosensor, J Solid State Electrochem, 17 (2013) 2887-2893.

[20] J. Liu, L. Han, T. Wang, W. Hong, Y. Liu, E. Wang, Enzyme immobilization and direct electrochemistry based on a new matrix of phospholipid-monolayer-functionalized graphene, Chem Asian J, 7 (2012) 2824-2829.

[21] C.M. Miyazaki, T.P. Pereira, D.B.T. Mascagni, M.L. de Moraes, M. Ferreira, Monoamine oxidase B layer-by-layer film fabrication and characterization toward dopamine detection, Mater. Sci. Eng. C, 58 (2016) 310-315.

[22] Y. Tian, J. Xia, L. Zhang, J. Zhang, Y. Jiang, Y. Zhang, L. Yang L, Q. Zhang, L. Xia, Ionic liquid based polymeric liposomes: A stable and biocompatible soft platform for bioelectrochemistry, Bioelectrochemistry, 111 (2016) 41-48.

[23] J. Yan, H. Guan, J. Yu, D. Chi, Acetylcholinesterase biosensor based on assembly of multiwall carbon nanotubes onto liposome bioreactors for detection of organophosphates pesticides, Pestic Biochem Physiol, 105 (2013) 197-202.

[24] M. Yoshimoto, C. Iida, A. Kariya, N. Takaki, M. Nakayama, A biosensor composed of glucose oxidase-containing liposomes and MnO_2-based layered nanocomposite, Electroanalysis, 22 (2010) 653-659.

[25] Q. Liu, B.J. Boyd, Liposomes in biosensors, Analyst, 138 (2013) 391-409.

[26] O.K. Nag, V. Awasthi, Surface engineering of liposomes for stealth behavior, Pharmaceutics, 5 (2013) 542-569.

[27] P. Milla, F. Dosio, L. Cattel, PEGylation of proteins and liposomes: a powerful and flexible strategy to improve the drug delivery, Curr Drug Metab, 13 (2012) 105-119.

[28] P. Girsch, S. de Vries, Purification and initial kinetic and spectroscopic characterization of NO reductase from *Paracoccus denitrificans*, Biochimica et biophysica acta, 1318 (1997) 202-216.

[29] M. Prudêncio, A.S. Pereira, P. Tavares, S. Besson, I. Cabrito, K. Brown, B. Samyn, B. Devreese, J.V. Beeumen, F. Rusnak, G. Fauque, J.J.G. Moura, M. Tegoni, C. Cambillau, I. Moura, Purification, characterization, and preliminary crystallographic study of copper-containing nitrous oxide reductase from *Pseudomonas nautica 617*, Biochemistry, 39 (2000) 3899-907.

[30] U.K. Laemmli, Cleavage of structural proteins during the assembly of the head of bacteriophage T4, Nature, 227 (1970) 680-685.

[31] C.G. Timóteo, A.S. Pereira, C.E. Martins, S.G. Naik, A.G. Duarte, J.J.G. Moura, P. Tavares, B.H. Huynh, and I. Moura, Low-spin heme b_3 in the catalytic center of nitric oxide reductase from *Pseudomonas nautica*, Biochemistry, 50 (2011) 4251-4262.

[32] A. Akbarzadeh, R. Rezaei-Sadabady, S. Davaran, S.W. Joo, N. Zarghami, Y. Hanifehpour, M. Samiei, M. Kouhi, K. Nejati-Koshki, Liposome: classification, preparation, and applications, Nanoscale Res. Lett, 8 (2013) 1-9.

[33] S. Garny, N. Beeton-Kempen, I. Gerber, J. Verschoor, J. Jordaan, The co-immobilization of P450-type nitric oxide reductase and glucose dehydrogenase for the continuous reduction of nitric oxide via cofactor recycling, Enzyme Microb Technol, 85 (2016) 71-81.

[34] M. Bhuvana, V. Dharuman, Tethering of spherical DOTAP liposome gold nanoparticles on cysteamine monolayer for sensitive label free electrochemical detection of DNA and transfection, Analyst, 139 (2014) 2467-2475.

[35] T.M. Oliveira, M.F. Barroso, S. Morais, M. Araujo, C. Freire, P. de Lima-Neto, A.N. Correia, M.B. Oliveira, C. Delerue-Matos, Sensitive bi-enzymatic biosensor based on polyphenoloxidases-gold nanoparticles-chitosan hybrid film-graphene doped carbon paste electrode for carbamates detection, Bioelectrochemistry, 98 (2014) 20-29.

[36] G. Alarcon-Angeles, G.A. Álvarez-Romero, A. Merkoçi, Electrochemical biosensors: Enzyme kinetics and role of nanomaterials, Reference Module in Chemistry, Molecular Sciences and Chemical Engineering, Elsevier, 2017.

[37] S. Datta, L.R. Christena, Y.R.S. Rajaram, Enzyme immobilization: an overview on techniques and support materials, Biotech, 3 (2013) 1-9.

[38] H. Yang, C. Gong, L. Miao, F. Xu, A glucose biosensor based on horseradish peroxidase and glucose oxidase co-entrapped in carbon nanotubes modified electrode, Int J Electrochem Sci, 12 (2017) 4958-4969.

[39] O. Matarredona, H. Rhoads, Z. Li, J.H. Harwell, L. Balzano, D.E. Resasco, Dispersion of single-walled carbon nanotubes in aqueous solutions of the anionic surfactant NaDDBS, J. Phys. Chem. B, 107 (2003) 13357-13367.

[40] D. Grieshaber, R. MacKenzie, J. Vörös, E. Reimhult, Electrochemical biosensors - Sensor principles and architectures, Sensors, 8 (2008) 1400-1458.

[41] F. Wang, X. Chen, Y. Xu, S. Hu, Z. Gao, Enhanced electron transfer for hemoglobin entrapped in a cationic gemini surfactant films on electrode and the fabrication of nitric oxide biosensor, Biosens. Bioelectron, 23 (2007) 176-182.

[42] F.W.P. Ribeiro, F.W. de Souza Lucas, L.H. Mascaro, S. Morais, P.N. da Silva Casciano, P. de Lima-Neto, A.N. Correia, Electroanalysis of formetanate hydrochloride by a cobalt phthalocyanine functionalized multiwalled carbon nanotubes modified electrode: characterization and application in fruits, Electrochim. Acta, 194 (2016) 187-198.

[43] M. Gamero, F. Pariente, E. Lorenzo, C. Alonso, Nanostructured rough gold electrodes for the development of lactate oxidase-based biosensors, Biosens. Bioelectron, 25 (2010) 2038-2044.

[44] Y.-M. Li, H.-H. Liu, D.-W. Pang, Direct electrochemistry and catalysis of heme-proteins entrapped in methyl cellulose films, J. Electroanal. Chem, 574 (2004) 23-31.

[45] L. Zhang, G.-C. Zhao, X.-W. Wei, Z.-S. Yang, A nitric oxide biosensor based on myoglobin adsorbed on multi-walled carbon nanotubes, Electroanalysis, 17 (2005) 630-634.

[46] L.M. Blomberg, M.R.A. Blomberg, P.E.M. Siegbahn, Reduction of nitric oxide in bacterial nitric oxide reductase—a theoretical model study, Biochim. Biophys. Acta, 1757 (2006) 240-252.

[47] M.R.A. Blomberg, P.E.M. Siegbahn, Mechanism for N_2O generation in bacterial nitric oxide reductase: A quantum chemical study, Biochemistry, 51 (2012) 5173-5186.

[48] Y. Shiro, Structure and function of bacterial nitric oxide reductases: Nitric oxide reductase, anaerobic enzymes, Biochim. Biophys. Acta, 1817 (2012) 1907-1913.

[49] J.P. Collman, Y. Yang, A. Dey, R.A. Decréau, S. Ghosh, T. Ohta, E.I. Solomon, A functional nitric oxide reductase model, Proc Natl Acad Sci U S A, 105 (2008) 15660-15665.

[50] J. ter Beek, N. Krause, J. Reimann, P. Lachmann, P. Adelroth, The nitric-oxide reductase from *Paracoccus denitrificans* uses a single specific proton pathway, J Biol Chem, 288 (2013) 30626-30635.

[51] X. Chen, H.-Y. Long, W.-L. Wu, Z.-S. Yang, Direct electrochemical behavior of cytochrome *c* on sodium dodecyl sulfate modified electrode and its application to nitric oxide biosensor, Thin Solid Films, 517 (2009) 2787-2791.

[52] S. Jia, J. Fei, J. Deng, Y. Cai, J. Li, Direct electrochemistry and electrocatalysis of hemoglobin immobilized in an amphiphilic diblock copolymer film, Sens Actuators B Chem, 138 (2009) 244-250.

[53] W. Wen, W. Chen, Q.-Q. Ren, X.-Y. Hu, H.-Y. Xiong, X.-H. Zhang, S.-F. Wang, Y.-D. Zhao, A highly sensitive nitric oxide biosensor based on hemoglobin–chitosan/graphene–hexadecyltrimethylammonium bromide nanomatrix, Sens Actuators B Chem, 166-167 (2012) 444-450.

[54] F. Li, M. Nie, X. He, J. Fei, Y. Ding, B. Feng, Direct electrochemistry and electrocatalysis of hemoglobin on a glassy carbon electrode modified with poly(ethylene glycol diglycidyl ether) and gold nanoparticles on a quaternized cellulose support. A sensor for hydrogen peroxide and nitric oxide, Microchim. Acta, 181 (2014) 1541-1549.

[55] A. Shrivastava, V. Gupta, Methods for the determination of limit of detection and limit of quantitation of the analytical methods, Chro Cron. Young Sci, , 2 (2011) 21-25.

[56] X. Liu, L. Shang, Z. Sun, G. Li, Direct electrochemistry of hemoglobin in dimethyldioctadecyl ammonium bromide film and its electrocatalysis to nitric oxide, J Biochem Biophys Methods, 62 (2005) 143-151.

[57] Y.-C. Liu, J. Zhao, W.-L. Wu, Z.-S. Yang, Direct electrochemical behavior of cytochrome *c* on DNA modified glassy carbon electrode and its application to nitric oxide biosensor, Electrochim. Acta, 52 (2007) 4848-4852.

[58] A.A. Abdelwahab, W.C. Koh, H.B. Noh, Y.B. Shim, A selective nitric oxide nanocomposite biosensor based on direct electron transfer of microperoxidase: removal of interferences by co-immobilized enzymes, Biosens. Bioelectron, 26 (2010) 1080-1086.

[59] W.C. Alvin Koh, M.A. Rahman, E.S. Choe, D.K. Lee, Y.-B. Shim, A cytochrome *c* modified-conducting polymer microelectrode for monitoring in vivo changes in nitric oxide, Biosens. Bioelectron, 23 (2008) 1374-1381.

[60] R.M. Santos, M.S. Rodrigues, J. Laranjinha, R.M. Barbosa, Biomimetic sensor based on hemin/carbon nanotubes/chitosan modified microelectrode for nitric oxide measurement in the brain, Biosens. Bioelectron, 44 (2013) 152-159.

CHAPTER 7

CONCLUDING REMARKS AND FUTURE PERSPECTIVES

“The best journeys answer questions that in the beginning you didn’t even think to ask.”

Jeff Johnson

Since the 1980s, it has been revealed that NO is one of the most important physiological regulators, playing a key role in signal transduction and cytotoxicity. In humans, NO controls many functions such as vasodilation, neurotransmission, immune response, platelet aggregation, apoptosis and gene expression. However, its overproduction can lead to several pathological conditions (hypertension, diabetes, arteriosclerosis and neurodegenerative diseases) [1]. In this work, NOR, a membrane-bound enzyme involved in the denitrification pathway, was purified from *Marinobacter hydrocarbonoclasticus* and used, for the first time, to develop third-generation biosensors. Successful purifications were accomplished originating two different batches of NOR with the specific activity of 760 and 307 U/mg. The specificity of NOR towards NO made it an ideal target to develop biosensing enzymatic devices to monitor NO, and can possibly be further explored to determine other reactive nitrogen species, in biological systems, namely in humans.

Due to NOR structural similarity to cytochrome oxidases, NOR is able to reduce O_2 to H_2O. Thus, the first main objective of this dissertation was to modify by drop casting a PGE with NOR to characterize NOR direct electrochemical behaviour and NOR bioelectrocatalytic activity towards NO and O_2. The attained sensitivities and the Michaelis Menten constants corroborated the higher affinity of NOR for its natural substrate. No significant interference on sensitivity towards NO was noted in the presence of O_2, while the O_2 reduction was significantly and negatively influenced by the presence of NO. These results suggested the high potential applicability of NOR in unmediated enzymatic biosensor for NO detection.

One of the main requirement to successfully develop enzymatic biosensors is the need to efficiently immobilize the biorecognition element on the selected solid support. Several immobilization strategies are available, namely through physical adsorption, electrostatic interactions, cross-linking, covalent bonding, encapsulation and entrapment. The preferred approach has a major impact on biosensor performance (sensitivity, reproducibility and response time) and long-term stability. The enzyme's structure and activity should remain unchanged after immobilization, and the enzyme should intimately and strongly link to the transducer surface. In addition, many anchorage sites are required to obtain high enzymatic catalytic currents in order to reach low detection limits. Therefore, 3D structures were explored in this work since, when compared to the direct immobilization of enzymes onto an electrode surface, incorporation of enzymes into a 3D structure has the potential to protect the enzyme from the surrounding environment maintaining its

total activity and to provide a model system to mimic and understand the action of some membrane-bound intracellular enzymes [2].

The first optimized nanocomposite, composed by carboxylated MWCNTs and a specific IL namely 1-butyl-3-methylimidazolium tetrafluoroborate ($BMIMBF_4$), demonstrated to be an effective microenvironment for the immobilization of NOR due to synergetic effects between MWCNTs (excellent electric conductivity and large surface area) and ionic liquid (biocompatibility, viscosity and ionic conductivity) with good electroanalytical characteristics. The second approach, the optimization of a biomimetic nanocomposite prepared with carboxylated SWCNTs, lipidic bilayer (DOPE:DOTAP:DSPE-PEG where 1,2-di-(9Z-octadecenoyl)-sn-glycero-3-phosphoethanolamine (DOPE), 1,2-di-(9Z-octadecenoyl)-3-trimethylammonium-propane (DOTAP) and 1,2-distearoyl-sn-glycero-3-phosphoethanolamine – polyethylene glycol (DSPE-PEG)) and NOR, exhibited higher sensitivity and Michaelis Menten constant, as well as wider linear range although the lowest activity of the used NOR. Both proposed nanocomposite-based biosensors exhibited acceptable long-term stability (about 1 month). However, further improvements are still needed in order to decrease the detection limits and fully characterize biosensors behaviour in complex samples and in the presence of interfering substrates (hydrogen peroxide, peroxynitrite, carbon dioxide and others reactive nitrogen species). Also, other alternatives for immobilization may be tested. Preliminary studies were already performed with promising results regarding the preparation of a nanocomposite based on the excellent capacity of film formation and biocompatibility of chitosan and also on the high electric conductivity of reduced graphene oxide. Other approaches previously assessed during this PhD work consisted in the development of carbon ionic liquid electrodes; limitation on the amount of the purified enzyme did not allow to conclude this full evaluation, which also generated encouraging results.

Altogether, the obtained data contributed with relevant information concerning NOR based–biosensors for NO detection. Still, some challenges remained unaddressed and should be explored in future works namely their application using NO donors. Direct measurement of NO released from endothelial cells (responsible for the inhibition of platelet aggregation and adhesion, and modulation of the vascular tone) is difficult because NO is generated in small amounts and degrades fast in biological system. However, the use of NO donors could help to work around this problem. Specific NO donors can be selected based on the timescales required for the application (short life time: N-(N-L-γ-glutamyl-S-nitroso-L-cysteinyl)-glycine (GSNO), 6-(2-Hydroxy-1-methyl-2-nitrosohydrazino)-N-methyl-1-hexanamine (NOC-9), sodium

nitroprusside (SNP) and diethylammonium (Z)-1-(N,N-diethylamino)diazen-1-ium-1,2-diolate (DEA NONOate) or high life time: (Z)-1-[N-(3-aminopropyl)-N-(n-propyl)amino]diazen-1-ium-1,2-diolate (PAPA NONOate), 3-(aminopropyl)-1-hydroxy-3-isopropyl-2-oxo-1-triazene (NOC-5), 3-ethyl-3-(ethylaminoethyl)-1-hydroxy-2-oxo-1-triazene (NOC-12) and (Z)-1-[N-(2-aminoethyl)-N-(2-ammonioethyl)amino]diazen-1-ium-1,2-diolate (NOC-18) [3-5].

The passage of pyrolytic graphite electrodes to microelectrodes could also have a major positive impact on the potential real biosensor applicability. Carbon fiber microelectrodes have been applied to the neurology field, in particular in rat brain [6], since the carbon fibers have usually less than 10 µm as diameter, and because they are flexible for implantation causing low tissue damage. However, some drawbacks have been described for these specific microelectrodes, when used as bare devices, namely some sensitivity and selectivity limitations that could be overpassed using the modifications developed in this thesis. Incorporation the benefits of microelectrodes with the inherent specificity of NOR could be the next step to get closer to *in vivo* applications of NO detection. Furthermore, the integration of several bio-recognitions elements with DET behavior in the same biosensor and, for example, in microfluidic biosensing systems could permit a detection of a broad range of analytes and a high degree of miniaturization/automation with a great cost-efficiency. Coupling the processing power of microelectronics with the excellent sensitivity and specificity of the biological recognition elements make biosensors exquisite tools for real-time and *in situ* biomonitoring of NO dynamics in living systems.

References

[1] S. Moncada, R.M. Palmer, E.A. Higgs, Nitric oxide: physiology, pathophysiology, and pharmacology, Pharmacol. Rev, 43 (1991) 109-142.

[2] C. Zhu, G. Yang, H. Li, D. Du, Y. Lin, Electrochemical sensors and biosensors based on nanomaterials and nanostructures, Anal. Chem, 87 (2015) 230-249.

[3] S. Griveau, C. Dumezy, J. Seguin, G.G. Chabot, D. Scherman, F. Bedioui, *In vivo* electrochemical detection of nitric oxide in tumor-bearing mice, Anal. Chem, 79 (2007) 1030-1033.

[4] L. Grossi, S. D'Angelo, Sodium Nitroprusside: Mechanism of NO Release Mediated by Sulfhydryl-Containing Molecules, J Med Chem, 48 (2005) 2622-2626.

[5] S. Jiang, R. Cheng, X. Wang, T. Xue, Y. Liu, A. Nel, et al., Real-time electrical detection of nitric oxide in biological systems with sub-nanomolar sensitivity, Nat. Commun, 4 (2013) 1-7.

[6] R.M. Santos, M.S. Rodrigues, J. Laranjinha, R.M. Barbosa, Biomimetic sensor based on hemin/carbon nanotubes/chitosan modified microelectrode for nitric oxide measurement in the brain, Biosens. Bioelectron, 44 (2013) 152-159.

APPENDIX

Appendix A

Cell growth conditions for Marinobacter hydrocarbonoclasticus nitric oxide reductase purification

Marinobacter hydrocarbonoclasticus or also called *Pseudomonas nautica* 617 ("Institute Pasteur Culture Collection" 617 / 1.85) was isolated from marine coastal sediments contaminated with the effluents from an oil refinery under denitrificans conditions and temperature of 30°C. Reactors of 200 L were used to cell growth with incorporation of 10 $mmolL^{-1}$ of nitrate as electron acceptor.

Culture medium is presented in table A.1 and the pH adjusted to 7.5 with 10 $molL^{-1}$ of HCl, sterilized and autoclaved. The culture medium was supplemented with the trace elements solutions (table A.2) and the $FeSO_4$ e K_2HPO_4 (table A.3), autoclaved separately. Cells were collected by centrifugation at the end of the stationary step. Yield of 1 g of cells/L of the culture medium (w/w) were resuspended in buffer 100 $mmolL^{-1}$ Tris-HCl pH 7.0 and broken in a French Press.

The extract was centrifuged at 8 000 × *g* for 20 minutes to separate whole cells and then ultracentrifuged twice at 125 000 × *g* for 1 hour to separate the cell membranes from the soluble extract. The membranes were stored at -70 ° C.

Table A.1. Culture medium composition for the bacteria *Marinobacter hydrocarbonoclasticus* growth.

Reagent	Amount to prepare 1 L (g)
NaCl	11.7
$MgSO_4.7H_2O$	12.3
KCl	0.75
Tris	6.05
NH_4Cl	3
$CaCl_2$	1.49
Yeast extract	1
Lactate	10

Table A.2. Trace elements solution composition (Starkey solution).

Reagent	Amount to prepare 1 L (g)
$F_2SO_4.7H_2O$	6.2
$ZnSO_4.7H_2O$	1.44
$MgSO_4.4H_2O$	1.12
$CuSO_4.5H_2O$	0.25
$CoSO_4.7H_2O$	0.9
BO_3H_3	0.6
$Mo_7(NH_4)_6O_{24}.4H_2O$	1
$Ni(NO_3)_3.6H_2O$	0.04
Na_2SeO_3	0.02
HCl conc.	51.4 mL

Table A.3. Supplementary solutions for the *Marinobacter hydrocarbonoclasticus* medium culture growth.

Solutions	Volume to prepare 1 L (mL)
$FeSO_4.7H_2O$ ($1 mgmL^{-1}$)	2
$K_2HPO_4.3H_2O$ (1.86%(p/v))	4
Trace elements (table 2)	0.2

Appendix B

Electrophoretic procedures

Denaturing polyacrylamide gel electrophoresis (SDS-PAGE) is used as a way of determining which proteins are present in each fraction throughout the purification, as well as the degree of purity of a sample. The technique consists of an adaptation of the Laemmli method [1] in which tricine is used instead of glycine in the running buffer and the samples are incubated at 40° C instead of boiled. Incubation at temperatures above 50 °C may lead to aggregation and complete loss of some membrane proteins from the samples. The solutions to be prepared to gel electrophoresis are shown in table B.1.

Table B.1. Solutions for gel and buffer preparation.

Solution	Reagents	Preparation	Storage
Acrylamide + bis-acrylamide	1,5 g bis-acrylamide 48 g acrylamide	Dissolve in 40mL with magnetic stirring Maku up to 100mL	4°C Dark bottle Use maximum of 30 days
Gel buffer 3.0 $molL^{-1}$	36.34 g Tris (Mw = 121.14 $gmol^{-1}$)	Dissolve in 80-90 mL	4°C Dark bottle
	+ 0.3 g SDS (attention: Foam!)	pH to 8.45 with HCl concentrated. Make up to 100 mL	
Tris-HCl 1.0 $molL^{-1}$, pH 7	12.11 g Tris (Mw = 121.14 $gmol^{-1}$)	Dissolve in 80-90 mL pH to 7.0 with HCl concentrated. Make up to 100 mL	4°C Dark bottle
Cathode buffer Solution 10 × concentrated	121.14 g Tris (Mw = 121.14 $gmol^{-1}$) +179.20 g tricine	Dissolve in 800-900 mL	4°C Dark bottle If precipitates are formed warm to room temperature
	+ 10.00 g SDS (attention: Foam!)	pH must be 8.45 Make up to 1000 mL	
Anode buffer Solution 10 × concentrated	121.14 g Tris (Mw = 121.14 $gmol^{-1}$)	Dissolve in 800-900 mL pH to 7.0 with HCl concentrated. Make up to 1000 mL	4°C Dark bottle If precipitates are formed warm to room temperature
Sample buffer	1.2 g SDS (attention: Foam!) + 3 g glycerol + 1.5 mL of Tris-HCl 1.0 $molL^{-1}$ pH 7 + 1.0 mg bromophenol blue + 600 µL of mercaptoethanol	10 mL	Aliquot in eppendorfs with 500 µL of sample buffer and freeze to -20°C
PSA (Ammonium persulfate)	1 g PSA	10 mL	Aliquot in eppendorfs with 150 µL of PSA and freeze to -20°C
Dye solution	0.25% Comassie R-250 blue 50% methanol 10% acetic acid	200 mL	Dark bottle Room temperature
Decolorizing solution	50% methanol 10% acetic acid	250 mL	Dark bottle Room temperature

The volumes necessary for the preparation of a 7 × 10 cm gel, 0.75 mm thick (Bio-Rad Mini-protean II-Mini Gel vial), are given in Table B.2.

Table B.2. Solutions for the separating and concentration gel.

Reagent	Separating gel	Concentration gel
Acrilamide	16%	4%
Acri. + bis. Acril. solution	3.34 mL	332 µL
Gel buffer	3.34 mL	1.00 mL
Glycerol	800 µL	---
Water	2.52 mL	2.66 mL
PSA	50 µL	30 µL
TEMED (use in hood)	5 µL	3 µL

The samples are prepared by adding the buffer of the samples so that it represents 1/4 of the final volume and incubated for 30 minutes at 40 °C.

After the gel is polymerized, the samples are applied to the wells and the gel is run at constant current. The initially applied current is 35 mA for 45 minutes, then increasing to 70 mA for an additional 45 minutes.

Appendix C

Protein quantification

Purification and characterization of proteins necessarily involves the determination of the total amount of protein present in a given sample. Although there are several very strict methods for quantification, they are not usually used routinely in a biochemistry laboratory because of their complexity, requirement and price. Routine procedures use colorimetric or spectrophotometric methods which, although not as rigorous, provide good results if applied correctly. The choice of the most appropriate method in each case depends on the nature of the protein, the presence of other components in the sample and the desired speed, accuracy and sensitivity. Lowry method was the chosen method and is based on the Biuret method but has a sensitivity about 100 times higher due to the use of the Folin-Ciocalteau reagent [2]. The colorimetric reaction yields Cu^{+}, which in this case is coupled to the reduction of phosphomolybdate and phosphotungstate by the tyrosine, tryptophan and cysteine residues present in the protein forming a complex of intense blue color. The color developed by mg of protein depends on the specific nature of the protein. This method is much more sensitive but is more time consuming, the color is unstable and depends on the tyrosine and tryptophan composition of the protein. Mercapto and NH_4^{+} compounds interfere with the reaction.

The protocol used is described below and used the solutions presented in table C.1.

1- 100 µL sample/ blank (water/ Tris-HCl/ phosphate buffer)/ standard;

2- Add 400 µL of Biuret Reagent and wait 10 minutes;

3- Add 3.5 mL of 2.3% Na_2CO_3 and mix;

4- Add 100 µL of Folin's Ciocalteu phenol reagent (directly from the bottle) and mix each tube immediately;

5- Measure Abs at 750 nm (20-120 minutes later).

Firstly, a calibration curve is prepared according with the volumes presented in table C.2 using a standard Bovine Serum Albumin (BSA) solution of 1 $mgmL^{-1}$.

Table C.1. Solutions for Lowry method.

Biuret Reagent (500 mL)*	
Reagent	**Weight (g)**
$CuSO_4.5H_2O$	0.75
KNa tartrate	3.0
NaOH	15.0
KI	0.5
2.3% Na_2CO_3 (500 mL)	
Na_2CO_3	11.5

* a) Dissolve $CuSO_4.5H_2O$ and KNa tartrate in approximately 250 mL of water; b) Dissolve NaOH in approximately 100 mL of water; Add b) to a), then add KI and make up to 500 mL. Store in plastic bottle and at room temperature.

Table C.2. Calibration in Lowry method using Bovine Serum Albumin as protein model.

Standard**	**Concentration ($mgmL^{-1}$)**	**Volume BSA (µL)*****	**Volume H_2O (µL)**	**v total (µL)**
0	0	-	500	500
1	0.050	25	475	
2	0.100	50	450	
3	0.125	62.5	437.5	
4	0.150	75	425	
5	0.200	100	400	
6	0.225	112.5	387.5	
7	0.250	125	375	
8	0.275	137.5	362.5	
9	0.300	150	350	

** Standards could be made with water, Tris-HCl or KPi.

*** BSA is stored in the freezer (-20°C) with a concentration of 10 $mgmL^{-1}$ and used with a concentration of 1 $mgmL^{-1}$.

A typical calibration curve could be observed in Fig. C.1 with a good correlation coefficient of 0.999 between absorbance and BSA concentration (mg/mL).

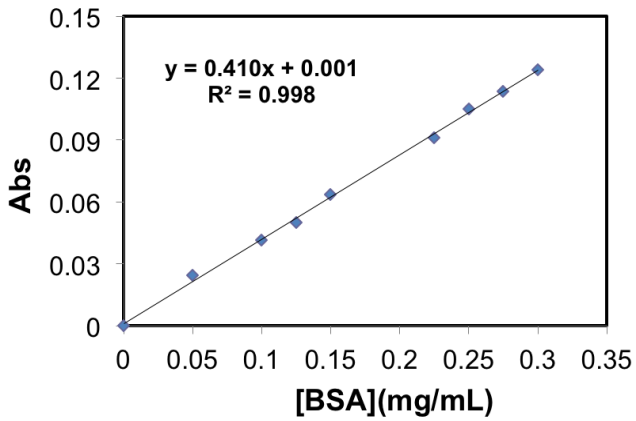

Fig. C.1. Calibration curve (Absorbance versus Bovine Serum Albumin concentration) used in Lowry method for protein quantification.

References

[1] U.K. Laemmli, Cleavage of structural proteins during the assembly of the head of bacteriophage T4, Nature, 227 (1970) 680-685.

[2] J.H. Waterborg, H.R. Matthews, The Lowry method for protein quantitation, in: J.M. Walker (Ed.) The protein protocols handbook, Humana Press, Totowa, NJ, 1996, pp. 7-9.